Sheffield Hallam University

A Sheffield Hallam University thesis

Remediation of Heavy Metals from Water using Modified Clay-Chitosan Composites

Hassan Mohammed Majiya

A thesis submitted in partial fulfilment of the requirements of
Sheffield Hallam University
for the degree of Doctor of Philosophy

December 2022

Declaration

I hereby declare that:

1. I have not been enrolled for another award of the University, or other academic or professional organisation, whilst undertaking my research degree.

2. None of the material contained in the thesis has been used in any other submission for an academic award.

3. I am aware of and understand the University's policy on plagiarism and certify that this thesis is my own work. The use of all published or other sources of material consulted have been properly and fully acknowledged.

4. The work undertaken towards the thesis has been conducted in accordance with the SHU Principles of Integrity in Research and the SHU Research Ethics Policy.

5. The word count of the thesis is 58,544.

Name	*Hassan Mohammed Majiya*
Date	*December 2022*
Award	*PhD*
Faculty	*College of Business, Technology and Engineering*
Director of Studies	*Dr Francis Clegg*

"Thousands have lived without love, not one without water."

-W.H Auden

Acknowledgement

Abstract

Water contamination with pollutants such as heavy metals is of significant concern because the toxicity exhibited by these metals can pose a severe threat to human health and the environment. Adsorption with the combined use of geological materials (such as clays) and biodegradable polymers (such as chitosan) seems to be a promising technique for purification of water contaminated with toxic metals. These materials not only provide a cost-benefit but are also materials derived from sustainable sources and are thus environmentally friendly. This study focuses on the preparation of functional composites (from bentonite clay and chitosan biopolymer) as cheaper, and sustainable adsorbents for effective removal of heavy metals from water. The work carried out in this thesis investigated the efficiency of mixing bentonite with two different chitosans via different preparation methods. The different forms of bentonite-chitosan (Bt-Ch), composites and beads, were prepared in the weight ratios of 90%/10%, 70%/30% and 50%/50%, and via solution blending and precipitation methods, respectively. The beads were further subdivided, identified as "beads-A" and "beads-B", and were formed by adding either bentonite suspension or bentonite powder, respectively, to solubilised chitosan solution. The composites and beads were characterised by thermogravimetric analysis (TGA), X-ray diffraction (XRD), and Fourier transform infrared spectroscopy (FTIR). Subsequently, the different forms of the prepared clay-chitosan composites were investigated for their ability to remove metal ions (Pb, Pb-Cu and As) from aqueous solutions. Batch adsorption procedures (via statistical design of experiments) were used to study the removal of these metal ions. Results showed that Pb (or Pb-Cu) ions can be removed from aqueous solutions effectively. The amount of chitosan present in the adsorbent and its distribution within or outside the interlayer space of the bentonite clay was shown to have pronounced effects on the Pb (or Pb-Cu) uptake by these clay-chitosan composites, and the adsorption of Pb was significantly affected by the presence of other multi-competing ions. However, these composites showed a poor loading capacity (very low removal efficiencies) towards As ions. This led to modification of bentonite clay with chitosan and Fe(III) cations; the Fe-modified composites have demonstrated effective removal of As ions from aqueous solution. The developed Bt-Ch and Fe-modified composites exhibited good potential for re-use after five cycles of regeneration, thus, indicating their potential as cost-effective adsorbents for removal of

these metal ions from both drinking and wastewater. Overall, this study provides insights and new valuable knowledge for inexpensive remediation of metal-contaminated water, especially when using composites made from cheap and sustainable materials.

Abbreviations

AC	Activated carbon
ANOVA	Analysis of variance
BDST	Bed depth service time
Bt	Bentonite clay
Bt-Ch	Bentonite-Chitosan composites or beads
BBD	Box-Behnken design
CEC	Cationic exchange capacity
CCD	Central composite design
Ch	Chitosan
EDTA	Ethylenediaminetetraacetic acid
FTIR	Fourier-transform infrared spectroscopy
ICP-OES	Inductively coupled plasma-optical emission spectrometry
Fe-Bt-Ch	Iron-modified Bentonite-Chitosan composites
MPSD	Marquardt's percent standard deviation
POU	Point of use
PAGMI	Presidential Artisanal Gold Mining Development Initiative
PFO	Pseudo-first order
PSO	Pseudo-second order
RSM	Response surface methodology
SEM	Scanning electron microscope
TAB	Thermally activated bentonite
TGA	Thermogravimetric analysis
WHO	World Health Organisation
XRD	X-ray Diffraction

List of symbols

C_e Equilibrium concentration (mg/l) or (mol/l)

C_i (or c_o)   Initial concentration or influent concentration (mg/l) or (mol/l)

C_t Effluent concentrations (at time t) of the column adsorption (mg/L)

d   Interlayer distance

E   Mean free energy of adsorption (KJ/mol)

b_L (or K_L)   Langmuir adsorption coefficient constant (L/mg)

k_1 Pseudo-first order rate constant (1/h) or (1/min)

k_2 Pseudo-second order rate constant (g/mg·min) or (g/(mg·h)

K_{AB} Adams–Bohart rate constant (ml/ min/ mg)

K_{BDST} Bed-depth-service-time rate constant (ml/min/mg)

K_C Equilibrium constant

K_F Freudlich coefficient constant (L/g)

K_{RD} Dubinin-Radushkevich constant related to the sorption energy (mol^2/kJ^2).

K_{Th} Thomas rate constant (ml/min/mg)

K_{YN} Yoon-Nelson rate constant (min^{-1})

M   Mass of adsorbent (g)

M_W Molecular weight (g/mol)

n   Freundlich exponent or heterogeneity factor (from 0 to 1)

N_0 Saturation concentration in column adsorption (mg /ml)

Q   Volume flow rate of the column adsorption (ml/min),

q_{DR} Dose-response column adsorption capacity in mg/g),

q_e Adsorption capacity at equilibrium (mg/g) or (μg/mg)

Q_{max} Maximum saturated monlayer adsorption capacity (mg/g) or (μg/mg)

q_{RD} Dubinin-Radushkevich adsorption capacity (mg/g) or (μg/mg)

q_t Adsorption capacity at time t (mg/g) or (μg/mg)

q_{TH} Thomas maximum adsorption capacity (mg/g) or (μg/mg)

R   Universal gas constant (J/mol·K)

R^2 Coefficient of correlation

t   Time (s), (min) or (h)

T   Temperature (K) or (^{O}C)

v	Influent stream linear velocity during column adsorption
V	Volume of the solution (L)
X^2	Nonlinear chi-square
Z	Column bed height in column adsorption (cm)
α	Elovich sorption rate (mg/g min) or the constant of the Dose–Response model
β	Elovich desorption coefficient (g/mg min)
ε	Polanyi potential (or adsorption potential) parameter
τ	Yoon-Nelson parameter; time required for 50% adsorbate breakthrough (min)
λ	Wavelength (nm)
ΔG	change in Gibbs free energy
ΔH	change in enthalpy
ΔS	change in entropy

Table of Contents

List of Figures

List of Tables

Chapter 1

Introduction

1.1. Overview

It is undisputed that water is one of the precious resources required for human survival. The world is now facing a threat in meeting the demands of unpolluted drinking water due to its excessive usage, the impacts of climate change, expanding industrialisation and improper disposal of effluents into water bodies [1]. Due to rapid industrialisation, there are reported cases of river pollution in everywhere [2]. The rivers in Africa, Asia and Latin American are reported to be contaminated with various kinds of pollutants [2]. About 90% of both domestic and industrial effluents in low-economy nations are being discharged into surface water bodies without prior treatment (Figure 1.1) [2]. Surface water (rivers and lakes) and ground water (wells and natural springs) serves as major sources of drinking water, which are mostly not protected leading to water pollution [2]. Deaths due to unsafe water and a lack of access to improved sources of drinking water and good sanitation are common in African and Asian regions [3]. In the next three decades, it is projected that the world population will climb to approximately 9 billion, this will put more pressure on the limited available fresh water and therefore effective purification methods for water are essential in order to continue supporting the life of both flora and fauna [3,4].

Human activities and some natural processes have resulted in polluting water resources to the extent that decontamination is required before using it for domestic and other applications [2]. Metal contamination of water results from intensive anthropogenic activities, including mining, agriculture, and disposal of industrial waste materials [1]. Industrial effluents are also a major source of toxic metal pollution in water and furthermore, releasing of wastewaters into surface waters also has a greater implication in addition to drinking water, since effects to aquatic animals culminate to critical misbalances in the ecosystem [4]. As nearly all heavy metals are dangerously harmful

and not degradable biologically, they have to be removed from the wastewater so as to meet steadily more strict quality standards of the environmental media [5].
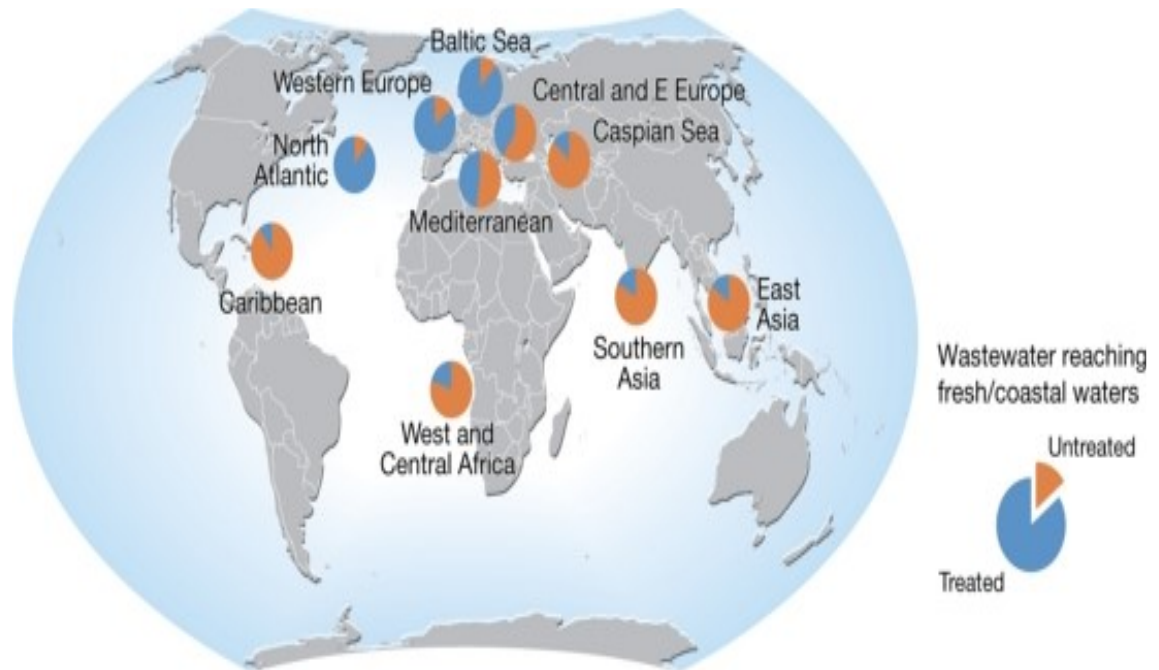
Figure 1.1: World map showing the ratio of treated and untreated wastewater before discharging into surface waters. Source: (GRID-Arendal)

1.2. Heavy metals: their toxic effects, and removal from water

The term "heavy metal" is often used as a group name for metals, semi-metals (e.g. arsenic) and non-metals (e.g. selenium), which have been associated with contamination and potential toxicity [6]. In particular, toxic heavy metals are some of the most hazardous substances to human health (and other living organisms) and have become a major public concern throughout the world [7–10]. Some water soluble heavy metals (such as lead, mercury, chromium, copper, nickel, manganese, and cobalt) can pose a severe threat to humans and other living organisms, because they can cause extended destruction to numerous biological systems [5]. For instance, serious damage to the central nervous system (lead, mercury), kidneys (copper, lead, mercury), skin, teeth (nickel, chromium), liver or lungs (nickel, mercury, lead, copper) [5]. Drinking water is one of the major routes of heavy metal exposure to the human body; their concentration in water may be safe (or favourable for dietary needs) at low concentration levels, but might also be harmful or deadly at higher concentration levels

[11]. Therefore, the World Health Organisation (WHO) in collaboration with other regulatory bodies set Guideline values in drinking water (Table 1.1) [12].

Table 1.1: Examples of heavy metals, their toxic effects, sources, and permissible limits

Heavy metals	Biological effects	Sources	Permissible limits (mgL^{-1})
Lead (Pb)	Congenital paralysis, high blood pressure, brain damage, reduced learning abilities, liver and kidney damage, infertility, and cardio toxic.	Mining, pesticides, automobile, burning coal.	0.01
Cadmium (Cd)	Lung cancer, renal dysfunction, and reproduction problems.	Fertilisers,electroplating, nuclear plants, paints, and plastics.	0.03
Mercury (Hg)	Destruction of nervous system, genetic defects, mental retardation, chest pain, and dyspnea.	Oil refining, mining, fertilisers, paints, pulp, and paper.	0.006
Arsenic (As)	Induces chromosomal abnormalities, affects foetuses (carcinogenic), nasal septum, skin changes, and peripheral neuritis.	Pesticides and herbicides for agricultural purposes.	0.01
Chromium (Cr)	Lung cancer, weakened immune system, kidney and liver damage, respiratory problems and skin rash.	Textile and steel industry.	0.05
Copper (Cu)	Anaemia, hypertension, liver and kidney damage, uraemia.	Mining, pesticide production and metal plating.	2.00
Uranium (U)	Disturbs hormone balance, nephrotoxic, neurotoxic, genotoxic and weakened immune system.	Mining.	0.03

Source: [12,13]

Unlike organic contaminants, heavy metal ions cannot be bio-degraded in nature, and too much intake of these toxic metals could even result in death [5]. Therefore, the removal of heavy metals from drinking and wastewater are of fundamental importance to protect the environment and ensure the wellbeing of the populations. Various important procedures have been used in removing heavy metals from drinking and

3

wastewaters; these are chemical precipitation, bio-sorption, ion-exchange, adsorption, membrane filtration, and electrochemical reduction methods [7,14–20]. All these techniques exhibit some level of limitation and currently adsorption is considered the most effective, efficient and cost-benefit method for water purification from heavy metal pollutants [14,15,19,20].

Generally, activated carbon is the most widely used absorbent, but due to its high cost of production, it has resulted in the search for better and low-cost alternatives [5,14,21–23]. Although, scattered research has already been done on numerous alternatives and potentially lower-cost sorbent materials (such as zeolites, biochar, agro-waste, clay minerals and polymers) for heavy metals uptake from contaminated water, more attention has recently shifted to combinations of biopolymers (e.g. chitosan or alginate) and clay minerals (e.g. bentonite, kaolinite) due to their excellent individual metal-binding capacities, availability, environmentally friendly nature and low-cost [14].

1.3. Problem statement and motivation

Heavy metals pollution and poisoning has been documented throughout history. Elevated arsenic concentration in water has affected the health of thousands of people, mostly living in developing countries due to lack of basic sanitation and infrastructures [8]. The contamination of groundwater by As occurs naturally and has been found in about 70 countries globally, but people living in Asian countries are particularly more at risk of higher arsenic exposure (Figure 1.2) [24,25]. The biggest mass As poisoning ever recorded in human history happened in Bangladesh, where about 57 million people were exposed to As concentrations above 0.01 mg L^{-1} [8]. In addition, about 6 million people are at risk of arsenic poisoning in West Bengal, India [8,26].

A recent Pb poisoning occurred in Zamfara State of North-Western Nigeria, this was considered the worst outbreak of heavy metals poisoning in modern history [11,27,28]. During this period, there were 7,000 incidences of lead poisoning, resulting in about 700 deaths, and the source of the widespread poisoning was traced to artisanal gold mining and ore processing in the villages of the Zamfara and Kebbi States of the North-western region [27,29]. The gold bearing deposits in the Zamfara region usually contains extremely high concentrations of Pb, and this explains why the water sources within this

district were highly contaminated with Pb and thus one of the major routes of human exposure [27]. In addition, the artisanal miners often discharged Pb-contaminated effluents carelessly, resulting in the passage of Pb into surface and ground-water sources. Drinking water and the surrounding ecosystem remains contaminated and the people of this area are continuously using the water without any purification (Figure 1.3) [27]. Even though artisanal gold mining has considerable environmental impacts, it also significantly contributes to the economic growth of the people living in the Zamfara region and overall, a real driving force towards the development and diversification of Nigerian Economy. Nigeria used to be a major crude oil-producing nation, but a recent collapse in oil prices slashed Nigeria's revenue by as much as 50%, causing a 20% cut in the nation's capital budget and an additional 25% cut in annual expenditure [30]. To address the dilapidated economic situation, the Nigerian government made a drastic move to diversify of the economy and comart foreign reserves towards the mining of solid minerals such as gold and other precious metals. To achieve this, the Presidential Artisanal Gold Mining Development Initiative "PAGMI" was launched in 2019 by the federal government of Nigeria [29]. PAGMI is a comprehensive artisanal and small-scale gold mining development programme, which will foster the rationalisation and amalgamation of artisanal gold mining activities into Nigeria's legal, economic, and institutional framework [29]. According to PAGMI, the Federal Government of Nigeria could realise an annual average of $150 million in taxes, $25 million in royalties, and $500 million accrual to foreign reserves from the consolidation of artisanal gold mining activities [29]. The optimistic contribution of artisanal gold mining to Nigeria's economy and national development should be considered as one of the major motivations to find a sustained, appropriate, and cost-effective waste management alternative that could meet the given environmental regulatory standards. The lasting economic development cannot be accomplished without considering the environmental impacts of artisanal mining in Nigeria and other developing nations and with the growing public awareness of the environmental issues and more stringent environmental legislation.

Generally, the treatment of the effluents containing heavy metals from the mining processing is challenging because conventional techniques are inadequate for the complete removal of heavy metal ions from wastewater. At the moment, there are no records or published works regarding the removal of Pb (and other heavy metals) from the water of the artisanal gold mines (Zamfara region) or about the treatment of

wastewater before discharging it into surface water sources or a dug pit (Figure 1.3). In South Africa, where the mining sector accounts for the biggest contribution of heavy metal pollution, the current methods used in remediating the metal-contaminated waters are liquid extraction, ion-exchange resin, electrodialysis, chemical precipitation, membrane filtration, and biosorption [31]. However, due to the large quantities of the metal waste generated (metal-bearing sludges which are difficult to dispose of), these traditional techniques are sometimes not effective, are very expensive, and energy, operationally and chemically intensive [31]. Furthermore, the technical and economic efficiencies of these conventional methods are limited in the treatment of dilute metal-contaminated effluents [32]. For these reasons, adsorption processes on an appropriate sorbent are the focus of this study, especially, using natural based materials such as chitosan biopolymers and bentonite clay. If local and cheap materials such as bentonite [33,34], and chitosan (obtained from sea animal wastes from food and fishery industries) are used for composite formation which then can be applied in the treatment of metal-contaminated waters, it will not only bring economic benefits but also decrease the environmental load. Therefore, a main focus of the research is to develop a composite which could be applied as a cleaning/remediation technology in the treatment of metal-contaminated drinking water and wastewater at the industrial scale.
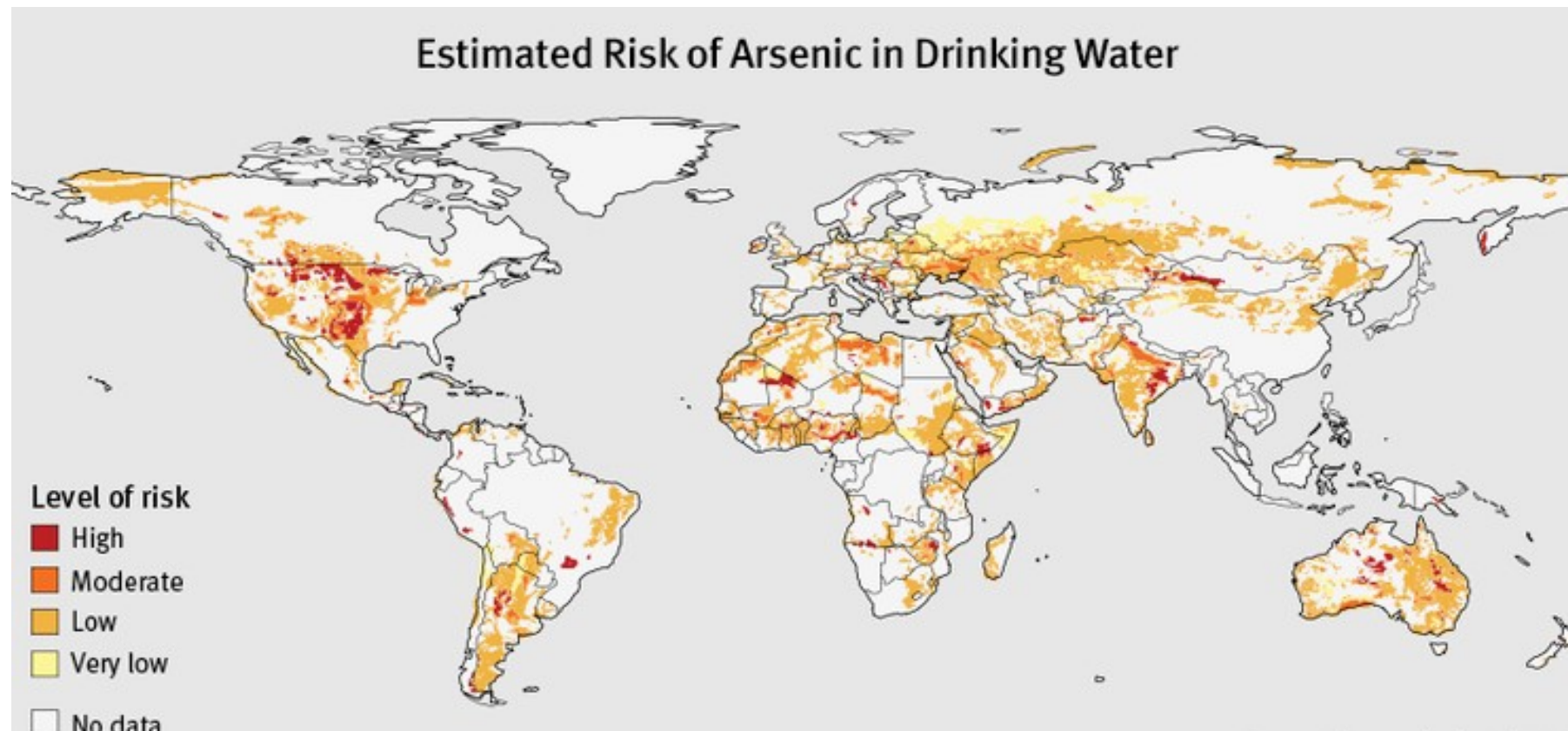
Figure 1.2: World map showing the global risk of arsenic in drinking water. Source: [35]

Figure 1.3: Pictures showing the artisanal gold ore washing and processing in some remote villages of Zamfara, North-western, Nigeria.
Source: (A) punchng.com; (B) myvillaafrica.blogspot.com; (C) globalsentinelng.com.

1.4. Aim and Objectives

The overall aim of this research is to develop a sustainable method, through preparation of clay-polymer composites (I.e., bentonite-chitosan) for effective removal of heavy metals from water.

The main objectives of this study include;

1. To prepare novel functional composites (and beads) from bentonite clay and chitosan biopolymer.

2. To prepare positively charged composites by modifying bentonite clay with chitosan and Fe(III) cation.

3. To characterise synthesised composites using a range of techniques including X-ray diffraction, thermogravimetric analysis and Fourier transform infrared spectroscopy.

4. To study the feasibility of using prepared composites for the removal of heavy metals (Pb, Cu and As) from aqueous metal solutions, through sorption experiments.

1.5. Outline of the thesis

In this thesis, the research work described herein is organised in ten different chapters (with appendices) and each chapter has a varying task as highlighted below.

Chapter 2 is devoted to a comprehensive literature review regarding the remediation of industrial wastewater, and common materials used for water treatment. The chapter also reviews the fundamentals of adsorption processes.

Chapter 3 is dedicated to brief description of analytical instrumentation used in the characterisation of clay-polymer composites and quantitative measurements of analysed metal ions.

Chapter 4 presents the first experimental reports of the research, which involves the successful preparation of functional composites or beads from bentonite clay and chitosan biopolymers. Through this different preparation methods were investigated to assess their effects on efficiency of mixing bentonite clay with chitosan biopolymer.

In Chapter 5, the feasibility of employing the prepared Bt-Ch composites and beads as an adsorbent is demonstrated to abstract Pb(II) ions from aqueous solutions via batch adsorption procedures.

Chapter 6 demonstrated the simultaneous removal of Pb(II) and Cu(II) ions from binary metal solution by Bt-Ch composites and beads.

In Chapter 7 the possibility of using prepared Bt-Ch composites and beads as an adsorbent to remove As(III) ions from aqueous solutions is investigated.

Chapter 8 reports the successful modification of bentonite clay with chitosan and Fe(III) cations for effective removal of As(III) from aqueous solutions.

Chapter 9 is related to column adsorption studies and specifically, the fixed-bed column technique was used to assess the adsorption performance wet-Bt-Ch composites towards Pb (II) ions.

Chapter 2

Literature Review

2.1. Management and remediation of industrial wastewater

Before the middle of the 20th century, elimination or minimisation of waterborne diseases was the primary focus of water pollution control policies [36]. These policies were adapted in all developed nations and mainly focused on the treatment of municipal wastewaters by the application of conventional remediation techniques (primary and/or secondary treatments) [36]. Sadly, until 1960's, the only pollution control approach taken in regard to industrial effluents, was the "dilution and disperse" strategy [36]. The policy-makers did not start making any new pollution control measures, until, only after a catastrophic toxic metal poisoning events took place [36]. The first and well-known heavy metal poisoning incident happened in Japan (in 1956), where a company (producing acetaldehyde) discharged tonnes of mercury into the Minamata bay [36]. This toxic metal entered the food chain and thousands of people whose usual diet comprised of fish and other sea foods developed symptoms of mercury poisoning, which is now called Minamata disease [36]. After this incident, it was then evident that the "dilution and disperse" procedure did not work and therefore, early environmental legislation was recommended in the 1960's, to deal with this kind of specific pollution problem [36]. For instance, strict international environmental policies are available currently, to regulate toxic chemicals such as heavy metal effluents emanated with discharge from various industries [24,36]. Since all heavy metals are potentially toxic and not biodegradable, the European Union environmental legislation recommends that their recovery and reuse are the only ways to prevent them being released into the environment (Table 2.1) [24,36–40]. Hence, under the Industrial Emission Directive (Directive 2010/75/EU) and IPPC Directive (Directive 2008/1/EC), the best advisory practice for heavy metals containing wastewater in the chemical industry includes the following [36,39,41]:

- separate effluents containing heavy metal compounds as far as possible

- treat the separated effluents streams at point of source before mixing with other streams

- make use of the techniques that enable recovery as broadly as possible

- if necessary, facilitate further elimination of heavy metals in a final effluent treatment plant as a polishing step, with subsequent treatment of sludge.

From the above recommendations, the policy encourages clean technologies (such as adsorption and membrane processes) by prioritising the separation and further recovery of heavy metals from wastewaters and therefore, promoting the recycling of certain wastes [36]. Apart from a legislative motive there are merits from purification of wastewater, for instance wastewater is reduced, it minimises environmental impairment by eliminating the discharges of harmful chemicals, there is recovery of valuable compounds and water re-use is promoted, thus reducing freshwater consumption [24].

Table 2.1: Summary of the European Union legislation concerning heavy metals

Substances	(Directive 2008/105/EC)		(Directive 2010/75/EU)	(Directive 2006/11/EC)	(Helcom recommendation 23/11 2002)
	Priority substance	Priority hazardous substance	Polluting substance to water	Dangerous substances to aquatic environment	Water discharge limits (mg/dm^3)
Pb	×		×	×	0.5
As			×	×	--
Cd	×	×	×	×	0.2
Hg	×	×	×	×	0.05
Cr			×	×	0.5; Cr (III) 0.1; Cr (VI)
Ni	×		×	×	1.0
Zn			×	×	2.0
Cu			×	×	0.5
Co			×	×	--

Source: [24,36–40]

Some of the numerous traditional technologies available to reduce heavy metal concentration from wastewater are precipitation, ion-exchange, adsorption, reverse osmosis (or electro-dialysis), cementation and electrocoagulation (Figure 2.1). Below is a brief explanation of some of these traditional methods [36,42].

- Chemical precipitation is a popular remediation technique used as a main method for treating metal-contaminated wastewater, which involves transformation of dissolved contaminant into insoluble solids. For decades, precipitation of toxic metals in industrial wastewaters has been accomplished by adding sodium hydroxide or lime as a coagulants or flocculants to increase the particle size. The process is less effective for low concentrations and chemically intensive, it lacks specificity and involves high cost of waste disposal due to the large volumes of generated sludge.

- Ion-exchange is a known method for recovery of heavy metals, and it is a reversible chemical reaction at which point an ion from wastewater solution is exchanged for a similarly charged ion attached to an immobile solid particle. However, this technique is not efficient in high ionic strength solutions and regeneration of resins are needed.

- Reverse osmosis/electrodialysis is another remediation which involves the use of semi-permeable membranes for removal of metal ions from effluents. Selective membranes such as cation and anion membranes are employed in electrodialysis, which are fitted between the electrodes in electrolytic cells for proper association of electrical current.

- Coagulation via electrolytic process (known as electro-coagulation) is an effective technique in recovery of dissolved metals and other suspended solids It involves an electrochemical procedure to recover metal ions from wastewater. In principle, when metal ions and charged contaminants counteract with ions of opposing charges, they become unsettled and form a stable precipitate.

- Electrowinning is a regular method used in remediation of metal-contaminated wastewater generated from mining, metallurgical and electronics/electrical industries. Most heavy metals in contaminated effluent can be removed by this process via insoluble anodes.

Figure 2.1: Some methods for removal of heavy metals from water

Unfortunately, the activities and discharging of waste products by small-scale industries in developing nations are frequently conducted without proper environmental or safety regulations [24]. Poverty and lack of resources are the main reasons why environmental standards are not implemented, and thus, simpler, recyclable and low-cost purification methods are needed now for remediation of wastewater in developing nations [24].

2.2. Treatment of domestic water in rural areas of developing nations

Unlike in developed countries, there are extremely limited centralised water treatment infrastructures in rural regions of developing nations. A potential solution backed by the World Health Organization (WHO) to overcome poor-quality household drinking water is to treat available water at the point of use (POU) [10,24,43].

Some technologies such as solar disinfection, ceramic filters (including silver-infused), amalgamated coagulant-chlorine disinfection systems, and bio-sand filters have been reviewed and applied for water treatment at POU and these tools have helped and provided a dramatic decrease in water-borne disease related with effective microbiological efficacy [24,44]. The techniques mentioned above are designed mainly

14

to reduce or avert all kinds of water borne illness. So, for water polluted with heavy metals, organic compounds and other toxic chemicals, these methods might not be enough and therefore, a particular treatment procedure is required [24]. For instance, reverse osmosis (RO), ion exchange and adsorption are likely POU tools for eliminating heavy metals and metalloids from drinking water [24].

It was reported in the mid-1990s that AdEdge Technologies Inc. developed an iron-oxide based granular sorbent (Bayoxide® E33) which can be used as an adsorption media for removing arsenic from drinking water in individual households [24]. It has been successfully used in large-scale drinking water applications and reduces up to 99% of total arsenic, including both arsenic (III) and arsenic (V) [24].

Mansoor and Meera [24,45] developed and studied a dual media filter consisting of manganese oxide-coated and iron hydroxide-coated sand for the simultaneous removal of heavy metals and bacteria from water with encouraging results; bacteria and zinc were removed at levels greater than 99% and 96%, respectively.

Sen and Khoo [46] studied zinc adsorption onto both kaolin and natural bentonite and the results obtained demonstrated that both can be used as an excellent natural adsorbent to remove Zn (II) from wastewaters with good efficiency and low cost. In addition, Masindi and Gitari [47] successfully fabricated cryptocrystalline magnesite/bentonite clay composite via a mechanical-chemical process and it was applied for removal of Co(II), Cu(II), Ni(II), Pb(II) and Zn(II) ions from aqueous solution to below permissible limits and therefore, from the experimental data and kinetic studies, they concluded that the synthesised composite could be used for remediation of metal contaminated wastewater.

Many more materials (as inexpensive adsorbents) have been developed, studied and reported in various literature for removal of pollutants (specifically, heavy metals) in water, but it has been concluded from most studies that more research is needed before a workable implementation is achievable [5,9,14,15,17,21,23].

2.3. Materials used as an adsorbent for water purification

There are numerous adsorbents used for water treatment which could either be of natural origin or obtained from industrial production and/or activation process (Figure 2.2). Common natural adsorbents are usually very cheap which includes clay minerals, natural zeolites, oxides, or biopolymers [48]. Adsorbents produced industrially, are often referred to as "engineered adsorbents", which are usually very expensive and can be classified as carbonaceous, polymeric, oxidic, and synthetic zeolite adsorbents [48]. Generally, engineered adsorbents usually display the highest adsorption capacities, because they are produced under strict quality control which show approximately constant properties [48]. Activated carbon (AC) produced from carbonaceous material by chemical activation or gas activation is perhaps the most popular adsorbents used in water treatment on account of its huge surface area (>600 m^2 g^{-1}), high adsorption capacity and excessive porosity [4,14,48]. However, because of its high cost of production, it has limited their use. Polymeric adsorbents are usually made by copolymerisation of nonpolar or weakly polar monomers, which also show higher adsorption capacities like activated carbons, but high material costs and costly regeneration have prevented a broader application till now [48]. The oxidic materials includes solid hydroxides, hydrated oxides, and other oxides, but among the engineered oxidic adsorbents, aluminium and iron materials are the most important and widely used in industrial water treatment [48]. Production of oxidic adsorbents is quite expensive and the process is based on the precipitation of hydroxides followed by a partial dehydration at elevated temperatures, and therefore, the resulting hydroxide products are thermodynamically metastable [48]. Although there are vast deposits of zeolites which occur naturally, often synthetic zeolites are used for practical applications. Synthetic zeolites can be manufactured from aqueous alkaline solutions of silicon and aluminium compounds under hydrothermal conditions [48]. Like oxidic adsorbents, zeolites have strong hydrophilic surface properties and they are suitable for ion exchange processes (e.g., softening) but not for the adsorption of neutral organic substances [48].

In recent decades, there has been an increasing interest in using natural materials (such as clays or biopolymers), wastes and by-products as alternative low-cost adsorbents to replace engineered adsorbents such as activated carbons, polymeric materials, oxidic

and zeolites molecular sieves [4,14,48]. Due to the expensive nature of engineered adsorbents, they are no longer attractive for water treatment in low-economy nations and other small-scale industries, thus, a search for better low-cost alternatives is necessary. Although, cost should be a major criterion for comparing different sorbents, it is rarely reported in the literature. The expense of individual sorbents varies depending on the degree of processing required and local availability [14]. Usually, a sorbent could be presumed as "low cost'' if it requires little processing, is abundant in nature, or is a by-product or waste material from agricultural or industry [14]. Therefore, to sustain an effective system of water purification, naturally abundant and cheaper materials such as clays could be used as an adsorbent.
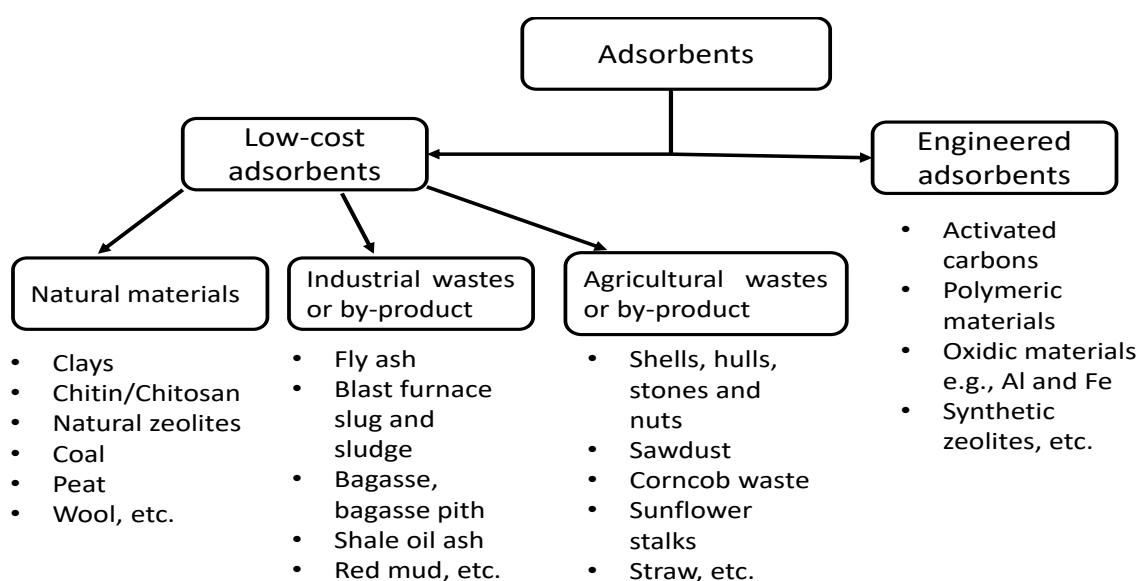
Figure 2.2: Some selected low-cost and Engineered adsorbents

2.3.1. Clay minerals: Structures and physiochemical properties

Clays and clay minerals are cheap and readily available inorganic materials, which have found their application in various fields of science and engineering. They are used as a filler in polymer composites, as catalysts in chemical reactions, as adsorbent in water treatment, hydraulic fluid in oil drilling and as an additive in paper, glass and ceramic making [49,50]. In general, the term "clay" is often used to refer to aluminosilicate minerals that have particle sizes in the micron range in addition to having cation-exchange features [51–53]. Essentially, clays are hydrous aluminosilicates made up of the colloid fraction of soils, sediments rocks and water [49,54]. In terms of structure,

most clay minerals have a distinctive arrangement of their constituent atoms in interlinked planes, which gives rise to the sheet structure within clays, thus, clays are generally referred to as sheet silicates or phyllosilicates [50,55,56]. There are various categories of clays, but the phyllosilicate (sheet silicate) family is the most important and usually used for most applications, they are often termed "clay minerals" [52,53]. Phyllosilicates have been classified into groups, and the smectite group includes bentonite (predominantly montmorillonite; see Figure 2.3), hectorite, saponite, vermiculite and sepiolite, these are very abundant in nature and have been used for metal sorption processes as well as a raw material for composite formation in many applications [49,53,57,58]. The fundamental component of most clay minerals comprises of the tetrahedral sheet of polymerised silica (SiO_4) and the octahedral sheet of alumina [52,53]. The alumina octahedra (like silica tetrahedra) can polymerise in two dimensions by sharing four oxygen atoms to form sheets [52,53].

One of the main phenomena which take place within clay minerals is 'isomorphous substitution', this occurs when cations of different charge (usually lower) replace Al or Si ions in both the octahedral or tetrahedral sheet, respectively which results in a negatively charged structure. The deficiency in positive charge is compensated by sorption of interlayer cations between the layers of the clay which hold the sheets together [50,55,56]. For instance, the isomorphous substitution of Al^{3+} for Si^{4+} in the tetrahedral sheet and Mg^{2+} or Fe^{2+} for Al^{3+} in the octahedral sheets will result in a negative surface charge on the clay [52,55,56]. These negative charges are permanent and usually are not affected by pH changes, which may vary with the nature of the host clay [52,59]. A negative charge can also take place because of dissociation of the hydrogen in numerous hydroxyl groups at broken edges of the clay, which includes SiOH and AlOH groups, to which dissociation readiness increases, as pH increases. In addition, a negative charge on the clays surface can originate due to their low coordination number edge atoms and these charges can be easily neutralised by compensation cations, i.e. Na^+ or Ca^{2+} [52,59].

It is this kind of layer arrangement in clay structures that allows expansion (swelling property) when in contact with water, and this provides an open mineral surface for cation adsorption [52,59]. A good example of swelling clay is type 2:1 clay including bentonite (montmorillonite) which possesses an exceptionally large surface area and

has been subjected to many studies involving clay nanocomposites commonly used in chemical and industrial applications [52]. Depending on the dominant exchangeable cation bentonite clay can be identified as Na-bentonites or Ca-bentonites, both with their unique properties, such as high cation exchange capacity, large chemically active surface area to volume ratio, and interlayer surfaces possessing unusual hydration properties [52,60]. The aforementioned features observed by bentonite allow it to be modified by a range of different surface treatments including acid-alkali treatment [61], reaction with organic molecule [62], and grafting polymer [63].
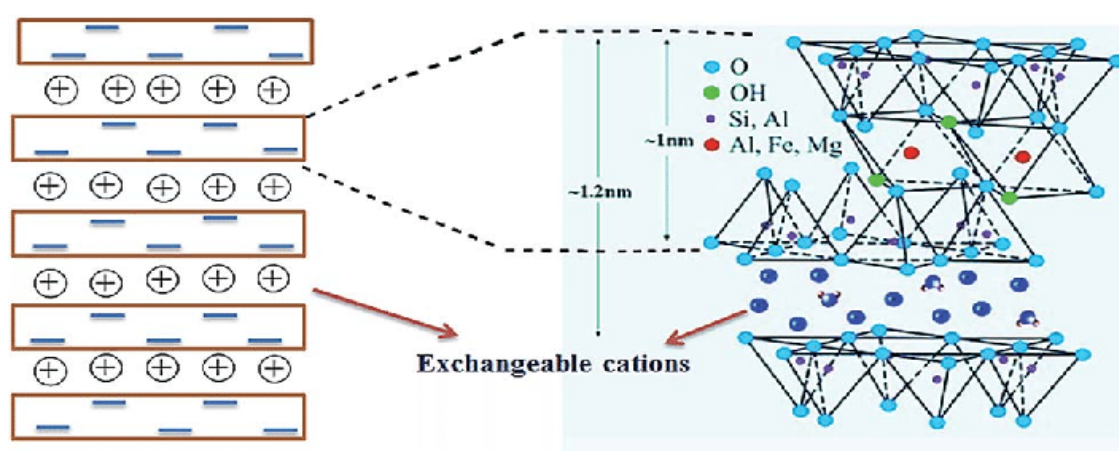
Figure 2.3: A diagrammatic sketch of the structure of Montmorillonite clay. Source: [64]

2.3.1.1 *Clay minerals as a low-cost adsorbent for heavy metals removal*

Large surface area to mass ratios coupled with vast negative exchange sites on their surfaces make clay particles a good adsorbent for metal adsorption [52]. From an environmental perspective, clays can act as a wholesome accumulator of pollutants by taking up charged ions (cations and anions) via ion exchange or adsorption process [49]. Therefore, clays can contain exchangeable charged ions held loosely to their surface, which includes; Ca^{2+}, Mg^{2+}, H^+, K^+, NH_4^+, Na^+, SO_4^{2-}, Cl^-, PO_4^{3-}, and NO_3^- [49,54,58].

Clays and their remodelled forms have received global attention as adsorbents for metal ions removal from water because of their cost-benefit and availability compared to other popular sorbents (activated carbon, zeolites and membranes) [49,54]. For instance, the use of bentonite based material was reported to be effective for removal of Cr (VI) [62,65] and Pb (II) [66] from aqueous solution. In addition, various studies

reported the performance of clay minerals, such as bentonite (montmorillonite), kaolinite, illite and Hydrotalcites, for the removal of heavy metals, which includes Pb, Zn, Ni and As [8,52,60]. The adsorption of heavy metals by clay minerals usually involves a complex mechanism which includes direct bonding between metal cations with the surface of clay minerals, surface complexation, and ion exchange [54].

In many studies, pre-treatment (acid, alkaline or thermal activation) is required to enhance the surface area, pore-volume, and number of acid sites on the surface of clays which will consequently increase their heavy metal adsorption capacity [67]. Bhattacharyya and Gupta [49] studied the adsorption of cobalt (II) using natural and acid activated kaolinite and montmorillonite from aqueous solution. The adsorption experiments were carried out using a batch procedure and investigated different pHs, initial Co (II) concentrations, interaction times, temperatures, and amount of clay. Adsorption of Co (II) on the clays increased continuously from pH 1.0 to 8.0 and reached equilibrium within 240 min. The results showed that the maximum adsorption capacity of the clays was within the range of 11.2 to 29.7 mg/g and Co (II) accumulation was in order as shown; acid-activated montmorillonite > natural montmorillonite > acid activated kaolinite > kaolinite. The kinetic experiments showed that adsorption interactions were best described by a second order model and successfully simulated by Langmuir isotherms. Thermodynamic studies showed that the adsorption of Co (II) on kaolinite and acid-activated kaolinite is endothermic (driven by entropy increase), but that of montmorillonite and acid-activated montmorillonite followed an exothermic process. Other studies concerning the adsorption of heavy metals by clay minerals is summarised in Table 2.2. From some of the extensive reviews, it was reported that due to the difficulty experienced in recovering clay particles from solutions after adsorption processes, neat clay minerals are not very efficient or attractive in removing micro-pollutants from water when compared with zeolites and activated carbon [49,54]. Therefore, an attractive solution to overcome these problems is to combine them with polymers.

Table 2.2: Adsorption capacities of clay minerals for various heavy metal removals from aqueous solutions

Adsorbent	Adsorbate (pollutant)	Adsorption capacity q_{max} (mg/g)	pH & Equil. time	Ref.
Naural Montmorillonite	Ni(II)	166.67	6.0; 3hrs	[68]
	Mn(II)	142.86	6.0; 3hrs	
Organo-modified montmorillonite.	Hg(II)	46.1	4.0; --	[69]
Organo-modified hectorite	Hg(II)	54.7	4.0; --	
Na-Montmorillonite	Cd(II)	5.20	≥ 5.5; --	[70]
	Cr(II)	5.13	≥ 5.5; --	
	Cu(II)	3.04	≥ 5.5; --	
	Mn(II)	3.22	≥ 5.5; --	
	Ni(II)	3.63	≥ 5.5; --	
	Pb(II)	9.58	≥ 5.5; --	
	Zn(II)	3.61	≥ 5.5; --	
Thermally activated bentonite (TAB)	U(VI)	196	9.0; --	[71]
Beidellite	Pb(II)	83.3-86.9	-- ; --	[72]
	Cd(II)	42-45.6	-- ; --	
Kaolinite	Mn(II)	0.446	-- ; --	[67]
	Co(II)	0.919	-- ; --	
	Ni(II)	1.669	-- ; --	
	Cu(II)	10.787	-- ; --	

2.4. Modification of clay minerals: the formation of clay-polymer composites

There are several methods used in the modification of clays to enhance their efficiency, functional (chemical) and mechanical properties. Literature includes, acid/alkali treatment, thermal treatment, and surfactant modifications [52]. However, the most effective methods to alter the surface properties of the clay minerals is surface modification using functional polymers [52].

The blending of inorganic clay minerals with polymers has led to a brand-new classification of materials which are usually referred to as clay-polymer micro- or nano-composites. The synthesis of layered silicate-polymer composites has been researched extensively and for many applications including potential adsorbents for purification of water contaminated with heavy metals. The clay materials may be well dispersed in the polymer component such that intercalation of polymer occurs within the interlayer space of the clay [73]. Among the different clays, bentonite (mainly montmorillonite) is good for composite formation in many applications [49,57,64,74], it is also very abundant in nature and widely used for metal sorption processes as a raw material [49,57,64,74,75].

The use of traditional non-biodegradable, synthetic polymers (produced from fossil fuels) for composite formation is becoming less attractive due to their damaging effect on the health of the ecosystem [76]. There is therefore a need to develop novel polymer composites which are non-toxic and biodegradable such as to allow degradation via natural composting processes [76]. The intercalation of positively charged biopolymers (e.g. chitosan) into layered silicates (e.g. bentonite) has only gained attention in recent decades. These alternative materials are interesting from a sustainability and environmental aspect, but also have potential to offer a cost-benefit.

Chitosan (molecular structure shown in Figure 2.4) is an abundant biopolymer and is derived from alkaline deacetylation of chitin, sourced from crustacean shells obtained from food and fishery industries [9,15]. Its popularity and numerous uses were attributed to its unique chemistry and easy dissolution in some aqueous solutions of mineral and organic acids [77–80]. The presence of free amine and hydroxyl groups (both being susceptible to modification) on the chitosan backbone structure has made it easy for composite formation to produce hybrid products with improved, complementary and synergistic properties [81,82]. Under slightly acidic conditions (at pH 6.0 or below), the amino groups of chitosan (pKa = 6.0 to 6.5) become protonated to form a soluble cationic polyelectrolyte which can easily be adsorbed onto layered silicate materials [77,81]. The driving force behind the clay-chitosan mixture is mainly a cationic exchange process through the positively charged amino groups ($-NH_3^+$) of the chitosan biopolymer and resident exchangeable cations located at the negative sites in the bentonite clay structure [81]. The chitosan biopolymer may also interact with bentonite

clay via hydrogen-bonding at hydroxyl groups located at the broken edges of clay layers. There is also the possibility of hydrogen bonding through water bridges, i.e. water strongly interacting with resident exchangeable cations through the electronegative oxygen group allowing the more electropositive hydrogen of water to form hydrogen bonds with the amine or hydroxyl groups of chitosan. Some of the prepared bentonite-chitosan composites developed through research have been employed to make sensors [83], absorbent materials for water treatments [84], and enzyme immobilization supports [85].
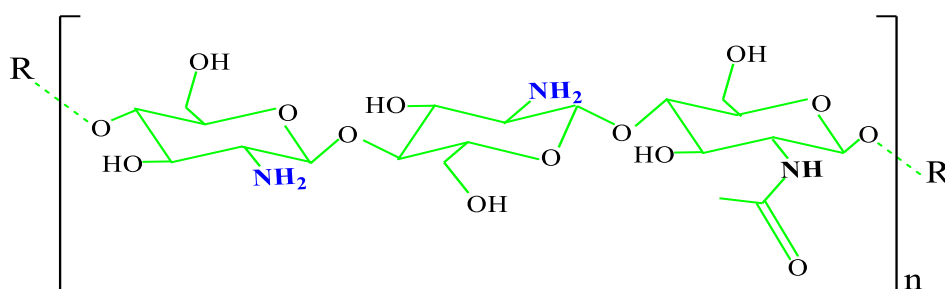
Figure 2.4: Chemical structure of chitosan biopolymer

In most studies, the most popular and usual approach of preparing bentonite-chitosan (Bt-Ch) composite materials is by a solution blending method, which involves mixing of solubilised chitosan (usually in dilute aqueous acetic acid) with bentonite clay suspension followed by centrifugation to remove water and non-adsorbed material [81,83–87]. Generally, the protonated amino functional groups of the chitosan promote strong electrostatic bonds with the clay surface by replacing a significant fraction of the resident exchangeable cations of the clay [85]. From previous studies, it is possible to control the extent of intercalation of the biopolymer such that mono- or a bilayers within the layers of layered silicates (the interlayer space) are formed; low amounts lead to monolayers, whereas bi-layers are formed with higher amounts [81,85].

Information about the quantity of biopolymer intercalated into clay layers is paramount because it has a great influence on the functional properties of the resulting materials [81,85]. For instance, in the formation of clay-chitosan composite, the ionic exchange behaviour of the composite material can be switched from a cationic to an anionic exchange capacity when the amount of adsorbed chitosan exceeds the cationic exchange capacity (CEC) of the pristine clay and the polymer is displayed as a bilayer

[81,85]. From previous studies, the usual way to characterise clay-polymer (specifically, bentonite-chitosan) composite materials is by using analytical techniques such as X-ray Diffraction (XRD), Fourier-transform infrared spectroscopy (FTIR), scanning electron microscope (SEM) and thermogravimetric analysis (TGA) [81,84,85,88]. In sum, modifying clays with chitosan has been reported to show improved properties (pore size, mechanical strength, hydrophilicity and chemical stability) in comparison with raw chitosan and neat clays [84].

2.4.1. Clay-polymer composite as a cheap and effective heavy metal removal

To overcome the disadvantages of both individual polymeric materials and neat clay adsorbents, clay–polymer composites are being developed and have gained increasing attention in the recent past [73]. From a comprehensive review, an initial comparative study about the interaction of charged and uncharged polysaccharides on homoionic smectites (Ca-montmorillonite) was carried out; it was found that positively charged polymers such as chitosan are adsorbed to the same extent as the most strongly adsorbed, neutral species [81,85].

Some studies have been published on the adsorption capacity of bentonite-chitosan composite to establish inexpensive large-scale adsorbent for the removal of heavy metals from wastewaters or drinking water. Futalan et al. [89], performed batch experiments and investigated the comparative adsorption of Cu (II), Ni (II), and Pb (II) from aqueous solution using chitosan-bentonite composite. Single and binary system adsorption data showed that Cu (II) and Pb (II) were best fits with Freundlich isotherm, while Ni (II) with Langmuir isotherm. In the binary systems, a decrease in adsorption capacities and isothermal constants was observed, indicating preferencial adsorption in the order of Pb (II) > Cu (II) > Ni (II). The kinetic experiments showed that the pseudo-second order model fitted better. Thermodynamic studies showed that the adsorption of these metals onto chitosan-bentonite was exothermic. Adsorption of Pb (II) is spontaneous, whereas Ni (II) is non-spontaneous at 25-55°C, and Cu (II) adsorption is only spontaneous at 25°C. Other studies reported on the adsorption of heavy metals by clay-chitosan composites are summarised in Table 2.3. Poor chemical stability (high solubility) of chitosan in strong acidic solution has restricted the use of chitosan

derivatives (such as clay-chitosan composite) for adsorption of heavy metals [9]. To overcome the poor chemical stability of chitosan or its derivative (e.g. clay-chitosan composite) in strongly acidic media, attempts have been made to carried out a suitable crosslinking of the materials [9,90]. Despite some advantages, crosslinked chitosan composite materials have not been fully used at the industrial scale, because it involves a decrease in the adsorption capacity, as amino groups involved in crosslinking are not available for complex formation of heavy metals [9,90].

Table 2.3: Adsorption capacities of clay-chitosan for various heavy metal removals from aqueous solutions

Adsorbent	Adsorbate (pollutant)	Adsorption capacity q_{max} (mg/g)	pH & Equil. time	Ref.
Chitosan saturated Montmorillonite	Pb(II)	47.45 (C_i = 200 mg/L)	5.0 ; 3hrs	[91]
	Cu(II)	31.85 (C_i = 200 mg/L)	5.0 ; 3hrs	
	Cd(II)	20.68 (C_i = 200 mg/L)	5.0 ; 3hrs	
ECH crosslinked chitosan-clay beads	Ni(II)	32.36(C_i = 100 mg/L)	6.0 - 4.5 ;	[92]
	Cd(II)	72.31(C_i = 100 mg/L)		
Chitosan-Montmorillonite	Co(II)	150 (C_i = 825 mg/L)	-- ; 12hr	[93]
Chitosan-Montmorillonite composite	Se(II)	18.4 / 98% removal	Not pH dependent	[94]
5%Bentonite-chitosan	Cr(VI)	223	5.0 ; > 2hrs	[95]
Crosslinked chitosan-Montmorillonite nanocomposite	As(V)	0.39 (0.4 mg/L) About 97.5% removal	7 ; 1.5hrs	[96]
Chitosan-clay nanocomposite	Cr(VI)	357.14	3 ; --	[97]
Chitosan-coated bentonite beads	indium(III)	17.89	4.0 ; --	[98]
Chitosan-palygorskite composite	Pb(II)	CP1; 201.5	6.0 ; 30 mins	[99]
		C2P; 154.5	6.0 ; 40 mins	
		CP2; 147.1	6.0 ; 40 mins	
Chitosan.-vermiculite biocomposite	Cd(II)	58.48	4	[100]
	Pb(II)	166.67	4	
Chitosan-modified vermiculite	As(III)	72.2	5; 30 mins	[82]

ECH = epichlorohydrin; Ci = initial concentration; CP1 = [Chitosan-palygorskite composite @ 1:1]; C2P = [Chitosan-palygorskite composite @1:2]; CP2 = [Chitosan-palygorskite composite @2:1]

2.5. Adsorption Technology and Processes

2.5.1. Adsorption Phenomena: from ancient discoveries to modern techniques

Even though certain phenomena related to adsorption have been known since classical times, the first quantitative observations were reported by Scheele [101] and Fontana [102] in 1773 and 1777, respectively, for their experimental work on the uptake of gases by charcoal and clays [103]. Experimental observations carried out by Lowitz [104,105] contributed to the modern application of adsorption, where he used charcoal for decolourisation of tartaric acid solutions as a result of organic impurities uptake [103]. In 1814, de Saussure [106,107] discovered the exothermic character of adsorption processes and concluded that all types of gases are taken up by porous substances (e.g. seafoam, cork, charcoal, and asbestos) [103]. Moreover, de Saussure observed that gases which undergo condensation readily, are taken up to the greatest extent by porous substances and he was the first to pay attention to the commonness of adsorption [103]. In the late 19th century other scientists such as Chappuis [108–110], Joulian [111] and Kayser [112,113] made some contributions towards absorption processes [103]. However, the real practical application of adsorption processes is based significantly on the selective uptake of individual components from their mixtures by other substances, which was discovered by Tswett in 1903 [114], and from his work, he took advantage of this phenomenon to separate chlorophyll and other plant pigments through silica materials [103]. The technique proposed by Tswett has been regarded, as "column solid-liquid adsorption chromatography" and this discovery was not only the beginning of a new analytical technique but also the origin of a new field of surface science which comprises of adsorption and catalysis [103].

2.5.2. What is adsorption?

Scientifically, , adsorption is a phase transfer process that is widely used to remove substances from fluid phases (gases or liquids) usually via batch or column procedures [48,115]. Adsorption technique is one of the universal and most economic methods for water purification and has been used for the removal of soluble and insoluble organics, inorganic and biological pollutants [17]. Adsorption is a surface phenomenon were

27

chemical species (e.g. pollutants) are adsorbed onto the uppermost atomic layers of a solid material (Figure 2.5) [16,17,23]. Adsorption mostly occurs by physisorption (i.e. physical forces including van der Waal interactions or hydrogen bonding), but also chemisorption (i.e. covalent or ionic bonding) [17]. The substance to be adsorbed, prior to adsorption on the surface is called the adsorptive substance, and when in an adsorbed state it is called the adsorbate. The material that adsorbs the molecules is the adsorbent [17].
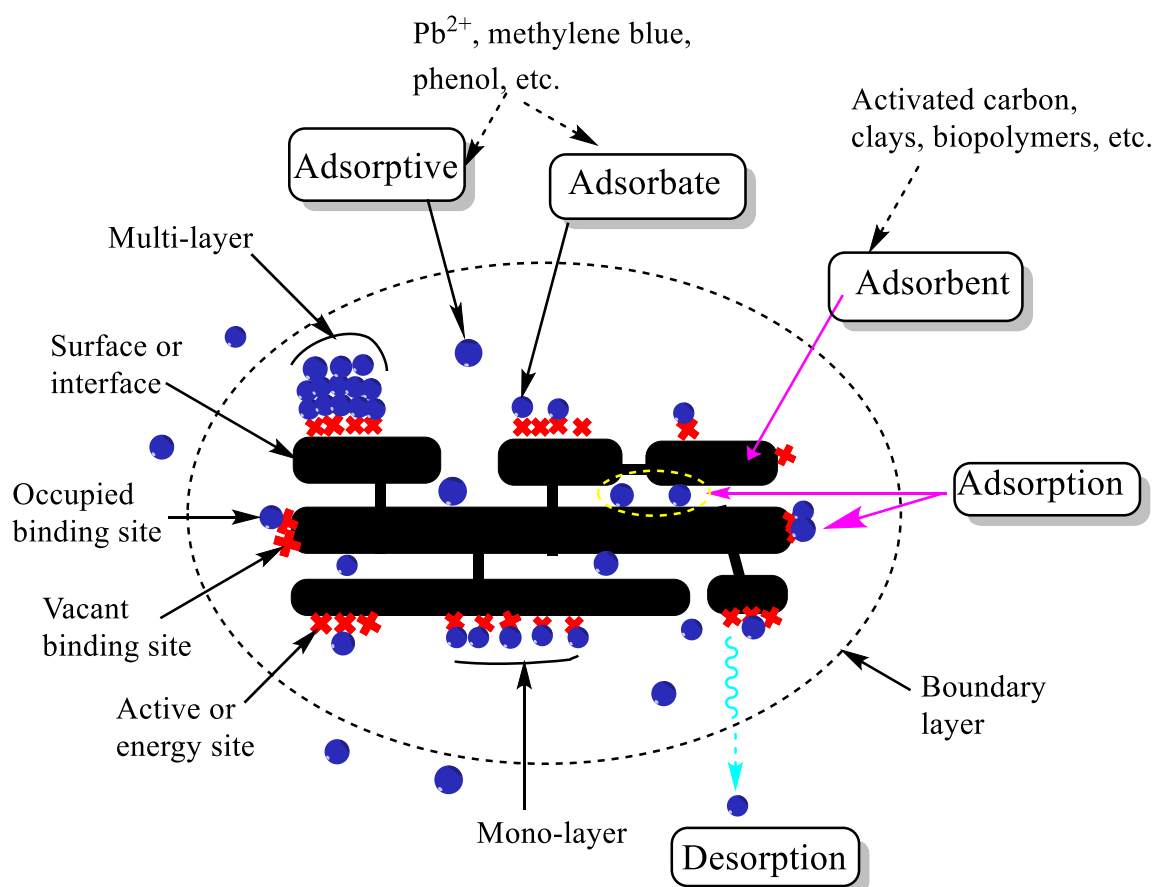
Figure 2.5: Schematic illustration of adsorption and desorption process in solid-liquid system, and some other fundamental concepts utilised in the field of adsorption science and technology.

Adsorption technology is a less expensive technique (compared to other conventional methods) which proffers flexibility in operational design and since it is sometimes reversible, adsorbents can be rejuvenated by appropriate desorption processes, thus, making it highly attractive for water treatment, especially in developing nations [5,15]. Numerous factors determine adsorption processes which includes; temperature, nature and amount of the adsorbate and adsorbent, the presence of other competing adsorbate(s) and experimental conditions (such as pH, contact time and particle size)

[17]. The adsorption performance can be expressed as the amount of adsorbate adsorbed at equilibrium or the percentage of removed adsorbate. The amount of adsorbate adsorbed at equilibrium (q_e; mg/g) is often calculated using the expression shown below in Equation 2.1, which is usually regarded to as a material balance of an adsorption system; this relates that adsorbate is removed through sorption process [116].

$$q_e = \frac{C_0 - C_e}{M} V \qquad (2.1)$$

Where, C_o and C_e are initial and equilibrium liquid-phase concentrations of the adsorbate, respectively, V(L) is the volume of the solutions and M (g) is the mass of the adsorbent used.

In summary, in order to have an in-depth understanding of the adsorption and desorption processes, there needs to be a comprehensive understanding of two basic aspects namely equilibria and kinetics [117,118]. Also, thermodynamic data may provide some information about the final state of an adsorption/desorption system, but kinetics plays the key role which deals with changes in chemical properties in time and is concerned especially with rates of change [117].

2.5.3. Adsorption kinetics and role of initial contact time

Adsorption kinetics is a curve (or line) that describes the rate of retention or release of a solute from an aqueous environment to solid-phase interface at a given adsorbents dose, temperature, flow rate and pH [115]. The time dependence of an adsorption process is very crucial because the information about the rate at which a chemical species (e.g. pollutant) is removed from aqueous solutions in order to design appropriate sorption treatment systems [118]. It is of interest to recognise both adsorption and desorption kinetics (determine their phenomenological coefficients characterising the transport of sorbate within sorbents) since the rate of desorption is important in the design and re-generation of the adsorbent [117]. In addition, the kinetics of adsorption is one of the fundamental studies necessary for better understanding of the controlling mechanism of the sorption [118].

The initial contact time of the adsorption kinetics data play an important role in performing accurate kinetics modelling and inferring valid deductions [116]. Depending on the affinity between the adsorbent and adsorbate, the initial adsorption rate may be extremely fast [116]. For Instance, Tran et al. [116,119] investigated the adsorption of Cd^{2+} ions onto orange-peel-generated biochar, and found that equilibrium can be reached rapidly (80.6 - 96.9% removal within 1 min). A similar result was reported by Guo et al. [116,120], with approximately 70.0 - 96.6% of the total Cd^{2+} ions in solution being removed within the first few minutes of contact. Muller et al. [116] carried out adsorption studies of Zn (II) ions and observed that about 90% were adsorbed onto (Lewatit-S1468) within 1 min, and reached equilibrium at around 5 min. In addition, for the adsorption of organic contaminants, Canzano et al. [116,121] carried out an investigation on the adsorption of anionic Congo-red dye by raw and acid-treated pinecone powder and observed that the entire process reached equilibrium within the first few minutes (< 5 min). Therefore, regarding the above-mentioned fast adsorption processes, it is observed that, with limited data points spanning the early adsorption process, the amount of adsorbate uptake per mass of adsorbent at any time t (qt) is almost or approaches that equilibrium (qe) and, therefore, plotting the kinetic data is bound to produce a straight line, independent of the real kinetic order accorded by the system [116]. In other words, the equilibrium data obtained from very fast adsorption processes cannot describe the way by which the system reaches equilibrium and as a result, the use of data recorded over a significant time interval after the attainment of equilibrium, or very close to equilibrium, is likely to lead to erroneous conclusions regarding the adsorption kinetics [116]. However, the adsorption of inorganic and organic contaminants onto most porous adsorbents (such as activated carbon, biochar, zeolite, and macroreticular resin) is usually slow and can take a longer time (hours, several days or weeks) to approach true equilibrium and therefore, it is necessary to provide a specified timeframe for the adsorption process in order to establish a real kinetics process [116].

In batch adsorption systems, pseudo-first order (PFO) and pseudo-second order (PSO) models are the most frequently used in adsorption studies, followed by Elovich and intra-particle diffusion models [48,116–118]. It should be noted that mere fitting of the kinetic models cannot be the only basis for determination of the adsorption mechanism, but rather, in combination with characterisation by several analytical techniques (such

as FTIR, NMR, XRD, XPS, SEM, Raman spectroscopy, TGA/DTA, DSC etc.) a good sense of the chemical nature of the adsorbate and adsorbent, adsorbent's surface, and chemical or physical interactions between the adsorbent and adsorbate is still required [48,116].

2.5.3.1 *Pseudo-first order (PFO) kinetic model*

The first order rate equation was first introduced by Lagergren [122], in his work on adsorption of oxalic acid and malonic acid onto charcoal [116,123]. Although, the equation is now generally used in the form proposed by Ho and McKay [116,124,125]. The PFO kinetic model for sorption systems is based on the initial solute concentration and most times, the model does not fit well for the full-length of contact time [72,115,124]. Both linear and non-linear forms of the PFO kinetic model are shown in Equations 2.2 and 2.3, respectively, as presented in Table 2.4. The two important parameters calculated from PFO kinetic equations are equilibrium adsorption capacity, q_e (mg/g) and pseudo-first order rate constant, k_1 (min^{-1}), these values (q_e and k_1) are usually determined by applying the commonly accepted linear regression procedure, based on the linearised form of the PFO equation [123].

Even though, the PFO equation is widely applied in adsorption systems, there are problems related to the application of PFO kinetic models, which have been adequately discussed in the literature. The PFO equation is only appropriate for the initial contact time (for example, 20-30 min; and not for the whole range), and the problem due to the two unknown parameters (q_e and k_1) in the equation has made the PFO kinetic model complicated [116,126]. The plots of the linearised form of the PFO equation are only linear over approximately the first 30 min; beyond this initial period, the experimental and theoretical data will not fit [116,127]. The selection of an appropriate q_e value is another major challenge, as the predicted adsorption capacity value at equilibrium time (q_e) should not be lower than the experimentally obtained adsorption capacity (q_t), or else it will create issues involving using the logarithm of a negative number. [116,123,125]. In addition, the calculated q_e value (when using the PFO linearised equation) is not usually equal to the q_e value obtained from experiments, and thus, this further indicates the inability of the PFO linearised equation to fit kinetic adsorption data [116,128]. The large differences observed in both calculated and experimental q_e when

fitting PFO model (especially, the linearised equation) could be due statistical issues, however, McKay et al. [127], in their review argued that the presence of a boundary layer or external resistance controlling the beginning of the sorption process could be responsible for this discrepancy [116].

Therefore, two methods have been recommended in order to curtail the problems associated when applying PFO equation for accurate estimation of the kinetic parameters, these are; (1) a trial and error process to obtain the optimal q_e values as suggested by McKay et al. [126] or (2) application of a nonlinear optimisation technique [116].

2.5.3.2 *Pseudo-second order (PSO) kinetic model*

The second order rate equation was initially proposed in 1984 by Blanchard et al. [129], for their work on the removal of heavy metals from water using natural zeolites [116,125]. It was not very popular until Ho and McKay [124] published their foremost paper in 1999 for their work on the analysis of the pseudo-second order model for sorption processes [125]. This kinetic model is based on the sorption equilibrium capacity which depends on the number of adsorption sites and the number of adsorbate ions in the solid/liquid system [48,124,130]. Like PFO, the PSO kinetic model has been widely used in most adsorption studies and can be expressed in both linear and non-linear forms as illustrated by Equations 2.4 and 2.5, respectively, presented in Table 2.4. The two parameters calculated from PSO equations are equilibrium adsorption capacity, q_e (mg/g) and pseudo-second order rate constant, k_2 (g/mg min). Also, the initial sorption rate constant $k_2 q_e^2$, (mg/g min) sometimes denoted as "h" was proposed by Ho et al. [131] in their work on the adsorption of dyes from waste streams by peat [116]. In most published literature, experimental data for adsorption kinetics are well fitted by the linear form of the PSO equation (K_2) in comparison to the linear form of the PFO (K_1) equation [48,116,125]. This could be due to a statistical advantage of the linear equation of the PSO equation over the linear equation of the PFO model. For instance, in the PSO plots of t/q_t vs. t, the points at equilibrium (q_t) are naturally well aligned because t/q_t approaches t/q_e when q_t is approximately to or very close to q_e and hence, incorporation of many data at equilibrium produces a fitting straight line of slope with a correlation coefficient R^2 close to 1 and a calculated, q_e value close to that of experimental, q_e

[48,125]. Since PSO fits most experimental kinetic data better in most adsorption studies, it is usually reported and concluded that the adsorption mechanism is chemisorption in nature, involving the transfer of electrons between the adsorbate and adsorbent [48]. However, it has been reported that this conclusion is wrong because the adsorption mechanism cannot be solely based on simple fitting of the PSO model [48,116].

2.5.3.3 *Elovich kinetic model*

This kinetic equation was proposed by Roginsky and Zeldovich [132] for their work on the adsorption of carbon monoxide onto manganese dioxide [116]. This equation is now generally known as the Elovich equation and it helps to further understand the chemisorption nature of adsorption [48,116,130]. It assumes that the actual solid adsorbent surfaces are energetically heterogeneous and no interactions occur among the adsorbed species [130]. The linear and non-linear forms of the Elovich model are described by Equations 2.6 and 2.7, respectively, presented in Table 2.4. The two parameters (referred to as Elovich coefficients) calculated from the equation are initial adsorption rate, α (mg/g min) and desorption coefficient, β (g/mg min) [130]. The numerical values of both constants (α and β) are usually obtained by a linear regression procedure and higher values of α indicate higher adsorption rates than desorption, which show viability of adsorption processes [130].

Table 2.4: List of different adsorption kinetics models

Kinetic models	Equations		Plots	Constants	Ref.
PFO					
(A) Linear	$\ln(q_e - q_t) = \ln(q_e) - k_1$	(2.2)	$\ln(q_e - q_t)$ Vs t	k_1 (min^{-1})	[124,125]
(B) Non-linear	$q_t = q_e - e^{-k_1 t}$	(2.3)	q_t Vs t		
PSO					
(A) Linear	$\dfrac{t}{q_t} = \dfrac{1}{k_2 q_e^{\;2}} + \dfrac{t}{q_e}$	(2.4)	t/q_t Vs t	k_2 (g/mg min) $k_2 q_e^{\;2}$ (mg/g min)	[116,125]
(B) Non-linear	$q_t = \dfrac{k_2 q_e^{\;2} t}{1 + k_2 q_e t}$	(2.5)	q_t Vs t		
Elovich					
(A) Linear	$q_t = \dfrac{1}{\beta} \ln(\alpha\beta) + \dfrac{1}{\beta} \ln(t)$	(2.6)	q_t Vs ln(t)	**α** (mg/g min) **β** (g/mg min)	[116,130]
(B) Non-linear	$q_t = \frac{1}{\beta} \ln(1 + \alpha\beta t)$	(2.7)	q_t Vs t		

Note: PFO = Pseudo-first order; PSO = Pseudo-second order; q_e and q_t are the adsorption capacities at equilibrium and time t respectively (mg/g); k_1 is the PFO rate constant (min^{-1}); k_2 is the PSO rate constant (g/mg min); $k_2 qe^2$ is the PSO initial sorption rate constant (mg/g min); α is the Elovich initial sorption rate (mg/g min); β is the Elovich desorption coefficient (g/mg min)

2.5.4. Adsorption equilibrium and Isotherm

The adsorption equilibrium refers to the distribution of a sorbate between the fluid and adsorbed phases [24]. For instance, the equilibrium is established when the amount of the adsorptive material adsorbed (solid phase) and that in the solution (liquid phase) becomes constant [17,24,116]. At equilibrium, the relationship between the quantities of adsorptive materials adsorbed (with respect to the initial amount added) and those in the liquid phase is often called an adsorption isotherm [17]. The knowledge of adsorption equilibrium data and shape of the adsorption isotherm reflects on the adsorption intensity, which also relates the attraction between the adsorptive and adsorbent, and can provide qualitative and quantitative information about the adsorption process [24,48]. Information about the equilibrium (adsorbate/adsorbent interaction) is crucial for designing a large-scale adsorption system, for instance, this will help in selection of an appropriate adsorbent, to design batch, flow-through, or fixed-bed adsorbers [48]. In addition, adsorption isotherms can significantly contribute to understanding and elucidating the adsorption mechanisms [116]. The adsorption equilibrium depends on the strength of the adsorbate/adsorbent interactions and is significantly affected by the properties of the adsorbate and the adsorbent but also by properties of the aqueous solution, such as initial concentration, temperature, pH value, and occurrence and type of competing adsorbates [24,48,116,133–135].

Most of the empirical isotherms for adsorption equilibrium were based on a single-solute system originally developed for gaseous or vapour adsorption, where the equilibrium loading is typically expressed as a function of gas or vapour pressure [48]. In order to use the same isotherm models for the adsorption of solutes in liquid-solid systems, the original models were modified and the equilibrium pressure was replaced with equilibrium concentration [24,48]. Graphically, the adsorption isotherm is given as the equilibrium adsorbed amounts (q_e) versus the equilibrium metal ion concentrations (C_e) at constant temperature as shown in Figure 2.6 [17,48].
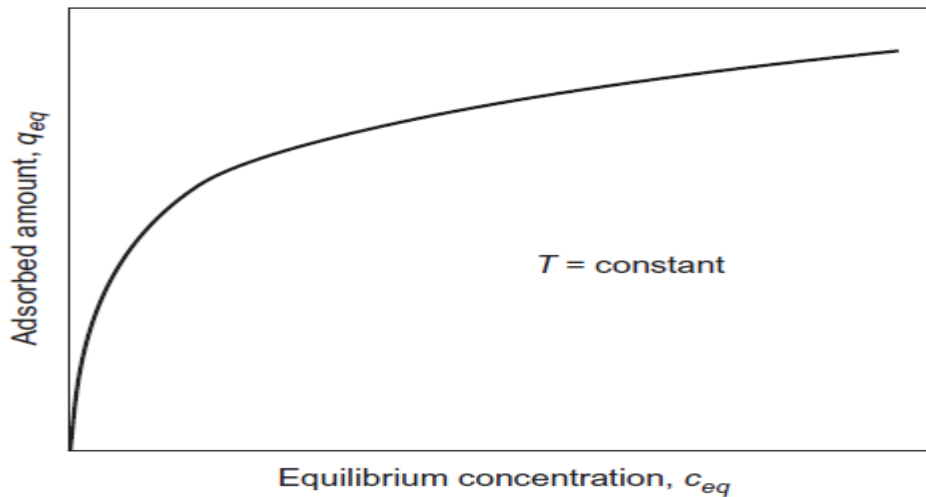
Figure 2.6: Schematic of a typical batch adsorption isotherm showing the variation in the equilibrium amount of adsorbate adsorbed onto the surface of the adsorbents with the change in equilibrium concentration (in a solid-liquid system) at a constant temperature.

As reported over the years, a diverse range of isotherm models have been applied to study adsorption processes which can be classified as follows [48,116,136–138]:

1) One-parameter isotherms, also referred to as irreversible isotherms (Henry Isotherm model).

2) Two-parameter isotherms which include Langmuir, Freundlich, Dubinin-Radushkevich, Temkin, Flory-Huggins and Hill models.

3) Three-parameter isotherms which include Redlich-Peterson, Sips, Toth, Koble-Corrigan, Khan, Fritz-Schluender, Vieth-Sladek, and Radke-Prausnitz models.

4) More than three-parameter isotherms which includes Weber-van Vliet, Fritz-Schlunder, and Baudu models.

Among all the isotherms mentioned above, Langmuir and Freundlich models (followed by Dubinin-Radushkevich model) are the most frequently used in adsorption studies, because of their simplicity, usefulness of their model parameters and ease to interpret [48,116,138]. Therefore, we will limit our discussion to these three adsorption isotherm models, which are all expressed in linear and non-linear forms in Equations 2.8 to 2.13, as presented in Table 2.5.

.

Table 2.5: List of different adsorption Isotherm models

Isotherm models	Equations		Plot	Constants	Ref.
Langmuir (A) Linear	$\dfrac{C_e}{q_e} = (\dfrac{1}{Q_{max}})C_e + \dfrac{1}{Q_{max}k_L}$	(2.8)	C_e/q_e vs C_e	Qmax (mg/g) k_L (L/g)	[116,138]
(B) Non-linear	$q_e = \dfrac{Q_{max}k_L C_e}{1 + k_L C_e}$	(2.9)	$q_e\ versus\ C_e$		
Freundlich (A) Linear	$\log q_e = n\log C_e + \log k_f$	(2.10)	$\log q_e\ vs\ \log C_e$	k_f (L/g) n (unitless)	[116,138]
(B) Non-linear	$q_e = k_f C_e{}^{n}$	(2.11)	$q_e\ vs\ C_e$		
Dubinin-Radushkevich (A) linear	$In q_e = In q_{DR} - k_{DR}\varepsilon^2$	(2.12)	$In q_e\ vs\ \varepsilon^2$	q_{DR} (mg/g) k_{DR}(mol^2/kJ^2)	[116,138]
(B) Non-linear	$q_e = (q_{DR})e^{-k_{DR}\varepsilon^2}$	(2.13)	$q_e\ vs\ \varepsilon^2$		

Note: C_e is the equilibrium concentration (mg/L), q_e is the equilibrium adsorption capacity (mg/g), Qmax (mg/g) is the maximum saturated monolayer adsorption capacity of an adsorbent, K_L is the solute absorptivity (L/mg), K_F is the adsorbent capacity (L/g), n is the heterogeneity factor (unitless-ranging from 0 to 1), q_{RD} is the Dubinin-Radushkevich adsorption capacity (mg/g), K_{RD} is the Dubinin-Radushkevich constant related to the sorption energy (mol^2/kJ^2).

2.5.4.1 *Langmuir isotherm model*

The Langmuir adsorption isotherm [139] is one of the most popular two-parameter isotherm models, which was originally developed to describe gas-solid-phase adsorption onto activated carbon, conventionally used to quantify and compare the adsorption efficiency among different bio-sorbents [116,138,139]. The theoretical Langmuir equation or empirical model in its formulation assumes that adsorption is monolayer and reversible; a fixed number of specific limited sites are available on the adsorbent surface and all the active sites have the same energy; once an adsorbate occupies a site, no further adsorption can occur on that same site; and there is no interaction among the adsorbate species [116,138,140]. Graphically, the Langmuir adsorption model is characterised by a plateau, an equilibrium saturation point where once all molecules occupy all sites, no further adsorption can take place [138,141,142].

Mathematically, the Langmuir isotherm model has been expressed in both linear and non-linear forms, which are illustrated by Equations 2.8 and 2.9, respectively, and presented in Table 2.5. The two key parameters calculated from Langmuir equations are the maximum saturated monolayer adsorption capacity of an adsorbent, Qmax (mg/g) and the solute absorptivity, K_L (L/g). For a good adsorbent, a high theoretical adsorption capacity Qmax and a steep initial sorption isotherm slope (i.e., high K_L) are generally desirable [116].

If the experimental data are adequately described by the Langmuir model, it is essential to calculate the separation factor (a dimensionless constant; R_L) [116,138]. The separation factor (R_L) was originally proposed by Hall et al. [143], and appropriately defined by Webber and Chakkravorti [144] which can be represented as shown below in Equation 2.14 [116,138]:

$$R_L = \frac{1}{1 + K_L C_o} \tag{2.14}$$

where R_L is a constant separation factor (dimensionless) of the solid-liquid adsorption system, K_L is the Langmuir equilibrium constant, and C_o (mg/L) is the initial adsorbate concentration.

Lower R_L value reflects that adsorption is more favourable and by deeper description, R_L value indicates the adsorption nature to be either unfavourable ($R_L > 1$), linear ($R_L = 1$),

favourable (0 < R_L < 1) or irreversible (RL = 0) [138,144]. The R_L value can predict the Langmuir isotherm shape and the relationship between R_L values, nature of adsorption and various isotherm shapes is summarised in Table 2.6 [116,144]. It should be noted that the above mathematical expression of the separation factor can only be employed for isotherms that obey the Langmuir model. R_L values will vary with the initial adsorbate concentration, irrespective of the shape of the isotherm, and R_L values at different initial adsorbate concentrations cannot be calculated directly from the Langmuir isotherm, but can be calculated from the Langmuir equilibrium constant K_L [116,138].

2.5.4.2 *Freundlich isotherm model*

The Freundlich isotherm [145], is one of the earliest empirical equations used to describe equilibrium data and adsorption characteristics for a heterogeneous surface [48,116,138,145]. It can be used in describing the non-ideal, reversible, monolayer and multilayer adsorption process, with non-uniform distribution of adsorption energies over the heterogeneous surface [138]. Contrary to the Langmuir model, the Freundlich isotherm can describe neither the linear range at exceptionally low concentrations nor saturation effect at very high concentrations [48,116]. Currently, Freundlich isotherm is widely applied for analysis of organic compounds or highly interactive species adsorbed onto activated carbon (and molecular sieves) [48,138].

The linear and non-linear forms of Freundlich models are given as Equations 2.10 and 2.11, presented in Table 2.5. The two important parameters calculated from Freundlich equations are the Freundlich constant K_F, $(mg/g)/(mg/L)^n$ and the Freundlich intensity parameter, also called Freundlich exponent n, (dimensionless) which indicates the magnitude of the adsorption driving force or the surface heterogeneity [116]. The Freundlich constant (K_F) characterises the strength of the adsorption and a higher K_F value indicates that higher loading of adsorbate onto adsorbent could be achieved as shown in Figure 2.7(a) [48]. The n value ranges between 0 to 1, which is a measure of adsorption intensity or surface heterogeneity. When the value gets closer to zero it implies that the system becomes more heterogeneous and usually, a value below unity implies a chemisorption process [138]. Also, the n value has an influence on the shape of the isotherm, the lower the n value , the more concaved (with respect to the concentration axis) will be the isotherm shape Figure 2.7(b) [48]. The relationship

between n values and nature of adsorption with various isotherm shapes is summarised in Table 2.6 [48,116].

2.5.4.3 *Dubinin-Radushkevich isotherm model*

The Dubinin-Radushkevich isotherm [146] is one of the two-parameter isotherm models, which was developed to account for the effect of the porous structure of an adsorbent [116,146]. It was developed based on the theory of filling micropores, which was originally used for the adsorption of vapour (gaseous molecules) onto microporous adsorbents [48,146]. In order to make the original Dubinin-Radushkevich isotherm model applicable to liquid-solid systems, the equilibrium and saturation pressure of the vapour in the original isotherm equation are replaced with concentration and saturation concentration of the adsorbate [48]. In practice, it is generally applied to express the adsorption mechanism with a Gaussian energy distribution onto a heterogeneous surface and also, the approach could be used to distinguish the physical and chemical adsorption of metal ions [103,138,147,148]. The Dubinin-Radushkevich isotherm model is expressed in both linear and non-linear models as given by Equations 2.12 and 2.13, respectively, presented in Table 2.5. The Polanyi potential also referred to as the adsorption potential (ϵ) parameter in the Dubinin-Radushkevich equation is usually calculated from Equation 2.15 [48,116,138];

$$\epsilon = RT \, In[1 + \frac{1}{C_e}]$$ (2.15)

where R, T and Ce represent the gas constant (8.314 J/mol K), absolute temperature (K) and adsorbate equilibrium concentration (mg/L), respectively.

The two parameters which could be obtained from the Dubinin-Radushkevich equation are the adsorption capacity, q_{RD} (mg/g), and the Dubinin-Radushkevich constant related to the sorption energy, K_{RD} (mol^2/kJ^2). The mean free energy, E, per molecule of adsorbate which is the energy required to remove a molecule from its location in the sorption space to infinity and can be computed by Equation 2.16 [116];

$$E = [\frac{1}{\sqrt{2k_{DR}}}]$$ (2.16)

Table 2.6: Relationship between isotherm parameters (RL and n), nature of adsorption and Isotherm shapes

Separation Factor (R_L)	Freundlich exponent (n)	Nature of adsorption	Isotherm shapes
$R_L = 0$	$n = 0$	Irreversible	Horizontal
$R_L < 1$	$n < 1$	Favourable	Concave
$R_L = 1$	$n = 1$	Linear	Linear
$R_L > 1$	$n > 1$	Unfavourable	Convex
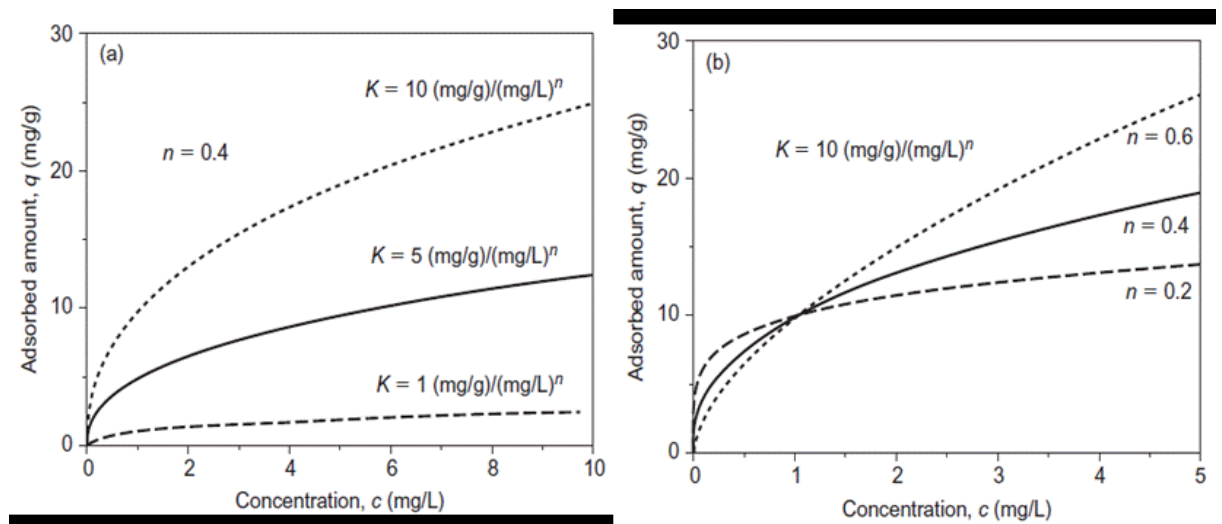
Figure 2.7: Scheme showing the influence of Freundlich parameters on adsorption isotherm.
(a) Freundlich constant (K_f) and (b) Freundlich exponent (n). Source:[48]

2.5.5. Multi-component adsorption

Adsorption has been identified as one of the most effective techniques for the treatment of wastewater containing different pollutants [149]. It is essential to understand the concept of multicomponent adsorption before applying it to the treatment of a liquid system containing multiple or competing pollutants (e.g., wastewater). This is because there are series of interactions among the components present in the wastewater, which are due to high concentrations of these pollutants [149]. Therefore, it is required

to estimate the movement of these pollutants and to investigate the influence of competitive interaction among the pollutants on the overall adsorption process [149]. Experimental equilibrium data are difficult to obtain for multi-component systems, and the practical way of estimating multicomponent adsorption equilibria, is to predict mixture isotherms from isotherm data of the single solutes [150]. However, it was observed that methods based solely on single solute equilibrium data often fail to calculate experimental mixture equilibria accurately [150]. In regard to this, several equations with additional empirical parameters which have to be determined from mixture experiments have been proposed to suit the purpose of multi-component adsorption system [150]. Multicomponent isotherm models are required to know the interaction among the molecules, and various isotherm models like Langmuir, Freundlich, etc., are modified to study multicomponent adsorption systems [149,151–155]. The extended forms of multi-component Langmuir and Freundlich models are shown in Equations 2.17 to 2.20, which are presented in Table 2.7.

Table 2.7: List of some multi-component adsorption Isotherm models

Multi-component Isotherm models	Equations		Ref.
Langmuir (1) Non-Modified competitive equation	$$q_{e,i} = \frac{q_{m,i}\, b_{L,i}\, C_{e,i}}{1 + \sum_{j=1}^{N}(b_{L,j} C_{e,j})}$$	(2.17)	[149,151–153]
(2) Modified competitive equation	$$q_{e,i} = \frac{q_{m,i}\, b_{L,i}\, (C_{e,i}/\eta_{L,i})}{1 + \sum_{j=1}^{N} b_{L,j}\, (C_{e,i}/\eta_{L,i})}$$	(2.18)	
Extended Freundlich (1) One-component equation	$$q_{e,1} = \frac{k_{f,1}\, C_{e,1}^{\; n_1 + x_1}}{C_{e,1}^{\; x_1} + y_1 C_{e,2}^{\; z_1}}$$	(2.19)	[149,151,155]
(2) Two-component equation	$$q_{e,2} = \frac{k_{f,2}\, C_{e,2}^{\; n_2 + x_2}}{C_{e,2}^{\; x_2} + y_2 C_{e,2}^{\; z_2}}$$	(2.20)	

Note: $q_{e,i}$ is equilibrium adsorption capacity for i component (mg/g); $C_{e,i}$ is the equilibrium concentration for i component (mg/L); $b_{L,i}$ is the Langmuir constant for i component (L/mg); $q_{m,i}$ monolayer adsorption capacity for i component (mg/g); N is total number of components in the solution; $\eta_{L,i}$ is the interaction factor for extended and modified Langmuir equation; $q_{e,1}$ and $q_{e,2}$ are the equilibrium adsorption capacities for component 1 and 2 respectively, (mg/g); $C_{e,1}$ and $C_{e,2}$ are the equilibrium concentration of component 1 and 2 respectively, (mg/L). $K_{f,1}$ and $K_{f,1}$ Freundlich constants for mono and binary adsorption system, respectively; n_1 and n_2 are adsorption intensities for mono and binary adsorption system, respectively; The constants x_1, y_1, z_1 and x_2, y_2, z_2 are obtained for a set of experimental values of $q_{e,1}$ vs $C_{e,1}$ and $q_{e,2}$ vs $C_{e,2}$ respectively, (by minimizing the error in non-linear regression analysis);

2.5.6. Column Adsorption design and modelling

The column or continuous adsorption method is usually employed to assess the performance of adsorbent materials for large scale adsorption systems [156]. Although there are different techniques used, fixed-bed adsorption is the most representative and mostly reported in the literature. Slurry columns are usually used for powdered adsorbents, whereas fixed-bed columns are applied for granular adsorbents [48]. Powdered adsorbents generally have the advantage of extremely high adsorption rates (i.e. adsorbate quickly removed) and attain equilibrium within short contact times. However, due to their inherent flow resistance, powdered adsorbents may not be suitable in fixed-bed column systems [48]. Unlike fixed-bed, adsorbent consumption may be higher for slurry columns, and an additional separation step may be needed to remove the loaded powdered adsorbent from the liquid phase [48]. In Fixed-bed column design, the adsorption kinetics, equilibrium, and material balance are needed for overall evaluation of the system. However, in some circumstances, only equilibrium data in combination with the material balance equation are needed to describe the adsorption process in slurry columns [48].

The fixed-bed adsorption system has a similar operational mode to the fixed-bed ion exchanger, i.e. at any time, there are three zones in the adsorption column namely, saturated, adsorption (mass transfer) and non-work zones (Figure 2.8) [156,157]. In principle, as time increases, the adsorption zone gradually moves downward, and the height of the non-work zone decreases. When the adsorption zone reaches the bottom of the column, the solute in the effluent will breakthrough [158].

The most important concept in fixed-bed adsorption systems is the breakthrough curve, it provides the basic but predominant information for the design of a column adsorption system and without it, one cannot determine a rational scale for practical application [159]. As described in the literature (depicted in Figure 2.9) [156,157]; when the adsorption column is saturated, the effluent concentration is usually quite low, with the increase of operation time, the adsorption zone gradually moves down and when it reaches the bottom, the effluent concentration begins to rise rapidly. When the effluent concentration reaches the desired concentration C_b, a breakthrough will occur (break

point). The point at which the effluent concentration reaches about $90 - 95\%$ of the influent concentration C_e is called the adsorption exhaustion point. The height of the adsorption zone (h) is the moving distance of the adsorption zone from break point to exhaustion point.
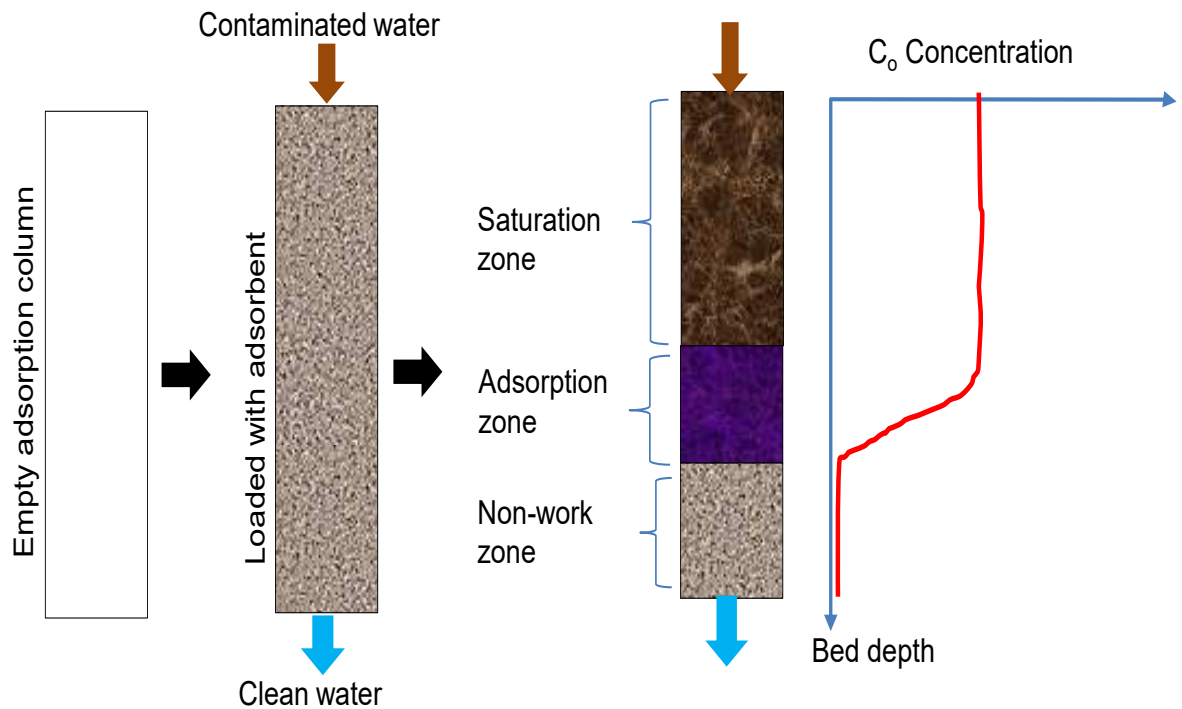
Figure 2.8: Schematic representation of fixed-bed adsorption system

Several mathematical models have been developed and used to model the breakthrough behaviour of an adsorption column (with a high degree of accuracy) for the evaluation of efficiency (and applicability) of potential adsorbents for large-scale operations; these includes Thomas, bed depth service time (BDST), the Adams and Bohart model, Yoon–Nelson, Clark, Wolborska and the modified dose–response model [156]. These models depend on the operational parameters such as initial concentration, volume flow rate, bed height and temperature [156].
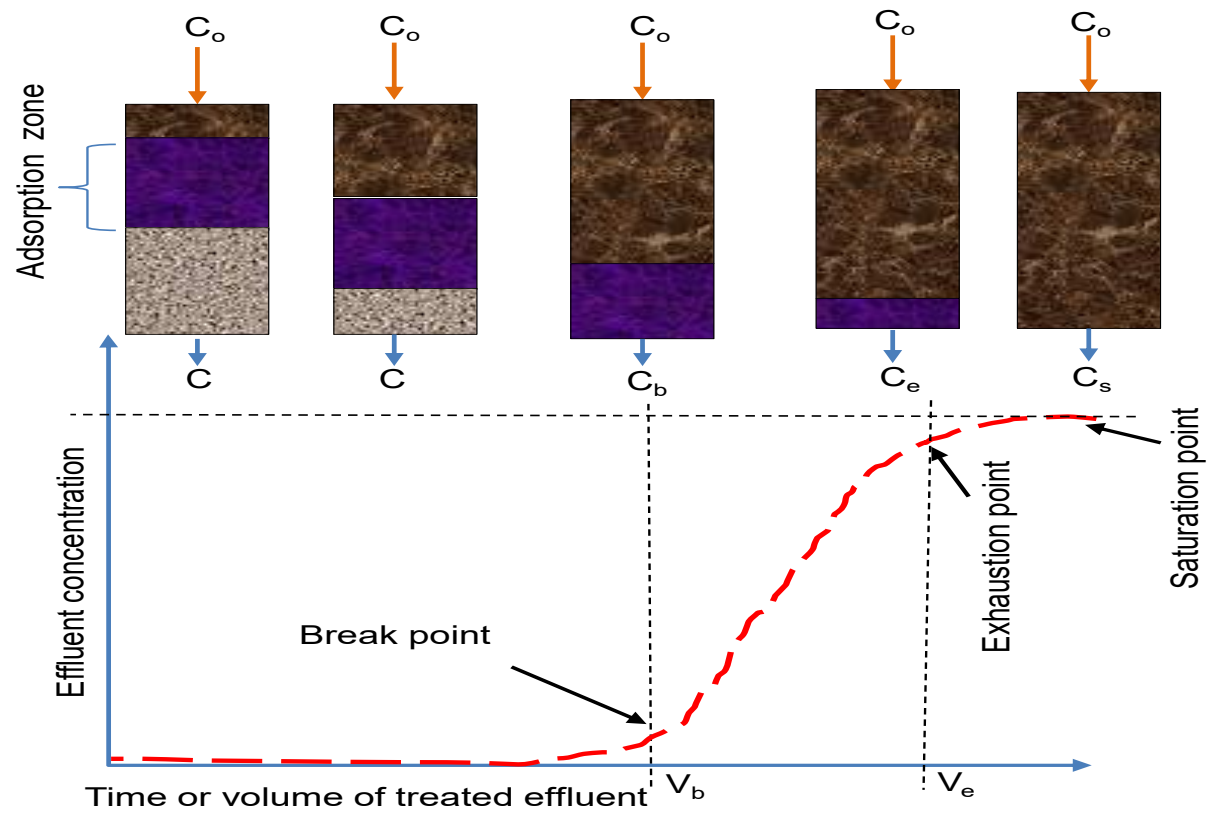
Figure 2.9: Schematic representation of breakthrough curve by movement of adsorption zone

2.5.6.1 *Thomas model*

The Thomas model [160] was developed based on the assumption of Langmuir kinetics of the adsorption-desorption process [156]. It is the most widely used mathematical model in column studies and usually applied to determine the maximum adsorption capacity of an adsorbent [156]. The non-linear form of the Thomas model is given by Equation 2.21, presented in Table 2.8. The two parameters calculated from the Thomas equations are K_{Th} (ml/min/mg) and q_{TH} (mg/g), referred to as the Thomas rate constant and maximum solid-phase concentration of the solute, respectively.

2.5.6.2 *Adams-Bohart model*

The Adams–Bohart model [161] assumes that the adsorption rate is proportional to both the residual capacity of the adsorbent and the concentration of the adsorbing species [156]. It is used to describe the initial part of the breakthrough curve and the non-linear equation form can be expressed as shown in Equation 2.22, presented in the Table 2.8. The main characteristic parameters determined from Adams-Bohart equations are K_{AB} (ml $min^{-1}mg^{-1}$) and N_0 (mg ml^{-1}), which are referred to as the Adams–Bohart rate constant and saturation concentration, respectively.

2.5.6.3 *Bed Depth Service Time (BDST) model*

The bed depth service time model is based on the Bohart-Adams quasi-chemical rate law and assumes that the rate of adsorption is directly proportional to the fraction of adsorption capacity remaining on the media [156]. The BDST model is provided by a relationship between bed depth and service time in terms of concentration and adsorption parameters [156]. The non-linear form of BDST model is given by Equation 2.23 and presented in Table 2.8. The main characteristic parameters determined from BDST equations are K_{BDST} (ml $min^{-1}mg^{-1}$) and N_0 (mg ml^{-1}) which are referred to as the BDST rate constant and saturation concentration, respectively.

2.5.6.4 *Yoon and Nelson model*

The Yoon and Nelson model [162] is a relatively simple mathematical model which is not only less complicated compared to other models but also requires no detailed data concerning the characteristics of adsorbate, the type of adsorbent, and the physical properties of the adsorption bed [156,163]. The non-linear form of Yoon and Nelson equation is given as Equation 2.24 and is presented in Table 2.8. The key parameters (for calculation of theoretical breakthrough curves for a single-component system) obtained from Yoon and Nelson equation are K_{YN} (min^{-1}) and τ (min), which are the rate constant, and the time required for 50% adsorbate breakthrough, respectively.

2.5.6.5 *Dose-Response*

The Dose-Response model is a recent mathematical column adsorption model which was developed to overcome the shortcomings of the older models [164,165]. The previous three column models including Thomas, Adams-Bohart, and Yoon-Nelson models predict a non-zero value of the ratio of effluent concentration (C_f) to influent concentration (C_i) at time (t) = 0, which is not true and may lead to too-low estimation of breakthrough time [164,165]. This limitation was addressed with Dose-Response to model breakthrough curves, which is commonly used in the field of pharmacology and now extends to column adsorption processes [164,165]. The non-linear form of the Dose-Response model is given as Equation 2.25 and is presented in Table 2.8. The parameter determined from Dose-Response model equations are q_{DR} (mg/g) and α (dimensionless) which are referred to as the adsorbate concentration in the solid phase (i.e., column adsorption capacity in mg/g) and Dose-Response constant, respectively.

Table 2.8: List of different column adsorption models

Column Adsorptions models (non-linear)	Equations		Plot	Constants	Ref.
Thomas	$$\frac{C_O}{C_t} = \frac{1}{1 + \exp.\left(\frac{K_{TH}q_{TH}M}{Q} - K_{TH}C_o t\right)}$$	(2.21)	$\frac{C_o}{C_t}$ VS t	K_{TH} q_{TH}	[156,163]
Adams-Bohart	$$\frac{C_t}{C_o} = \exp\left(K_{AB}C_o t - K_{AB}N_o\frac{Z}{\mu}\right)$$	(2.22)	$\frac{C_t}{C_o}$ VS t	K_{AB} N_o	[156,166]
Bed Depth Service Time (BDST)	$$\frac{C_t}{C_o} = \frac{1}{1 + \exp\left[K_{BDST}C_o\left(\frac{N_o}{C_o v}Z - t\right)\right]}$$	(2.23)	$\frac{C_t}{C_o}$ VS t	K_{BDST} N_o	[156]
Yoon and Nelson	$$\frac{C_t}{C_o} = \frac{\exp(K_{YN}t - \tau K_{YN})}{1 + \exp(K_{YN}t - \tau K_{YN})}$$	(2.24)	$\frac{C_t}{C_o}$ VS t	K_{YN} τ	[156,163]
Dose-Response	$$\frac{C_t}{C_o} = \frac{1}{1 + \left(\frac{C_o Q t}{q_{DR}M}\right)^\alpha}$$	(2.25)	$\frac{C_t}{C_o}$ VS t	q_{DR} α	[165]

Note: C_o and C_t are the influent (at t = 0) and effluent (at time t) concentrations, respectively (mg/L), q_{TH} is the is the maximum concentration of the adsorbate in the solid phase in mg/g, K_{Th} is the Thomas rate constant (ml/min/mg), M is the mass of sorbent in the column (g), Q is the volume flow rate (ml/min), K_{AB} is the Adams–Bohart rate constant (ml/ min/ mg), N_0 is the saturation concentration (mg /ml), Z is the column bed height (cm), v is the influent stream linear velocity, K_{BDST} is the BDST rate constant (ml/min/mg), K_{YN} is the Yoon and Nelson rate constant (min⁻¹) and τ the time required for 50% adsorbate breakthrough (min), q_{DR} is the adsorbate concentration in the solid phase (i.e., column adsorption capacity in mg/g), and α *is the constant of the Dose–Response model (dimensionless)*

2.5.7. Linear and nonlinear forms of kinetic and isotherm models

The linear regression analysis of the linear forms of the kinetic and isotherm equations has been frequently employed in sorption studies for accessing the quality of fits and adsorption efficiency [138,167]. This is essentially due to its wide usefulness in a variety of experimental adsorption data and the simplicity of the linearised forms of the kinetic and isotherm equations [138,168,169]. However, Lima et al. [170] confirmed that using linearised equilibrium and kinetic adsorption models could generate errors and make the parameters determined from these models meaningless. Also, it was reported that linearisation isotherms models (for instance, Langmuir and Freundlich isotherm models) have been demonstrated inappropriate in predicting the goodness of fit for a set of conditions and thus unable for providing a fundamental understanding of the adsorption systems, resulting in an improper conclusion [138].

The interest in the utilisation of nonlinear optimisation modelling has gained more attention in recent years [138,171]. The use of nonlinear equilibrium and kinetic adsorption models gives values that are reliable and statistically relevant for modelling the isotherm and kinetics of adsorption [138]. Therefore, many researchers [116,138,170,172–174] have recommended the use of nonlinear methods instead of the linear method, to calculate the parameters of kinetic and isotherm models accurately in both batch and column adsorption experiments.

Although, the coefficient of determination (R^2) has been widely used to identify the best-fit model, others such as Marquardt's percent standard deviation, nonlinear chi-square have lately been used [116,138].

2.6. Adsorption factors and statistical design of experiments

The various parameters, namely, pH, initial concentration, temperature, adsorbent dose, and adsorbent particle diameter, have been proven to influence the adsorption efficiency [175]. The vital features of an adsorption process are extremely complicated and therefore finding the optimum values of operating parameters (conditions) become essential to get the optimum pollutant (e.g. heavy metals) removal efficiency [176].

Thus, process optimisation becomes a vital platform to determine the values of design parameters at which the response reaches its optimum level [175,176].

The traditional way of conducting experimental work is by using one factor at a time strategy, where the effect of each factor is investigated separately. In this way the variable to be studied is varied while the rest of the factors are maintained constant. However, in the case of studying the effect of multiple factors, this approach will involve large number of experiments and, therefore, leading to waste of resources, such as time and chemical reagents. In addition, the effect of one factor might be dependent on the level of other factors, i.e. a factor interaction effect. The use of the one variable at a time approach may often miss important conclusions about the effect of (one) experimental variable when the level of another variable is changed. Further, the process optimisation is inefficient due to the difficulty of finding the true optimum with a reasonable amount of experiments [36,177,178].

Therefore, to overcomes the limitations discussed above, the utilisation of statistical design of experiments is an alternative methodology in conducting experimental work. Unlike "one factor at a time approach", in statistical experimental designs, the values (levels) of the factors are varied in each experiment following a systematic experimental plan. In addition, an empirical model is fitted to the multivariate experimental data, which is used to get a better understanding of the system studied. In comparison to the traditional approach, statistical design of experiments has the advantages of evaluating relatively large number of factors in a smaller number of experiments [36,177–179]. Statistical experimental designs usually involve mathematical or statistical manipulation with some complexity, but nowadays, user-friendly software is available to generate economical tailor-made experimental plans considering any practical and logistical complications. Further, the resulting data are easily analysed, and conclusions are drawn from the analysis.

There are a wide variety of experimental designs that can be used in a study, and the type of experimental design to be used can be selected based on the objective of the study (screening designs or response surface designs).

1) Screening designs are usually used at the inception of a study, and their main objective is to identify which main factors affect the response. So, screening designs allow the screening of relatively large number of factors in a relatively

small number of experiments. Results obtained in the screening experiments can also be used to redesign the range of the factors studied [36,180].

2) Response surface designs are used to evaluate the important factors of a study in more detail. They are often used after identifying the main factors affecting the response of the experiment [36,180]. A better and more visual understanding of the relationship between the responses and factors, are obtained with response surface plots. In addition, response surface designs are used for finding optimum conditions. Finding the optimal conditions can be achieved by maximising or minimising a response or by approximating the response to a targeted value [36,180].

Chapter 3

Analytical Instrumentation

3.1. Instruments used for characterisation of clay-polymer composites

3.1.1. Thermogravimetric Analysis (TGA)

TGA is an instrumental analysis technique repeatedly employed in thermal investigation, which is mainly used to characterise materials by measuring their change in mass with respect to temperature [181,182]. The important properties usually measured by TGA include purity, composition, decomposition temperatures, decomposition reactions, and adsorbed moisture contents [181,182]. Both TGA and Differential-Scanning-Calorimetry (DSC) techniques are frequently used together to provide complementary information that could facilitate the interpretation of thermal experiments [181].

In a defined atmosphere (of TGA), the mass of a sample is measured as it is heated, cooled, or held at a constant temperature. As shown in Figure 3.1 (left), there can be five different steps involved in a regular mass-loss curve of a material (such as polymer) during a thermal analysis. Step-1 is the loss of volatile components (e.g., moisture), step-2 refers to a decomposition stage, step-3 is when the atmosphere is switched from nitrogen to oxygen, step-4 is the combustion/oxidation of carbon and step-5 relates to the inert inorganic residue of ash fillers. The detail description of any TGA instrument is beyond the scope of this thesis, but a schematic diagram of how a system works for thermogravimetry is shown in Figure 3.1 (right).

Regarding the work carried out in this thesis, a computer programmed TGA/DSC-1 instrument (Mettler-Toledo; Star^e System) was used to quantify the amount of chitosan present in the final synthesised Bt-Ch composite or beads (Figure 3.2). All analyses were performed with 5 mg samples in alumina pans under an air purge (40ml/min) between 35 and 1000°C at heating rate 20 ^{o}C / min.
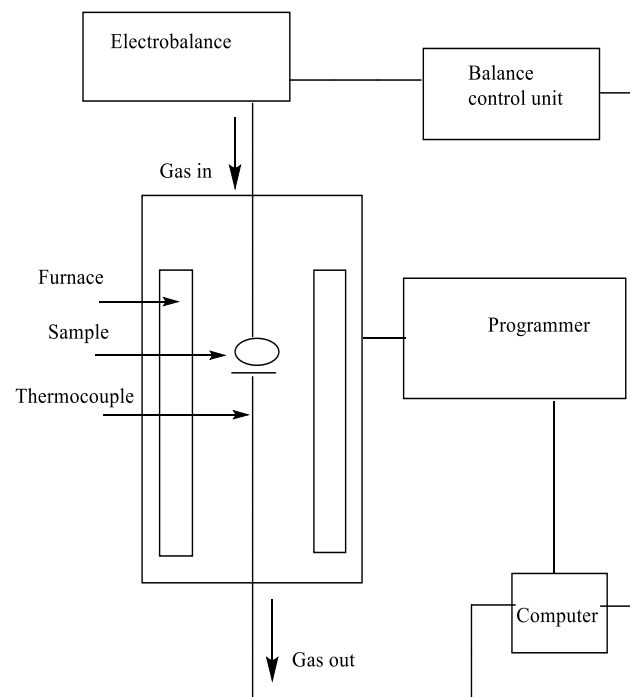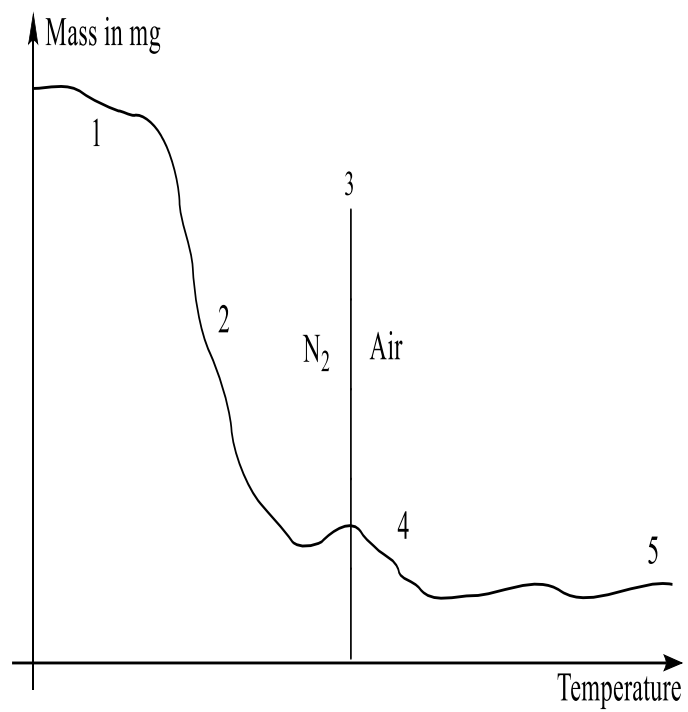
Figure 3.1: Schematic diagram of a typical mass-loss curve of a material (left), and a system for thermogravimetry instruments (right)

Figure 3.2: Laboratory set-up of Mettler-Toledo TGA/DSC-1 instrument (Stare System) for Thermal analysis

3.1.2. X-ray diffraction (XRD)

X-rays are part of the electromagnetic spectrum and are frequently used for structure elucidation by identifying the crystalline phases with the specimen sample through XRD [182]. X-rays are generated in a X-ray tube and usually produced by the sudden deceleration of fast-moving electrons. Generally, when X-rays interact with the specimen sample of interest, they produce a diffraction pattern (i.e., constructive interference) as shown in Figure 3.3. The mathematical relationship that describes the wavelength of the radiation λ, the angle θ between the incident beam of radiation and the parallel planes of atoms causing the diffraction, and the spacing d between these planes is called Bragg's Law (Equation 3.1) [183].

$$2d.\sin\theta = n\lambda \hspace{6cm} 3.1$$

Where d is the distance of separation of the planes, θ is the angle of incidence, n is an integer and λ is the wavelength of the X-ray.
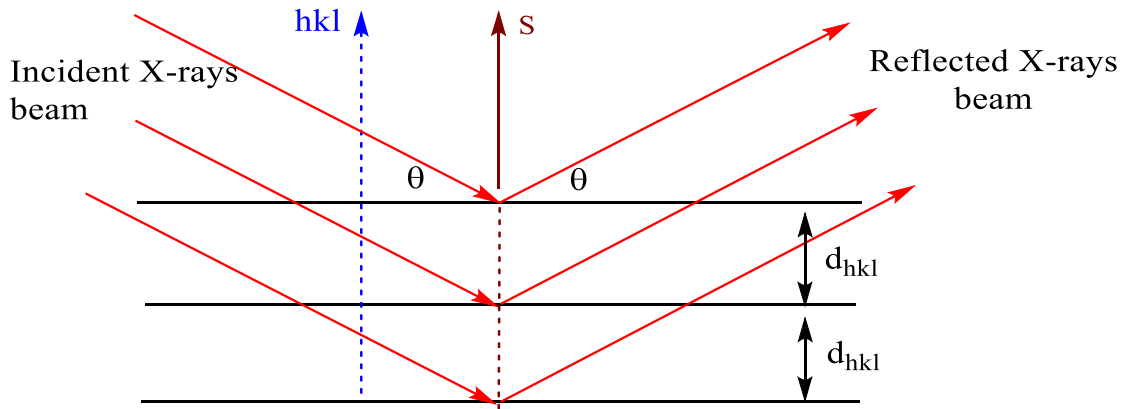
Figure 3.3 Schematic diagram to illustrates simple Bragg's Law model

To keep the X-ray beam properly focused, several powder diffractometers use the Bragg-Brentano geometry as shown in Figure 3.4 (left). Usually, the incident angle (omega) changes in conjunction with another angle (2theta), and this can be accomplished by rotating the sample or by rotating the X-ray tube. Also, the detector could move in a circle around the sample, and the detector position is recorded as the angle 2θ.

In summary, if the values of θ and λ are known, the d value could easily be calculated, which represents the distance between the layers of the clay [183]. Obviously, clay minerals are frequently orientated in such a way that diffraction will take place only from the 001 plane, and the resultant d-value calculated is known as the d-spacing (d_{001} spacing) or interlayer spacing in clay minerals [183]. These values can be used to determine if intercalation has been successful (or not) when a clay mineral (e.g., bentonite) is combined or treated with intercalants such as polymer [183].

For experimental work carried out in this thesis, XRD was used to determine whether the chitosan was located within the interlayer of the bentonite clay. The X-ray diffraction (XRD) analysis of Bentonite-Chitosan composites or beads samples was performed using a computer programmed Philips X'Pert X-ray diffractometer (with pixel detector) as shown in Figure 3.4 (right) with a Cu target ($K_{\alpha}1$, λ = 0.154056 nm) radiation at supplied anode power 40 kV and 40 mA. XRD patterns of the samples were recorded between the diffraction angles 2θ = 2 − 45°.
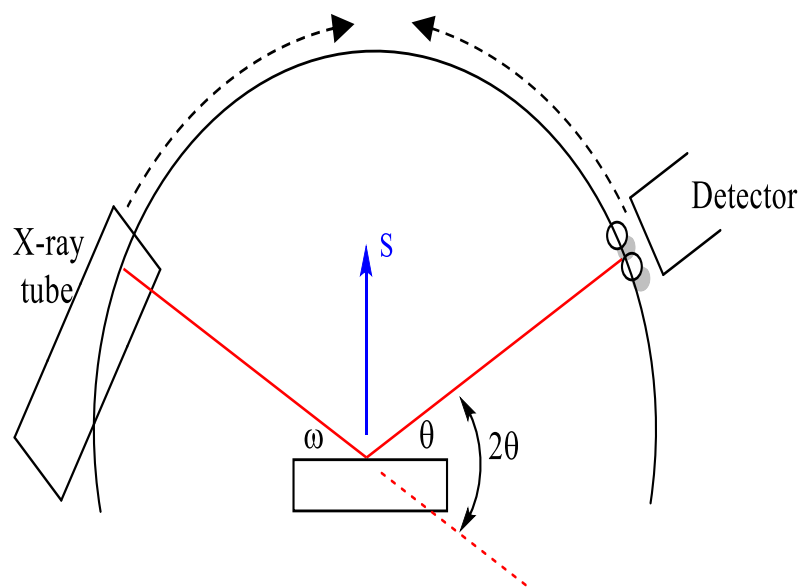
Figure 3.4: Schematics of Bragg-Brentano diffraction geometry (left) and photograph showing the X-ray tube, sample spinner and detector (right)

3.1.3. Fourier Transform Infrared Spectroscopy (FTIR)

Fourier Transform Infrared Spectroscopy (FTIR) is currently the most widely used technique of infrared spectral analysis and it has numerous advantages over the conventional dispersive methodologies [183]. Some of the advantages of FTIR spectrometers include high sensitivity, resolution, and speed of data acquisition (i.e., data for an entire spectrum can be obtained in few seconds). Unlike dispersive instruments, FTIR instruments contain no dispersing element (a prism or grating), and all wavelengths are detected, resolved, and measured simultaneously using a Michelson-interferometer. This can allow all the infrared frequencies of the source to be recorded in the time domain as an interferogram. During the mathematical conversion an apodisation function is used to truncate the interferogram which removes unnecessary data [183,184]. Although the detailed mathematical theory of Fourier-transform measurement (by using Michelson-interferometer) is beyond the scope of this thesis, a simple schematic illustration of how it is configured is shown in Figure 3.5 (left).

In terms of instrumentation, the basic building blocks for most FTIR spectrometers are a source of radiation, collection optics, a means to discriminate between wavelengths and a detector [184]. Usually, the infrared beam is passed from a source through an interferometer, then through the sample, and onto the detector. In this way, an interferogram is recorded, by a single scan, over the full wavenumber range within a few seconds [184]. Technically, to reduce the noise contribution, several scans are recorded, which are summed up and averaged. An FTIR spectrum of the sample is usually generated by ratioing it against a background spectrum, which has been previously recorded under the same conditions as the sample spectrum, but without the sample in place [184].

Concerning the work carried out in this thesis, infrared spectra covering the spectral range 500– 4000 cm^{-1} were measured with a Nicolet FTIR spectrometer (Figure 3.5-right) coupled with ATR (Attenuated total reflection) accessory, which consists of a diamond disc as an internal reflection element. Compared to other FTIR-sampling techniques, ATR enjoys some advantages: (1) it requires only a minimal sample with little

sampling preparation. (2) it is a fast, easy and non-destructive technique, which gives a more efficient and accurate result with a low signal-to-noise ratio [184]. The instrument was equipped with a deuterated triglycine sulphate (DTGS) detector, and the powdered samples of the bentonite-chitosan composites or beads were placed on the ATR crystal, and then the spectrum was recorded. Both background and sample spectra were taken at room temperature, and each spectrum was the average of 64 scans collected at 4 cm^{-1} resolution.
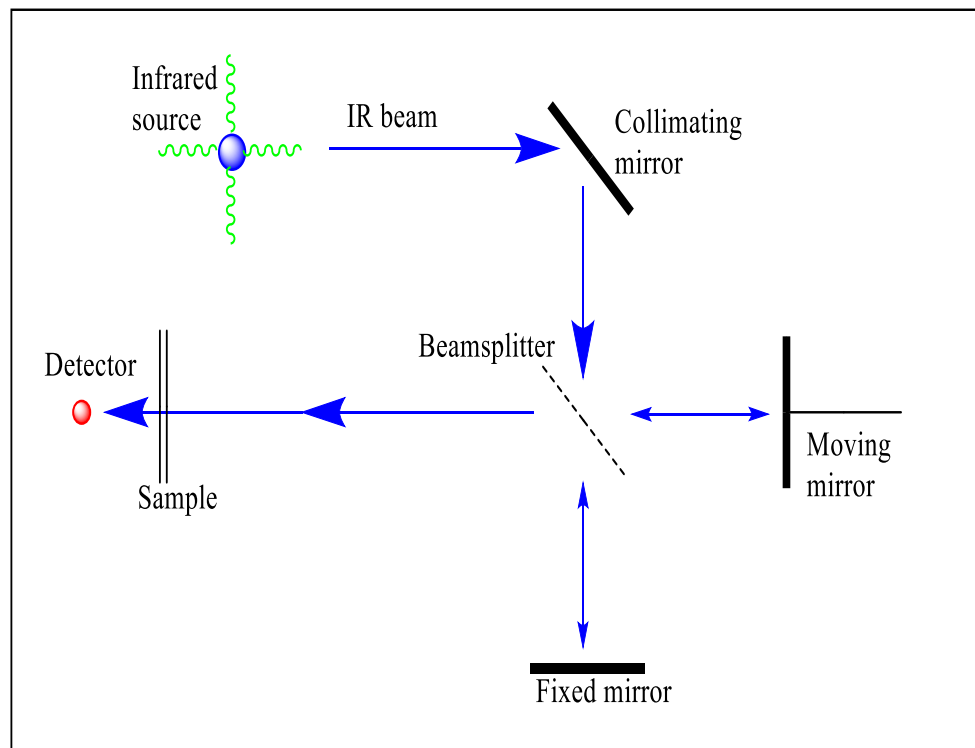
Figure 3.5: (left) the optical diagram of a Michelson interferometer (right) picture showing the laboratory set-up of a Nicolet FTIR Spectrometer Instrument for infrared spectral analysis.

3.2. Instrument used for the quantitative analysis of heavy metals

3.2.1. Inductively coupled plasma – optical emission spectrometry (ICP-OES)

Inductively coupled plasma-optical emission spectrometry (ICP-OES) is one of the popular and most powerful analytical tools for analysis (quantitative and qualitative) of trace elements in various samples, mostly in fluid state [182,185]. This technique is based on the spontaneous emission of photons from atoms and ions which have been excited. Both gaseous and liquid samples may be injected directly into the instrument, while the solid samples requires appropriate sample preparation to make the analytes available in a solution prior to analysis [182,185].

In terms of operation, a typical ICP-OES instruments uses argon gas and an intense electromagnetic field to create superheated plasma at very high temperatures of about 7000 K. Usually, a pump will steadily supply the fluid sample into a nebulizer, which then transforms the liquid into mist, and sends it to the ICP-emission source (plasma) [186]. The high temperature plasma will then heat the sample causing significant excitation and ionisation of sample into atoms and charged ions [182,185]. Once the atoms or ions are in their excited state, they can fall back to lower states to emit light at different wavelengths. The intensity of the light emitted at specific wavelengths is measured and used to determine the concentration of the element(s) of interest [182,185]. One advantage of thermal excitation sources (in ICP-OES analysis) is that it can populate many atoms or ions with different energy levels for several different elements at the same time [186]. Since all the excited atoms and ions can emit respective characteristic radiation at the same time, then this makes ICP-OES more flexible to choose from several different emissions and allows the analysis of multiple elements concurrently [186].

For the adsorption experimental work undertaken in this thesis, the quantitative measurements of Pb(II), Cu(II), Zn(II), Ni(II) and As(III) ions were carried out by ICP-OES (Agilent 5110 model), equipped with a torch having an axial viewing mode coupled with an autosampler (Figure 3.6). The following wavelengths 220. 353, 327.395, 206.200, 231.604, 278.022 nm were selected during ICP-OES analysis of Pb(II), Cu(II), Zn(II), Ni(II)

and As(III), respectively. The instrument operating conditions were; radio frequency (RF) power of 1.2 kW, plasma gas flow rate of 12 L/min, auxiliary gas flow rate of 1.0 L/min, nebulizer flow rate of 0.7 L/min, sample aspiration rate of 2.0 mL/min and stabilisation time of 15 seconds. The measurements were performed in triplicate and the read time was 5 seconds for each replicate. The metal ion concentrations were determined by the optical emission at the respective wavelength of each element of interest. Standard solutions of metal ion concentrations 10, 20, 50, 100, 200, 300, and 500 mg/L were used for the calibration curve of the respective metal ions measurements. The calibration standard solutions were prepared by diluting a standard stock solution of 1000 mg/L in HCl.

Figure 3.6: Inductively Coupled Plasma – Optical Emission Spectrometry (ICP-OES; Agilent 5110 model) equipment used for heavy metals analysis

Chapter 4

Bentonite-Chitosan composites and beads: design, preparation, and characterisation

4.1. Introduction

The synthesis of layered silicate-polymer composites for many applications has been researched extensively, but the intercalation of positively charged biopolymers (such as chitosan) into layered silicates (e.g., bentonite) has only gained attention recently. The combination of bentonite clay and chitosan biopolymer to form composite materials has been reviewed earlier, in Chapter 2, Section 2.4.3. Not much is known about the multiple synthetic procedures used, and the usual way of preparing Bt-Ch composite materials is by a solution blending method [81,83–85,87]. In their previous work, Darder et al. [81], exclusively reported that the initial chitosan-clay ratio employed in their composite preparation did not necessarily reflect the final chitosan biopolymer amount adsorbed on the clay, which is likely to be due to loss of solubilised, unabsorbed chitosan during the washing step of the composite formation. Knowing the amount of the chitosan available (and position with respect to the clays interlayer) in the synthesised composites is critical to providing more understanding about their application, true composition, and form. Although some works have already been conducted regarding the formation of clay-chitosan composites; however, the interaction of Bt-Ch composites has never been investigated by using different synthetic methods. Herein, the amounts of chitosan in the final clay-polymer composites are determined with respect to, starting compositions, location of chitosan within the clay and synthetic preparation procedure.

This chapter describes and investigates the efficiency of mixing bentonite in two different states with two types of chitosan via two different preparation methods. Using two different states of bentonite clay, in powdered form and aqueous suspension, it was hoped to determine whether the state of the bentonite clay during the preparation procedure had any influence on the extent of chitosan intercalation and interaction.

Also, this study contributes to the ongoing debate concerning the understanding of the interaction of clay (bentonite) and biopolymer (chitosan) in the formation of bentonite-chitosan composites or beads. The Bt-Ch composites and beads were developed by focussing on changing the starting composition in the weight ratios of 90%/10%, 70%/30% and 50%/50%. A solution blending method involving washing by centrifugation was used to produce mixtures termed 'composites' and a precipitation method without the need for centrifugation was used to produce mixtures termed 'beads'. TGA was used to quantify the amount of chitosan present in the final composite or beads. XRD was used to determine whether the chitosan was present within the interlayer of the bentonite, and FTIR was used to assess any chemical changes within the chitosan, and any chemical interaction between the chitosan and clay.

4.2. Experimental

4.2.1. Materials

The bentonite, Cloisite® Na$^+$, was obtained from Rockwood Additives (now BYK Limited) and used as the layered silicate starting material. Two different chitosan biopolymers were obtained from Sigma-Aldrich (now Merck). The first chitosan (190, 000 – 310, 000 medium molecular weight) has a degree of deacetylation (DD) within the range of 75 - 85% and was tagged "Chitosan-1". The second chitosan was derived from crab shells stated as highly viscous and with no documented deacetylation degree value or molecular weight and was tagged "Chitosan-2". The highly viscous nature of chitosan-2 indicated a high molecular weight. Acetic acid (≥ 99.99% - metal purity based) and hydrochloric acid (32% w/v; specific gravity = 1.16) were used to prepared aqueous acidic solutions. Sodium hydroxide (reagent grade, 97%, pellets) was used to prepare aqueous basic solutions. Acetic acid and sodium hydroxide were also obtained from Sigma-Aldrich (now Merck). Hydrochloric acid was obtained from Fisher Scientific, UK. All chemicals used, unless otherwise stated, were of analytical grade purity and preparations were made using deionised water.

4.2.2. Preparation of Bentonite-Chitosan (Bt-Ch) composites and beads

The experimental work on this research project began by dissolution testing of both chitosan biopolymers with a chosen acid solution. Dissolution testing with various acid concentration ranges (acetic acid; 1×10^{-3} to 2.0 M and hydrochloric acid; 5×10^{-4} to 1.0 M) showed that both chitosan (0.08 mmol/L) was completely soluble in acetic acid when its concentration is $\geq$ 0.05 M ($\approx$ 0.3% w/v). However, the same amount of both chitosan only becomes soluble in aqueous HCl solutions within a short concentration range of 0.05 - 0.3 M ($\approx$ 0.2 – 0.9% w/v). Outside this concentration range (i.e., below 0.05 and above 0.3 M), chitosan was observed to be insoluble in aqueous HCl solutions. For the work carried out in this chapter, two different preparation methods were investigated; i) solution blending to form composites, and ii) precipitation to form beads-A and beads-B. In each case, the preparation experiments were conducted in triplicate. Acetic and hydrochloric acid were used to solubilised chitosan biopolymer for synthesis of Bt-Ch composites (solution method) and Bt-Ch beads (precipitation method), respectively.

4.2.2.1 *Solution blending method*

The solution method was used to form Bt-Ch composites. First, chitosan solution was prepared by dissolving appropriate mass (see Table 1) of chitosan into a specific volume of 0.5% w/v aqueous acetic acid solution accompanied by vigorous stirring (650 rpm) for 2 hours using a magnetic stirrer. At the same time, bentonite was allowed to undergo a partial swelling in an appropriate volume of deionised water and stirred (650 rpm) for 1 hour (see Table 4.1). Thereafter, the chitosan solution was slowly added to the bentonite suspension and the mixture stirred (650 rpm) for 24 hours at 60 °C. The resulting homogenised mixture was centrifuged at 3000 rpm for 2 hours using a Sorvall RC6 Superspeed Centrifuge. The sediment (wet composite) was separated from the supernatant and as part of a cleaning process approximately 300 ml of deionised water was added to the sediment, shaken (using a rotator mixer) for 2 hours and the mixture centrifuged again as above. This process was further repeated twice. Finally, drying of the sediment was carried out at a temperature of 70 °C overnight using a conventional oven.

4.2.2.2 *Precipitation method*

The precipitation procedure was used to form Bt-Ch beads-A and beads-B. The Bt-Ch beads were prepared using a procedure reported in the literature [187] with modifications. First, chitosan solution was prepared by dissolving an appropriate mass of chitosan (Table 4.1) in aqueous HCl solution (0.25% w/v; 350 ml capacity) and stirring at 650 rpm for 2 h. Then after that, 100 ml of bentonite suspension (for synthesis of beads-A) or appropriate weight of powdered bentonite (for synthesis of beads-B) was slowly added to the chitosan solution and continuously stirred for another 24 hours at 650 rpm. A pH electrode was then placed into the beaker (containing Bt-Ch mixtures) and a burette was suitably positioned to allow addition of NaOH solution (1.0 M). The pH of the mixture was measured and recorded before any addition of NaOH solution. As the stirring of the mixture continued (450 rpm), NaOH solution from the burette was carefully added to the Bt-Ch mixture until its neutralisation (pH 7) and the polymer precipitated from solution. The precipitate (wet Bt-Ch beads) was separated from supernatant using a Fisherbrand test sieve (250 µm) and washed three times with 200 ml of deionised water. It was then dried in an oven for 24 h at 70 °C. Note that during the preparation of 90%Bt-10%Ch beads concerning chitosan-1, no precipitate was formed (at pH 7), and so it was centrifuged to recover the sediments.

4.2.2.3 *Percentage product yield of Bt-Ch composites and beads recovered*

The percentage yield of Bt-Ch composite and beads produced via the solution and precipitation methods were calculated using Equation 4.1:

$$Percentage\ (\%)\ yield = \frac{Actual\ yield}{Theoretical\ yield} \times 100 \qquad (4.1)$$

Actual yield = the amount of product recovered from experiment after drying.

Theoretical yield = the amount of product based on the sum of the starting materials = 5 g

4.2.3. Characterisation of Bt-Ch composites and beads

The synthesised Bt-Ch composites and beads samples were characterised by using TGA, XRD, and FTIR as previously described in Sections 3.1.1, 3.1.2 and 3.1.3, respectively.

Table 4.1: Proportions for synthesis of Bt-Ch-1 (and Bt-Ch-2) composites and beads via solution blending and precipitation method, respectively

Sample composition	Wt. of Bt. (g)	Wt. of Ch. (g)	Vol. of Bt. suspension (ml)	Vol. of Ch. Solution (ml)	Total vol. of the mixture (composites & beads-A)	Total vol. of the mixture (beads-B)
90%Bt-10%Ch	4.5	0.5	100	350	450	350
70%Bt-30%Ch	3.5	1.5	100	350	450	350
50%Bt-50%Ch	2.5	2.5	100	350	450	350

Note: Wt. = weight; Bt. = bentonite; Ch. = chitosan; Vol. = volume
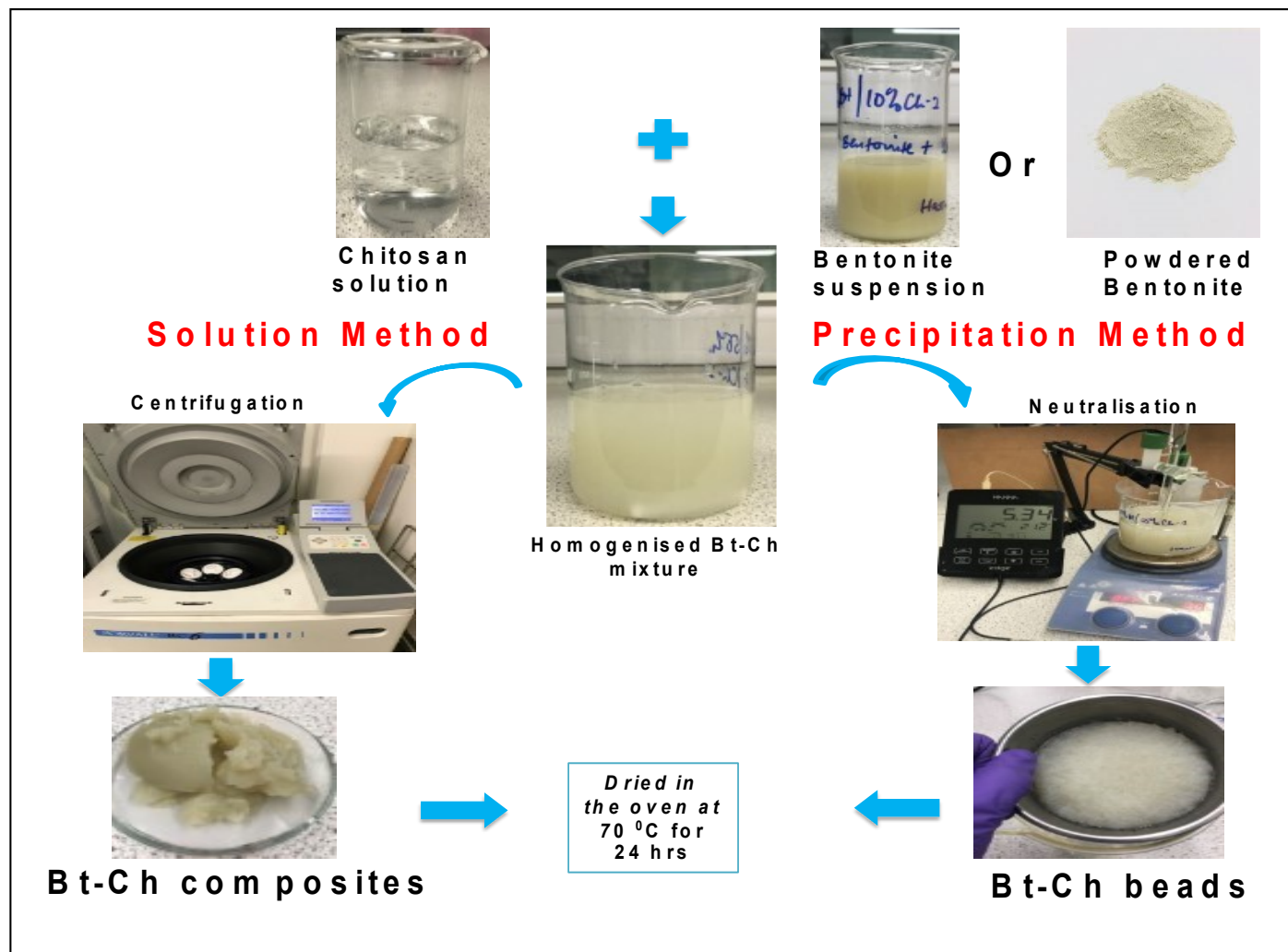
Figure 4.1 : Images and schemes showing the making of Bt-Ch composites and beads

4.3. Results

4.3.1. Synthesis of Bt-Ch composites and beads

Bt-Ch composites and beads were made using solution blending and precipitation methods, respectively. The product yields of Bt-Ch composites, beads-A, and beads-B made from the medium and high molecular weight chitosans are shown in Figure 4.2 (A) and (B), respectively. It is anticipated any observed weight loss in the yield of all 18 samples will be mostly due to the loss of chitosan, though it should be noted that the initial clay mass includes adsorbed water ($\approx$ 8 wt. % as evidenced by TGA), which can be replaced when chitosan is adsorbed.

From the six composites prepared via the solution blending method, the yield was lower compared to the respective beads (both A & B) recovered through the precipitation method. This is mostly due to loss of non-adsorbed and solubilised chitosan during the washing step. From the composites prepared via the solution blending method, the percentage yield recovered increased in order of increasing bentonite content: 90%Bt-10%Ch > 70%Bt-30%Ch > 50%Bt-50%Ch. More weight loss with higher chitosan loading indicates that there is excess chitosan not absorbed on to the clay.

Generally, the yields of the Bt-Ch-1 beads-A or beads-B from the precipitation method were between 85 - 93% and 72 - 88%, respectively. While the yields of the Bt-Ch-2 beads-A and beads-B were between 91 - 93% and 83 - 88%, respectively. There was approximately 5 - 13 % less yield for Bt-Ch-1 beads-B compared to beads-A. Likewise, about 5 - 8 % less yield for Bt-Ch-2 beads-B compared to beads-A. Powdered bentonite (instead of bentonite suspension) was used in the preparation of beads-B, and the wash collected (during the washing stage) was observed to be slightly cloudy. Thus, there is the possibility that some amount of bentonite particles in the mixtures were unable to be trapped by the chitosan as it precipitated during the neutralisation stage and eventually washed away.

For solution blending method, there was approximately 12 - 38 % and 6 - 36 % less yield for Bt-Ch-1 composites compared to Bt-Ch-1 beads-A and beads-B, respectively. Also, there was about 16 - 48 % and 8 - 43 % less yield for Bt-Ch-2 composites compared to

Bt-Ch-2 beads-A and beads-B, respectively. This may be due to the high portion of chitosan been washed away during the centrifugation and washing stage of the solution method.
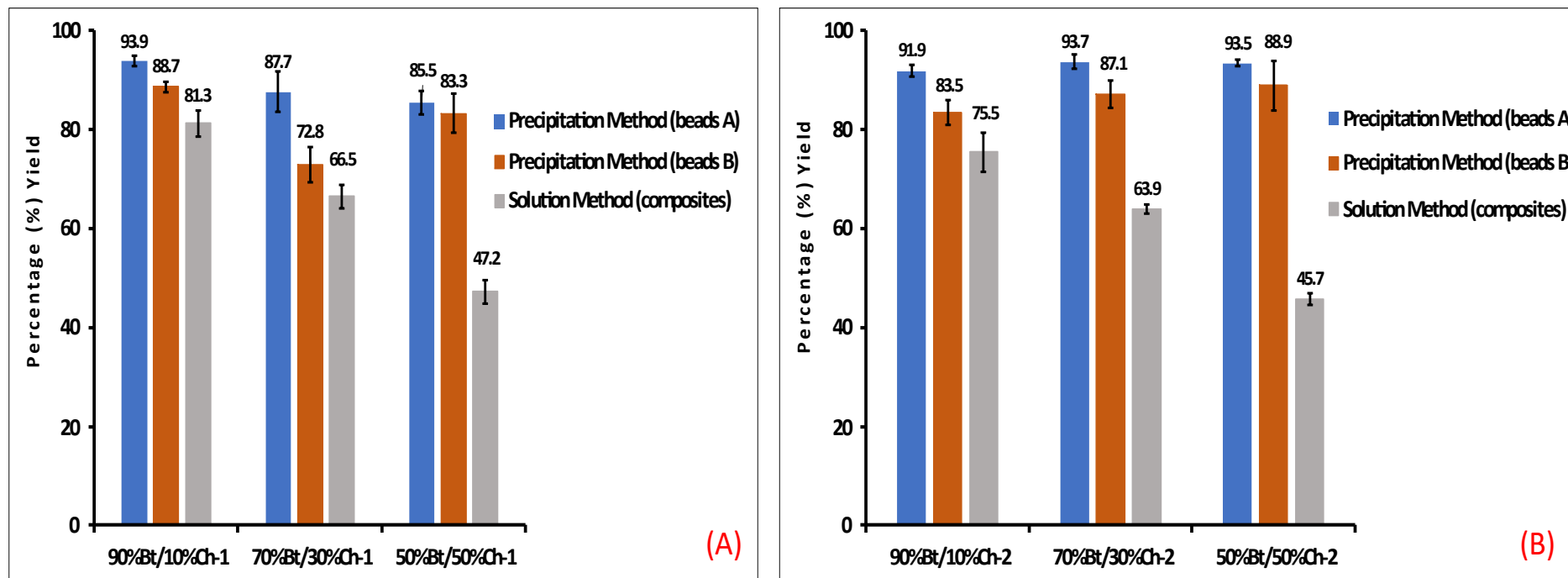
Figure 4.2: Charts showing percentage (%) yield of (A) Bt-Ch-1 and (B) Bt-Ch-2 composite product recovered via precipitation and solution methods

Note: Each bar represents mean ± standard error of three different samples (n = 3). Beads-A = (Bt. suspension + Chitosan solution); beads-B = (powdered Bt. + Chitosan solution).

4.3.2. Thermogravimetric Analysis (TGA)

TGA was used to quantify the amount of chitosan present in the final composition of the prepared Bt-Ch composites or beads. TGA curves (and first derivatives) of bentonite, and representative chitosans (i.e., Ch-1 & Ch-2) and Bt-Ch composites/beads are shown in Figure 4.3. It was observed that bentonite has only two major weight loss occurrences; 90-100 °C, which correspond to the evaporation of physisorbed water, and 600-700 °C, which is caused by de-hydroxylation (loss of structural hydroxyl groups). The TGA curves of chitosan, Bt-Ch beads and composites can be characterised by three stages of weight loss. In the first stage, minor weight loss is observed between 100-120 °C. In the second stage, major weight loss is observed between approximately 200-450 °C and in the third stage a subsequent lower weight loss is observed between approximately 600-700 °C. To estimate the amount of chitosan in each of the Bt-Ch beads and composites, the mass due to de-hydroxylation was subtracted from the total weight lost between 200 – 700 °C. The weight loss due to de-hydroxylation of pure bentonite clay was found to be 4.88 ± 0.07% (n= 3). To reflect the amount of bentonite clay in each composite or bead sample the following values were calculated; 4.39%, 3.42% and 2.44% as the weight loss due to de-hydroxylation, for 90%Bt-10%Ch, 70%Bt-Ch30% and 50%Bt-50%Ch composite and bead samples, respectively. The calculated amounts of chitosan in each Bt-Ch-1 composite/beads sample are shown in Figure 4.4A. For all 90%Bt-10%Ch-1 samples, approximately 10 wt% of chitosan was observed, indicating that almost all the chitosan-1 might have been retained by the bentonite. For 70%Bt-30%Ch-1 samples, about 25 wt% of chitosan was observed for the beads, but only 12 wt% of chitosan for the composites. Possibly, about 5 wt% of chitosan was lost (of the 30 wt% offered) for the beads, but a lot more, approximately 18 wt% for the composites was observed. A low amount of chitosan in composites indicates that a large portion of chitosan has been washed away during the centrifugation and washing stage of the solution method. An observed decrease in the yield for beads-B compared to beads-A, despite similar amounts of chitosan present, may be due to loss of some bentonite particles which were not trapped by the chitosan as it precipitated during the neutralisation stage (as evidenced by % product yield; Figure 4.2A). For 50%Bt-50%Ch-1, a similar trend is

observed, though there is less of a decrease in % product yield. The greater weight loss is attributed to more chitosan present in the beads compared to composites.

The calculated amounts of chitosan in each Bt-Ch-2 composite/beads samples are shown in Figure 4.4B. As can be seen, similar trends are observed for Bt-Ch-2 beads compared to the calculated amount of chitosan obtained for Bt-Ch-1 beads. However, less chitosan was observed for Bt-Ch-2 composites compared with those obtained for Bt-Ch-1 composites. The lower values obtained for Bt-Ch-2 composites is attributed to the high viscous nature of chitosan-2, resulting in poor mixing with clay suspension and a larger portion of chitosan-2 being washed away during the preparation stage.
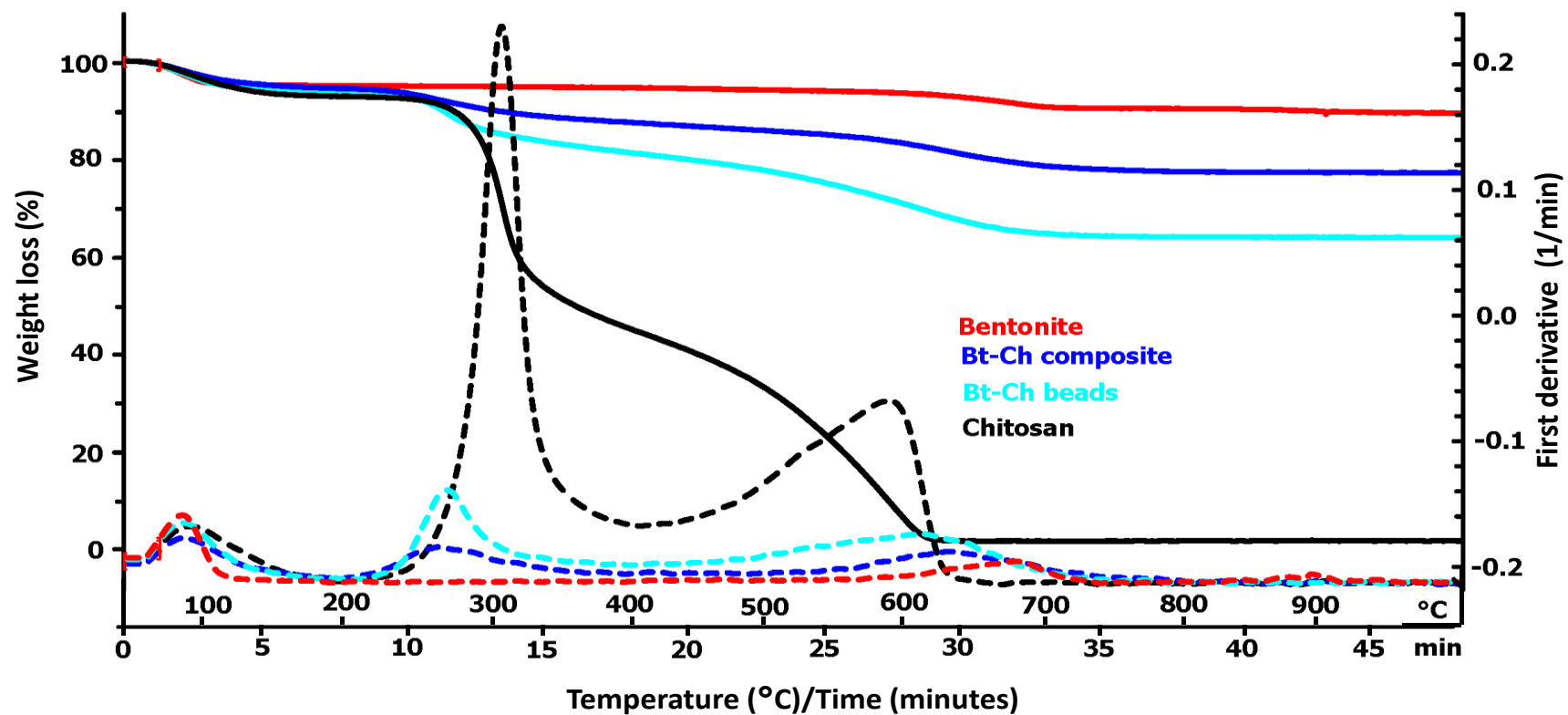
Figure 4.3: TGA curves and first derivatives of bentonite, chitosan-1, and Bt/Ch-1 composites/beads

Note: smooth lines represent weight loss; break line represents first derivatives; similar trends observed for chitosan-2 and Bt-Ch-2 composites/beads
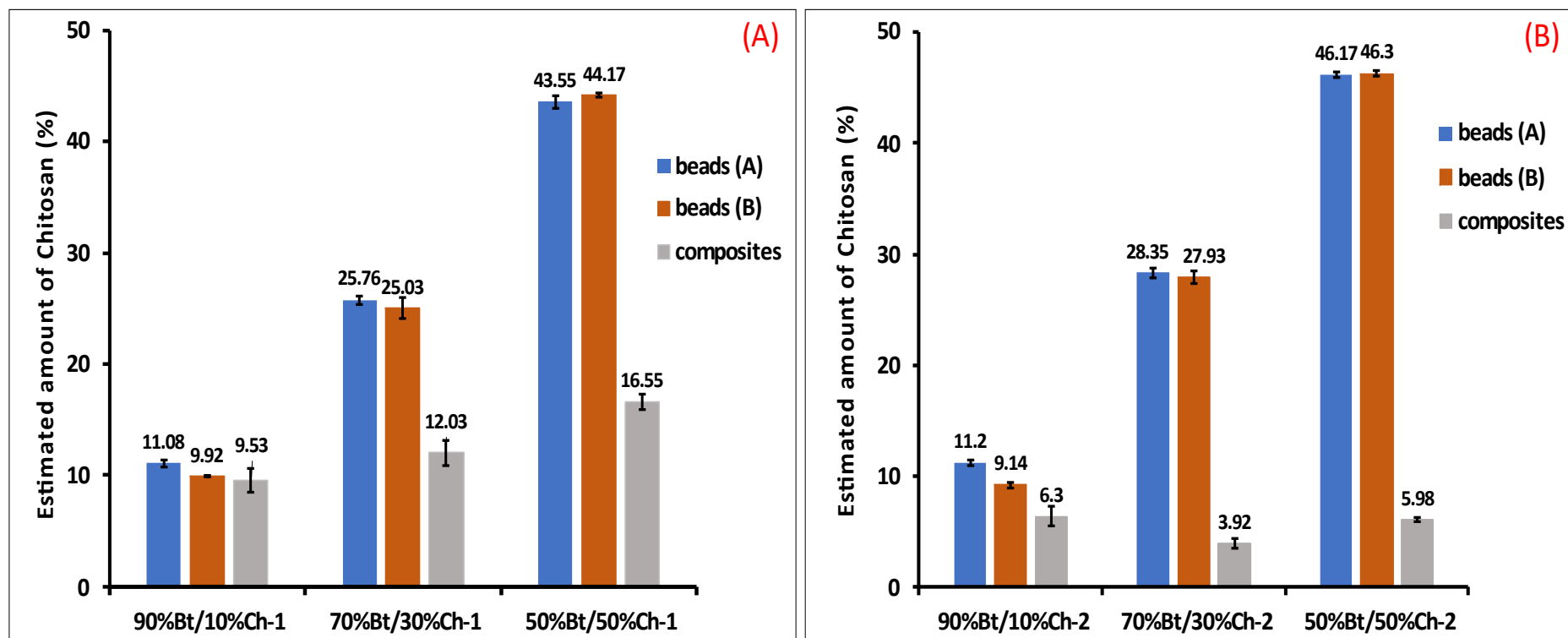
Figure 4.4: Charts showing the estimated amounts of chitosan (%) present in (A) Bt-Ch-1 composites/beads (B) Bt-Ch-2 composites/beads

Each bar represents mean ± standard error of three different samples (n = 3).

4.3.3. XRD Analysis

XRD was used to determine whether the chitosan was located within the interlayer of the bentonite clay. The XRD patterns of prepared Bt-Ch-1 composites and beads are shown in Figure 4.5A. A large significant increase in d-spacing from 1.26 nm to 1.59, 1.72 or 1.75 nm was observed for 90%Bt-10%Ch-1, 70%Bt-30%Ch-1 and 50%Bt-50%Ch-1 composites, respectively. For Bt-Ch-1 beads-A, and like for the composites, the d-spacing reflections show a significant shift towards lower angle (larger d-spacing) with a much larger difference compared to pristine clay, however, there are differences in relative intensity of the reflections and interlayer spacings. This is as anticipated given the higher loadings of chitosan as determined by the TGA analysis (Figure 4.4A). The calculated d-spacings of 1.87, 1.92 and 2.02 nm were observed for 90%Bt-10%Ch-1, 70%Bt-30%Ch-1 and 50%Bt-50%Ch-1 beads-A, respectively. In addition, a shoulder (with less significant shift) to the right of these reflections is still clearly observed for both 90%Bt-10%Ch-1, 70%Bt-30%Ch-1 beads-A; these represent a single layer of chitosan. The relative amount of these single layers decreases with increasing amounts of chitosan, as expected since the additional chitosan will convert single layer into bilayers. The higher d-spacing value obtained with the highest amount of chitosan (50%Bt-50%Ch-1 beads-A) indicates that it is predominantly due to bilayers of chitosan intercalated between the clay layers. This agrees with the similar higher d_{001}-spacing value (2.04 nm) obtained from the previous work carried out by Darder et al. [81,83], which has been related to chitosan bilayers intercalated into clay structures. For the XRD traces collected from all Bt-Ch-1 beads-B samples, the dominant reflections were positioned at 1.26 nm indicating higher single layer loadings, which is the opposite for the observations noted in the composite and beads A samples. There is some evidence of bilayer structures in the Bt-Ch-1 beads-B samples, as evidenced by the shoulders representing d_{001}-spacings of approximately 1.75 nm, but their relative intensities and thus inferred amounts are significantly less. Overall, similar reflection shifts were expected for Bt-Ch-1 beads-B in comparison to Bt-Ch-1 beads-A because similar amounts of chitosan are present (Figure 4B), however this is not the case. The shifts are even smaller than those of the Bt-Ch-1 composites, which have considerably less chitosan present. This data suggests that the preparation process, i.e., the addition of

powdered bentonite rather than as a suspension significantly affects (i.e., lowers) the distribution of chitosan within the interlayer space of the clay (as illustrated in Figure 4.6).

For Bt-Ch-2 composites/beads (Figure 4.5B), the XRD traces collected for Bt-Ch-2 beads-B samples show slight observable intercalation (with shoulders to the left of reflections) just like those obtained for Bt-Ch-1 beads-B. But a significant increase in d-spacing from 1.26 nm to 1.86 nm (with a slight shoulder to right), was observed for 50%Bt-50%Ch-2 beads-A. However, two reflections are observed in the traces of both 90%Bt-10%Ch-2 and 70%Bt-%30Ch-2 beads-A. The first reflection shows no change from that of the pristine bentonite (still at d-spacing of 1.26 nm). The second reflection (d-spacing of 1.86 nm) shows a much larger difference compared to pristine clay and increases in relative intensity with respect to chitosan loading. This likely to be due to bilayers of chitosan intercalated between the clay layers. Regarding the composites prepared from chitosan-2, a slight increase in d-spacing (from 1.26 nm to 1.48 nm) was observed for 90%Bt-10%Ch-2 composites, but no observable intercalations were observed for 70%Bt-30%Ch-2 and 50%Bt-50%Ch-2 composites. Although, a shoulder (with less significant shift) to the left of the reflections is slightly observed for both 70%Bt-30%Ch-2 composites, which might represent a single layer of chitosan. Overall, the lower in reflection-shift towards lower angle (smaller d-spacing) for Bt-Ch-2 composites/beads (compared to Bt-Ch-1 composites/beads) may be attributed to the high molecular weight of chitosan-2. The highly viscous nature of chitosan-2 resulted a poor mixing during preparation stage and may indicate more disordered within the clay layers.
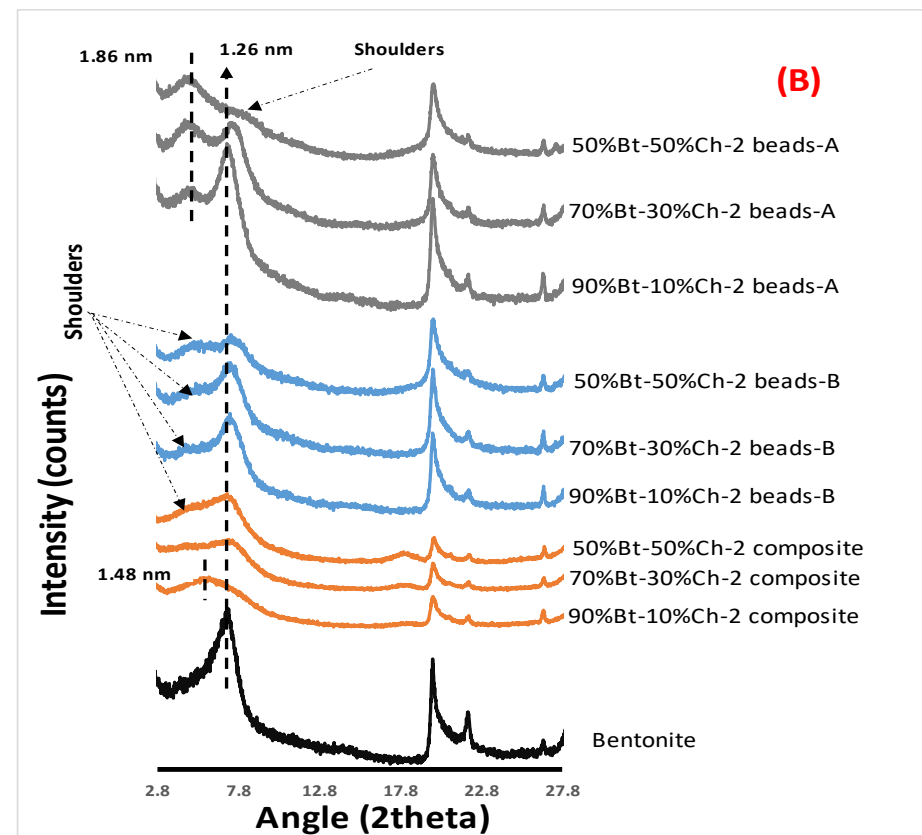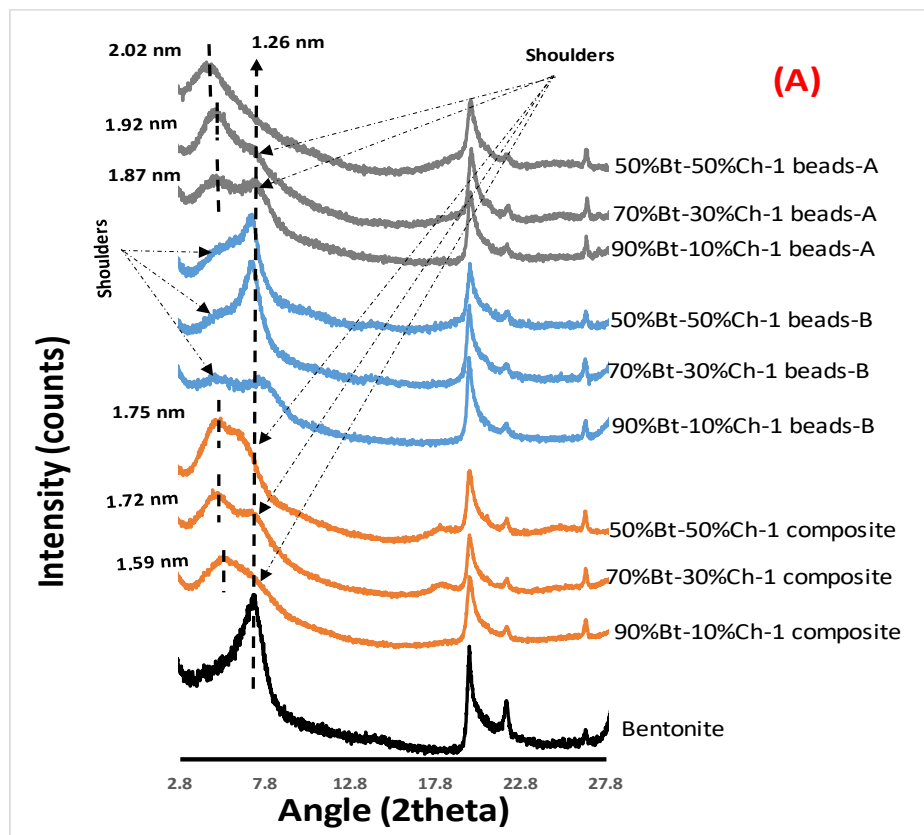
Figure 4.5: XRD patterns of (A) bentonite, Bt-Ch-1 composites/beads and (B) bentonite, Bt-Ch-2 composites/beads
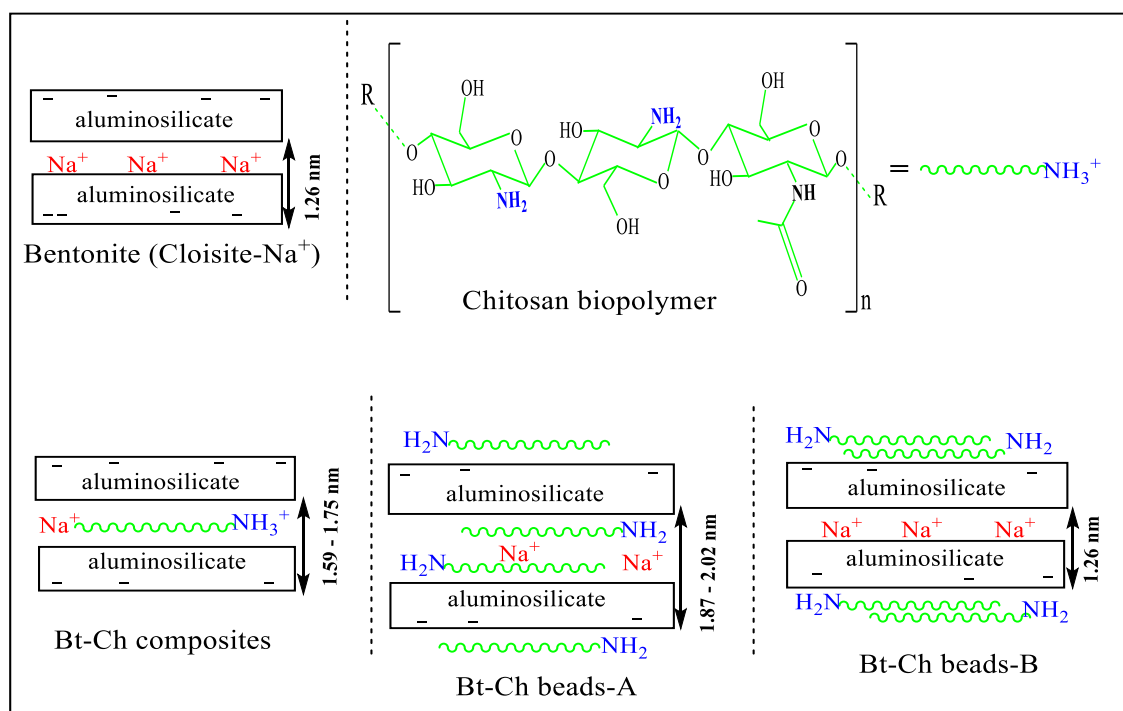
Figure 4.6: Scheme illustrating how chitosan interacted (or intercalated) with bentonite clay

4.3.4. FTIR Analysis

Figure 4.7 shows the FTIR spectra of bentonite, Bt-Ch-1 beads-A, and chitosan. The bands assignments are shown in Table 4.2. FTIR spectra of Bt-Ch-1 beads-B and Bt-Ch-1 composites samples are presented in Appendix A1 and A2, respectively.

The FTIR spectrum of pristine bentonite (Figure 4.7a) shows dominant bands due to montmorillonite as reported in the literature [97]; the band at 3627 cm^{-1} is attributed to the O-H stretching vibration of structural OH groups and the band at 1635 cm^{-1} is attributed to the O-H deformation vibration of adsorbed water molecules. The intense band at 1003 cm^{-1} corresponds to the Si-O stretching vibration bonds of montmorillonite.

The spectrum of pure chitosan (Figure 4.7a) looks similar to that previously reported in the literature [20,188–190]; the broad bands centred around 3282 cm^{-1} are due to overlapping bands from O-H and N-H stretching vibrations. The bands observed at 2875 cm^{-1} are attributed to the symmetric stretching vibrations of C-H bonds of -CH$_3$/-CH$_2$ groups. The bands at 1648 cm^{-1} and 1564 cm^{-1} are due to C=O stretching vibration of the carboxamide group (O=C-NHR) and N-H bending vibration of amine groups (-NH$_2$), respectively. The bands at 1420 cm^{-1} and 1314 cm^{-1} are related to the bending vibration

of -C-H bonds and the band at 1026 cm^{-1} is attributed to stretching vibrations of C-O groups.

The spectra of the Bt-Ch beads-A with different weight-ratios of chitosan (90%Bt-10%Ch, 70%Bt-30%Ch, and 50%Bt-50%Ch; (Figure 4.7b, c and d, respectively) are combinations of the spectra of pristine bentonite and chitosan. The characteristic bentonite bands at 3627 cm^{-1} and 1008-1014 cm^{-1} appear in the spectra of all the Bt-Ch beads-A and the intensity of the former decreases with increasing chitosan loading. The chitosan bands between 1200-1600 cm^{1} also increase with chitosan loading and corresponds with the chitosan loadings derived by TGA. The band at 1648 cm^{-1} in pristine chitosan shifts to slightly lower frequencies for all the beads-A samples, however, it is not certain whether these band changes are due to a shift of the C=O stretching band of carboxamide or an overlap of the O-H deformation vibration of water molecules (as noted at 1635 cm^{-1} for bentonite). The N-H deformation band due to amine groups at 1564 cm^{-1} in the pristine chitosan does shift to lower frequencies for all Bt-Ch beads-A samples. A shift to lower frequencies would indicate a lower degree of interaction of the N-H bond (i.e. less energy required to move the constrained hydrogen) when complexed with clay and presumably results from the breakup of a strong hydrogen-bonding network within the chitosan molecules when present alone, and a weaker N-H interaction with the clay. Since it was shown by XRD that there is less intercalated chitosan in beads B than beads A, (but relatively similar amounts of chitosan) different interactions of the N-H bonds may be occurring, however, there was spectral evidence to suggest this as the spectra of the Bt-Ch beads-B samples were respectively relative to loading like those obtained for beads-A (see supplementary data).

The trends in the spectra of Bt-Ch composites samples were similar to those of beads A and B samples though the intensity of the bands due to chitosan were less intense, which was due to less chitosan being present. The presence of a very weak band at ≈1720 cm^{-1} was additionally observed for all the Bt-Ch composites and this was attributed to the v_{CO} stretching band of traces of acetate ions present in the composites, that were introduced by the use of acetic acid to adjust pH [81].

The spectra of Bt-Ch-2 composites/beads are not different from those of Bt-Ch-1 composites/beads. Therefore, the spectra of Bt-Ch-2 composites/beads samples were

not presented in this thesis as similar trends were observed compared to those of Bt-Ch-1 samples.
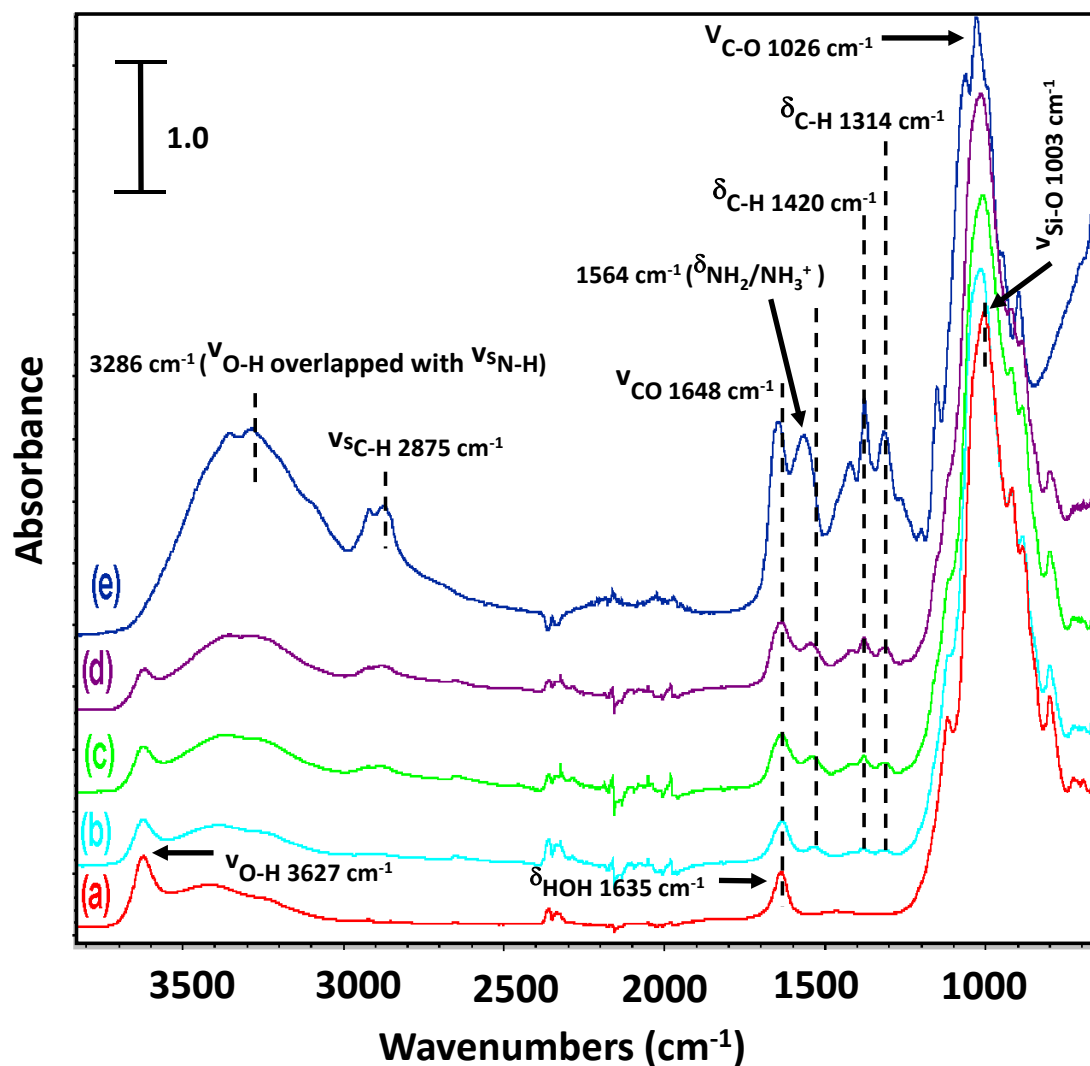
Figure 4.7: FTIR spectra of (a) pristine bentonite (b) 90%Bt-10%Ch-1 beads-A (C) 70%Bt-30%Ch-1 beads-A (d) 50%Bt-50%Ch-1 beads-A and (e) pure chitosan-1

Note: V = stretching vibration; δ = bending vibration; v_s = symmetric stretching vibration.

Similar trends were observed for the spectra of 90%Bt-10%Ch-1, 70%Bt-30%Ch-1, 50%Bt-50%Ch-1 beads-A, and pure chitosan-2.

Table 4.2: Assignments of FTIR Adsorption Bands for Bentonite clay and Chitosan biopolymers

Wavenumbers (cm^{-1})	Band Assignment
3627	O-H stretching vibration of hydroxyl groups in Bt. clay
3500 - 3000	O-H stretching vibration of hydroxyl groups (both Bt. Clay and chitosan), N-H stretching vibrations of Amine groups (in chitosan).
2875	Symmetric stretching vibrations of C-H bonds of -CH$_3$/-CH$_2$ groups in chitosan
1648, 1635	C=O stretching vibration of the carboxamide group (in chitosan), O-H deformation vibration of adsorbed water molecules (in Bt. Clay)
1564	N-H bending vibration of amine groups in chitosan
1420, 1314	C-H bending vibration of -C-H bonds in chitosan
1026, 1003	C-O stretching vibrations of -C-O groups (in chitosan), Si-O stretching vibration of montmorillonite in Bt. clay

Note: Bt = Bentonite

4.4. Conclusion

A bio-hybrid and functional material based on natural, abundant, low-cost, and environmentally friendly resources was successfully synthesised. A series of bentonite-chitosan composites (via solution blending method) and beads (via precipitation method) were prepared and characterised by TGA, XRD and FTIR. It was observed that higher product yield (%) was recovered for bead samples synthesised via the precipitation method, compared to the composite samples recovered through the solution blending method. This is attributed to loss of solubilised chitosan during the washing step of the products recovered via the solution blending method. The products synthesised via precipitation method (beads) contain more chitosan which is supported by the TGA results. A high portion of chitosan can be washed away as evidenced through the solution blending method. The XRD results show that a reasonable amount of chitosan has been intercalated into the interlayers of the clay for Bt-Ch-1 beads-A and Bt-Ch-1 composites, whereas much less has been intercalated with Bt-Ch-1 beads-B.

Similar result was obtained for beads-A and beads-B of Bt-Ch-2 samples. The calculated interlayer spacings increases with respect to chitosan loading and this correlates well with the results of TGA. The evidence shows that both mono- and bi-layer of chitosan were intercalated into clay layers for all Bt-Ch-1 composites. The higher d-spacing value obtained for Bt-Ch-1 beads-A (most especially for 50%Bt-50%Ch) are due to bilayers of chitosan intercalated between the clay layers. The chitosan is clearly interacting with the interlayers as there is clear evidence the chitosan is penetrating between the layers. Although, not all the chitosan may be in the interlayer region, perhaps the interlayer region is full and no more can enter. The clay layers are not able to expand further than 2 layers (i.e. become exfoliated) so any excess will be associated at the outer layers of clay stacks, at the edges of clay layer stacks and perhaps as an excess between stacks. Less intercalation of chitosan into clay layers for Bt-Ch-2 samples (compared to Bt-Ch-1) may be attributed to the high molecular weight of chitosan-2. FTIR results show that N-H bands (in chitosan) shifted to lower wavenumbers for all the Bt-Ch composites and beads, this may be due to the extent of protonation, location in clay exchange sites and how chitosan interacts with clay. The application of using Bt-Ch composites/beads as an adsorbent for removal of heavy metals is described in Chapter 5, 6 and 7 of this thesis.

Chapter 5

Adsorption of lead (Pb) onto Bentonite-Chitosan composites and beads: screening, optimisation, equilibrium, desorption, and mechanism studies

5.1. Introduction

The contamination of water by toxic metals, like lead (Pb), exceeding the permissible limits is an issue of great concern to the public with health implications. Adsorption with the combined use of composites (made from bentonite clays and chitosans) seems to be a promising technique for removal of toxic metals (e.g., Pb) from water. These developed functional composites have a lot of active adsorption sites (containing hydroxyl and amino groups of the chitosan biopolymer) capable of abstracting Pb from water. Very few studies have been published on the adsorption of Pb by Bt-Ch composites. This work aims to gain more understanding of the adsorption of Pb by these composites; this includes chitosan loading, molecular weight, and their form, for example, how each component is distributed, and how they interact resulting from systematic preparation procedures.

Batch adsorption procedures were used to study the removal of Pb ions (from aqueous solutions) by the Bt-Ch composites and beads. To fully understand the multiple factors affecting the adsorption process, a statistical design of experiments was explored in which two-level fractional factorial and I-optimal designs were used for screening and optimisation studies, respectively. During the screening phase, seven potential factors namely, pH, initial concentration, agitation rate, temperature, adsorbent dosage, agitation time and adsorbent type were examined for their significance on adsorption of Pb (II) onto Bt-Ch composites or beads. Only three variables (pH, initial concentration, and adsorbent dosage) as identified from the screening experiment and within the levels assessed were observed to have a significant effect on the adsorption of Pb (II) onto Bt-Ch composites or beads. These significant variables were further examined in more detail for optimisation analysis. Optimum adsorption conditions were estimated by a

numerical optimisation tool which was adjusted by changing the significance of each response involved. An adsorption equilibrium study was then performed based on the optimal experimental conditions (pH and adsorbent dosage) obtained from surface response-optimal designs. A non-linear modelling method was employed to analyse the adsorption equilibrium process by using the "Solver add-in" in Excel Microsoft 365 (Latest Version). Finally, selectivity towards Pb (II) adsorption, regeneration of adsorbents and mechanism studies were carried out.

5.2. Experimental

5.2.1. Materials

All the Bt-Ch-1 and Bt-Ch-2 composites/beads were prepared as described in Chapter 4. Lead (II) nitrate (≥ 99.95%), copper (II) nitrate hydrate (≥ 99.95%), zinc (II) nitrate (≥ 99.95%), nickel (II) nitrate (≥ 99.95%), sodium (meta) arsenite salt (≥ 90.0%), sodium hydroxide (reagent grade, 97%, pellets), Ethylenediaminetetraacetic acid (EDTA; disodium salt), and the stock standard solutions (for ICP) of Pb (II), Cu (II), Zn (II), Ni (II), As (III), Ca (II) Mg (II), K (I) and Na (I) were obtained from Sigma-Aldrich (now Merck). Hydrochloric acid and nitric acid were obtained from Fisher Scientific, UK. All chemicals used, unless otherwise stated, were of analytical grade purity and preparations were made using deionised water.

5.2.2. Adsorption experiments

In this chapter, a batch adsorption procedure was used to assess the adsorption capability of Bt-Ch composites/beads towards Pb(II) ions. The adsorption experiments were designed and performed based on two-level fractional factorial (screening) and I-optimal designs (surface response), as shown in Appendix B1 and B2, respectively. During the screening phase, seven potential factors namely, pH, initial concentration, agitation rate, temperature, adsorbent dosage, agitation time and adsorbent type were examined for their significance on adsorption of Pb(II) onto Bt-Ch composites/beads. Only three variables (pH, Initial concentration, adsorbent dosage) as identified from the screening experiment were observed to have a significant effect on the adsorption of Pb

(II) onto Bt-Ch composites/beads, and therefore, these variables were further examined in more detail for the optimisation analysis.

The effect of pH on the adsorption of the Pb(II) ion was carried out within the range that was not influenced by a precipitation process. It has been reported that the predominant species of Pb (II) ions at pH > 7 are $Pb(OH)^+$, $Pb(OH)_2$ and $Pb(OH)_3^-$, hence studying the effect of pH within the range of 7 and above, could lead to erroneous conclusions [66]. Therefore, the adsorption experiments were carried out at pH of less than 7 to ensure Pb (II) ions are removed just by adsorption processes without the effect of precipitation. In this study, the effect of pH was examined by varying the pH value from 2 to 6.

First the stock solution (1000 mg/L) of Pb(II) ions was prepared by dissolving 1.599 g of lead (II) nitrate in ultrapure deionised water and preserved with 10 ml of aqueous 5% w/v HNO_3 solution. The stock solutions of other ions (Cu (II), Zn (II), Ni (II) and As (III) for the competing ions experiments were prepared in the same manner by dissolving a known weight of their salts. Adsorption experiments were conducted in cleaned and sterilised Nalgene centrifuge plastic tubes (50-mL capacity). The centrifuge plastic bottles together with their contents were agitated using a Gyrotory Water Bath shaker (Model G76D; Figure 5.1). After that, the mixtures were centrifuged (using a Sorvall RC6 Superspeed Centrifuge) at 3000 rpm for 5 minutes and the supernatant collected and stored in cleaned and sterilised Fisherbrand PP centrifuge tubes (15 mL capacity) appropriately labelled for analysis of Pb (II) ions. The quantitative measurement of Pb (II) and that of other ions (Cu, Zn, Ni and As from competing ions experiments) were carried out by inductively coupled plasma – optical emission spectrometry (Agilent 5110 ICP-OES) , with instrument operating conditions as stated in Section 3.2.1.

The batch procedure was followed when determining the adsorption equilibrium, and the selectivity studies (effect of competing ions using multi-component solution).

The amount of Pb (II) or any metal ions per unit mass of Bt-Ch composites/beads (adsorbents) and percent adsorption performance (%) were calculated using Equations 5.1 and 5.2, respectively.

$$q_e = \frac{C_i - C_f}{M} \times V \qquad (5.1)$$

$$\% \text{ Adsorption} = \frac{C_i - C_f}{C_i} \times 100 \qquad\qquad (5.2)$$

Where q_e (mg Pb (II) ions g^{-1} Bt-Ch composites/beads) is the adsorption capacity, and C_i and C_f (mg L^{-1}) are initial and final concentrations of the Pb (II) ions before and after the adsorption experiment, respectively. V(L) is the volume of solutions and M (g) is the mass of the Bt-Ch composites /beads (adsorbent).

Figure 5.1: Water Bath Shaker equipment used for batch adsorption experiments

5.2.2.1 *Screening: two-level fractional factorial design*

In this study, six quantitative factors were examined for their significance on adsorption of Pb (II) onto Bt-Ch beads/composites (Code A to F, Table 5.1). These quantitative factors were tested for two different adsorbents (composites and beads-A, labelled as X and Y, respectively) simultaneously, which represent a single categorical factor "adsorbent type" (Code G, Table 5.1). Beads-B (labelled as Z) were not used during the screening experiment, since it has a close resemblance to beads-A. Therefore, with seven factors in total (six quantitative and one categorical factor) a fraction factorial design, which requires only sixteen experiments was designed (by using Design-Expert® 13 as shown in Appendix B1). This design enables the estimation of eight interaction effects, in addition to the main effects.

In general, the effect (E_X) of each variable "X" on each response "Y" is estimated as follows in Equation 5.3 [180].

$$E_X = \frac{\sum Y(+1) - \sum Y(-1)}{\frac{N}{2}} \tag{5.3}$$

From the above equation, $\sum Y(+1)$ and $\sum Y(-1)$ represent the sum of the responses, where factor "X" is at (+1) and (-1) levels, respectively. N is the number of experimental runs.

Table 5.1: Factors and their levels investigated during the screening stage in the batch adsorption experiments of Pb (II) onto Bt-Ch composites/beads

Serial Number	Code	Factors	Unit	Levels	
				Lower values (-1)	Higher values (+1)
1	A	pH	---	2	6
2	B	Initial concentration	mg/L	50	250
3	C	Agitation rate	rpm	180	280
4	D	Temperature	°C	25	55
5	E	Adsorbent dosage	g	0.1	0.5
6	F	Agitation time	minute	10	60
7	G	Adsorbent type	---	X	Y

Note: A - F are quantitative variables, while G is a categorical variable; X = Bt-Ch composites; Y = Bt-Ch beads

5.2.2.2 *Surface response methodology – I-optimal designs*

A response surface methodology (RSM) was used for the optimisation of significant variables. Three numeric variables (pH, initial concentration, adsorbent dosage, Table 5.2) as identified from the screening experiment were observed to have significant effect on the adsorption of Pb (II) ions onto Bt-Ch composites/beads. In addition, one categorical factor (variation in three different adsorbent types) was added to the three stated numeric variables and all were used within the optimisation studies. The optimal conditions and combined effect (interaction) of these significant variables on Pb (II) adsorption could have been studied using central composite design (CCD) or Box-Behnken design (BBD), which may have provided correct picture of the optimised parameters [176,191,192]. However, these two classical design choices require many experimental analyses runs (i.e. 60 and 51 runs, respectively) for one adsorbent sample alone, so considering the number of adsorbent samples to test for this adsorption work, which includes Bt-Ch composites and Bt-Ch beads (A & B) the less experimentally intensive, alternative method was chosen. Each of these three Bt-Ch beads/composites adsorption-types consisted of three different Bt-Ch ratios, *viz.*, 90%Bt-10%Ch, 70%Bt-30%Ch and 50%Bt-50% and were each prepared from two different chitosan biopolymers (Chitosan-1 & Chitosan-2). This makes a total of nine different Bt-Ch samples for each chitosan biopolymer, and a total of eighteen Bt-Ch samples to be investigated as adsorbents for adsorption of Pb (II) ions. Therefore, due to limitations of time and other resources, an optimal (Custom) design was opted for, which gave flexibility and fewer experimental preparations.

Optimal designs of experiment are computer-generated designs which are good alternatives considered in lieu of classical designs [178,193]. In the last few years, there has been an increased emphasis on the use of "Optimal" design of experiments [193]. With current improvement, it has been shown that optimal designs are flexible and can be used to solve many problems at hand [193].In addition, it can be tailored to a particular problem and situation, and in fact, can be utilised for almost any scenario [194]. The optimal Custom Designer incorporating some popular software such as Design-Expert® (software version 13), can give much more flexibility in creating

response surface designs, which are often much more efficient than the classical designs [194,195].

In the scenario herein, since one categoric factor is incorporated (in addition to three numeric factors), a response surface experiment was created with a 28-run Optimal Custom design (I-optimal), including five replicates, using Design-Expert® 13 software (Appendix B2). Every factor level combination was used in a randomised order. This design enabled to fit for a second-order polynomial model, which has main factors, two-factor interactions, and quadratic terms. These quadratic terms will capture the curvature in the relationship between the response (adsorption capacity) and the experimental variables. Also, a comparison among three different adsorbents-types (Bt-Ch composites, Bt-Ch beads-A, and Bt-Ch beads-B), was made possible for each chitosan/bentonite ratio. In summary, the equation model was defined as:

$$Y = \alpha + aA + bB + cC + dD + abAB + acAC + adAD + bcBC + bdBD$$
$$+ cdCD + aaA^2 + bbB^2 + ccC^2$$

(5.4)

where Y is the measured response (e.g., Pb-adsorption capacity, mg/g or efficiency, %) associated with every variable level combination, **α** is the intercept (mean value), A, B, C and D are the main factors (A = pH of Pb (II) ion solution; B = adsorbent dosage; C = initial concentration of Pb (II) ion solution; D = adsorbent type). AB, AC, AD, BC, BD, CD are the two-factor (binary) interactions. A^2, B^2, C^2 are the quadratic numerical (quantitative) factors, and a, b, c, d or ab, ac, ad, bc, bd, cd or aa, bb and cc are the coefficients of the main factors, interaction factors, and quadratic numerical factors, respectively.

Analysis of variance (ANOVA) was carried out to describe the coefficients of the quadratic equation. Significance of the adsorption variables were checked by p-value and F-value and the lack-of-fit test was used as a support test for adequacy of the fitted model.

In terms of optimisation and desirability function of adsorption parameters, the optimum adsorption conditions are determined by a numerical optimisation method, and one of the popular strategies for selecting the best alternatives is to use the simultaneous optimisation technique which was put forward by Derringer and Such (1980) [178,196]. This method adopts an objective function D, often referred to as the

desirability function, which transforms calculated response into a free scale value (d_i) called desirability [196]. The desirability ranges from zero to one (i.e., least to most desirable, respectively). The factor settings with best total desirability are the optimal conditions. The simultaneous objective function is a geometric mean of all transformed responses, which is given as;

$$D = (d_1 \times d_2 \times d_3 \ldots\ldots d_n)^{\frac{1}{n}}$$
(5.5)

where D is the desirability function, d_1, d_2, d_3 and d_n are the desirability ranges for each response, and n is the number of responses in the measurement.

Table 5.2: Factors and their levels investigated during optimisation stage of the batch adsorption experiments of Pb (II) ions onto Bt-Ch composites/beads

Levels	Numeric continuous factors			Categoric nominal factor
	A-pH	B-Adsorbent dosage (g)	C-Initial concentration (mg/L)	D-Adsorbent type
Low (-1)	2	0.05	50	Bt-Ch composites (X)
Centre point (0)	varied	varied	varied	Bt-Ch beads-A (Y)
High (+1)	6	0.5	250	Bt-Ch beads-B (Z)

Note: The centre points (0) for each continuous factor maybe slightly different due to the algorithms of the Optimal-I designs

5.2.2.3 *Adsorption equilibrium study and Isotherm modelling*

An adsorption equilibrium study was performed based on the optimal experimental conditions (pH and adsorbent dosage) obtained from the surface response-optimal designs in the previous section. Although to determine the equilibrium adsorption capacity of Bt-Ch composites/beads to absorb Pb(II) ions from aqueous solutions, a wider range of concentrations (i.e., from 10 to 500 mg L^{-1}) that differs from the one used in the optimal experiment (50 to 250 mg L^{-1}; Table 6.1). Thus, 0.05 g of each adsorbent was exposed to 25 mL of aqueous solutions containing Pb(II) ions with varying concentrations (as stated above) at pH 4.5, agitation time of 60 minutes (with the speed of 230 rpm) and at room temperature (approximately 21°C). The equilibrium adsorption capacities, q_e (mg/g) were calculated and then plotted against the corresponding respective equilibrium concentrations, Ce (mg/L) for adsorption isotherm modelling. Modelling equilibrium data with isotherm equations can provide qualitative and quantitative information about the adsorption process, which could contribute to understanding about the adsorption mechanisms [24,48,116]. In the study carried out in this chapter, two well-known adsorption isotherm models, viz; Langmuir [139], and Freundlich [145], were used to fit the equilibrium data obtained from adsorption of Pb(II) ions onto Bt-Ch composites/beads. Both Langmuir and Freundlich isotherm models have been fully reviewed previously in Sections 2.5.4.1 and 2.5.4.2 respectively. The non-linear equations of these models are shown in Equation 2.9 and 2.11, respectively, presented in Table 2.5.

5.2.2.4 *Desorption studies*

In this study, aqueous HCl and EDTA solutions were used as a stripping (desorbing) agent. Inorganic-strong acids (such as HCl) and chelating agents (e.g., EDTA) are widely used in desorption of metal ions from chitosan, its derivatives, and other adsorbents [197]. When strong acids are used, desorption is achieved by supplying plenty H^+ ions, which shifts the equilibrium and 'weakens' the interaction between adsorption groups (such as -NH_2) and metal ions (e.g., Pb). At the same time, the chloride ions (from HCl) readily complex with metal ions and help to solubilise [197]. On the other hand, strong

chelating agent such as EDTA has affinity towards metal ions and form a bond with them [197]. The desorption processes using strong acids or chelator can be described according to Equations (5.6) and (5.7), respectively.

$$Bt/Ch{\sim}NH_2Pb + 2H^+Cl^- \rightleftharpoons 2Bt/Ch{\sim}NH_3^+ + Pb^{2+}Cl_2 \qquad (5.6)$$

$$Bt/Ch{\sim}NH_2Pb + EDTA \rightarrow Bt/Ch{\sim}NH_2 + EDTAPb \qquad (5.7)$$
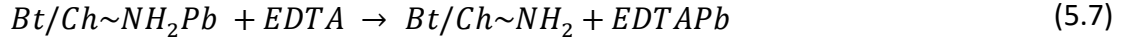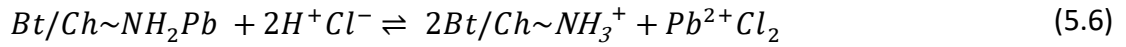
The regeneration of developed Bt-Ch composites/beads was carried out by exposing 0.2 g of each adsorbent sample to 150 mg/L Pb (II) solutions (25 ml; pH 4.5; agitation time = 10 minutes). The loaded adsorbents were agitated with 25 mL 1.0 M HCl or 0.01 M EDTA solutions for 120 minutes, filtered and washed with de-ionised water (3 times) prior to re-use. The HCl treated adsorbents were stabilised with NaOH before washing three times. The adsorption-desorption cycles were repeated 5 times for the sake of exploring the reusability of Bt-Ch beads or composites. The percent desorption (%) was calculated using Equation 5.8 [68].

$$\% \text{ Desorption} = \frac{C_d V_d}{M q_e} \times 100 \qquad (5.8)$$

Where C_d (mg/L) is the concentration of Pb(II) ions desorbed from Bt-Ch composites/beads, V_d (L) is the volume of desorbed solution, M (g) is the mass of adsorbent (Bt-Ch composites/beads), and q_e (mg/g) is the adsorption capacity of Bt-Ch composites/beads for Pb (II) ions.

5.2.2.5 *Ion-Exchange experiment: adsorption mechanism study*

An ion exchange experiment was carried out to investigate the possibility of cation exchange of Pb with the resident cations located in exchange sites of the clay that were not exchanged during the chitosan modification process. This was conducted based on the procedure previously reported in the literature [198–200]. Under the optimum experimental conditions, the ion exchange study was conducted in the range of 10 – 90 mg/L of Pb (II) ions solutions for all the adsorbent samples. The initial pH of the solution was adjusted to 4.5, and the final pH of the solution was also measured after the adsorption. The amounts of Pb (II) adsorbed and cations (Ca^{2+}, Mg^{2+}, K^+ and Na^+ ions)

released were quantitatively determined. To determine the possibility of leaching of these four cations from the adsorbents, a blank experiment was also conducted for the adsorbent with ordinary deionised water. The net release of cations was calculated by subtracting the amounts of cations released in the blank from the amounts of cations measured in the effluent after Pb (II) ions adsorption.

5.3. Results

5.3.1. Screening designs

The influence of seven factors, which includes pH (A), initial concentration (B), agitation rate (C), temperature (D), adsorbent dosage (E), agitation time (F) and adsorbent type (G) on the adsorption of Pb (II) ions by Bt-Ch beads/composites was determined using fractional factorial design (Resolution IV). The data were subjected to normal plot, ANOVA, fit and diagnostic statistics to select the statistically significant factors (or combination of factors) affecting the adsorption of Pb (II) ions onto Bt-Ch beads/composites. A Pareto chart is usually used to check for significant factors that have been selected from a half-normal plot [5]. Within the Pareto chart, the selected factors that are above the Bonferroni Limit show undoubtedly important factors, while those that are above the t-critical limit (but lower than Bonferroni Limit) are still likely to be important factors [5]. However, factors that are below the t-critical limit are insignificant, and they should not be included in further models, except those that support hierarchy [5].

Figure 5.2 shows the Pareto chart for Pb (II) adsorption capacity (mg/g) by 90%Bt-10%Ch-1 composites/beads. The Pareto chart for other adsorbent samples (70%Bt-30%Ch-1, 50%Bt-50%Ch-1, 90%Bt-10%Ch-2, 70%Bt-30%Ch-2 and 50%Bt-50%Ch-2 composites/beads) shows similar trends and are not presented in this thesis. As can be seen, it appears that from all the fifteen effects (7 main effects + 8 two-factor interactions) studied, only three of the seven estimated main effects are significantly important. These are the pH (A), initial concentration (B) and adsorbent dosage (E). They are critical factors for multivariate optimisation of Pb (II) adsorption onto Bt-Ch composites/beads via optimal-I design in the next step. The observed effects by pH (A) and initial concentration (B) were determined to have a positive influence, while that of adsorbent dosage (E) showed a negative influence towards Pb (II) adsorption capacity. Similar trends were observed for 70%Bt-30%Ch-1, 50%Bt-50%Ch-1, 90%Bt-10%Ch-2, 70%Bt-30%Ch-2, 50%Bt-50%Ch-2 composites/beads (as shown in Appendix III – VII, respectively).
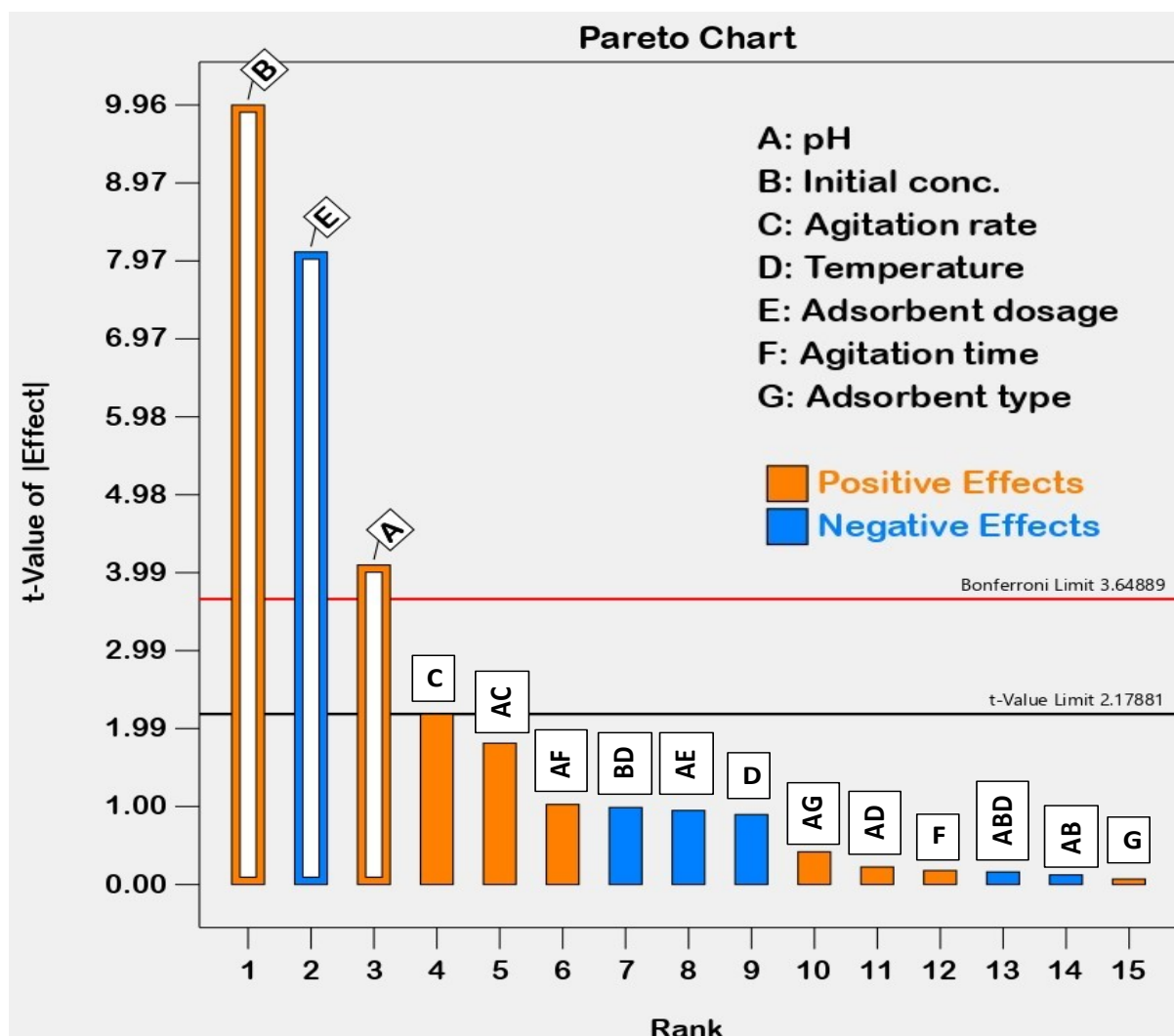
Figure 5.2: Pareto Chart for the seven factors (main effects and interactions) on the response analysis of adsorption capacity of Pb (II) onto 90%Bt-10%Ch-1 composites/beads

Note: this chart was plotted and obtained from Design-Expert®13. Base 10 log transformation (k = 0); ANOVA = significant; R^2 = 0.94; R^2_{adj} = 0.92; R^2_{pred} = 0.89; Shapiro-Wilk test (W-value = 0.91 and p-value = 0.24)

Similar trends were observed for 70%Bt-30%Ch-1, 50%Bt-50%Ch-1, 90%Bt-10%Ch-2, 70%Bt-30%Ch-2, 50%Bt-50%Ch-2 composites/beads.

5.3.2. Surface response (I-optimal) approach and chemometric analysis

To study the surface response, I-optimal design was employed to examine the respective and combined effects of pH (A), initial concentration (B) and adsorbent dosage (C), as the three significant and independent factors on the adsorption capacity (mg/g) of the Bt-Ch composites/beads for Pb (II) ions. The results for the experimental runs with their corresponding experimental and predicted response (adsorption capacity) of Pb (II) ion adsorption onto Bt-Ch-1 and Bt-Ch-2 composites/beads are all presented in Appendix B3 and B4, respectively. To check the significance and acceptability (sufficiency) of the regression model obtained by optimal response, the model was subjected to Analysis of variance (ANOVA). For the categorical factor-D (Adsorbent type), two coefficients are provided due to the need to use multiple coefficients associated with multi-level factors. The significance of regression model and each coefficient terms are usually determined by F and P-values using Fisher's and null hypothesis test [178,192]. Generally, the larger F-value and smaller P-value indicates a higher significance of regression model and each coefficient [178,192]. The model reduction was carried out where appropriate and this was done by deleting or reduction of non-significant terms to improve the proposed model. The adequacy of the model was checked with lack of fit tests, and evaluated by correlation coefficients values (R^2, $R^2_{adjusted,}$ and $R^2_{predicted}$). The coefficient of determination (R^2) value examines the goodness of fit of the model, and for a significant model, R^2 value should be close to unity [201].

The mathematical relationships between the three studied independent factors (i.e., pH, adsorbent dose, and initial concentration) and the response (adsorption capacity) were also provided by Design Expert 13 software. The equation in terms of actual factors (with regards to respective adsorbent (X, Y & Z) which describes the various parameters regarding the Pb(II) adsorption onto Bt-Ch-1 composites/beads are all shown in from Equations 5.9 to 5.17. While the equations related to adsorption of Pb(II) onto Bt-Ch-2 composites/beads are all presented in Appendix B5.

90Bt-10%Ch-1

$$Log_{10}(Adsorption\ capacity)X = 0.0776 + 0.4689A - 2.7332B + 0.00648C - 0.1562AB + 0.0037BC - 0.05204A^2 + 2.5178B^2 - 0.0002C^2 \tag{5.9}$$

$$Log_{10}(Adsorption\ capacity)Y = 0.0871 + 0.5202A - 3.0909B + 0.0061C - 0.1562AB + 0.0037BC - 0.0520A^2 + 2.5178B^2 - 0.00002C^2 \tag{5.10}$$

$$Log_{10}(Adsorption\ capacity)Z = 0.1431 + 0.4961A - 3.1018B + 0.0065C - 0.1562AB + 0.0037BC - 0.0520A^2 + 2.5178B^2 - 0.00002C^2 \tag{5.11}$$

70Bt-30%Ch-1

$$Log_{10}(Adsorption\ capacity)X = 0.402 + 0.3228A - 2.661B + 0.0038C - 0.102AB + 0.0003AC + 0.0038BC - 0.0358A^2 + 2.123B^2 - 0.00001C^2 \tag{5.12}$$

$$Log_{10}(Adsorption\ capacity)Y = 0.795 + 0.2991A - 3.093B + 0.0033C - 0.102AB + 0.0003AC + 0.0038BC - 0.0358A^2 + 2.123B^2 - 0.00001C^2 \tag{5.13}$$

$$Log_{10}(Adsorption\ capacity)Z = 0.513 + 0.359A - 2.973B + 0.0029C - 0.102AB + 0.0003AC + 0.0038BC - 0.0358A^2 + 2.123B^2 - 0.00001C^2 \tag{5.14}$$

50Bt-50%Ch-1

$$Log_{10}(Adsorption\ capacity)X = -0.741 + 0.867A - 2.014B + 0.0057C - 0.1446AB + 0.00031AC + 0.0004BC - 0.1062A^2 + 1.931B^2 - 0.00001C^2 \tag{5.15}$$

$$Log_{10}(Adsorption\ capacity)Y = -0.911 + 0.895A - 1.820B + 0.0057C - 0.1446AB + 0.00031AC + 0.0004BC - 0.1062A^2 + 1.931B^2 - 0.00001C^2 \tag{5.16}$$

$$Log_{10}(Adsorption\ capacity)Z = -0.778 + 0.937A - 2.6315B + 0.0057C - 0.1446AB + 0.00031AC + 0.0004BC - 0.1062A^2 + 1.931B^2 - 0.00001C^2 \tag{5.17}$$

Note: A = pH; B = Adsorbent dosage; C = Initial concentration; D = Adsorbent type; X = Bt-Ch composites; Y = Bt-Ch beads-A; Z = Bt-Ch beads-B

5.3.2.1 *Analysis of variance (ANOVA)*

The summary of ANOVA results for the adsorption capacity (mg/g) of Pb (II) ions by 90%Bt-10%Ch-1 composites/beads are shown in Appendix B6. After data-fitting was carried out, the modified quadratic models concerning the response were significant (F = 714.37; P<0.0001) for adsorption capacity (mg/g). The non-significant "lack-of-fit" for adsorption capacity (F = 0.4012; P = 0.8515 > 0.05) suggest the adequacy of the model to explain data in the experimental region. This implies that there are 85.15% chances that the F-value (for Lack of Fit) could be due to noise concerning adsorption capacity. The R^2 values for this model was found to be 0.99 which indicates that about 99% of the experimental data could be matched with the predicted value, and only 1% of it was not explained by the model. The predicted R^2 values (0.99) were in reasonable agreement with adjusted R^2 (0.99), i.e., the difference is less than 0.2. The small value of coefficient of variance, CV = 1.81, implies that deviation between the predicted and experimental data values were minimal. Adequate precision measures the signal to noise ratio, and a ratio greater than 4 is desirable [195], for this model, the ratio values were found to be 104.77, which indicates an adequate signal for Pb adsorption. P-values less than 0.05 indicate model terms are significant, and therefore, A, B, C, D, AB, AD, BC, BD, CD, A², B², and C² are significant terms in the modified quadratic model related to adsorption capacity. However, p-values greater than 0.10 indicate model terms are not significant and so, they were completely removed or deleted from the model. The estimated coefficients for these significant terms, as obtained by coded equation, are useful for identifying their relative impact. When comparing the factor coefficients (second column shown in Appendix B6) a positive and negative coefficient signifies increasing and decreasing effects, respectively.

The ANOVA results of the adsorption capacity (mg/g) of Pb (II) obtained for other adsorbents viz; 70%Bt-30%Ch-1, 50%Bt-50%Ch-1, 90%Bt-10%Ch-2, 70%Bt-30%Ch-2 and 50%Bt-50%Ch-2 composites/beads have similar trends (compared to that of 90%Bt-10%Ch-1), and are clearly described and presented from Appendix B7 to B11, respectively).

In terms of diagnostic statistics, both the normal probability plot and the correlation graph for Pb (II) adsorption by 90%Bt-10%Ch-1 composites/beads were obtained to

understand further the data generated (Figure 5.3). Figure 5.3a represent the normal probability plots of studentised residuals for adsorption capacity (mg/g). This plot indicates whether residuals follow a normal distribution, i.e., the points should lie on an approximately straight line without any apparent deviation. However, when the distribution is not normal, it signifies a nonlinear pattern, which may be corrected by a proper transformation [202]. As can be seen almost all data clearly lie on a straight line for both responses, and therefore, it can be assumed that they are normally distributed. Figure5.3b represents the correlation (relationship) between actual and predicted values of adsorption capacity (mg/g). The actual values are the measured values of the adsorption capacity obtained for 90%Bt-10%Ch-1 composites/beads, which was determined experimentally by using Equation 5.1. While, predicted values were generated by using Equations 5.9 to 5.11. As can be seen, the predicted values for adsorption capacity of 90%Bt-10%Ch-1 composites/beads for Pb(II) adsorption, obtained from the model, are in good agreement with the actual experimental data. It should be noted that these models predict data that was used to develop the model, and this may introduce some inherent bias for these models.

The normal probability plot and the correlation graph for of the adsorption capacity (mg/g) of Pb(II) obtained for other adsorbents have a similar trend as obtained for 90%Bt-10%Ch-1 sample.
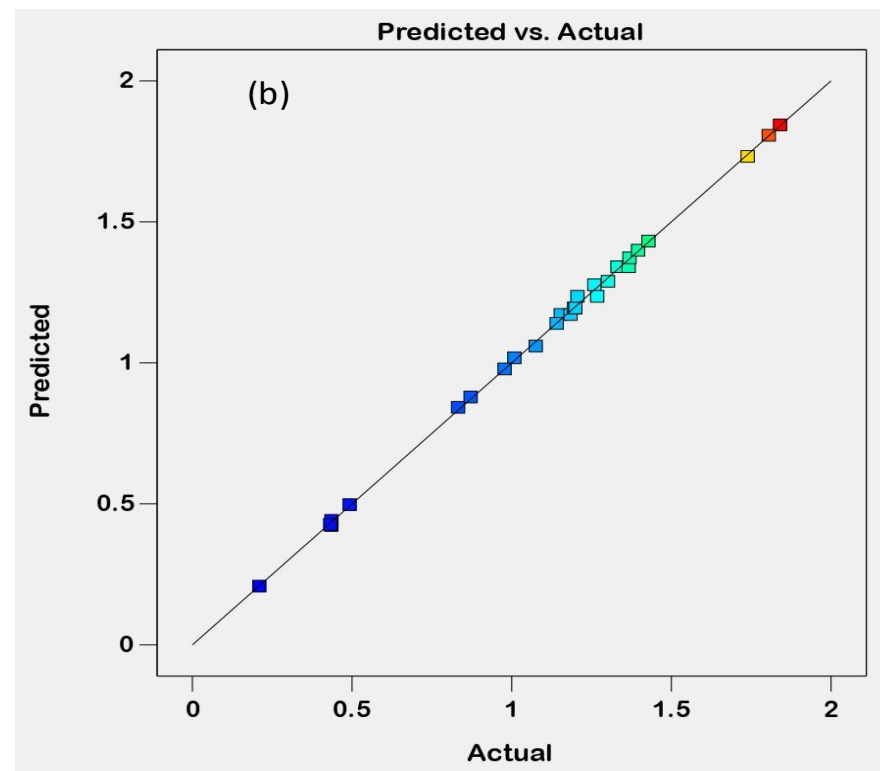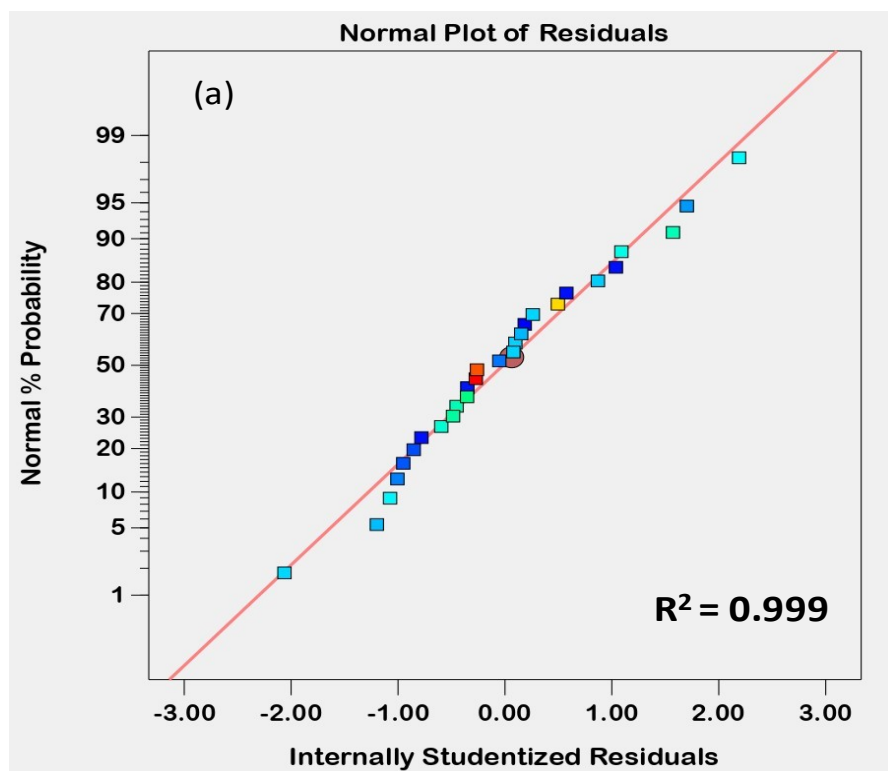
Figure 5.3: Normal probability plot of studentised residuals(a) and correlation between actual and predicted values (b) of Pb (II) ion adsorption capacity for 90%Bt-10%Ch composites/beads

Note: these graphs were plotted and obtained from Design-Expert®13; similar trends were observed for 70%Bt-30%Ch-1, 50%Bt-50%Ch-1, 90%Bt-10%Ch-2, 70%Bt-30%Ch-2, 50%Bt-50%Ch-2 composites/beads

5.3.2.2 *Effects of main factors and their interactions*

The model-graphs showing the effect of each quantitative factor and 2-way interaction effects on the adsorption capacity (mg/g) of Pb(II) by 90%Bt-10%Ch-1 composites/beads are shown in Figure 5.4 and 5.5, respectively. The model-graphs (concerning the main effects and interaction terms) obtained for the remaining adsorbent samples shows a similar trend but not presented in this thesis. As shown in Figure 5.4(a, b, c), adsorption capacity of Pb ions increases from pH of 2 to 4, maintained at this value from pH 4 to 5. The effect of the pH is more noticeable for beads (Figure 5.4b and c)) compared to the corresponding composites (Figure 5.4a). In terms of adsorbent dosage, it was observed that the adsorption capacity of Pb(II) ions decreases with an increase in the adsorbent dose from 0.05 to 0.5 g (Figure 5.4d, e, and f). Regarding initial concentration(as shown in Figure 5.4g, h, and i), the Pb(II) adsorption capacities increases with initial concentration from 50 to 200 mg/L and then maintain this high value for the remaining part of initial concentration (200 to 250 mg/L).

In terms of the model-graphs showing 2-way interaction effects (Figure 5.5); when the effects of two factors appear as two non-parallel lines, it indicates that the effect of one factor depends on the level of another factor, and vice versa [202,203]. Interactive effects were observed for pH-adsorbent dosage (Figure 5.5a b and c) and adsorbent dosage-initial concentration (Figure 5.5a b and c). At higher adsorbent dose (0.5 g), the effect of pH was insignificant. However, the influence of solution pH was more pronounced at the lowest value of adsorbent dosage (0.05 g).

Similar trends of the main and interactive effects were observed for all the remaining adsorbent samples.

5.3.2.3 *3D response surface plot*

To visualise the interactive influence among the significant variables on the adsorption of Pb (II) ions onto Bt-Ch composites/beads, a 3-dimensional (3D) response surface plot was used. The 3D response surface plots are graphical representation of regression equation showing the simultaneous interaction effect of two variables (on response), while maintaining the other variable constant [192,201].

(A) Interactive effect of solution pH and adsorbent dosage

Figure 5.4(a, b, & c) shows the 3D response surface plot for the interaction effect of pH and adsorbent dosage (at constant 200 mg/L initial conc.) on Pb (II) adsorption capacity (mg/g) for 90%Bt-10%Ch-1 composites, beads-A and beads-B, respectively. It has been widely reported that the initial pH of the adsorbate solution plays a significant role in the adsorption process and this can affect the removal of heavy metal ions from aqueous solution [20]. Although the speciation experiment was not conducted in this study, from the study carried out by Yang et al. (2010) [66] to determine the relative proportion of Pb species as a function of pH, they found that about 99% of the Pb ions present in the solution (at pH of 2 to 5) were in the free form (i.e., Pb(II) ions) prior to sorption with Na-bentonite. In this study, It was observed that the adsorption capacity of Pb(II) ions per unit weight of adsorbent increased from 21.21 to 54.41 mg/g, 18.21 to 63.41 mg/g, and 28.60 to 72.87 mg/g for 90%Bt-10%Ch-1 composites, beads-A, and beads-B, respectively, with an increase in pH level from 2 to 5 (Figure 5.4-a, b and c, respectively). The observed decreased in Pb (II) ions uptake (mg/g) for all 90%Bt-10%Ch-1 adsorbent samples at pH 2 maybe due to competition from hydronium ions (H_3O^+) and protonated active sites of the adsorbent. At lower pH (highly acidic conditions) the active sites present in the adsorbent such as silanol groups (present on bentonite) and amino groups (present on chitosan biopolymer) are more protonated and hence, they are less available/less inclined for Pb (II) ion adsorption [70,204]. As the pH increases, the active sites (silanol and amino groups) on the adsorbent are largely deprotonated and thereby, encouraging more Pb(II) ions uptake by the adsorbent [204]. The influence of solution pH was more pronounced at the lowest value of adsorbent dosage (0.05g). Also, it was noticed that the pH (A) may have a slightly negative effect on the Pb (II) adsorption capacity in a non-linear manner (A^2, check the coefficient in Appendix B6). Even though this quadratic effect of pH (A^2) is minimal (in comparison to the linear effect of pH (A)), it is suspected that this could be the reason for the characteristic curve-shape of the 3D Surface plot.

As shown in Figure 5.4 (a, b, and c), adsorbent dosage (B) was another significant factor but with a negative effect (check the coefficient in Appendix B6) on adsorption capacity (mg/g) of Pb (II) ions, it was also highly pH dependent. At the lowest pH value of 2, it was observed that the adsorption capacity of Pb (II) ions per unit weight of adsorbent

decreases from 21.03 to 13.72 mg/g, 18.19 to 10.64 mg/g, and 28.88 to 13.33 mg/g for 90%Bt-10%Ch-1 composites, beads-A, and beads-B, respectively, with an increase in adsorbent dose from 0.05 to 0.5 g. At higher pH level of 5, the corresponding adsorption capacity of Pb (II) ions per unit weight of adsorbent decreases from 57.66 to 13.81 mg/g, 65.17 to 13.99 mg/g, and 75.13 to 12.55 mg/g for 90%Bt-10%Ch-1 composites, beads-A, and beads-B, respectively. So, the effect of adsorbent dosage was much more pronounced at higher pH in comparison to lower pH values. Generally, with an increase in adsorbent dose, more active adsorbent sites (Bt-Ch-1 composites/beads) remain uncovered during the adsorption process, thus the Pb (II) uptake capacity may decrease. This agrees with previous similar results reported in the literature [205,206]. Similar trends were observed for 70%Bt-30%Ch-1, 50%Bt-50%Ch-1, 90%Bt-10%Ch-2, 70%Bt-30%Ch-2, 50%Bt-50%Ch-2 composites/beads.

(B) Interactive effect of initial concentration and adsorbent dosage

The effect of initial concentration (factor C) on the Pb (II) adsorption capacity (mg/g) is described in Figure 5.5 (a, b, & c), which represent the 3D surface plots for interaction effect of initial concentration and adsorbent dosage on adsorption capacity of Pb (II) ions (at constant pH 5) for 90%Bt-10%Ch-1 composites, beads-A, and beads-B, respectively. Due to mass transfer effects, adsorption of most heavy metals (e.g., Pb, Fe, etc.) are an extremely concentration-dependent process. This implies that the concentration driving force is directly proportional to the initial concentrations of the metal solutions, and consequently, the removal of metals ions depends on the initial concentration [206]. It was noticed that the effect of initial concentration on Pb (II) adsorption capacity is much more pronounced at lowest adsorbent dosage. At higher value of adsorbent dosage (0.5 g), and with an increase in initial concentration from 50 to 250 mg/L the adsorption capacity of Pb (II) ions increases from 2.78 to 13.81 mg/g, 2.81 to 13.99 mg/g, and 2.53 to 12.56 mg/g for 90%Bt-10%Ch-1 composites, beads-A, and beads-B, respectively, whereas at lowest value of adsorbent dosage (0.05 g), the corresponding adsorption capacity of Pb (II) ions increases are more pronounced from 24.96 to 57.66 mg/g, 28.21 to 65.17 mg/g, and 32.08 to 74.11 mg/g. At lower initial concentration of Pb(II) ions, although the adsorption process maybe extremely fast, most of the adsorbent active sites may remain unsaturated, and consequently this accounts for lower value of Pb (II) uptake (mg/g). At higher initial concentration, the

active sites available on the surface of the 90%Bt-10%Ch-1 composites/beads could be surrounded by more Pb (II) ions; therefore, Pb (II) ions are not only adsorbed in a monolayer at the outer interface of 90%Bt-10%Ch-1 composites/beads, but also diffuse within the adsorbent particles. Consequently, more Pb (II) ions uptake (mg/g) could be accomplished, and this is similar to what is frequently reported in previous literature [206,207].

Similar trends were observed for 70%Bt-30%Ch-1, 50%Bt-50%Ch-1, 90%Bt-10%Ch-2, 70%Bt-30%Ch-2, 50%Bt-50%Ch-2 composites/beads.
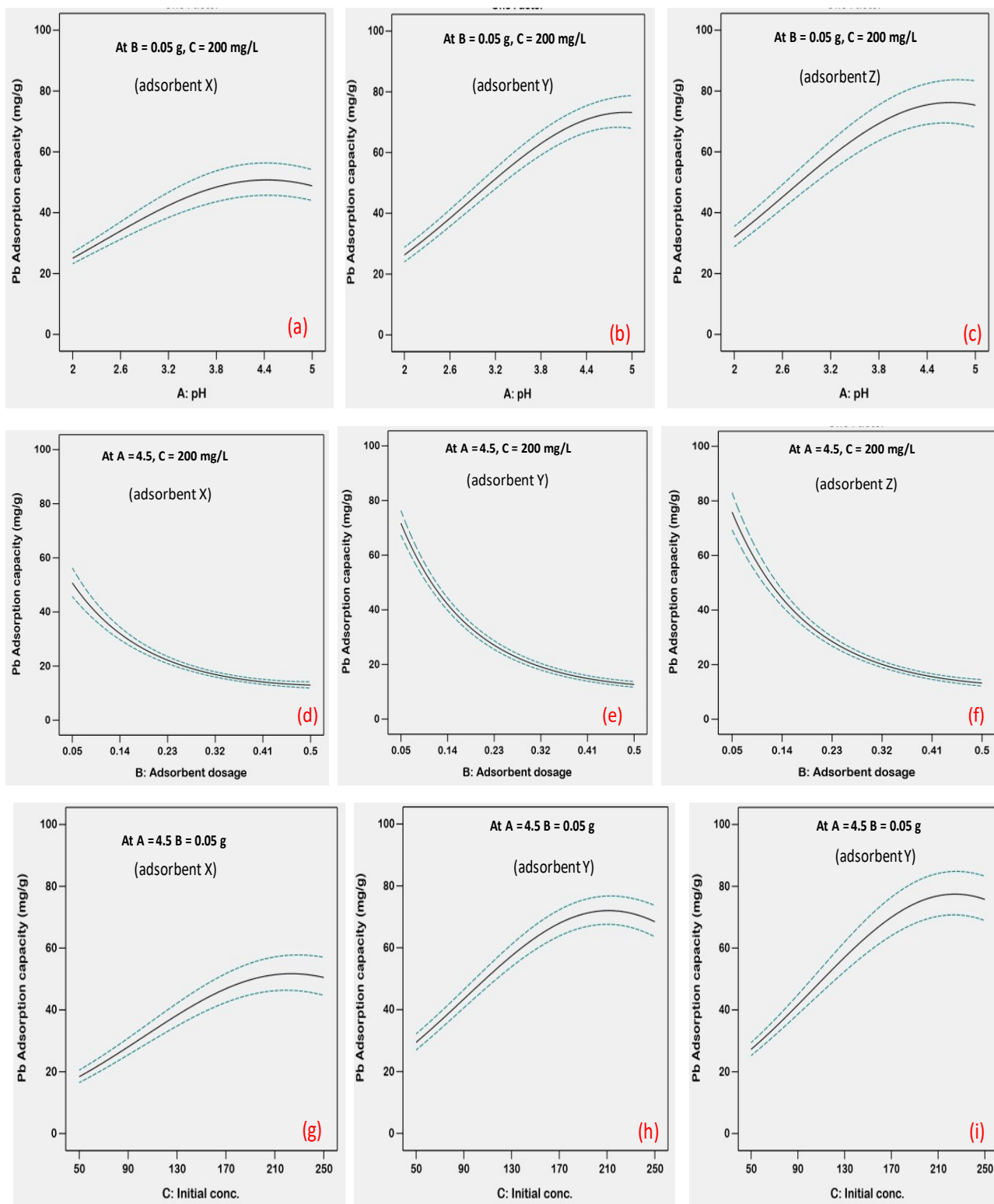
Figure 5.4: Graphs showing the effect of each factor on the Pb(II) adsorption capacity by Bt-Ch composites (a, d, g), beads-A (b, e, h) and beads-B (c, f, i).

Note: these graphs were plotted and obtained from Design-Expert®13; dashed lines represent 95% confidence interval bands of the experimental data; similar trends were observed for 70%Bt-30%Ch-1, 50%Bt-50%Ch-1, 90%Bt-10%Ch-2, 70%Bt-30%Ch-2, 50%Bt-50%Ch-2 composites/beads
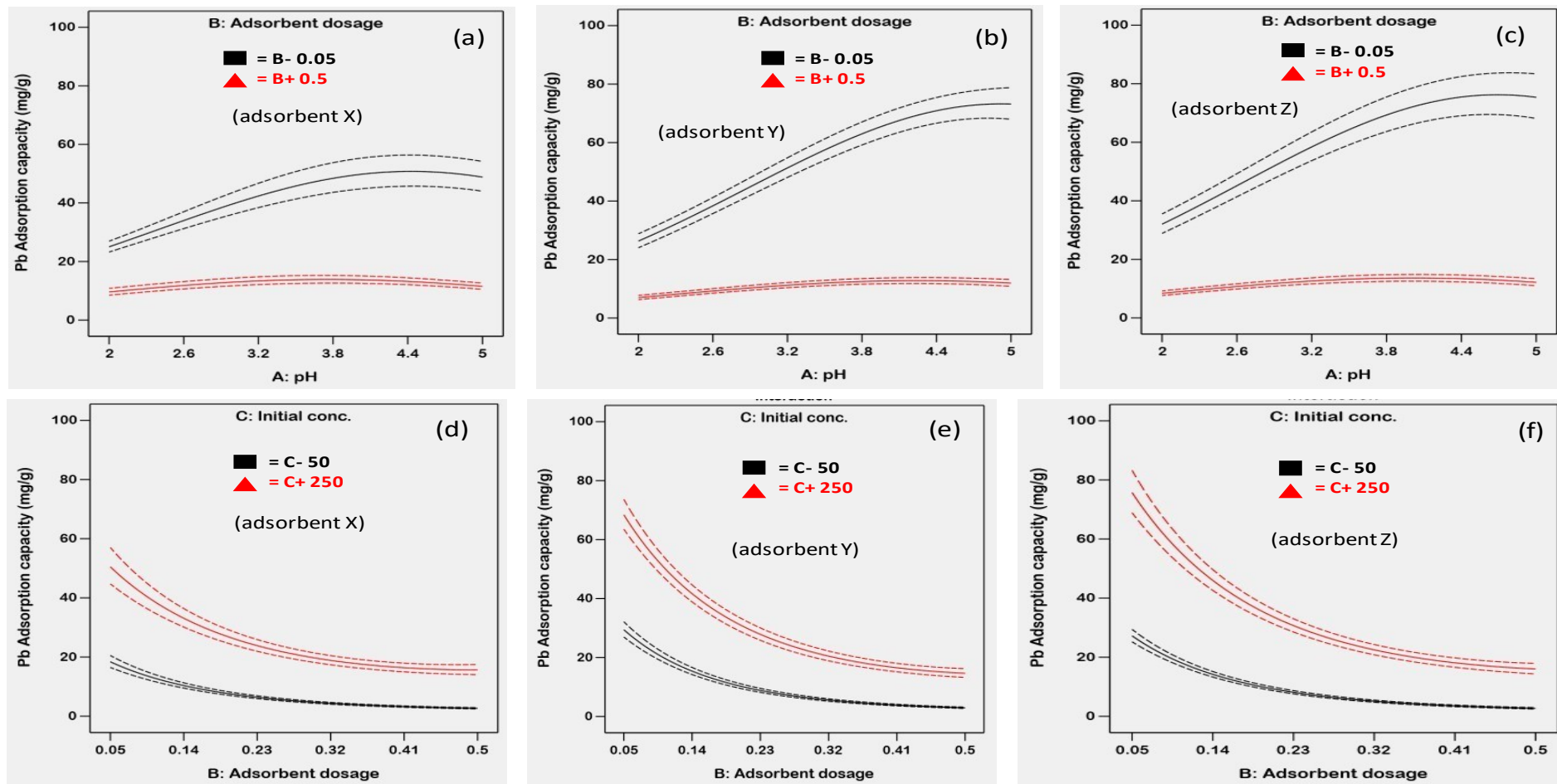
Figure 5.5: Graphs showing two-factor interactions and their effects on the Pb(II) adsorption capacity onto 90%Bt-10%Ch-1 composites/beads

Note: these graphs were plotted and obtained from Design-Expert®13; dashed lines represent 95% confidence interval bands of the experimental data; adsorbent X, Y and Z represent Bt-Ch composites, beads-A and beads-B, respectively. *S*imilar trends were observed for 70%Bt-30%Ch-1, 50%Bt-50%Ch-1, 90%Bt-10%Ch-2, 70%Bt-30%Ch-2, 50%Bt-50%Ch-2 composites/beads.
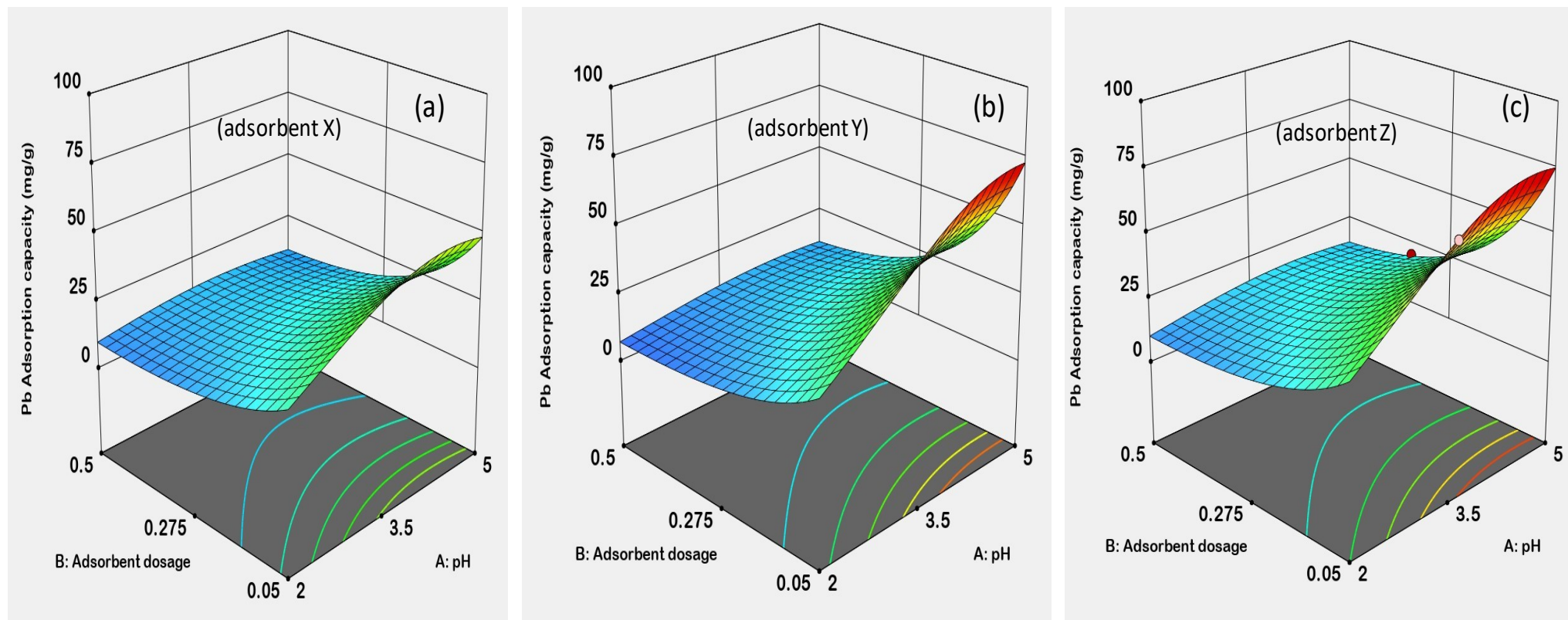
Figure 5.6: 3D response surface plot for the interaction effect of pH and adsorbent dosage (at constant 200 mg/L initial conc.) on Pb (II) adsorption capacity (a, b & c) for 90%Bt-10%Ch-1 composites, beads-A and beads-B, respectively

Note: these 3D surface plots were plotted and obtained from Design-Expert®13; similar trends were observed for 70%Bt-30%Ch-1, 50%Bt-50%Ch-1, 90%Bt-10%Ch-2, 70%Bt-30%Ch-2, 50%Bt-50%Ch-2 composites/beads
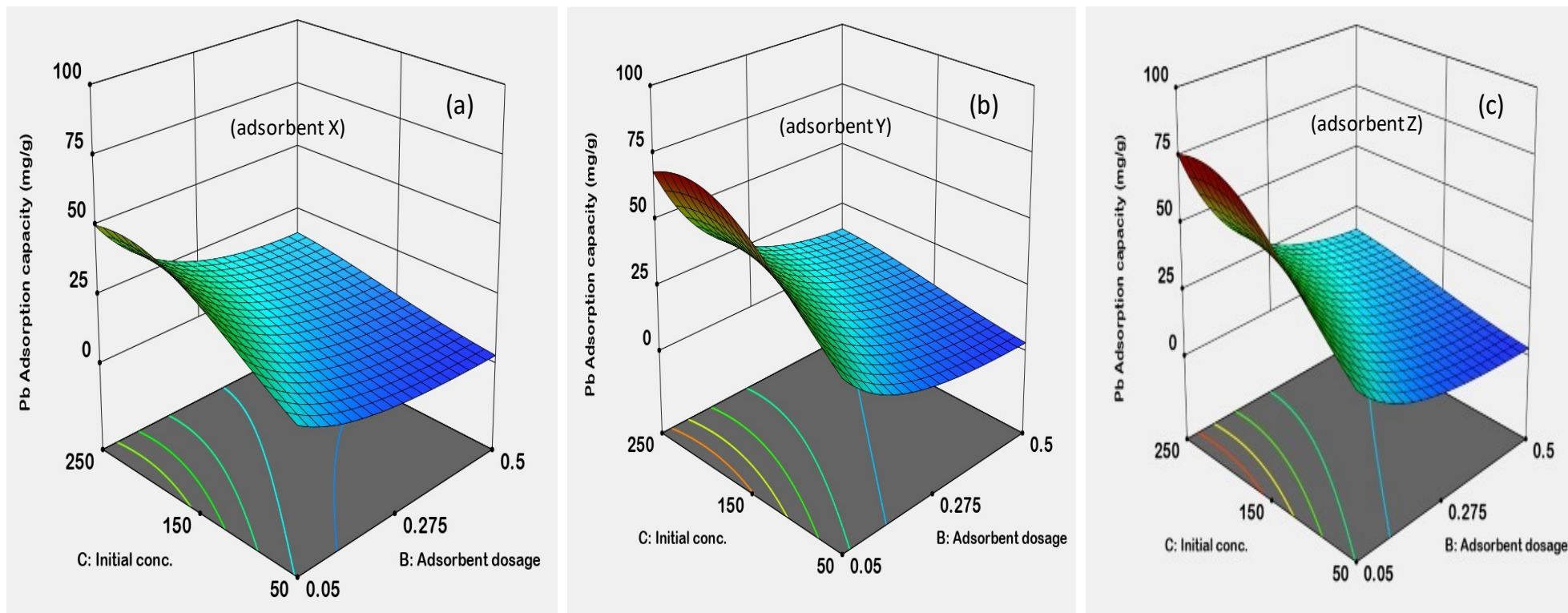
Figure 5.7: 3D response surface plot for the interaction effect of Initial conc. and adsorbent dosage (at constant pH 5) on Pb (II) adsorption capacity (a, b & c) for 90%Bt-10%Ch-1 composites, beads-A and beads-B, respectively

Note: these 3D surface plots were plotted and obtained from Design-Expert®13; similar trends observed for 70%Bt-30%Ch-1, 50%Bt-50%Ch-1, 90%Bt-10%Ch-2, 70%Bt-30%Ch-2, 50%Bt-50%Ch-2 composites/bead

5.3.2.4 *Optimisation of parameters for Pb(II) adsorption by Bt-Ch composite/beads*

A numerical optimisation was performed to determine the optimum point for the Pb(II) adsorption capacity (mg/g) by setting the target values of pH, adsorbent dosage, initial Pb(II) concentration, and selecting the specific adsorbents. The obtained optimal experimental conditions (selected by the models) estimated for the adsorption of Pb (II) by Bt-Ch-1 and Bt-Ch-2 composites/beads were pH of 4.5 and adsorbent dose of 0.05 g. The initial Pb (II) concentrations varied slightly, and therefore a harmonised value (i.e., 150 mg/l) was chosen and used. At these conditions, the predicted optimum Pb(II) adsorption capacity (mg/g) for Bt-Ch-1 and Bt-Ch-2 composites/beads are shown in Figure 6.7A and 6.7B, respectively. The optimum adsorption capacity estimated for both 90%Bt-10%Ch-1 and 70%Bt-30%Ch-1 beads (A & B) is higher compared to corresponding composites. However, 50%Bt-50%Ch-1 composites show a slightly higher adsorption capacity compared to corresponding beads-A (but lower compared to beads-B). Concerning all Bt-Ch-2 samples, the predicted adsorption capacity (mg/g) estimated for beads (A & B) is higher compared to corresponding composites. These results show some correlation towards the amount of chitosan present in each of the composites or beads as evidenced by TGA analysis (Figure 4.4; Section 4.3.2), which accounts for more adsorption sites (probably amine groups of chitosan) available on the surface of the beads or composites. The comparison of optimum adsorption capacity values obtained for various Bt-Ch composites and beads is only tentative, as this will be confirmed during the equilibrium isotherm modelling where the maximum adsorption capacity (Q_{max}) of respective adsorbents will be determined and compared.

In summary, additional experimental runs were performed to confirm the robustness of the predicted model under these optimal conditions (selected above). As shown in Table 5.3, the results obtained were within the accuracy and precision of the design space (95% for both prediction and confidence intervals), which indicates adequate predictability of the model for the response analysed.
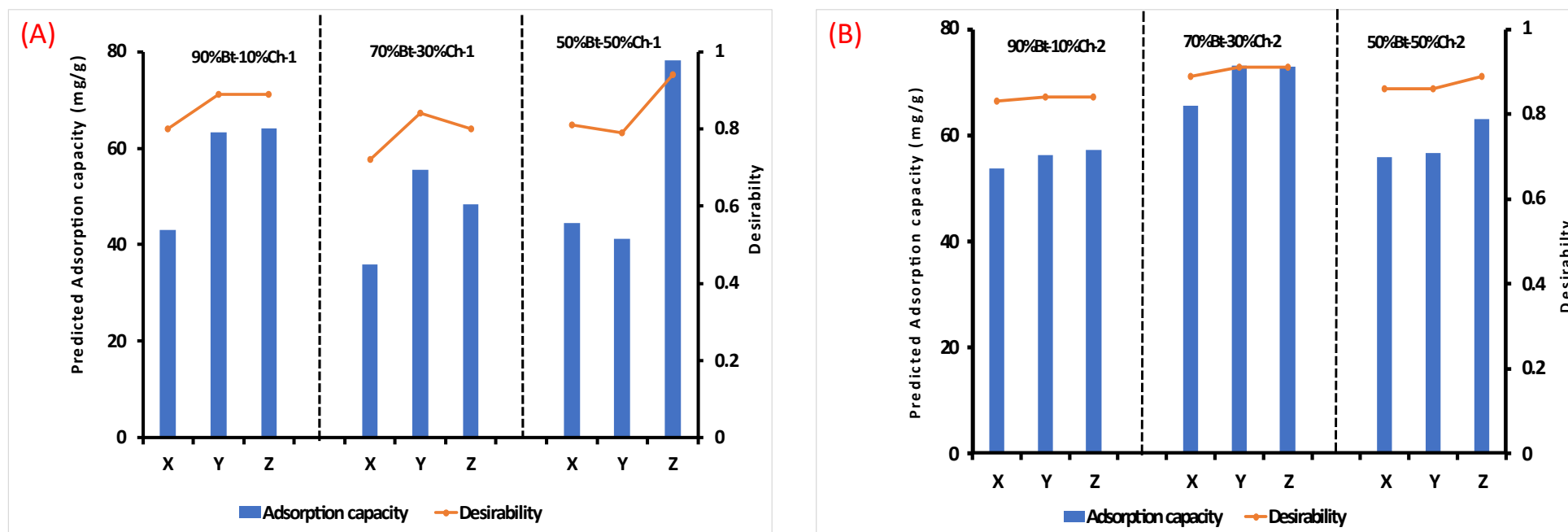
Figure 5.8: Charts showing predicted optimum Pb(II) adsorption capacity (mg/g) for (A) Bt-Ch-1 and (B) Bt-Ch-2 composites/beads

Table 5.3: Confirmation of experimental runs for analysed Optimal-I design model (Pb-adsorption capacity)

Adsorbent type	Target	Predicted Mean	Desirability	Confirmation experiment	Confidence Interval (95%)	
					Low	High
90%Bt-10%Ch-1 (X)	Maximize	42.95 ± 1.99	0.79	44.29 ± 1.99	38.29	48.08
70%Bt-30%Ch-1 (Y)	Maximize	55.45 ± 5.52	0.84	45.82 ± 0.66	45.79	66.49
50%Bt-50%Ch-1 (Z)	Maximize	78.25 ± 8.15	0.94	65.58 ± 2.42	61.62	93.31
90%Bt-10%Ch-2 (X)	Maximize	53.79 ± 7.11	0.83	55.23 ± 2.50	41.09	69.20
70%Bt-30%Ch-2 (Y)	Maximize	73.07 ± 15.52	0.91	58.81 ± 0.26	49.32	103.57
50%Bt-50%Ch-2 (Z)	Maximize	62.99 ± 4.44	0.89	56.47 ± 0.71	54.53	72.41

X = composites; Y = beads-A; Z = beads-B; pH = 4.5; adsorbent dose = 0.05 g; Initial concentration = 150.0 mg/L. For confirmation experiment, each value represents mean ± standard deviation of three (3) different samples (n = 3)

5.3.2.5 *Comparison of Pb uptake by pristine bentonite clay and Bt-Ch composites/beads*

To compare the Pb(II) adsorption capacity of pure bentonite with those of the prepared Bt-Ch composites/beads, a batch adsorption experiments were conducted with pure Na-bentonite as an adsorbent. The design experimental conditions (i.e., experimental run #1, #2, and #3, as Tabulated in Appendix B2) were used to perform this experiment. As demonstrated in Figure 5.9, a major limitation noted when using pristine bentonite clay as an adsorbent for Pb(II) adsorption was difficulty in recovery of clay particles after adsorption process, centrifugation was required to recover the clay particles.

 From the results of experimental runs #1, #2, and #3, the corresponding Pb uptake (mg/g) obtained for Na-bentonite were found to be 8.05, 0.59 and 1.57 mg/g, respectively (Figure 5.10A and 5.10B). The adsorption capacity (mg/g) using the same experimental conditions for all Bt-Ch-1 composites/beads were obtained and shown in Figure 5.10A (also check Appendix B3), and these show similar trends to those of Bt-Ch-2 composites/beads (Figure 5.10B., Appendix B4). A comparison between these data shows some drastic improvement in Pb(II) uptake by Bt-Ch beads/composites (about 50% more) when compared to pristine Na-bentonite.
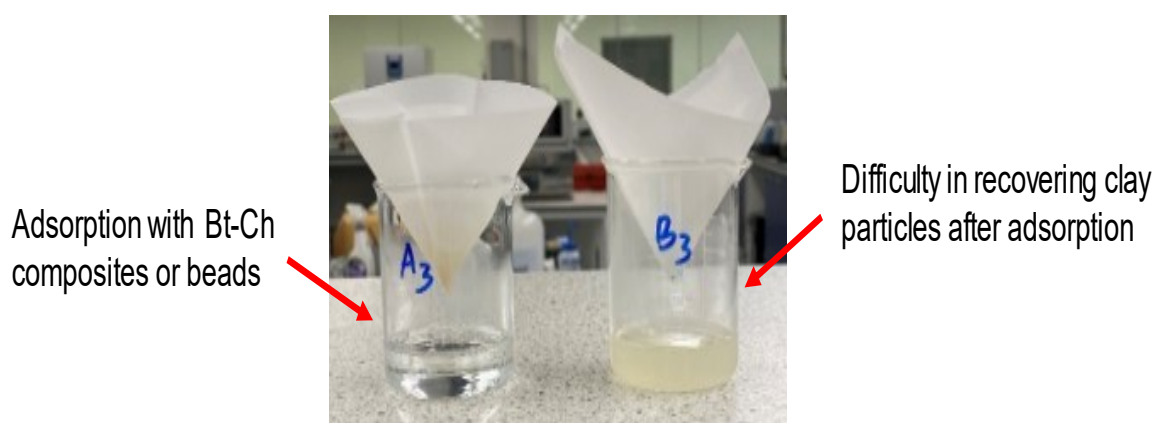
Figure 5.9: Filtration after batch adsorption experiments

119
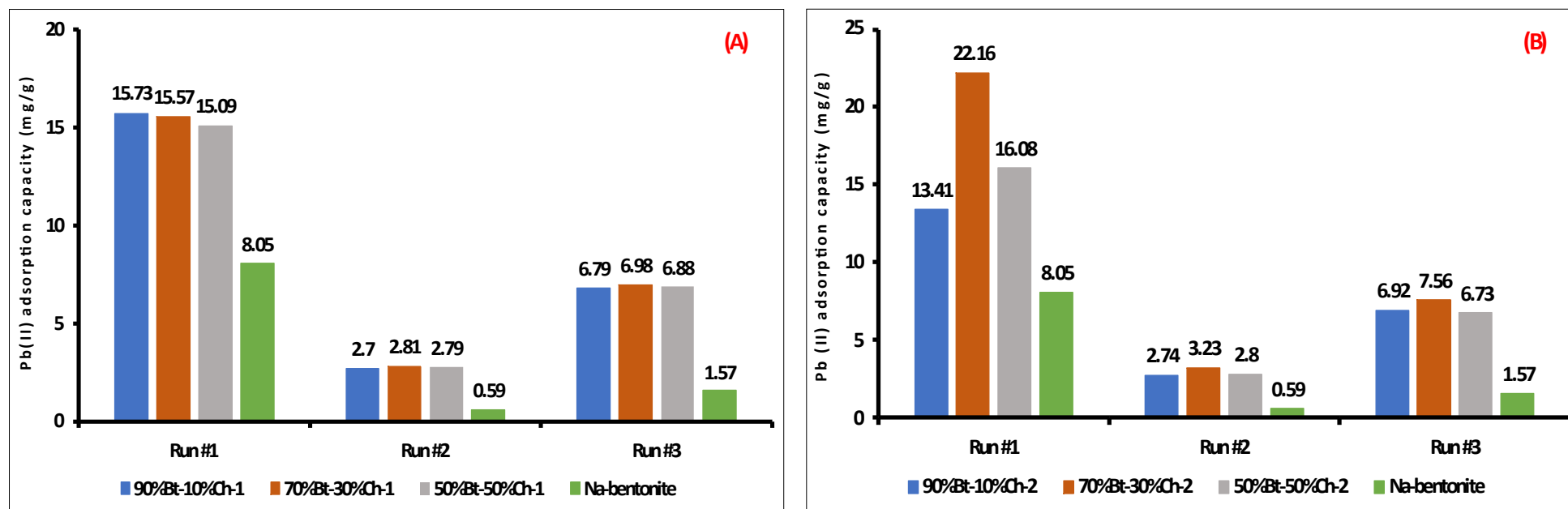
Figure 5.10: Charts showing the Pb (II) adsorption capacities (mg/g) of Na-bentonite as compared to values obtained for (A) Bt-Ch-1 and (B) Bt-Ch-2 composites/beads

Note: The experimental conditions of pH 3.5, 3.5, 5.0; an adsorbent dose of 0.28, 0.5, 0.2g; and initial Pb (II) concentration of 150, 50, 50mg/l for experimental run #1, #2, and #3, respectively (Appendix B2), were used to perform this experiment.

5.3.3. Adsorption equilibrium and isotherms modelling

Adsorption isotherms were obtained by fitting experimental data to both Langmuir and Freundlich equations. Figure 5.11 illustrates both Langmuir and Freundlich isotherm models for Pb (II) adsorption by 90%Bt-10%Ch-1 composites, and the same plots for all the adsorbents vis; 90%Bt-10%Ch, 70%Bt-30%Ch, 50%Bt-50%Ch composites/beads are presented in Appendix B12, B13 and B14, respectively. The values (or constants) obtained from these isotherms modelling for all the adsorbent samples(i.e., Bt-Ch-1 and Bt-Ch-2 composites/beads), are presented in Table 5.4 and 5.5, respectively. The Non-linear chi-square (X^2) was employed to access the quality of the fits concerning the isotherm modelling of the adsorption of Pb(II) ions onto Bt-Ch-1 and Bt-Ch-2 composites/beads. Very low values (e.g., close to zero) indicate that experimental data is very close to data obtained using a model, and vice versa [116]. In addition, the equilibrium data obtained from adsorption of Pb(II) ions (onto Bt-Ch-1 and Bt-Ch-2 composites/beads) correlated well with both Langmuir and Freundlich isotherms studied (correlation coefficient, R^2 = 0.999), indicating that under these experimental conditions, both monolayer and heterogeneous adsorption processes may coexist. This sometimes happens when the adsorbent has various functional groups, which provide active sites for the adsorbate of interest. The adsorption process occurs until a monolayer coverage occurs, as explained by the Langmuir model, but due to the different affinity of functional groups for metal ions from aqueous solution, the experimental data also fit well with the Freundlich isotherm model. This is similar to a previous study conducted by Ngah and Fatinathan [200], they observed that the equilibrium data obtained for Pb (II) biosorption (onto chitosan and chitosan-GLA) fitted well for both Langmuir and Freundlich isotherm models.

The Langmuir constant 'K_L' is an indicator of the favourability of adsorption via determination of the separation factor (R_L). The R_L values were calculated using Equation 2.14 (Section 2.5.4.1) and are given in Table 5.4 and 5.5 for Pb(II) adsorption onto Bt-Ch-1 and Bt-Ch-2, respectively. R_L values reflect the favourability of adsorption, adsorption nature is either unfavourable ($R_L > 1$), linear ($R_L = 1$), favourable ($0 < R_L < 1$) or irreversible ($R_L = 0$) [116,138,143,144]. In this study, the values of R_L have been found to within the range of 0 to 1.0 for all the adsorbent used, showing that the adsorption

of Pb(II) ions by both Bt-Ch-1 and Bt-Ch-2 composites/beads is favourable under these experimental conditions.

The Q_{max} value which represents the maximum adsorption capacity of Pb(II) ions at monolayer coverage as determined through the Langmuir isotherm, was much higher for Bt-Ch-1 beads compared to their corresponding, weight ratio, composites. This is expected since more chitosan as evidenced from TGA (Figure 4.4(A); Section 4.3.2) is present in the beads, and therefore, more possible active sites through the chitosan are available for Pb (II) adsorption. Similar Q_{max} values may be anticipated for both beads-A and beads-B because of the similar amounts of chitosan present, however this is not the case. The Q_{max} values obtained for beads-A are lower than those of the corresponding beads-B. This suggests that the distribution of chitosan within the interlayer space or external surfaces of the bentonite clay as evidenced by XRD results (Figure 4.5(A); Section 4.3.3) can affect Pb (II) uptake. XRD results indicate more chitosan is intercalated within the clay interlayers for beads-A, than for beads-B, and thus infers less chitosan is available for the adsorption of Pb ions. The more active sites for Pb(II) adsorption are therefore located with chitosan on external surfaces. In addition, the Qmax increases for beads-B with chitosan loading but not for beads-A (or composites). This confirmed that the chitosan available on the clay surface contributed more to Pb adsorption.

Except for 90%Bt-10%Ch-2 beads-A, the obtained Q_{max} values were much higher for all other Bt-Ch-2 beads samples compared to their corresponding, weight ratio, composites. The comparison of the Q_{max} values obtained for both beads-A and beads-B of Bt-Ch-2 samples (Table 5.3) show similar trends to those obtained for Bt-Ch-1 beads (Table 5.2). On the other hand, the Q_{max} values obtained for Bt-Ch-2 composites samples (Table 5.3) were much higher (compared to their corresponding Bt-Ch-1 composites), even though there is less chitosan present in Bt-Ch-2 composites (compared to corresponding Bt-Ch-1 composites) as evidenced by TGA (Figure 4.4; Section 4.3.2). This shows that there is no correlation between the Q_{max} values and the quantity of chitosan present in the Bt-Ch composites samples. Overall, the higher Pb(II) adsorption capacities were observed for Bt-Ch-2 samples compared to corresponding Bt-Ch-1 adsorbents. This may be due to a higher degree of deacetylation (DD) of Chitosan-2,

and it has been reported that, chitosan biopolymers with more DD, will contains more free amine (−NH$_2$) groups on their polymer structures [208].

To assess the respective contribution of either bentonite or chitosan towards Pb-adsorption in the composites and beads, the expected Q$_{max}$ due to the fraction of chitosan in the composites or beads were estimated from the Q$_{max}$ of 100% chitosan. The Q$_{max}$ due to 100% chitosan-1 and chitosan-2 were found to be 116.97 ± 2.14 and 119.06 ± 3.24 mg/g, respectively (see Appendix B15). As you can see (from Appendix B16), the general observation is that the amounts of Pb adsorbed by the composites and beads is considerably more than that anticipated from chitosan alone, therefore it suggests either the bentonite clay also contributes towards Pb(II) adsorption or there is a synergistic adsorption mechanism between bentonite and chitosan enhancing Pb(II) adsorption. The contribution of a cation exchange mechanism with the resident cations on the bentonite is discussed further below.

The Q$_{max}$ values obtained from adsorption of Pb (II) with Bt-Ch-1 and Bt-Ch-2 composites/beads were compared with other adsorbents reported in the literature (Table 5.6), and the higher adsorption capacities indicates that Bt-Ch composites/beads could serve as potential and better adsorbent. Futalan et al. (2011) [89] studied the removal of Pb(II) ions from a single-component solution using chitosan-immobilized-on-bentonite, which had an inferior Q$_{max}$ value (26.39 mg/g), but a similar optimum pH range as obtained in this study. Although, they reported that the adsorbent used was prepared in the weight ratios of 95% bentonite clay and 5% chitosan biopolymer. This may account for lower Pb(II) uptake (mg/g) because less chitosan present in the composite (compared to composites prepared in this study). Moreover, their procedure seems time-consuming, as it took about 4 hours to attain removal equilibrium at higher concentration of Pb(II) ions. In this study, the adsorption of Pb(II) ions onto Bt-Ch composites/beads was very fast and reached equilibrium within 10 - 60 minutes. In another study, Tirtom et al. (2012) [209] reported the removal of Pb(II) ions using crosslinked chitosan-clay composite beads with maximum removal capacity (Q$_{max}$) of 7.93 mg/g, which is quite smaller compared to the results obtained in this study. Beside the low loading capacity, crosslinking of the chitosan-clay composites could be relatively costly as an adsorbent for removal of metal ions. Hu et al., (2017) [91] demonstrated

the removal of Pb(II) ions from a single-component solution using montmorillonite-chitosan composite, where the Q_{max} value was found to be 47.95 mg/g, but it took more than 3 hours to attain equilibrium. In this regards, Bt-Ch composites/beads represents a good alternative for Pb (II) removal, considering its high loading capacity, fast adsorption equilibrium, and easy preparation of the composites/beads.

The estimated adsorbent capacities (also referred to as Freundlich constant (K_F)) determined from the Freundlich isotherms, are generally high for all the Bt-Ch composites/beads concerning Pb (II) adsorption. The Freundlich constant (K_F) characterises the strength of the adsorption, and a higher K_F value indicates that higher loading of adsorbate (such as Pb (II) ions) onto adsorbent could be achieved [48]. The observed Freundlich exponent (n) values calculated fall within the range of 0 to 1, and since it is closer to zero, this implies that the surfaces of these adsorbents in contact with Pb (II) ions are heterogeneous, a value below unity also usually suggests a chemisorption process [138].
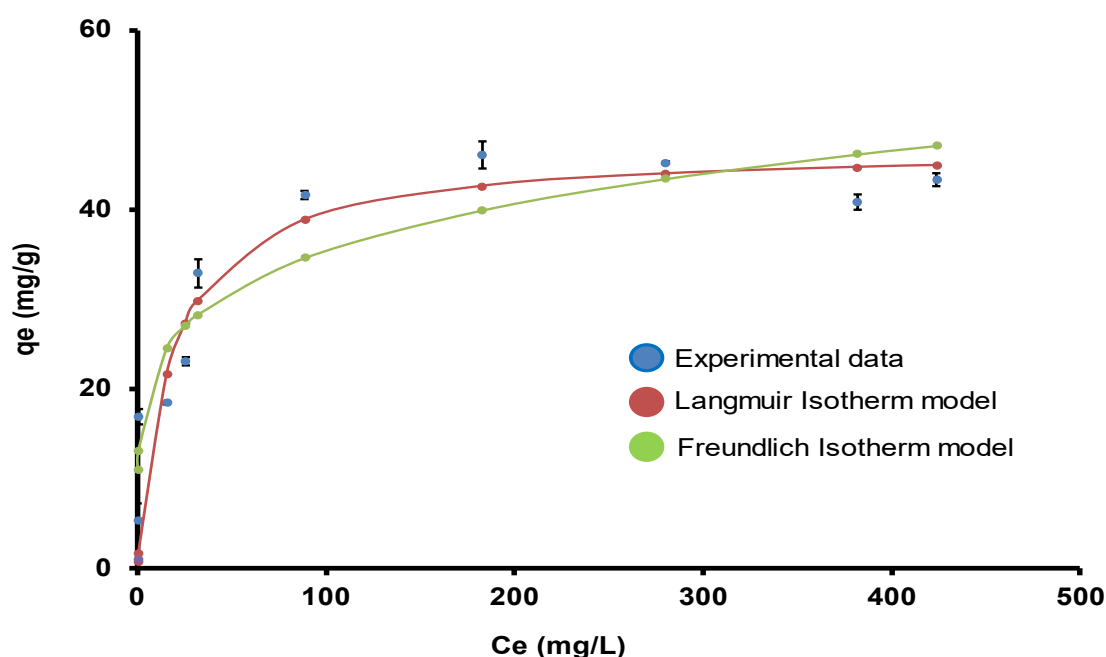
Figure 5.11: The non-linear Langmuir and Freundlich isotherms for adsorption of Pb (II) by 90%Bt-10%Ch composites (adsorbent X)

Note: pH = 4.5; adsorbent amount = 0.05 g; agitation time (at 230 rpm) = 60 minutes; Initial Pb concentrations = 10 - 500 mg/L; Each data-point represents mean ± standard deviation of three (3) different experiments (n = 3).

Table 5.4: The fitting parameters of Langmuir and Freundlich isotherms for the adsorption of Pb (II) onto Bt-Ch-1 composites or beads

Adsorbents	Langmuir					Freundlich			
	Q_{max}	K_L	R_L	R^2	X^2	K_F	n	R^2	X^2
90%Bt-10%Ch-1									
composites	46.60 ± 0.38	0.056	0.641-0.034	0.999	1.125	5.7×10^5	0.199	0.999	0.980
Beads-A	59.22 ± 0.47	0.851	0.105-0.002	0.999	0.928	3.7×10^{14}	0.130	0.999	1.120
Beads-B	69.21 ± 0.64	0.350	0.222-0.006	0.999	0.623	4.7×10^8	0.178	0.999	1.279
70%Bt-30%Ch-1									
composites	42.48 ± 4.22	0.052	0.658-0.037	0.999	0.865	1.3×10^5	0.211	0.999	0.567
Beads-A	53.60 ± 5.99	0.425	0.190-0.005	0.999	1.393	4.5×10^8	0.176	0.999	0.482
Beads-B	87.24 ± 2.22	0.073	0.578-0.027	0.999	3.076	6.9×10^4	0.282	0.999	0.644
50%Bt-50%Ch-1									
composites	40.73 ± 4.04	0.057	0.637-0.034	0.999	1.645	3.3×10^6	0.208	0.999	2.009
Beads-A	58.61 ± 2.81	0.020	0.833-0.091	0.999	1.655	3.5×10^2	0.336	0.999	1.853
Beads-B	94.60 ± 5.63	0.132	0.431-0.015	0.999	3.469	2.5×10^8	0.238	0.999	2.166

Note: Qmax (mg/g) is the maximum saturated monolayer adsorption capacity of an adsorbent, K_L is the Langmuir constant (L/mg), R_L is the separation constant (dimensionless), K_F is the Freundlich constant (L/g), n is the heterogeneity factor (unitless-ranging from 0 to 1), R^2 is the coefficient of correlation, and X^2 is nonlinear chi-square. Concerning K_L, K_F, n, and R^2, each value represents only average mean of three (3) different samples (n = 3). For Q_{max} each value represents mean ± standard deviation of three (3) different samples (n = 3). R_L values were calculated based on K_L and initial Pb (II) concentration, (C_O) ranging from $10 - 500$ mg/L.

Table 5.5: The fitting parameters of Langmuir and Freundlich isotherms for the adsorption of Pb (II) onto Bt-Ch-2 composites or beads

Adsorbents	Langmuir					Freundlich			
	Q_{max}	K_L	R_L	R^2	X^2	K_F	n	R^2	X^2
90%Bt-10%Ch-2 composites	60.98 ± 3.22	0.087	0.534-0.022	0.999	1.605	2.0×10^6	0.214	0.999	1.936
Beads-A	57.74 ± 3.23	0.624	0.138-0.003	0.999	0.640	4.5×10^9	0.154	0.999	0.961
Beads-B	91.88 ± 7.00	0.239	0.295-0.008	0.999	1.028	4.8×10^6	0.227	0.999	1.422
70%Bt-30%Ch-2 composites	64.38 ± 6.15	0.184	0.351-0.011	0.999	0.996	3.8×10^7	0.196	0.999	1.418
Beads-A	78.94 ± 10.15	0.300	0.250-0.007	0.999	1.526	3.5×10^8	0.207	0.999	1.581
Beads-B	95.58 ± 7.05	0.115	0.465-0.017	0.999	2.227	4.7×10^5	0.273	0.999	1.349
50%Bt-50%Ch-2 composites	60.95 ± 0.40	0.071	0.585-0.027	0.999	1.849	1.8×10^7	0.213	0.999	2.046
Beads-A	80.83 ± 0.30	0.034	0.746-0.056	0.999	1.175	4.5×10^4	0.325	0.999	0.664
Beads-B	96.60 ± 0.83	0.128	0.439-0.015	0.999	2.338	8.4×10^4	0.269	0.999	0.893

Note: Qmax (mg/g) is the maximum saturated monolayer adsorption capacity of an adsorbent, K_L is the Langmuir constant (L/mg), R_L is the separation constant (dimensionless), K_F is the Freundlich constant (L/g), n is the heterogeneity factor (unitless-ranging from 0 to 1), R^2 is the coefficient of correlation, and X^2 is nonlinear chi-square. Concerning K_L, K_F, n, and R^2, each value represents only average mean of three (3) different samples (n = 3). For Q_{max} each value represents mean ± standard deviation of three (3) different samples (n = 3). R_L values were calculated based on K_L and initial Pb (II) concentration, (C_O) ranging from 10 − 500 mg/L.

5.3.4. Effect of competing ions

To investigate the selectivity of Bt-Ch composites/beads towards Pb (II) ions, batch adsorption experiments were conducted in the presence of other competing ions using multi-component metal solutions containing Pb (II), Zn (II), Cu (II), Ni (II) and As (III) ions each with initial concentration of 0.45, 1.58, 1.59, 1.71 and 1.43 mmol/L respectively. These metal concentrations are actually the same in terms of mass concentration (i.e., 100 mg/L) but varies with molar concentration due to the molar mass of the respective metal ions. The removal percentages (%) of these metal ions from the multi-component solution by 90%Bt-10%Ch-1 and 90%Bt-10%Ch-2 are shown in Figure 5.12(A) and 5.12(B), respectively. Similar plots for the other adsorbents vis; 70%Bt-30%Ch and 50%Bt-50%Ch composites/beads are presented in Appendix B17 and B18, respectively.

One can see that the adsorption of Pb(II) from multi-component solution by Bt-Ch composites/beads was significantly affected by the presence of other competing ions, and the calculated removal efficiency showed a lower value compared to that from a single component Pb(II) solution (Appendix B19). This is because available adsorption sites on these adsorbents cannot accommodate all these metal ions at the same time. Pb showed highest removal percentages for 90%Bt-10%Ch, 70%Bt-30%Ch and 50%Bt-50%Ch composites and 90%Bt-10%Ch beads-A & beads-B, showing high affinity towards Pb, even in the presence of other competing ions. The common observation from these adsorbents is that they contain less chitosan in their composition as evidenced by TGA (Figure 4.4; Section 4.3.2). Cu showed highest removal percentages with the adsorbents; 70%Bt-30%Ch and 50%Bt-50%Ch beads-A & beads-B and these adsorbents contain more chitosan. It has been reported that among all the transition metals, Cu forms the most stable complexes with glucosamine (a monomer of chitosan biopolymer), and this correlates with the higher adsorption efficiency of Cu(II) ions by Bt-Ch beads [210]. Also, a binary adsorption study carried out by Ngah and Fatinathan (2009), showed that chitosan-triphosphate beads had higher affinity for Cu(II) ions in comparison to Pb(II) ions [199]. They reported that Cu(II) ions seem to be a stronger competitor, and its presence significantly depressed the adsorption of Pb(II) ions [199]. In general, the fact that the amount of Pb adsorbed by these adsorbents is reduced, the

overall total metal ion concentration adsorbed is more than that of Pb adsorbed when present alone.

Table 5.6: Comparisons of Pb (II) adsorption capacity by Bt-Ch composites/beads with other similar adsorbents

Adsorbents	pH; Equilibrium time	Q_{max} (mg/g)	Ref.
Na-Montmorillonite	≥ 5.5; --	9.58	[70]
Chitosan saturated Montmorillonite	5.0; 3hrs	47.45	[91]
Chitosan-clay composite beads	4.5; 1hr 20mins	7.93	[209]
Montmorillonite-TOA	7.0; 1hr 20mins	33.01	[211]
Chitosan-coated sand	6; 4hrs	8.18	[212]
Chitosan immobilized on bentonite (CHB)	4; 4hrs	26.39	[89]
Chitosan	4.5;	34.98	[200]
Chitosan-GLA	4.5;	14.24	[200]
Chitosan-alginate beads	4.5;	60.27	[200]
Chitosan-triphosphate beads	4.5; 1hr 40 mins	57.33	[199]
90%Bt-10%Ch-1 composites	4.5; 1hr	46.60 ± 0.38	this study
90%Bt-10%Ch-1 beads-A	4.5; 1hr	59.22 ± 0.47	this study
90%Bt-10%Ch-1 beads-B	4.5; 1hr	69.21 ± 0.64	this study
70%Bt-30%Ch-1 composites	4.5; 1hr	42.48 ± 4.22	this study
70%Bt-30%Ch-1 beads-A	4.5; 1hr	53.60 ± 5.99	this study
70%Bt-30%Ch-1 beads-B	4.5; 1hr	87.24 ± 2.22	this study
50%Bt-50%Ch-1 composites	4.5; 1hr	40.73 ± 4.04	this study
50%Bt-50%Ch-1 beads-A	4.5; 1hr	58.61 ± 2.81	this study
50%Bt-50%Ch-1 beads-B	4.5; 1hr	94.60 ± 5.63	this study
90%Bt-10%Ch-2 composites	4.5; 1hr	60.98 ± 3.22	this study
90%Bt-10%Ch-2 beads-A	4.5; 1hr	57.74 ± 3.23	this study
90%Bt-10%Ch-2 beads-B	4.5; 1hr	91.88 ± 7.00	this study
70%Bt-30%Ch-2 composites	4.5; 1hr	64.38 ± 6.15	this study
70%Bt-30%Ch-2 beads-A	4.5; 1hr	78.94 ± 10.2	this study
70%Bt-30%Ch-2 beads-B	4.5; 1hr	95.58 ± 7.05	this study
50%Bt-50%Ch-2 composites	4.5; 1hr	60.95 ± 0.40	this study
50%Bt-50%Ch-2 beads-A	4.5; 1hr	80.83 ± 0.30	this study
50%Bt-50%Ch-2 beads-B	4.5; 1hr	96.60 ± 0.83	this study

TOA = tri-n-octylamine; GLA = Glutaraldehyde
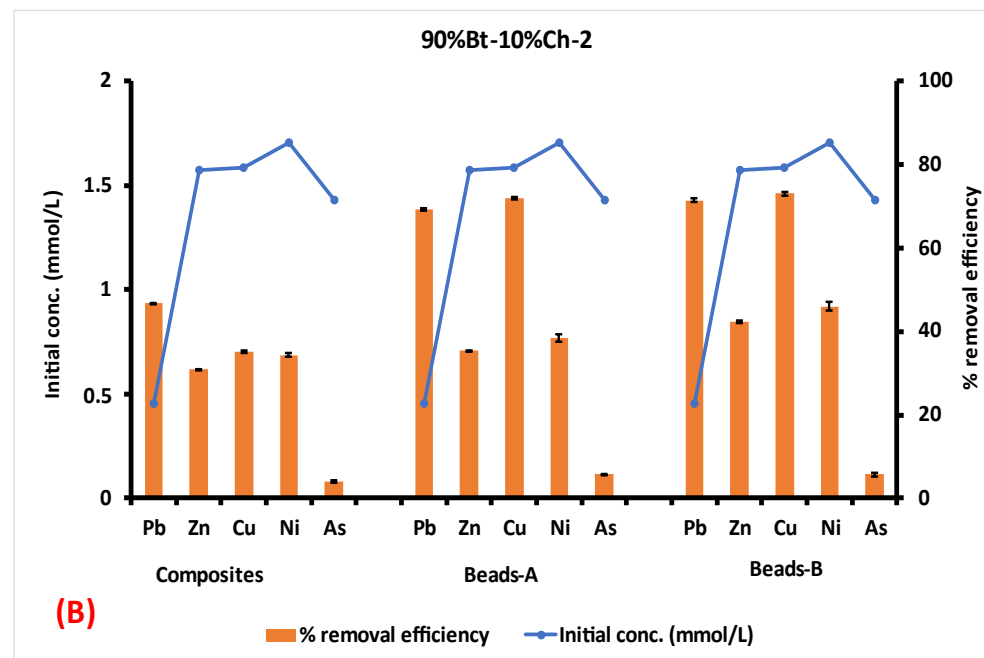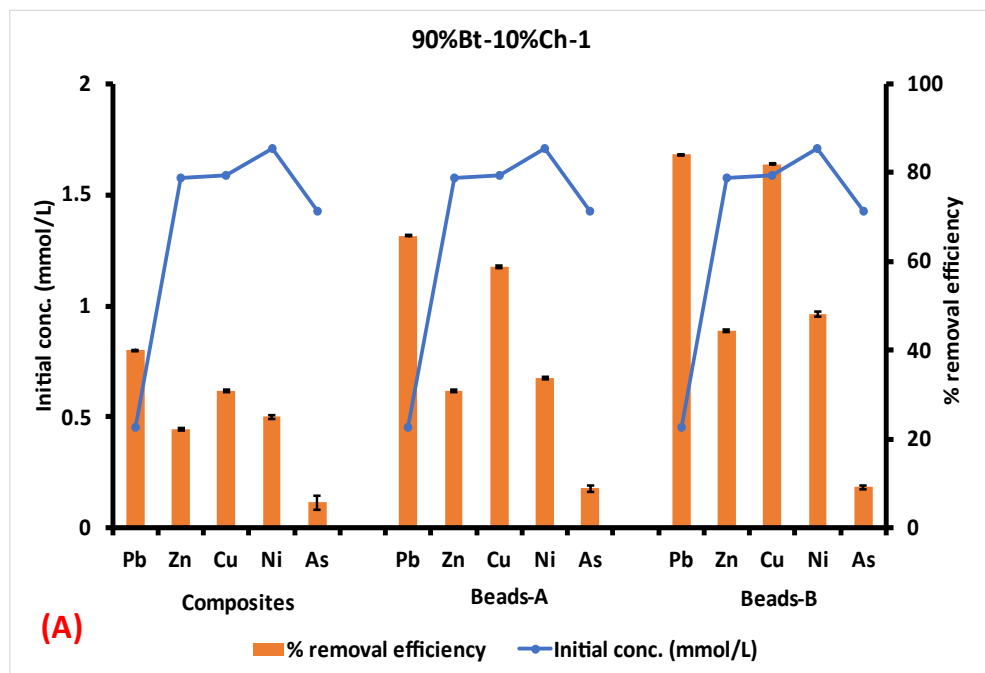
Figure 5.12: Charts showing the % removal efficiency of various metal ions from multi-component solutions by (A) 90%Bt-10%Ch-1 and (B) 90%Bt-10%Ch-2 composites/beads

Note: In multi-component solution, the initial concentrations of Pb, Zn, Cu, Ni, and As were 0.45, 1.58, 1.59, 1.71 and 1.43 mmol/L respectively. These metal concentrations are actually the same in terms of mass concentration (i.e., 100 mg/L) but varies with molar concentration due to the molar mass of the respective metal ions; pH = 4.5; adsorbent amount = 0.2 g; agitation time (at 230 rpm) = 60 minutes. Each bar represents mean ± standard deviation of three (3) different samples (n = 3)

5.3.5. Desorption studies and characterisation of regenerated Bt-Ch composites/beads

An appropriate adsorbent must not only be effective and have good adsorption capacity it should also have good potential for subsequent easy removal of metal ions [68,197]. Therefore, the desorption (recovery) of adsorbed Pb(II) ions and regeneration of Bt-Ch composites/beads were investigated. The results for the desorption (recovery) of adsorbed Pb(II) ions by different HCl and EDTA concentrations ranging from 1.0×10^2 to 2.0×10^3 mmol/L and 1.0 to 5.0×10^2 mmol/L, respectively (corresponding to 1.0×10^2 to 2.0×10^3 mEq/L and 1.0 to 5.0×10^2 mEq/L, respectively). The optimal recovery of Pb(II) ions was achieved with a 1.0×10^3 mmol/L HCl or 1.0×10^1 mmol/L EDTA aqueous solutions (corresponding to 1.0×10^3 mEq/L HCl or 1.0×10^1 mEq/L EDTA). Also, this concentration of HCl was chosen because chitosan is highly unlikely to be soluble, as demonstrated in our preliminary dissolution experiments.

Regarding HCl (1.0×10^3 mEq/L) as a desorbing agent, the Pb (II) adsorption and desorption percentages recovered from 90%Bt-10%Ch-1 composites/beads are shown in Figure 5.13. The adsorption-desorption plots for all the adsorbent samples (I.e., Bt-Ch-1 and Bt-Ch-2 composites/beads) are presented in Appendix B20 and B21, respectively. The desorption percentages in the 1st cycle observed for all the adsorbents was above 80%. This value, though slightly lower compared to adsorption percentages (about 90 to 99%), still portrayed good recoveries. For practical applications, it is imperative to investigate the stability of the same adsorbent by re-using it in multiple regeneration processes (adsorption-desorption cycles) [68,197]. In this regard, serial adsorption-desorption steps were conducted up to five times, and the observed percentages obtained for both adsorption and desorption of Pb (II) ions remained similar as those obtained for the first initial adsorption-desorption cycle. This indicates that all the used adsorbents were stable without apparent loss of the adsorption capacity up to at least 5 cycles. Similar trends were observed for all other adsorbents, excluding 90%Bt-10%Ch-2 and 50%Bt-50%Ch-2 composites samples. Although the desorption percentages obtained for both 90%Bt-10%Ch-2 and 50%Bt-50%Ch-2 composites samples remained steady, the adsorption of Pb (II) ions decreased significantly from

stage one to five. Even though a small amount of Pb (II) remains bound to Bt-Ch composites/beads after each desorption process, the subsequent adsorption process was excellent, effective and remained the same. The moderate consistency of the removal efficiency (%) observed for all adsorbents could be attributed to the sufficient active sites (such as amino groups of chitosan) available for each successive adsorption. This implies that, chitosan is still present in the regenerated Bt-Ch composites/beads.

In terms of EDTA (1.0×10^1 mEq/L) as a desorbing agent, the Pb (II) adsorption and desorption percentages recovered from 90%Bt-10Ch-1 composites/beads are shown in Figure 5.14. The adsorption-desorption plots for all the adsorbent samples (I.e., Bt-Ch-1 and Bt-Ch-2 composites/beads) are presented in Appendix B22 and B23, respectively. Generally, a better desorption percentage (about 90 to 99%) were achieved with EDTA (compared with HCl), and these values are higher compared to adsorption percentages which indicates excellent recoveries of Pb(II) ions.

Overall, the results indicated that the Bt-Ch composites/beads exhibited good reusability and can be recovered for consecutive uses.
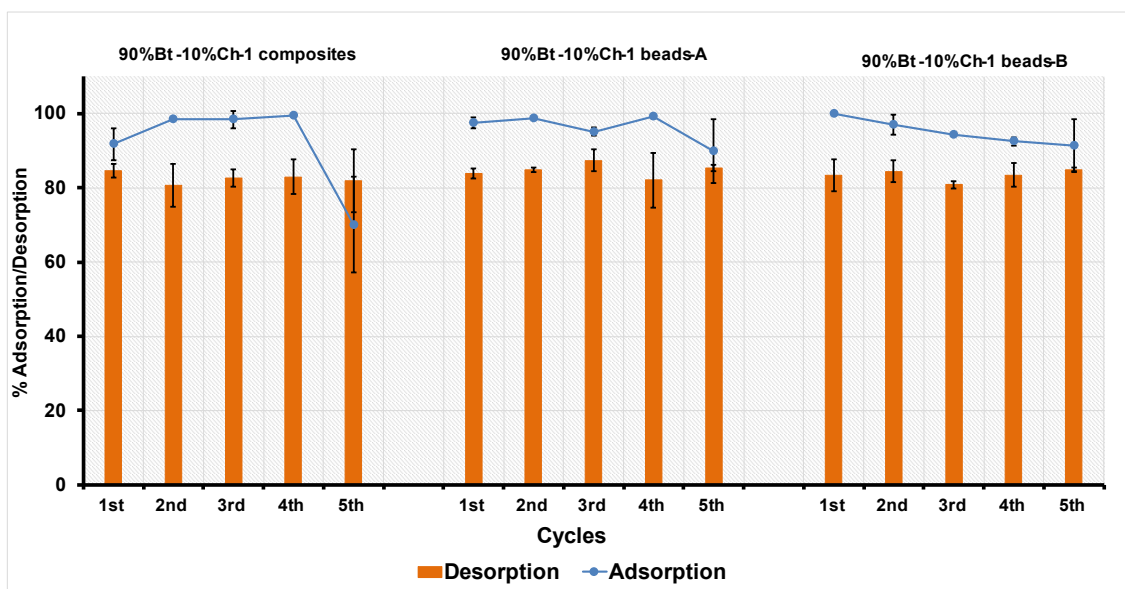
Figure 5.13: Charts showing the serial % Adsorption/Desorption of Pb (II) ions adsorbed onto 90%Bt-10%Ch-1 composites/beads.

Note: Initial Pb(II) concentrations = 1.44 mEq/L (corresponding to 150 mg/L); pH = 4.5; adsorbent amount = 0.2 g; adsorption agitation time (at 230 rpm) = 10 minutes; **desorbing agent = HCl (1.0×10^3 mEq/L)**; desorption agitation time (at 230 rpm) = 120 minutes. Each bar represents mean ± standard deviation of three (3) different samples (n = 3).
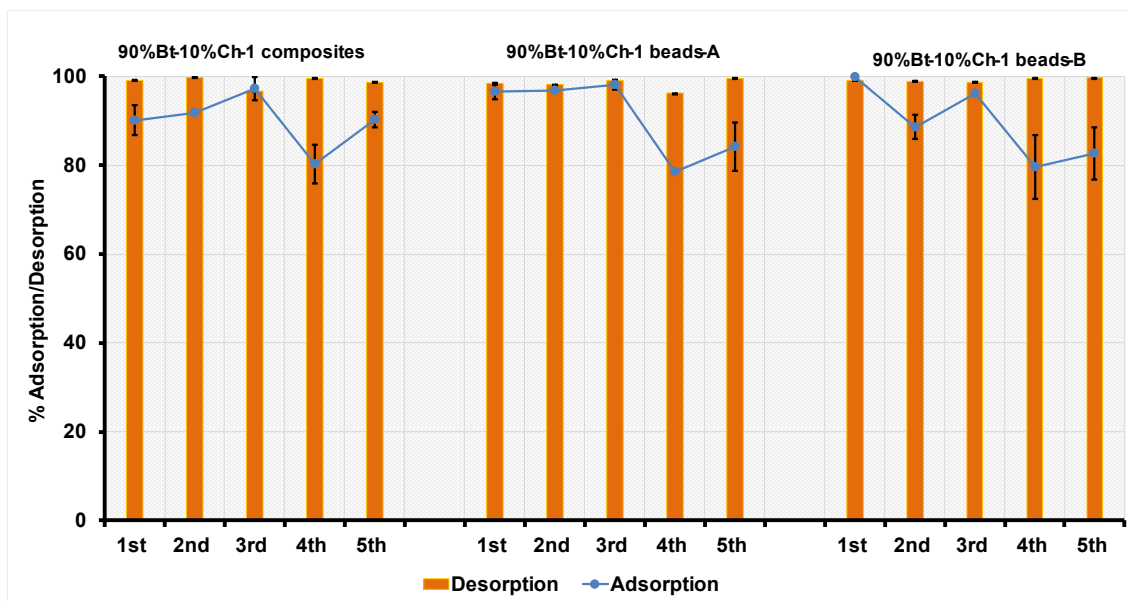
Figure 5.14: Charts showing the serial % Adsorption/Desorption of Pb (II) ions adsorbed onto 90%Bt-10%Ch-1 composites/beads

Note: Initial Pb(II) concentrations = 1.44 mEq/L (corresponding to 150 mg/L); pH = 4.5; adsorbent amount = 0.2 g; adsorption agitation time (at 230 rpm) = 10 minutes; **desorbing agent = EDTA (1.0 x 10^1 mEq/L);** desorption agitation time (at 230 rpm) = 120 minutes. Each bar represents mean ± standard deviation of three (3) different samples (n = 3).

5.3.6. Adsorption mechanism

In this study, only the adsorbent samples of Bt-Ch-1 composites/beads were used. To help further understand the adsorption mechanism of Pb(II) ions on Bt-Ch composites/beads, changes in the pH of the Pb (II) solution were measured before and after the adsorption process. It was observed that the pH of the solution increased after the adsorption of Pb (II) ions for all the adsorbents (from the adjusted pH of 4.5 ± 0.2 to 5.8 ± 0.9). A similar observation was also obtained by Ngah and Fatinathan [200], when they studied the sorption of Pb (II) ions onto chitosan (and its derivatives). From the control experiments (containing only adsorbents and no Pb) pHs of 6.5 ± 0.2 and 7.4 ± 0.2 were observed for Bt-Ch composites and beads, respectively. Therefore, the observed increased pH of the Pb (II) solution (after adsorption) might not be due to a decrease in the hydronium (H^+) ions concentration, but because of a pH contribution from the adsorbents used. Thus, ruling out the ion-exchange mechanism for the adsorption of Pb(II) ions onto Bt-Ch composites/beads becomes more difficult, and therefore, further investigation is required. [213,214].

The ion-exchange mechanism of the bentonite was further considered with regards to the ratio of heavy metals ions (Pb^{2+}) adsorbed onto the adsorbent to the total sum of light metal ions (Ca^{2+}, Mg^{2+}, Na^+, K^+) potentially released during adsorption process. These light metal ions can be typically found as exchangeable cations on bentonites. The mathematical ratio equation (abbreviated as $R_{b/r}$) was given by Sciban et al., [198]:

$$R_{b/r} = \frac{[Pb^{2+}]}{[Ca^{2+}] + [Mg^{2+}] + \frac{[Na^+]}{2} + \frac{[K^+]}{2} + \frac{[H^+]}{2}} \tag{5.18}$$

In Equation 5.18, the concentrations of all cations involved are expressed in mmol/L. The adsorption process is predominantly an ion-exchange mechanism when the $R_{b/r}$ value is equal to unity, while a higher $R_{b/r}$ value indicates that the sum of cations released is smaller compared to the amount of Pb (II) ions adsorbed [198–200]. The calculated $R_{b/r}$ values obtained for adsorption of Pb (II) ions onto Bt-Ch composites/beads are shown in Table 5.7. The calculated Rb/r values were less than 1.0 or close to unity for almost all the adsorbents. Although there are few cases where the estimated Rb/r values

were slightly greater than 1.0, this result indicates that the amount of Pb (II) ions adsorbed was slightly greater than (or equal to) the sum of the cations released. This proves that an ion-exchange mechanism with the bentonite plays some role in the adsorption of Pb (II) ions onto Bt-Ch composites/beads. At low initial Pb (II) concentration of 10 mg/L, lower $R_{b/r}$ values were observed for Bt-Ch beads compared to their corresponding composites. The graphs showing the simultaneous adsorption of Pb (II) ions and displacement of Na^+, Ca^{2+}, Mg^{2+}, K^+, and H^+ by 90%Bt-10%Ch composites/beads are shown in Figure 5.15. Similar graphs for other adsorbent samples are presented in Appendix B24. As can be seen, the amount of Pb (II) ions adsorbed onto all the adsorbents is proportional to the initial concentration of Pb (II) solution. Except for the Na^+ ion, the release of the other three cations (Ca^{2+}, Mg^{2+}, K^+) during the uptake of Pb (II) ions was insignificant. This is expected since the layered silicate used as starting material for composite/beads formation is the modified Na-bentonite type. The amounts of Na^+ cations released are small for all the composites compared to their corresponding beads. Unlike beads, the amounts of Na^+ cations released during adsorption of Pb(II) does not show steady trend as the initial concentration Pb(II) ions increases. This may be due to the high portion of Na^+ ions been exchanged (with chitosan) and washed away during the centrifugation or washing stage of the composite formation via the solution method. However, the amount of Na^+ ions released (for 90%Bt-10%Ch beads-A/beads-B) during the adsorption is almost twice the amount of Pb(II) ions adsorbed and increases with Pb (II) concentrations. This showed that Na^+ cations played some role in the ion-exchange process for the 90%Bt-10%Ch beads-A/beads-B. Except for 70%Bt-30%Ch beads-B, similar trends were observed for other adsorbents (70%Bt-30%Ch beads-A, 50%Bt-50%Ch beads-A, and 50%Bt-50%Ch beads-B).

To further understand the adsorption process of Pb(II) ions, FTIR spectra were collected for Bt-Ch composites/beads before and after Pb (II) adsorption to identify the possible sites of Pb (II) binding. Unfortunately, no major changes or evidence was observed. Previous study reported that both nitrogen and oxygen atoms (of the amino and hydroxyl groups, respectively) are the main adsorption sites for Pb(II) ions during the adsorption of Pb(II) ions onto chitosan-immobilized-on-bentonite composites [89]. But contribution of oxygen atoms seems to be less significant compared to nitrogen atoms

[215]. There are lone pairs of electrons on both nitrogen and oxygen atoms which can be complexed with metal ions via electron pair sharing, however due to the stronger attraction of the lone pair of electrons to the nucleus associated with the oxygen atom compared to that in the nitrogen atom, the tendency to donate the lone pair of electrons for sharing with a metal ion will be greater for nitrogen atoms than with oxygen atoms [215]. The nitrogen groups must therefore contribute majorly to the Pb (II) adsorption process which as described by the Freundlich isotherm fitting is chemical adsorption. Overall, the scheme illustrating the possible adsorption mechanisms concerning the adsorption of Pb(II) ions onto Bt-Ch composites/beads is shown in Figure 5.16.

Table 5.7: The Rb/r values at different Pb (II) concentrations for respective Bt-Ch composites/beads

Initial Pb (II) conc. (mg/L)	$R_{b/r}$								
	90%Bt-10%Ch			70%Bt-30%Ch			50%Bt-50%Ch		
	composite	beads-A	beads-B	composite	beads-A	beads-B	composite	beads-A	beads-B
10	0.68 $\pm$0.28	0.09 $\pm$0.04	0.18 $\pm$0.02	0.76 $\pm$0.26	0.17 $\pm$0.10	0.51 $\pm$0.20	0.54 $\pm$0.40	0.08 $\pm$0.04	0.17 $\pm$0.07
30	0.92 $\pm$0.28	0.24 $\pm$0.00	0.60 $\pm$0.16	1.03 $\pm$0.06	0.37 $\pm$0.14	1.35 $\pm$0.13	0.99 $\pm$0.44	0.56 $\pm$0.30	0.59 $\pm$0.33
50	0.99 $\pm$0.12	0.45 $\pm$0.09	1.43 $\pm$0.98	2.18 $\pm$0.70	0.46 $\pm$0.10	0.86 $\pm$0.14	0.99 $\pm$0.12	0.56 $\pm$0.16	0.67 $\pm$0.23
70	1.46 $\pm$0.40	0.58 $\pm$0.01	0.89 $\pm$0.01	1.41 $\pm$0.10	0.61 $\pm$0.09	1.46 $\pm$0.33	0.95 $\pm$0.06	0.61 $\pm$0.09	0.69 $\pm$0.16
90	1.51 $\pm$0.25	0.67 $\pm$0.02	0.94 $\pm$0.04	1.45 $\pm$0.05	0.66 $\pm$0.03	1.24 $\pm$0.26	1.03 $\pm$0.03	0.66 $\pm$0.09	0.72 $\pm$0.14

Note: each value represents mean ± standard deviation of three (3) different samples (n = 3).
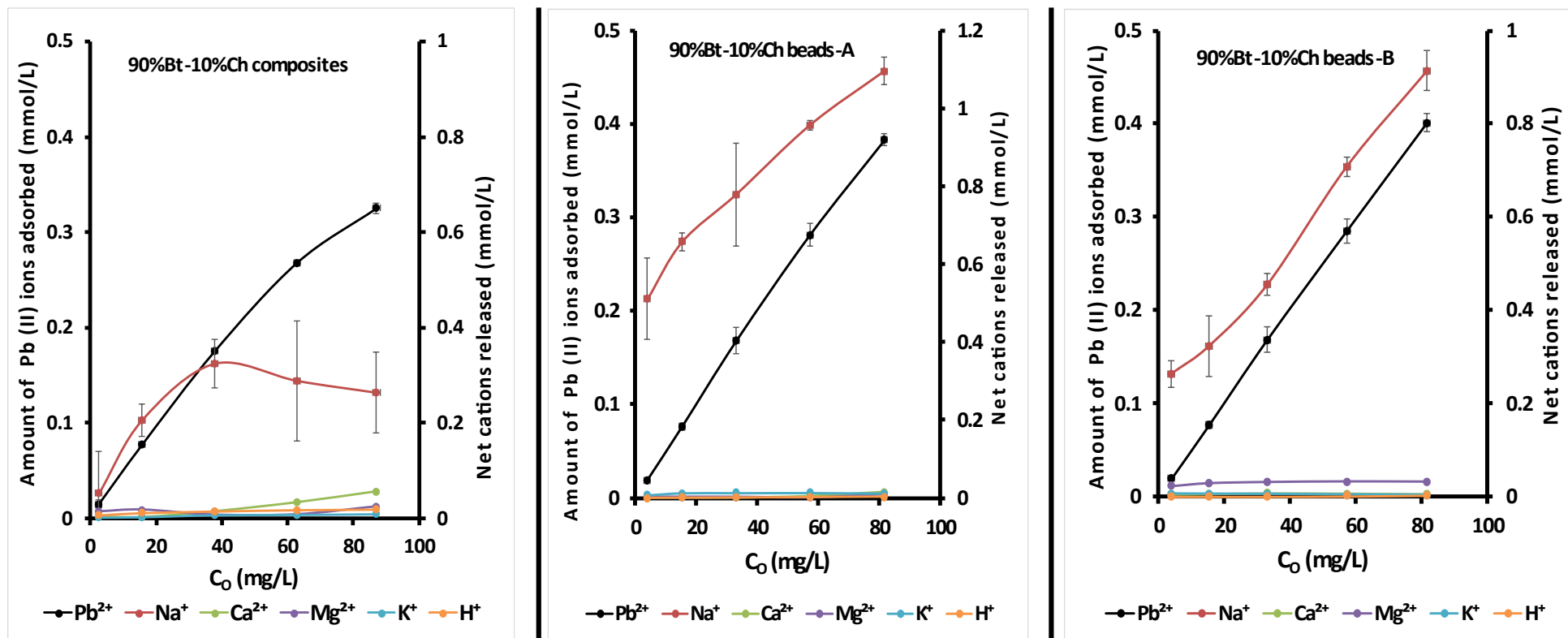
Figure 5.15: Graphs showing the adsorption of Pb (II) ions and displacement of Na+, Ca2+, Mg2+, K+, and H+ by 90%Bt-10%Ch composites/beads

Note: Initial Pb concentrations = 2.5 - 90 mg/L; pH = 4.5; adsorbent amount = 0.05 g; adsorption agitation time (at 230 rpm) = 60 minutes. Each bar represents mean ± standard deviation of three (3) different experiment (n = 3).
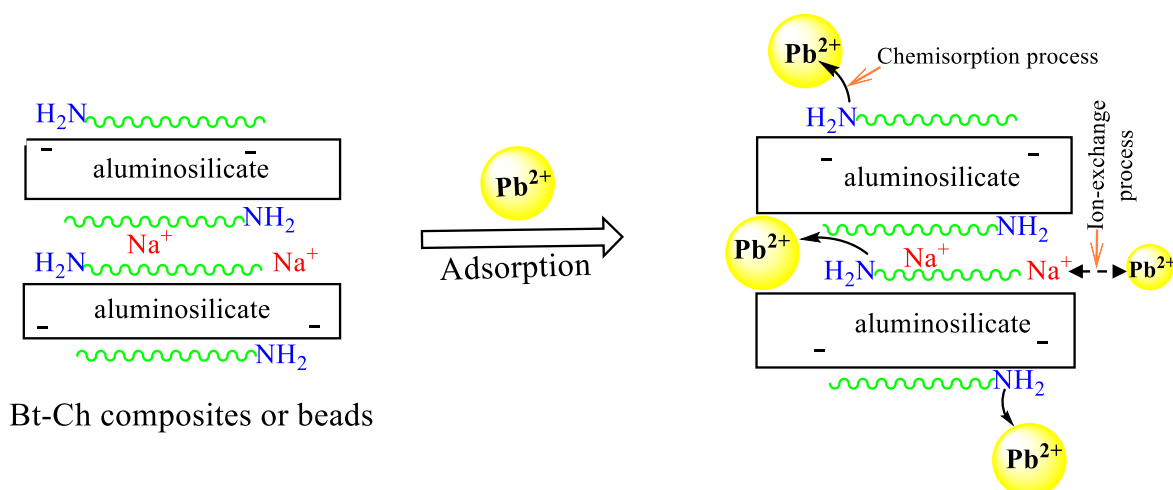
Figure 5.16: Scheme illustrating possible adsorption mechanisms concerning Pb(II) adsorption onto Bt-Ch composites/beads

5.3.7. Conclusion

The capability of different forms of prepared Bt-Ch composites/beads as an adsorbent have been investigated for their ability to remove Pb(II) ions from aqueous solution. This study demonstrated how to apply screening and optimal-I designs for identifying and optimising significant parameters for adsorption of Pb (II) ions with multiple adsorbents. It was observed that adsorption capacity (mg/g) of Pb (II) increases with pH and initial concentration and decreases with adsorbent dosage. On the other hand, the adsorption efficiency (%) of Pb (II) increases with pH and adsorbent dosage but decreases with initial concentration. The optimisation of the Pb(II) adsorption onto multiple adsorbents (Bt-Ch composites/beads) was carried out utilising a numerical optimisation tool. The optimal experimental conditions (pH = 4.5 and adsorbent dosage =0.05 g) obtained from surface response-optimal-I designs were used to perform an adsorption equilibrium study. The adsorption experimental data correlated well with both Langmuir and Freundlich isotherm models. High maximum Pb(II) adsorption capacities, Q_{max}, were recorded from 42.48 ± 4.22 to 94.60 ± 5.63 mg/g and 57.74 ± 3.23 to 96.60 ± 0.83 for Bt-Ch-1 and Bt-Ch-2 composites/beads, respectively. The Chitosan type (used to form the composites/beads), composition of Bt-Ch composites/beads, as well as chitosan distribution within the interlayer space of the bentonite clay has a pronounced effect on the Pb(II) uptake. In single-component Pb(II) solutions, excellent extents of adsorption

were obtained for all the prepared Bt-Ch beads/composites. Adsorption of Pb (II) from multi-component solution by Bt-Ch composites/beads was significantly affected by presence of other competing ions (including Zn, Cu, Ni, and As ions). The developed Bt-Ch composites/beads exhibited good potential for re-use after many cycles of regeneration up to the fifth cycle. Thus, indicating the potential of using Bt-Ch beads/composites as a cost-effective adsorbent for removal of Pb (II) ions from both drinking and wastewater. Both chemisorption process (complexation) and physical adsorption (ion-exchange process) are the main mechanisms regarding the adsorption of Pb (II) onto Bt-Ch composites/beads.

Chapter 6

Bentonite-Chitosan composites or beads: for co-adsorption of lead (Pb) and copper (Cu) from binary aqueous solutions

6.1. Introduction

There is growing public concern over the presence of multiple heavy metal ions in different water sources. The two metal ions that have garnered particular attention are Pb(II) and Cu(II) ions [199]. Pb(II) ion can be found in the effluents of battery recycling plants, metal mining and electronic assembly plants, and its cumulative effect can result in brain damage and dysfunction of the kidneys, liver and central nervous system in humans [199]. While Cu(II) ion is an essential trace element, high levels of induced Cu(II) can be fatal. Due to their widespread use in different industries, there is now a pressing need to develop effective methods for removing Pb(II) and Cu(II) ions from wastewater [199].

Numerous studies reported in the literature involve single-component adsorption of heavy metal ions. Since industrial effluents usually contain these metals, this necessitates simultaneous removal of two metals from the binary component systems. Both Pb(II) and Cu(II) ions have a greater affinity towards amine ($-NH_2$) and hydroxyl ($-OH$) groups of the chitosan, which are available on the composites or beads [199]. This was demonstrated from the results of the experimental work (Chapter 5, Section 5.3.5) to determine the effect of competing ions towards Pb(II) adsorption from a multiple-component solution. Therefore, the present study aims to explore the co-adsorption of Pb(II) and Cu (II) ions onto Bt-Ch composites and beads in binary metal systems. The optimisation and influence of multiple parameters on Pb(II)-Cu(II) adsorption with two adsorbent samples were investigated simultaneously using a statistical design of experiment *(*DoE*)*. The experimental adsorption data from equilibrium studies were subjected to various multi- and single-component equilibrium isotherm equations for the best fits, and the obtained parameters were compared. The adsorption efficiency

and effects of competing ions towards co-adsorption of Pb(II) and Cu(II)adsorption were investigated.

6.2. Experimental

6.2.1. Materials

In this study, only two adsorbent samples were tested for co-adsorption of Pb(II) and Cu(II) ions; 70%Bt-30%Ch-1 composites and beads-B were prepared as described from Chapter 4. All chemicals were obtained as described in Section 5.2.1.

6.2.2. Adsorption experiments

The batch adsorption procedure as described in Section 5.2.2 was used. The batch adsorption experiment was designed based on Optimal-I designs (Appendix C1). In this study, screening experiment was not conducted because fewer adsorbent was tested and all the factors (including pH, Initial concentration, adsorbent dosage) were examined (Optimal-I designs) for their effects (and significance) on the co-adsorption of Pb(II) and Cu(II) onto Bt-Ch composites/beads. Careful consideration was looked into during this sorption experiment as these metals can easily precipitates at higher pH levels. For instance, the Cu(II) ion, also known as the cupric ion, is soluble and exists as a free form particularly in low pH conditions (generally below pH 6), and above the pH of 6.0, it precipitates readily as copper hydroxide [216]. Similar chemistry was observed for Pb ions as indicated in Section 5.2.2. Therefore, the adsorption experiments were carried out at pH of less than 6 to ensure Pb and Cu ions are removed just by adsorption processes without the effect of precipitation. In this study, the effect of pH was examined by varying the pH value from 2 to 6.

The quantitative measurements of Pb(II) and Cu(II) ions were carried out using the Agilent 5110 ICP-OES instrument using wavelengths of 220.353 nm and 327.395 nm, respectively. The operating conditions of instrument are as stated in Section 3.2.1.

The amount of Pb(II) and Cu(II) ions per unit mass of Bt-Ch composites/beads (adsorbents) and percent adsorption performance (%) were calculated using Equations 5.1 and 5.2, respectively as shown in Section 5.2.2.

6.2.2.1 *Response Surface Methodology - Optimal-I designs*

In this study, four factors including pH, adsorbent dosage, initial concentration, and agitation time (Table 6.1) were investigated for the co-adsorption of Pb(II) and Cu(II) onto Bt-Ch composites/beads. Therefore, a 30-experimental-run of I-optimal design (based on four numeric factors, plus one categoric factor) was created using Design-Expert 13 software and included five replicates (Appendix B). Each factor level combination was used in a randomised order. This design enabled to fit for a second-order polynomial model, which has main effects, two-factor interactions, and quadratic terms. The equation model was summarily defined as:

$$Y = \alpha + aA + bB + cC + dD + eE + abAB + acAC + adAD + aeAE + bcBC + bdBD + beBE + cdCD + ceCE + deDE + aaA^2 + bbB^2 + ccC^2 + ddD \tag{6.1}$$

where Y is the measured response ((e.g., metal-adsorption capacity, mg/g or efficiency, %) associated with every variable level combination, $\boldsymbol{\alpha}$ is the intercept (mean value), A, B, C, D, and E are the main factors (representing pH, adsorbent dosage, initial concentration, agitation time, and adsorbent type, respectively); AB, AC, AD, AE, BC, BD, BE, CD, CE, and DE are the two-factor (binary) interactions; A^2, B^2, C^2, and D^2 are the quadratic numerical (quantitative) factors; a, b, c, d, e, or ab, ac, ad, ae, bc, bd, be, cd, ce, de, or aa, bb, cc, dd and ee are the coefficients of the main factors, interaction factors, and quadratic numerical factors, respectively.

Table 6.1: Factors and their levels investigated for co-adsorption of Pb(II) and Cu(II) ions onto Bt-Ch composites/beads

Levels	Numeric continuous factors				Categoric nominal factor
	A-pH	B-Adsorbent dosage (g)	C-Initial concentration (mg/L)	D-Agitation time (min)	E-Adsorbent type
Low (-1)	2	0.05	50	10	X
Centre point (0)	varied	varied	varied	varied	--
High (+1)	6	0.5	250	300	Y

Note: X = Bt-Ch composites; Y = Bt-Ch beads-B

6.2.2.2 *Adsorption equilibrium and Isotherm*

To determine the equilibrium adsorption capacity of Bt-Ch composites/beads to simultaneously absorb Pb(II) and Cu(II) ions from binary aqueous solutions, a wider range of concentrations (i.e., from 10 to 500 mg L^{-1}) that differs from the one used in the optimal experiment (50 to 250 mg L^{-1}; Table 6.1). The experiment was performed based on the optimal experimental conditions obtained from the surface response-optimal designs of the previous section. Thus, 0.05 g of each adsorbent was exposed to 25 mL of binary solutions containing Pb(II) and Cu(II) ions with varying concentrations (as stated above) at pH 4.5, agitation time of 60 minutes (with the speed of 230 rpm) and at room temperature (25°C). The equilibrium adsorption capacities, qe (mg/g) were calculated and then plotted against the corresponding respective equilibrium concentrations, Ce (mg/L) for adsorption isotherm modelling. The experimental adsorption data from equilibrium studies were subjected to various multi- and single-component Langmuir and Freundlich isotherm equations for the best fits, and the obtained parameters were compared. The single-component Langmuir and Freundlich equations (non-linear) are shown in Equation 2.9 and 2.11, respectively, presented in Table 2.5. The multi-component isotherms: non-modified Langmuir, modified Langmuir and extended Freundlich models are shown in Equations 2.17, 2.18 and 2.20, respectively, presented in Table 2.7. The correlation coefficient (R^2) and nonlinear chi-square test (χ^2) were used to evaluate the goodness of fit for single-component isotherm modelling. In addition to correlation coefficient (R^2), the Marquardt's percent standard deviation (MPSD) was used to identify the best-fit of the multi-component isotherm model.

6.2.2.3 *Desorption studies*

It has been reported that most heavy metal ions (Pb and Cu inclusive) have a strong affinity towards chelating agents such as ethylenediaminetetraacetic acid (EDTA) [197]. Therefore, dilute aqueous solutions of EDTA were used as a stripping (desorbing) agent to simultaneously recover both Pb and Cu ions adsorbed onto Bt-Ch composites/beads. The batch desorption procedure as described in Section 5.2.2.4 was used.

6.3. Results

6.3.1. Surface Response: I-optimal designs

In this study, only one response (i.e., adsorption capacity, mg/g) was used for the analysis of the optimal model related to both Pb(II) and Cu(II) adsorption. Although, the adsorption of these metals was done simultaneously, DoE has made it possible to assess each metal separately. The results for the 30 experimental-runs with their corresponding experimental and predicted response (adsorption capacity) for Pb(II) and Cu(II) ions adsorption onto Bt-Ch composites/beads are presented in Appendix C1. The mathematical relationships between the four studied independent factors (i.e., pH, adsorbent dose, initial concentration, and agitation time) and the response (adsorption capacity) were also provided by Design Expert 13 software. The equation in terms of actual factors (with regards to respective adsorbent (X & Y) which describes the various parameters regarding the Pb(II) adsorption onto Bt-Ch composites are all shown in Equations 6.2 and 6.3 respectively. While the equations related to Cu(II) adsorption are presented in Equations 6.4 and 6.5, respectively.

Pb-adsorption

$$(\text{Pb} - \text{adsorption capacity})X = -16.344 + 12.675A + 129.84B + 0.01069C + 0.0245D + 0.1618BC - 1.3846A^2 + 333.48B^2 - 0.0003C^2 - 0.0001D^2 \tag{6.2}$$

$$(\text{Pb} - \text{adsorption capacity})Y = -14.982 + 12.675A + 129.84B + 0.01069C + 0.0381D + 0.1618BC - 1.3846A^2 + 333.48B^2 - 0.0003C^2 - 0.0001D^2 \tag{6.3}$$

Cu-adsorption

$$(\text{Cu} - \text{adsorption capacity})X = -17.695 + 12.540A - 74.491B + 0.0068C + 0.0263D - 10.404AB + 0.0085AC + 0.2247BC - 1.2837A^2 + 324.73B^2 - 0.0002C^2 - 0.0001D^2 \tag{6.4}$$

$$(\text{Cu} - \text{adsorption capacity})X = -17.001 + 13.909A - 99.539B + 0.0379C + 0.0263D - 10.404AB + 0.0085AC + 0.2247BC - 1.2837A^2 + 324.73B^2 - 0.0002C^2 - 0.0001D^2 \tag{6.5}$$

6.3.1.1 *Analysis of variance (ANOVA)*

The summary of ANOVA results for the adsorption capacity (mg/g) of Pb(II) and Cu(II) ions by Bt-Ch composites/beads are presented in Appendix C2 and C3, respectively. After data-fitting was carried out, the modified quadratic models concerning both analysed metals were significant (Coefficient = 15.93; F = 40.13; P<0.0001; Appendix C2) and (Coefficient = 14.25; F = 32.46; P<0.0001; Appendix C3) for Pb-adsorption capacity (mg/g) and Cu-adsorption capacity (mg/g), respectively. The non-significant "lack-of-fit" for Pb-adsorption capacity (F = 4.32; P = 0.058 > 0.05; Appendix C2) and Cu-adsorption capacity (F = 4.18; P = 0.065 > 0.05; Appendix C3) suggest the adequacy of both models to explain data in the experimental region. The R^2 values for these models were found to be 0.96 and 0.97 for Pb-adsorption capacity and Cu-adsorption capacity, respectively. The predicted R^2 values (0.88 and 0.78; for Pb-adsorption capacity and Cu-adsorption capacity, respectively) were in reasonable agreement with adjusted R^2 (0.94 for both Pb-adsorption capacity and Cu-adsorption capacity), i.e., the difference is less than 0.2. The relatively small value of coefficient of variance, CV = 11.50 and 16.96; for Pb-adsorption capacity and Cu-adsorption capacity, respectively, implies that deviation between the predicted and experimental data values were minimal. In addition, concerning adequate precision for these models, the ratio values were found to be 21.10 and 19.81 for Pb-adsorption capacity and Cu-adsorption capacity, respectively, which indicates an adequate signal for both Pb and Cu adsorption. P-values less than 0.05 indicate model terms are significant, and therefore, A, B, C, E, BC, DE, A^2, B^2, C^2 and D^2 are significant terms in the modified quadratic model related to Pb-adsorption capacity (Appendix C2). Also, the significant terms in the model related to Cu-adsorption capacity are A, B, C, E, AB, AC, AE, BC, BE, A^2, B^2 and C^2 (Appendix C3). However, p-values greater than 0.10 indicate model terms are not significant and so, they were completely removed or deleted from the model.

Like Pb-adsorption capacity, the adsorption capacity of Cu(II) ions by Bt-Ch composites/beads was linearly affected by pH (A), adsorbent dosage (B), initial concentration (C) and adsorbent type (E). Interaction effects between AB, AC, AE, BC and BE were also observed concerning the absorption capacity of Cu(II) by Bt-Ch composites/beads. However, only three quadratic effects (A^2, B^2 and C^2) are significant in the model.

Regarding diagnostic statistics, Figure 6.1a & c represent the normal probability plots of studentised residuals for Pb(II) and Cu(II) adsorption capacity (mg/g), respectively. As can be seen almost all data clearly lies on a straight line for both responses, and therefore, it can be assumed that they are normally distributed. Figure 6.1b & d represent the correlation (relationship) between actual and predicted values of Pb(II) and Cu(II) adsorption capacity (mg/g), respectively. The actual values are the measured values of the adsorption capacity obtained for both Pb(II) and Cu(II) ions, which was determined experimentally by using Equation 5.1. While, predicted values were generated by using Equations 6.2 – 6.5. As can be seen, the predicted values obtained for both Pb(II) and Cu(II) adsorption capacity from the model, are in good agreement with the actual experimental data. It is important to consider that these models may contain inherent bias, as they were developed using data that is also predicted by the model.
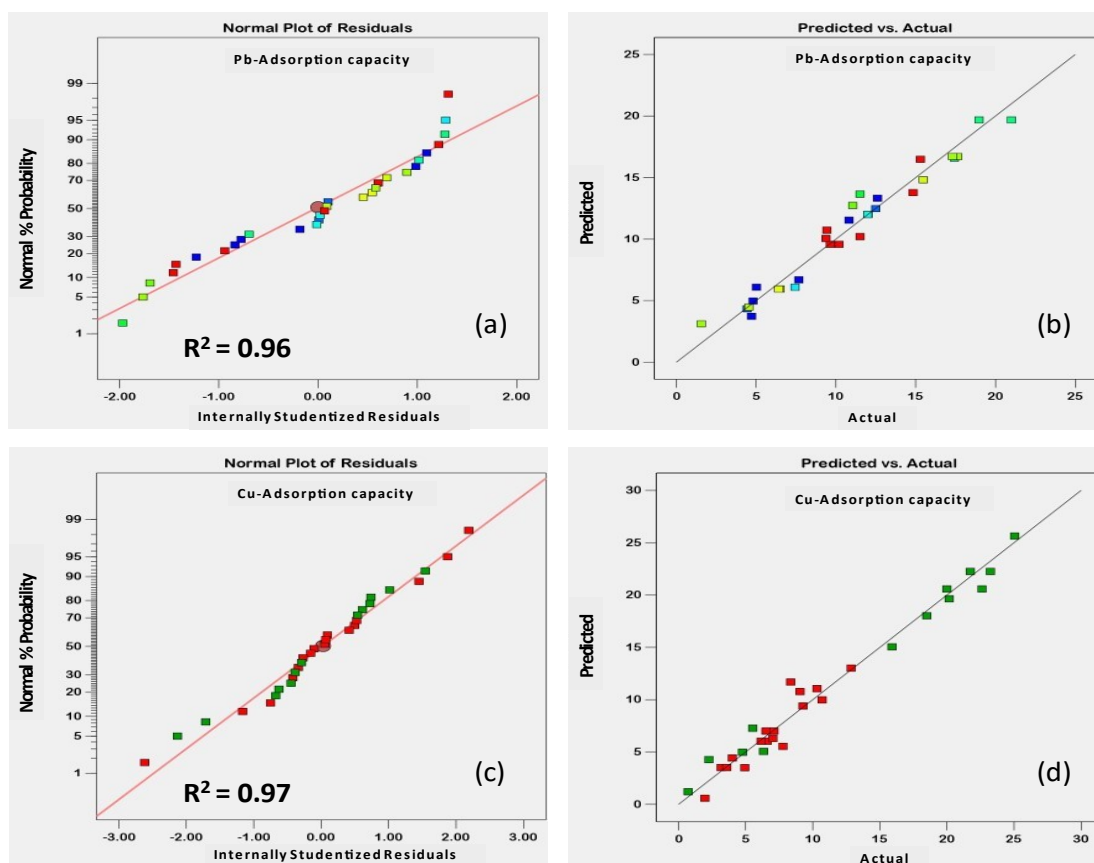
Figure 6.1: Normal probability plot of studentised residuals (a & c) and correlation between actual and predicted values (b & d) of Pb(II) and Cu(II) adsorption capacity, respectively.

Note: these graphs were plotted and obtained from Design-Expert®13

6.3.1.2 *Effects of main factors and their interactions*

Model-graphs showing the effect of each quantitative factor on the adsorption capacity (mg/g) of Pb(II) and Cu(II) by 70%Bt-30%Ch composites (adsorbent X) are shown in Figure 6.2. The model-graphs (concerning the main effect on the Pb(II) and Cu(II) adsorption) obtained for the second adsorbent sample (70%Bt-30%Ch beads) show a similar trend and is not presented herein. Generally, similar trends were observed for the effects of these factors towards both Pb(II) and Cu(II) adsorption. As can be seen in Figure 6.2 (a/d), adsorption capacity or Pb and Cu ions increases from pH of 2 to 4.5, maintained at this high value at pH 5 and then slightly decreases at pH 6. In terms of adsorbent dosage, it was observed that the adsorption capacity of Pb(II) ions slightly decreases with an increase in the adsorbent dose from 0.05 to 0.2 g (Figure 6.2b). However, adsorption capacity of Cu(II) ions slightly decreases initially (and then increases) as adsorbent dose increases from 0.05 to 0.2 g (Figure 6.2e). Regarding initial concentration, the Pb(II) and Cu(II) adsorption capacities slightly increase with initial concentration from 50 to 150 mg/L and then slightly decreases for the remaining part of initial concentration (200 to 250 mg/L).

The model-graphs showing 2-way interaction effects on the Pb(II) and Cu(II) adsorption capacity are presented in Figure 6.3 and Figure 6.4, respectively. When the effects of two factors appear as two non-parallel lines, it indicates that the effect of one factor depends on the level of another factor, and vice versa [202,203]. Concerning Pb(II) adsorption capacity, the interactive effects were only observed for adsorbent dosage-initial concentration (BC). Similar trends for this interactive effect were observed for both Bt-Ch composites (adsorbent X) and beads (adsorbent Y).

Regarding Cu(II) adsorption capacity, interactive effects were observed for pH-adsorbent dosage (AB), pH-initial concentration (AC), and adsorbent dosage-initial concentration (BC). Also, the way these factors interacted with regards to Cu(II) adsorption differed slightly for the two adsorbents (Bt-Ch composites and beads).

6.3.1.3 *The 3D response surface plots and combined effects of significant factors*

(A) Pb(II) adsorption capacity (mg/g) of Bt-Ch composites/beads

Concerning Pb(II) adsorption capacity (mg/g) of Bt-Ch composites/beads, the 3D response surface plot for the combined or interaction effect of adsorbent dosage and initial concentration, while the pH of the solution and agitation time were kept constant at 4.5 and 60 minutes, respectively, is shown in Figure 6.5. Pb(II) adsorption capacity (mg/g) of the Bt-Ch composites or beads slightly increases, when the initial concentration of the binary solution was increased from 50 to 150 mg/L, but flattened out when the initial concentration varied from 150 to 250 mg/L. It was noticed that the effect of initial concentration on Pb(II) adsorption capacity is much more pronounced at lowest adsorbent dosage. It was noticed that the initial concentration has a strong negative effect on the Pb(II) adsorption capacity in a non-linear manner (C^2, check the coefficient in Appendix C2). The strength of this quadratic effect (C^2) is greater (but opposing sign) in comparison to the linear effect contributed to the curve-shape of the 3D plot in the direction of initial concentration.

In terms of adsorbent dosage, it was observed that, the adsorption capacity (mg/g) of Pb(II) ions slightly decreased with an increase in the adsorbent dose from 0.05 to 0.2 g. The influence of adsorbent dosage may have a positive effect on the P(II) adsorption capacity in a non-linear manner (B^2, check the coefficient in Appendix C2). The quadratic effect of adsorbent dosage (B^2) was observed to have a similar strength (but opposing sign) in comparison to the linear effect of adsorbent dosage (B), which may account for the slight characteristic curve-shape of the 3D surface response plot.

(B) Cu(II) adsorption capacity (mg/g) of Bt-Ch composites/beads

The 3D surface response plots showing all the combined effects on the Cu(II) adsorption capacity are presented in Figure 6.6 and described below.

   ❖ *Interactive effect of solution pH and adsorbent dosage*

Figure 6.6a and 6.6d show the 3D response surface plot for the interaction effect of pH and adsorbent dosage (at constant initial conc. of 150 mg/L and agitation time of 60 minutes) on Cu(II) adsorption capacity (mg/g) for Bt-Ch composites and beads, respectively. We made the assumption that under the experimental pH condition, Cu and Pb metal ions in the binary solutions would exist primarily in the form of free Cu(II) and Pb(II) ions [66,216]. At lower adsorbent dosage, the adsorption capacity (mg/g) of Cu(II) ions increases for both adsorbents (i.e., 70%Bt-30%Ch composites and beads), with an increase in pH from 2 to 6. At very acidic medium (i.e., low pH level), the

151

hydronium ions (H_3O^+) are at high concentration, which then compete with Cu(II) ions for available active sites during adsorption. This accounts for the lower amount of Cu(II) uptake (mg/g) at lower pH of 2. However, as the pH increases, less hydronium ions (H_3O^+) will be present and thereby, allowing more Cu(II) ions uptake by the adsorbent [204]. At higher adsorbent dose (0.2 g), the adsorption capacity of Cu(II) ions slightly increases and then decreases for both adsorbents as pH of the solution increases from 2 to 6. It was observed that the pH has a strong negative effect on the Cu(II) adsorption capacity in a non-linear manner (A^2, check the coefficient in Appendix C3). The observed quadratic effect of pH (A^2) has a similar strength (but opposing sign) in comparison to the linear effect of pH (A), which may account for the slight characteristic curve-shape of the 3D surface response plot.

In terms of adsorbent dosage: at lower pH, the adsorption capacity (mg/g) of Cu(II) ions slightly increases for both adsorbents, with an increase in adsorbent dose from 0.05 to 0.2 g. However, at higher pH, the adsorption capacity (mg/g) of Cu(II) ions slightly decreases for both adsorbents as adsorbent dose increases from 0.05 to 0.2 g. The influence of adsorbent dosage may have a positive effect on the adsorption capacity (mg/g) in a non-linear manner (B^2, check the coefficient in Appendix C3). The quadratic effect of adsorbent dosage (B^2, check the coefficient in Appendix C3) is minimal and have a similar strength (but opposing sign) in comparison to the linear effect of adsorbent dosage (B).

❖ *Interactive effect of solution pH and initial concentration*

Figure 6.6b and 6.6e shows the 3D response surface plot for the interaction effect of pH and initial concentration (at constant adsorbent dosage of 0.05 g and agitation time of 60 minutes) on Cu(II) adsorption capacity (mg/g) for Bt-Ch composites and beads, respectively. At lower initial concentration, the adsorption capacity (mg/g) of Cu(II) ions increases, and then slightly decreases for both adsorbents as pH of the solution increase from 2 to 6. However, at higher initial concentration, the adsorption capacity (mg/g) of Cu(II) ions increases as pH varies from 2 to 6.

In terms of initial concentration: at lower pH, the adsorption capacity (mg/g) of Cu(II) ions slightly increases for both adsorbents as initial concentration varies from 50 to 250 mg/L. But at higher pH, the adsorption capacity (mg/g) of Cu(II) ions slightly increases (and then, decreases) for Bt-Ch composites as initial concentration increases from 50 to

250 mg/g. However, as for the Bt-Ch beads, the adsorption capacity (mg/g) of Cu(II) ions increases when the initial concentration varies from 50 to 250 mg/g. Overall, the influence of initial concentration may have a negative effect on the adsorption capacity (mg/g) in a non-linear manner (C^2, check the coefficient in Appendix C3). The quadratic effect of initial concentration (C^2, check the coefficient in Appendix C3) have a similar strength (but opposing sign) in comparison to the linear effect of initial concentration (C).

❖ *Interactive effect of adsorbent dosage and initial concentration*

Figure 6.6c and 6.6f shows the 3D response surface plot for the interaction effect of adsorbent dosage and initial concentration (at constant pH of 4.5 and agitation time of 60 minutes) on Cu(II) adsorption capacity (mg/g) for Bt-Ch composites and beads, respectively. At both lower and higher initial concentration, the adsorption capacity (mg/g) of Cu(II) ions slightly increases for Bt-Ch composites (but decreases for Bt-Ch beads) as adsorbent dose increases from 0.05 to 0.2 g. The quadratic effect of adsorbent dosage (B^2) has been previously discussed above.

In terms of initial concentration: at both lower and higher adsorbent dosage, the adsorption capacity (mg/g) of Cu(II) ions slightly increases for both adsorbents as initial concentration varies from 50 to 250 mg/L. The quadratic effect of initial concentration (C^2) has been previously discussed above.
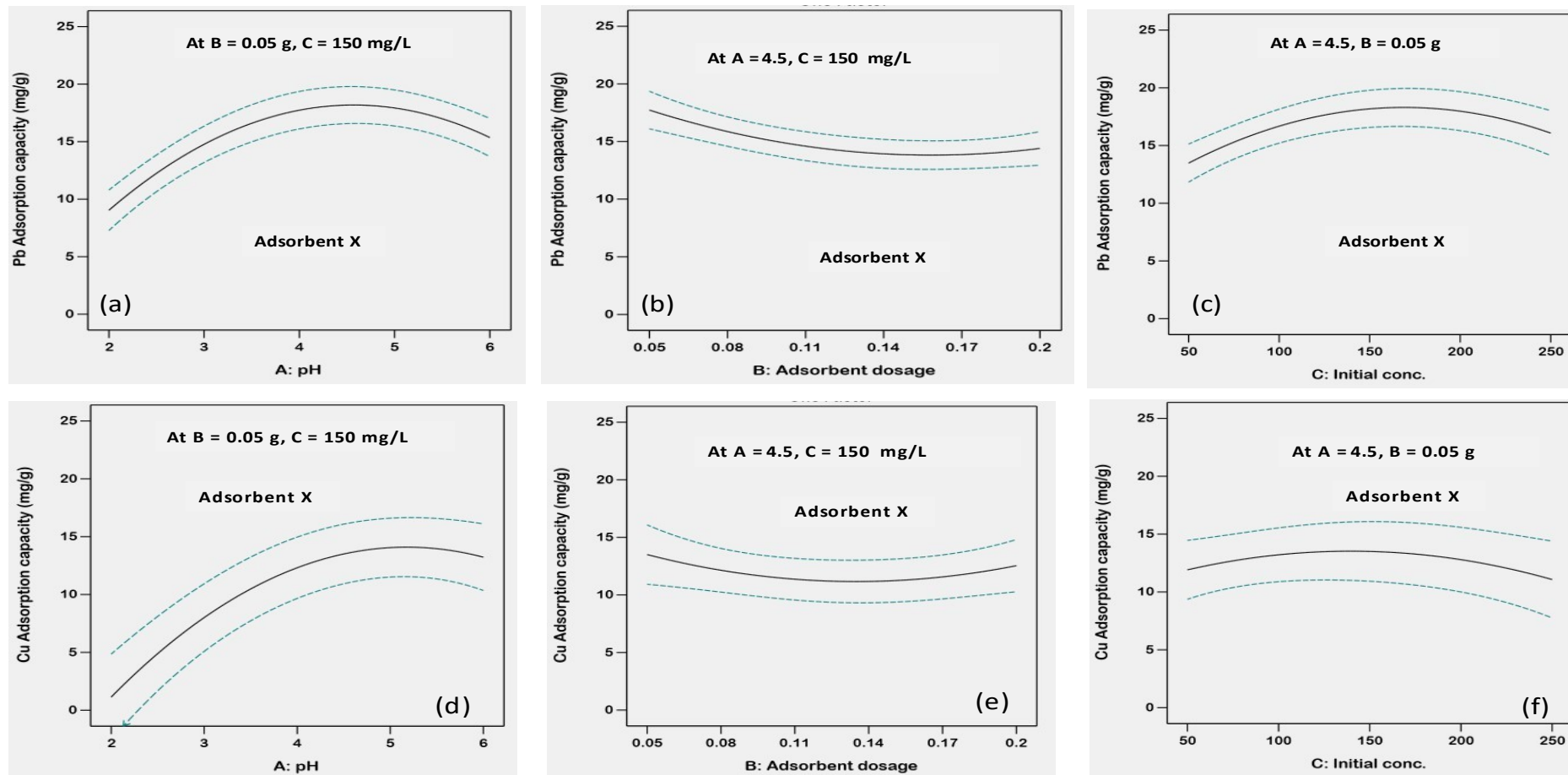
Figure 6.2: Graphs showing the effect of each factor on the Pb(II) adsorption capacity (a-c) and Cu(II) adsorption capacity (d-f) by Bt-Ch composites.

Note: these graphs were plotted and obtained from Design-Expert®13; dashed lines represent 95% confidence interval bands of the experimental data; (a/d) A-pH; (b/e) B-Adsorbent dose; (c/f) C-Initial concentration. Similar trends were observed for second adsorbent (Y = Bt-Ch beads).
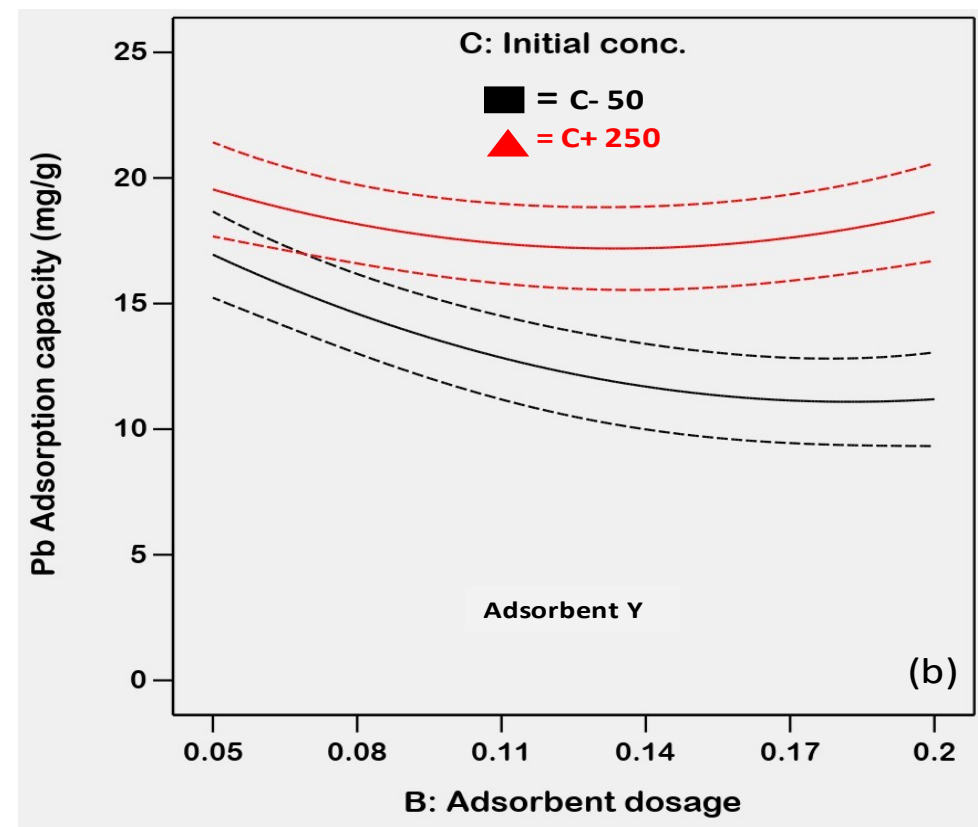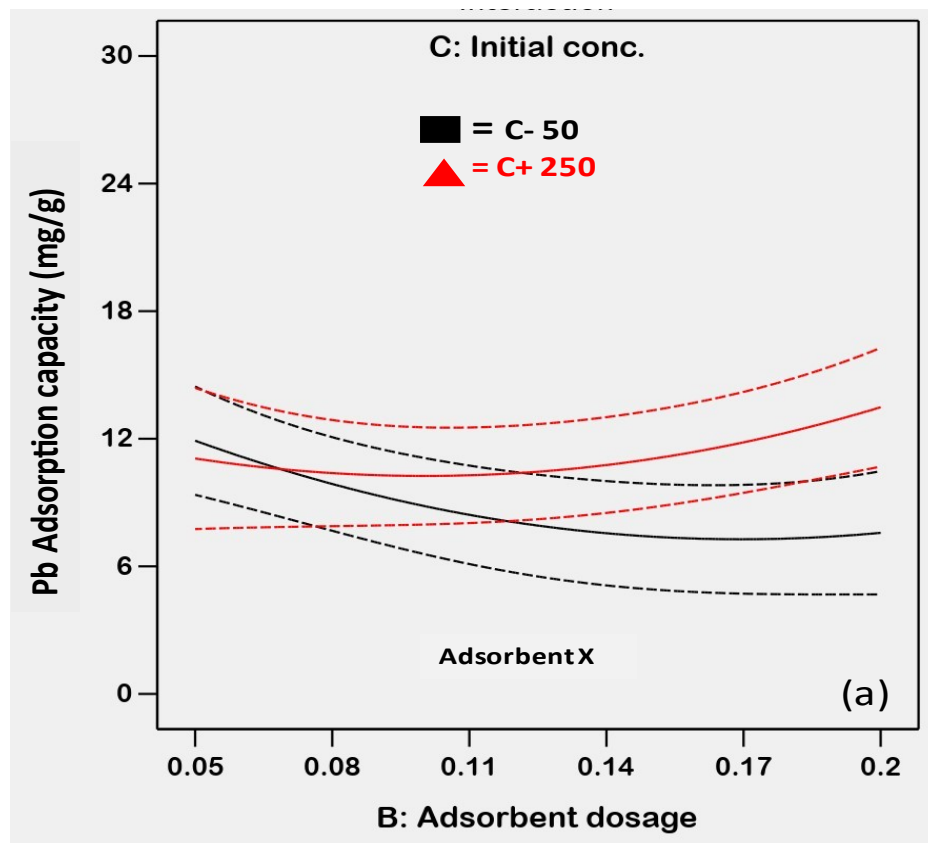
Figure 6.3: Figure Graphs showing two-factor interactions and their effects on the Pb(II) adsorption capacity

Note: these graphs were plotted and obtained from Design-Expert®13; dashed lines represent 95% confidence interval bands of the experimental data (a/b) Adsorbent dosage-Initial conc. (a) Adsorbent X = Bt-Ch composites; (b) Adsorbent Y = Bt-Ch beads.
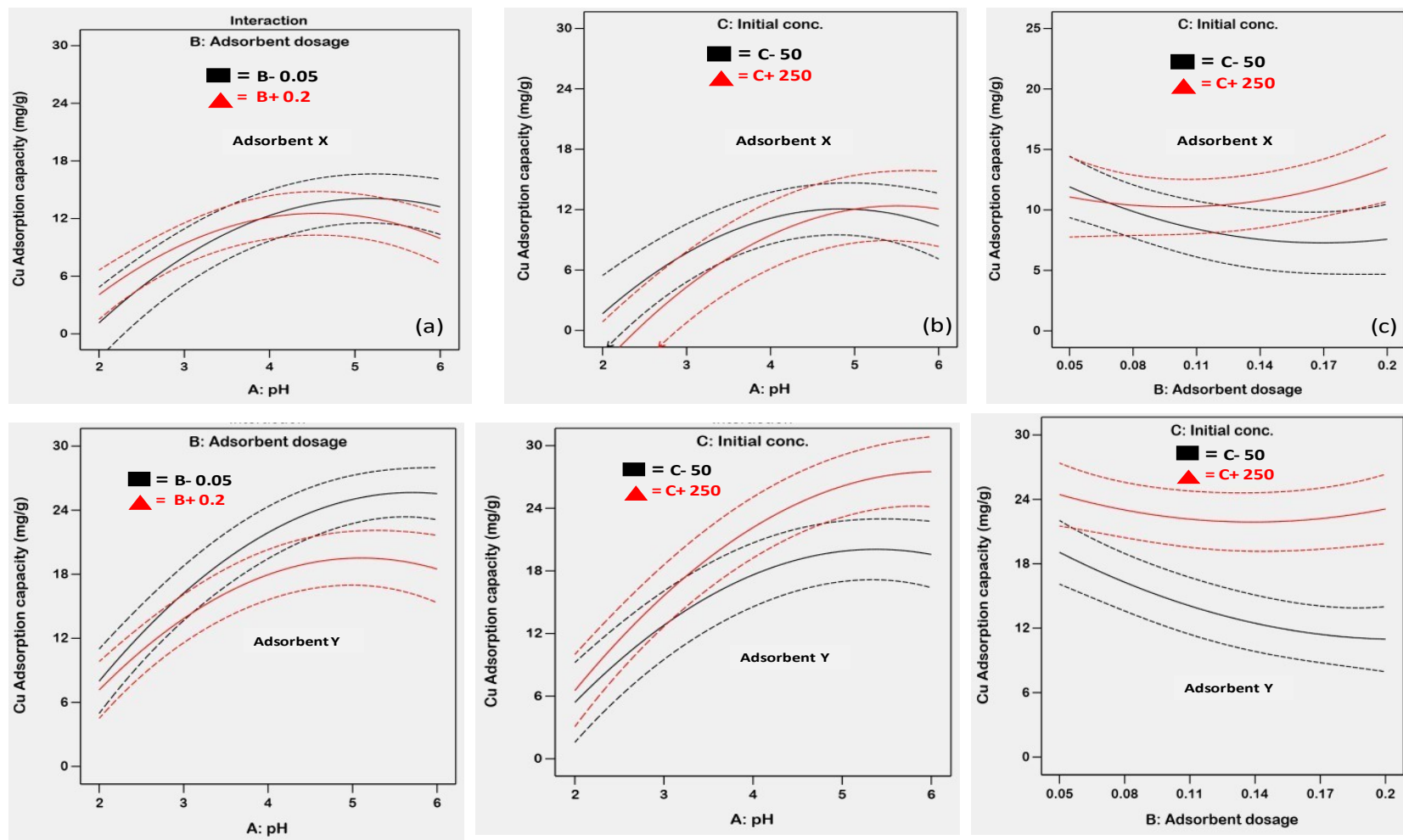
Figure 6.4: Figure Graphs showing two-factor interactions and their effects on the Cu(II) adsorption capacity (mg/g)

Note: these graphs were plotted and obtained from Design-Expert®13; dashed lines represent 95% confidence interval bands of the experimental data; (a/d) pH-Adsorbent dosage; (b/e) pH-Initial conc.; (c/f) Adsorbent dosage-Initial conc.; (a, b and c) Adsorbent X = Bt-Ch composites; (d, e and f) Adsorbent Y = Bt-Ch beads.
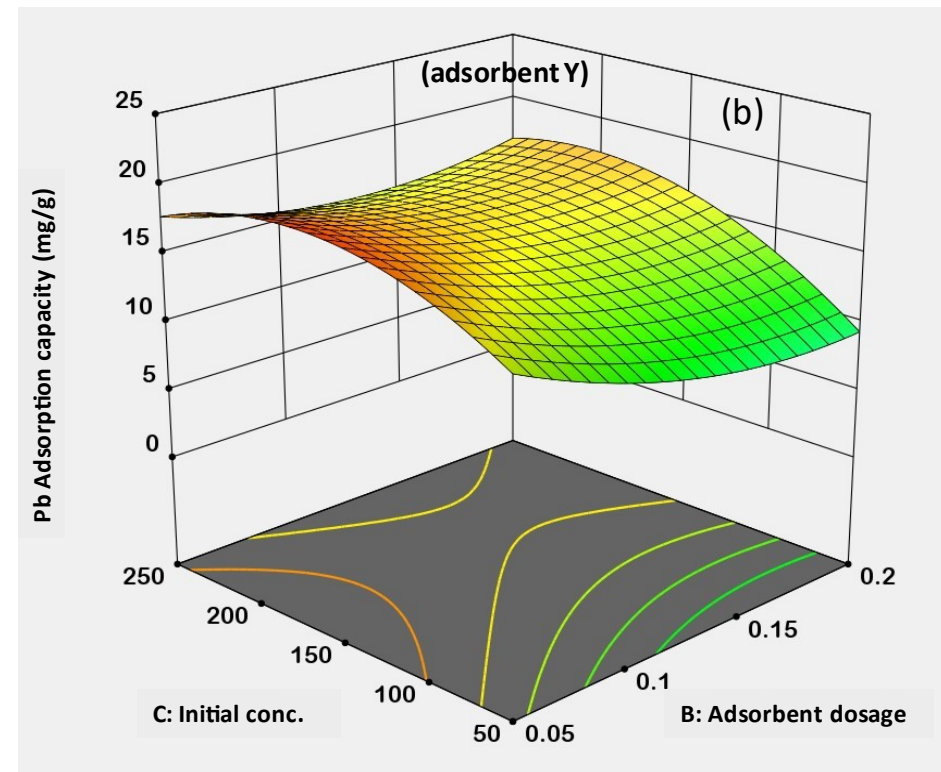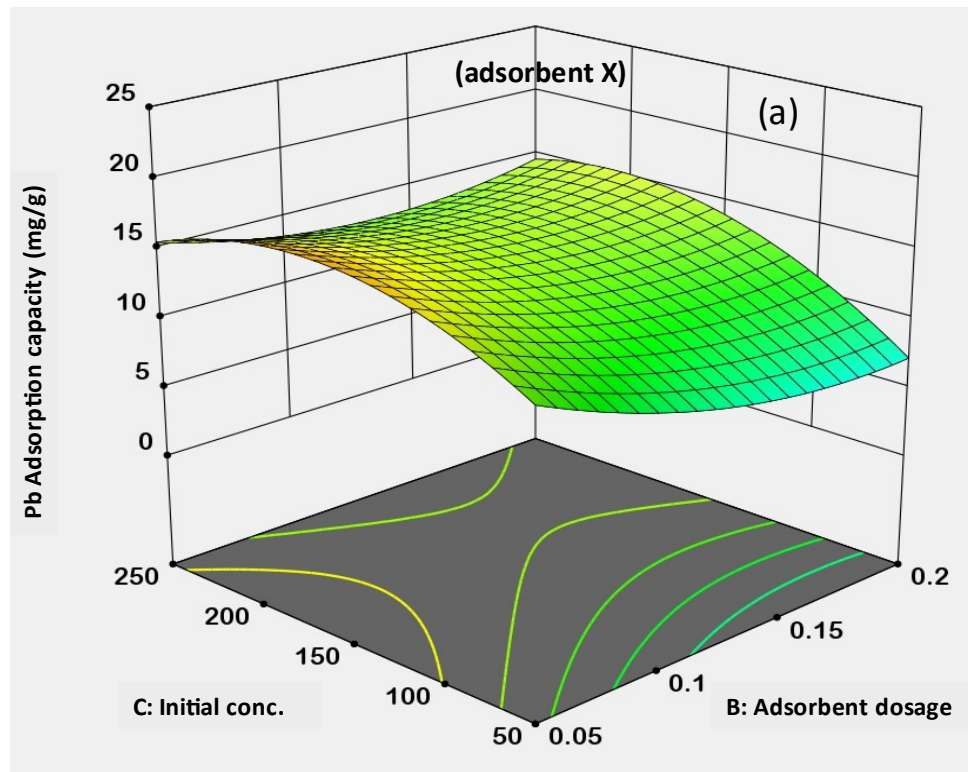
Figure 6.5: 3D response surface plots showing the combined effect of significant factors on the Cu(II) adsorption capacity (mg/g)

Note: these 3D surface plots were plotted and obtained from Design-Expert®13; (a/b) adsorbent dosage and initial concentration (at constant pH of 4.5 and agitation time of 60 minute). (a) Adsorbent X = Bt-Ch composites; (b) Adsorbent Y = Bt-Ch beads.
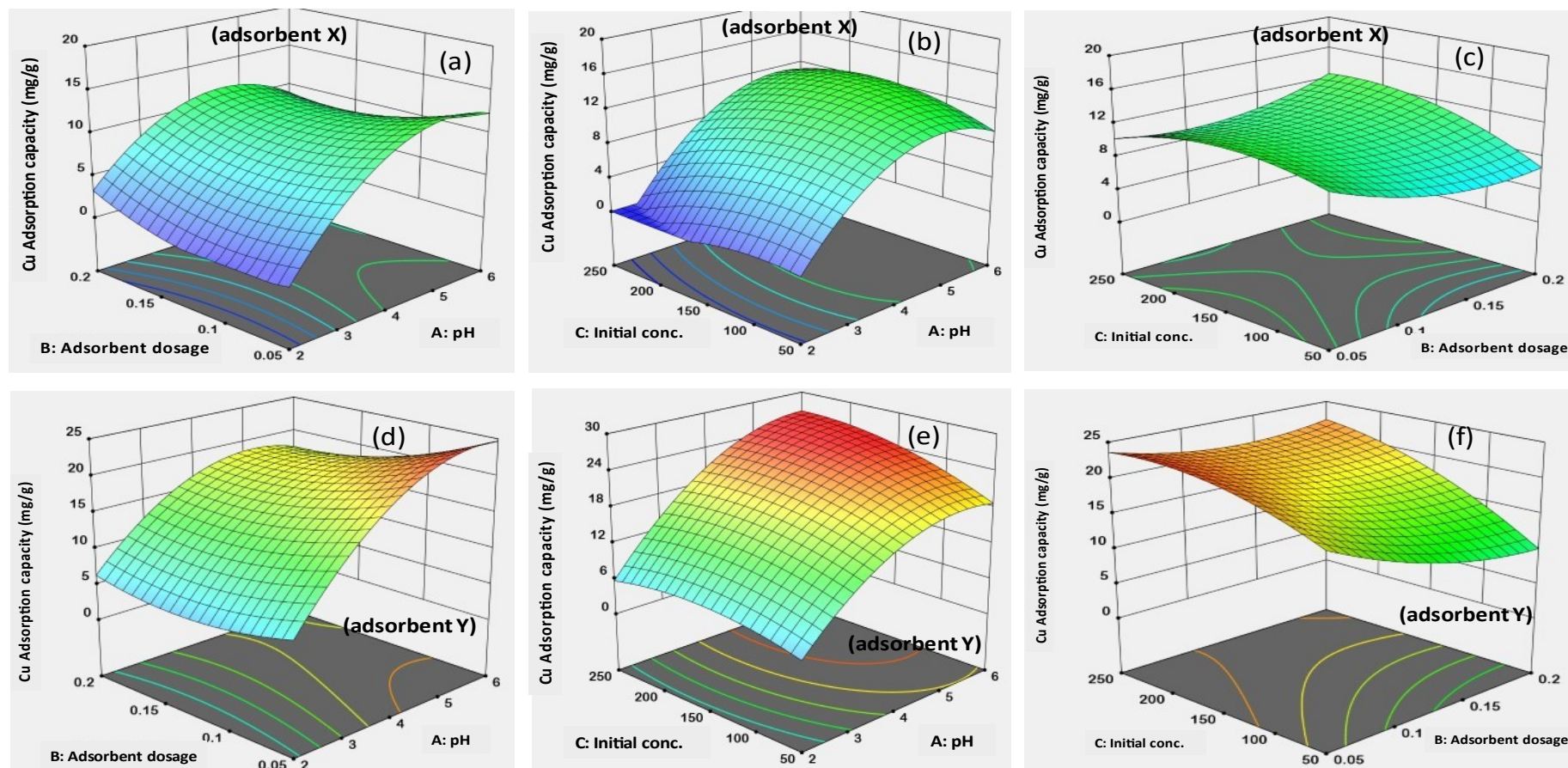
Figure 6.6: 3D response surface plots showing the combined effect of significant factors on the Cu(II) adsorption capacity (mg/g)

Note: these 3D surface plots were plotted and obtained from Design-Expert®13; (a/d) pH and adsorbent dosage (at constant initial conc. of 150 mg/L and agitation time of 60 minute); (b/e) pH and initial concentration (at constant adsorbent dosage of 0.05 g and agitation time of 60 minute); (c/f) adsorbent dosage and initial concentration (at constant pH of 4.5 and agitation time of 60 minute); (a, b and c) Adsorbent X = Bt-Ch composites; (d, e and f) Adsorbent Y = Bt-Ch beads

6.3.1.4 *Optimisation of parameters for Pb(II) and Cu(II) ions adsorption by Bt-Ch composites/beads*

The optimum conditions were derived so that there was a balance and an optimum adsorption for each of Pb and Cu ions was achieved. The experimental conditions selected to achieve this optimum adsorption were pH of 4.5, adsorbent dose of 0.05, initial concentrations of 150 mg/l, and agitation time of 60 minutes. Contour graphs (although not presented in this thesis) were used to estimate the optimum adsorption capacity and the obtained values are shown in Figure 6.7. As can be seen, the adsorption capacities values obtained for Pb(II) ions by Bt-Ch composites and beads were 17.67 mg/g and 19.85 mg/g, respectively. Also, the adsorption capacities values obtained for Cu(II) ions by Bt-Ch composites and beads were 12.67 mg/g and 22.94 mg/g, respectively. Relative to Pb, the optimum adsorption capacity of Cu ions obtained for beads was higher. However, for composites, the results were in contrast whereby the optimum adsorption capacity of Pb ions obtained was significantly higher compared to the value obtained for Cu ions. This demonstrates that composites have high affinity towards Pb, while beads show a strong affinity towards Cu during competitive adsorption. It has been reported that among all the transition metals, Cu forms the most stable complexes with glucosamine (a monomer of chitosan biopolymer), and this correlates with the higher loadings of Cu ions by Bt-Ch beads [210]. Higher Pb adsorption for composites is attributed to higher contribution from clay adsorption sites because there is less chitosan as evidenced from TGA results (Figure 4.4A; Section 4.3.2).

Under these conditions, the simultaneous adsorption of Pb(II) and Cu(II) ions was tested with one of the adsorbents (sample X; Bt-Ch composites) to confirm the robustness of the predicted model. As shown in Table 6.2, the experimental values (adsorption capacity) obtained from confirmation runs was found to be 18.52 ± 0.73 mg/g and 13.30 ± 0.25 mg/g which agrees well with the predicted values of 17.67 ± 1.24 mg/g and 12.67 ± 1.73 mg/g for Pb(II) and Cu(II) ions, respectively. The accuracy and precision of the design space is within 95% for both prediction and confidence intervals.
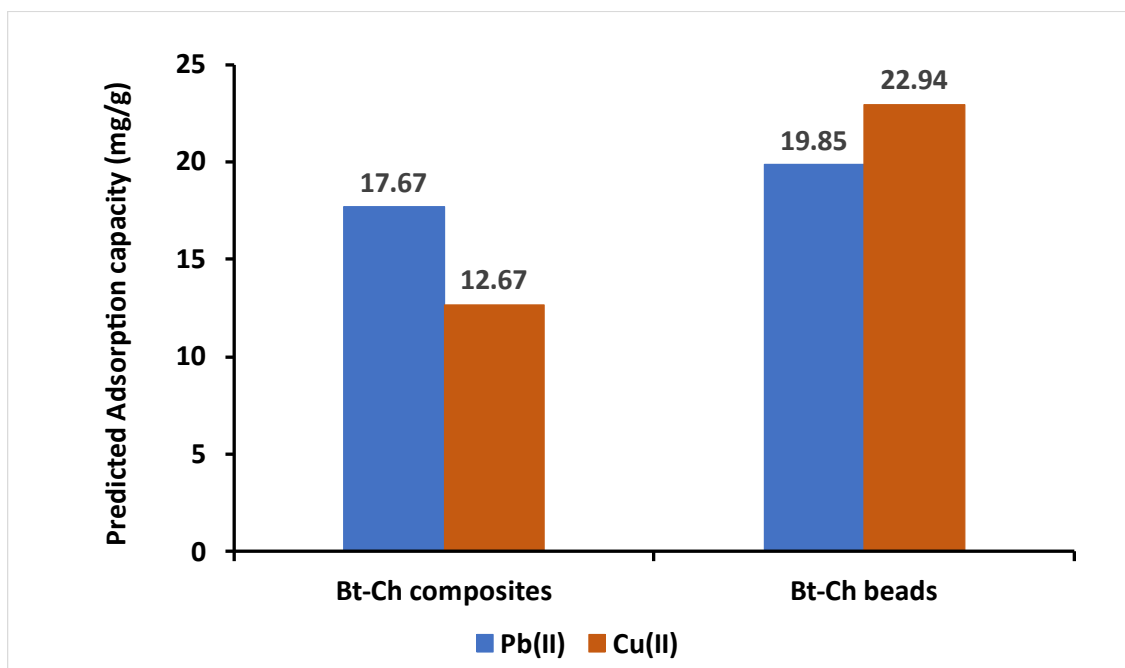
Figure 6.7: Charts showing predicted optimum Pb(II) and Cu(II) adsorption capacity (mg/g) for 70%Bt-30%Ch composites/beads

Table 6.2: Confirmation of experimental runs for analysed Optimal-I design model

Response	Adsorbent type	Target	Predicted Mean	Desirability	Confirmation experiment	Confidence Interval (95%)	
						Low	High
Pb-Adsorption capacity (mg/g)	X	Maximize	17.67 ± 1.24	1.00	18.52 ± 0.73	15.42	19.91
Cu-Adsorption capacity (mg/g)	X	Maximize	12.67 ± 1.73	1.00	13.30 ± 0.25	9.30	16.04

X = 70%Bt-30%Ch composites; pH = 4.5; adsorbent dose = 0.05 g; Initial concentration = 150.0 mg/L; agitation time = 60 minutes. For confirmation experiment, each value represents mean ± standard deviation of three (3) different samples (n = 3)

6.3.2. Adsorption Isotherm studies

The equilibrium adsorption data for the co-adsorption of Pb(II) and Cu(II) were fitted with various non-linear single- and multi-component isotherm models. In terms of single-component isotherms, both Langmuir and Freundlich equations were used. However, non-modified Langmuir, modified Langmuir and extended Freundlich model equations were further employed for multi-component isotherm modelling. Figure 6.8 illustrates both single- and multi-component isotherms models for co-adsorption of Pb(II)-Cu(II) by 70%Bt-30%Ch composites. Similar isotherm plots for the second

160

adsorbent sample (70%Bt-30%Ch beads) is presented in Appendix C4, but the calculated values (or constants) obtained from isotherm equations for the two adsorbent samples are presented in Table 6.3.

6.3.2.1 *Single-component Isotherm modelling*

Generally, the equilibrium data obtained from co-adsorption of Pb(II)-Cu(II) ions (onto Bt-Ch composites/beads) correlated well with both Langmuir and Freundlich isotherms studied (correlation coefficient, R^2 = 0.999) Also, the chi-square (X^2) values obtained were quite similar, indicating that under these experimental conditions, both monolayer and heterogeneous adsorption processes may coexist. This is like the previous adsorption isotherm studies of Pb(II) ions in a single-metal system as reported in Section 5.3.4. However, the Q_{max} value (based on the Langmuir isotherm) obtained in this binary study were twice or three times lower compared to the Q_{max} values obtained from the previous single Pb study for 70%Bt-30%Ch composites and beads, respectively (Table 5.2; Section 5.3.4). This result demonstrates that Cu(II) ions compete with Pb(II) ions for the available adsorption sites (on the Bt-Ch composites/beads) and reduces Pb(II)-loadings significantly. This is similar to the previous binary adsorption study carried out by Ngah and Fatinathan (2010), which showed that the Pb uptake (mg/g) by chitosan-triphosphate beads in a binary metal system (Pb-Cu) was three times lower compared to the value obtained by the same adsorbent in a single metal system [199]. In terms of adsorbent performance, the Q_{max} value (for both Pb and Cu) is higher for Bt-Ch beads (both individually and combined totals) compared to the corresponding composites (Table 6.3). This is because more chitosan is present in the beads as evidenced from TGA (Figure 4; Section 4.3.2) and therefore, more active sites through the chitosan are available for simultaneous adsorption of Pb(II) and Cu(II) ions. The maximum adsorption capacities (Q_{max}) values obtained for Pb(II) ions by Bt-Ch composites and beads were 18.26 ± 1.73 mg/g and 21.05 ± 3.70 mg/g, respectively. Also, the adsorption capacities values obtained for Cu(II) ions by Bt-Ch composites and beads were 12.15 ± 0.51 mg/g and 24.06 ± 0.44 mg/g, respectively. The trends in the Q_{max} values were similar to those optimum adsorption capacity values (Figure 6.7) obtained in the previous Section 6.3.1.4.

The R_L values were calculated using Equation 2.14 (Section 2.5.4.1) and are given in Table 6.3 for co-adsorption of Pb(II) and Cu(II) onto Bt-Ch composites/beads. In this study, the values of R_L have been found to be below 1.0 for both Pb(II) and Cu(II) ions, showing that the simultaneous adsorption of Pb(II) and Cu(II) by Bt-Ch composites/beads is favourable under the current experimental conditions.

From the Freundlich isotherms, the estimated Freundlich constant (K_F) values obtained (in this study, binary-metal system) for Pb(II) ions by Bt-Ch composites and beads were 8.88 ± 1.39 and 13.27 ± 2.52, respectively. These values were much lower compared to the K_F values obtained from previous study (i.e., single-metal system) for Pb(II) ions by Bt-Ch composites and beads, i.e., 1.3×10^5, and 6.9×10^4, respectively (Check Table 5.2; Section 5.3.4). The values of K_F obtained for Pb(II) ions were slightly higher compared to values obtained for Cu(II) ions regarding the binary adsorption by Bt-Ch composites/beads (Table 6.3). The Freundlich constant (K_F) characterises the strength of the adsorption, and a higher K_F value indicates that higher loading of adsorbate (such as metal ions) onto adsorbent could be achieved [48]. This explains (for composites, and not beads) the higher maximum adsorption capacity obtained for Pb (18.26 ± 1.73 mg/g) compared to the amount obtained for Cu (12.15 ± 0.51 mg/g; Table 6.3). This contrasts with the previous study carried out by Ngah and Fatinathan (2010), which showed that the K_F values obtained for Cu(II) ions were higher compared to the values obtained for Pb(II) ions during binary adsorption by chitosan-triphosphate beads [199]. The n value known as Freundlich exponent, was generally very low for both Pb(II) and Cu(II) ions regarding the two adsorbents studied. The observed n values fall within the range of 0 to 1, and since it is closer to zero, this implies that the surfaces of these adsorbents in contact with Pb(II) and Cu(II) ions are heterogeneous, a value below unity also usually suggests a chemisorption process [138].

6.3.2.2 *Multi-component Isotherm modelling*

The equilibrium adsorption data of Pb(II) and Cu(II) ions in simultaneous adsorption were fitted using three different multi-component isotherm models as shown in Figure 6.8, and the all the calculated parameters are summarised in Table 6.3. Based on the correlation coefficients ($R^2 = 0.999$), the co-adsorption of Pb(II)-Cu(II) ions onto Bt-Ch composites/beads correlated well with non-modified Langmuir, modified Langmuir and

extended Freundlich isotherm models. In addition, Marquardt's percent standard deviation (MPSD) was further employed to access the quality of the fits concerning multi-component isotherm modelling of binary adsorption of Pb(II)-Cu(II) onto Bt-Ch composites/beads. High MPSD values (e.g., close to 100) indicate high bias between the experimental data and the model [217]. In this study, the MPSD value obtained were generally low (i.e., below 25), showing a good fit to the experimental data.

The multi-component non-modified Langmuir model predicted quite similar Q_{max} values for both Pb(II) and Cu(II) ions (in the binary metal system) as compared to the Q_{max} values derived from the single-component Langmuir model for the binary adsorption system (Table 6.3). Even though the Langmuir constants ($K_{L,i}$) obtained from the multi-component non-modified Langmuir model differs slightly (with respect to the values obtained from single-component Langmuir model), the model could describe the behaviours of the simultaneous adsorption of Pb(II) and Cu(II) ions in binary solutions by Bt-Ch composites/beads.

Concerning the multi-component modified Langmuir model, the Q_{max} value predicted from the modified Langmuir model in respect to Cu(II) ions were also similar to the values obtained from the corresponding single-component Langmuir model. However, the Q_{max} values for Pb(II) for both adsorbents (Bt-Ch composites and beads) were higher compared to the values predicted by the single-component Langmuir and multi-component non-modified Langmuir models. The introduction of the interaction term ($\eta_{L,i}$) as per the modified Langmuir model may only have little influence on the model, since the $\eta_{L,i}$ values estimated were less than 1.0, and therefore, the parameters obtained from the modified Langmuir model are less reliable compared to those obtained from non-modified Langmuir. It has been suggested that when the estimated $\eta_{L,i}$ value is much greater than 1.0, the parameters obtained from modified Langmuir model should be used (instead of those obtained from non-modified Langmuir) to predict the binary-system adsorption [151]. Overall, the resulted slight deviance and overestimation of Pb(II) ions loadings by Bt-Ch composites/beads, may be due to some complexities resulted from the shortcoming of this model.

Like the single-component Freundlich model, the multi-component Freundlich isotherm model fitted well regarding the simultaneous adsorption of Pb(II) and Cu(II) ions assuming multilayer coverage and heterogeneous surface sites of Bt-Ch

composites/beads. Although the obtained values of Freundlich constant ($K_{f,i}$) and Freundlich exponent ($n_{,i}$) were slightly different from those obtained from the single-component Freundlich model.
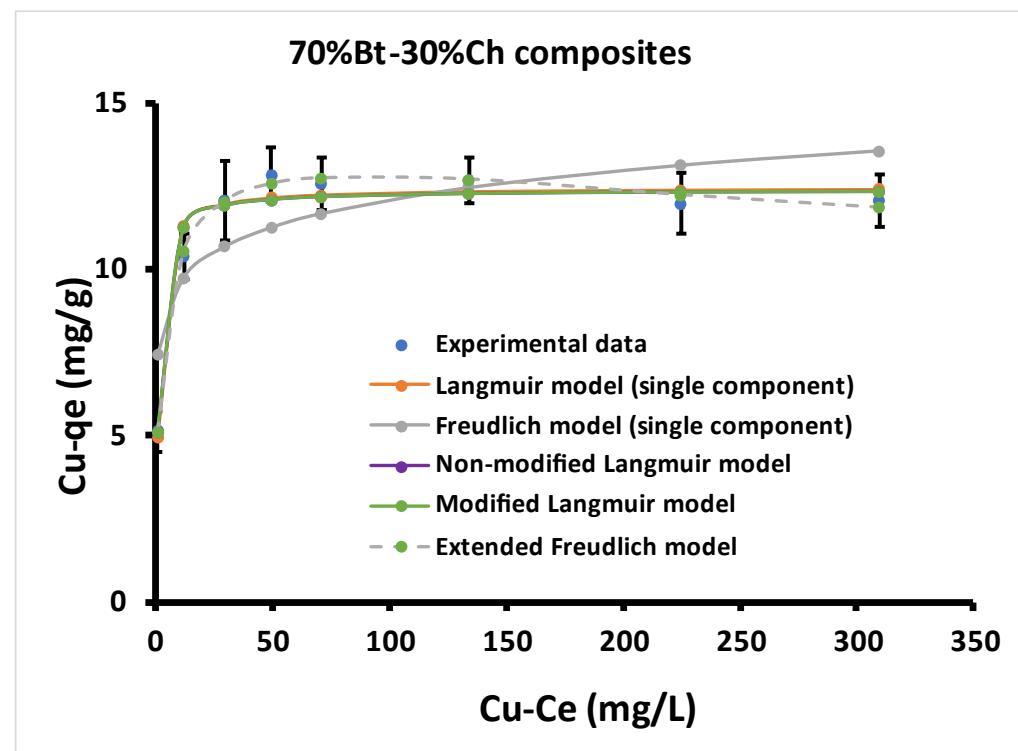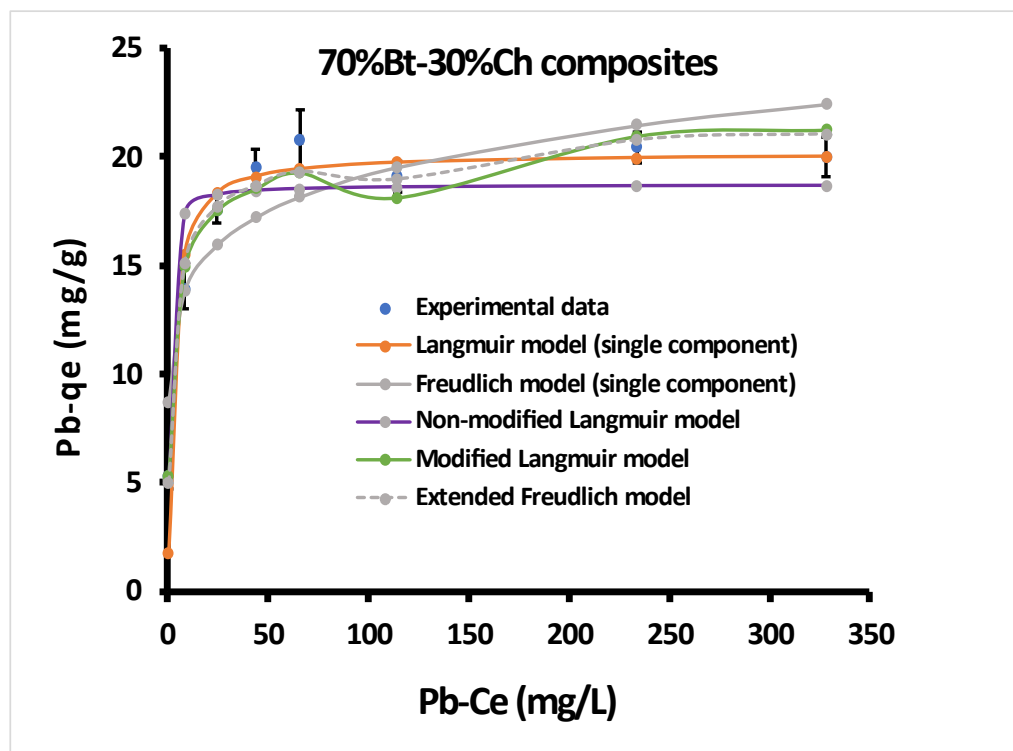
Figure 6.8: The non-linear single- and multi-component isotherms for co-adsorption of Pb(II)-Cu(II) by 70%Bt-30%Ch composites

Note: at 25 ^{O}C. pH = 4.5; adsorbent amount = 0.05 g; agitation time (at 230 rpm) = 60 minutes; Initial concentrations of Pb(II) and Cu(II) ions in binary solution = 10 - 350 mg/L; Each data-point represents mean ± standard deviation of three (3) different experiments (n = 3).

Table 6.3: The fitting parameters of Single-component and multi-component isotherms for the co-adsorption of Pb(II)-Cu(II) onto Bt-Ch composites/beads

Single-component Isotherm Models	70%Bt-30%Ch composites		70%Bt-30%Ch beads	
	Pb	Cu	Pb	Cu
Langmuir				
Q_{max}	18.26 ± 1.73	12.15 ± 0.51	21.05 ± 3.70	24.06 ± 0.44
K_L	0.280 ± 0.12	1.004 ± 0.20	1.877 ± 0.79	0.906 ± 0.52
R_L	0.010–0.263	0.003–0.091	0.002–0.051	0.003–0.099
R^2	0.999 ± 0.00	0.999 ± 0.00	0.999 ± 0.00	0.999 ± 0.00
X^2	0.188 ± 0.06	0.045 ± 0.02	0.214 ± 0.07	0.266 ± 0.03
Freundlich				
K_F	8.883 ± 1.39	7.223 ± 0.31	13.27 ± 2.52	13.57 ± 1.02
n	0.143 ± 0.01	0.109 ± 0.01	0.100 ± 0.11	0.122 ± 0.01
R^2	0.999 ± 0.00	0.999 ± 0.00	0.999 ± 0.00	0.999 ± 0.00
X^2	0.206 ± 0.05	0.119 ± 0.05	0.298± 0.06	0.145 ± 0.06

Multi-component Isotherm Models	70%Bt-30%Ch composites		70%Bt-30%Ch beads	
	Pb (i =1)	Cu (i =2)	Pb (i =1)	Cu (i =2)
Non-modified Langmuir				
$q_{m,i}$	16.36 ± 2.07	11.99 ± 0.51	21.09 ± 3.54	23.24 ± 1.44
$K_{L,i}$	1.55 ± 1.02	1.126 ± 0.25	1.771 ± 1.41	1.198 ± 0.46
R^2	0.999 ± 0.00	0.999 ± 0.00	0.999 ± 0.00	0.999 ± 0.00
MPSD	15.56 ± 4.60	8.025 ± 2.57	8.041 ± 3.40	13.67 ± 1.23
Modified Langmuir				
$q_{m,i}$	65.92 ± 22.7	11.99 ± 0.51	26.42 ± 6.15	22.64 ± 2.03
$K_{L,i}$	0.224 ± 0.19	0.680 ± 0.07	0.630 ± 0.74	1.701 ± 0.52
$\eta_{L,i}$	0.649 ± 0.46	0.616 ± 0.08	0.405 ± 0.46	1.011 ± 0.83
R^2	0.999 ± 0.00	0.999 ± 0.00	0.999 ± 0.00	0.999 ± 0.00
MPSD	8.694 ± 2.32	10.36 ± 3.32	9.281 ± 4.59	21.21 ± 6.16
Extended Freundlich				
$K_{f,i}$	13.85 ± 10.3	5.498 ± 0.19	30.47 ± 25.01	23.43 ± 8.78
$n_{,i}$	0.115 ± 0.12	0.332 ± 0.12	0.813 ± 0.50	0.290± 0.01
$x_{,i}$	2.794 ± 2.78	0.053 ± 0.05	0.000 ± 0.00	0.000 ± 0.00
$y_{,i}$	0.204 ± 0.25	0.054 ± 0.05	1.107 ± 0.91	0.582 ± 0.45
$z_{,i}$	1.342 ± 1.12	0.913 ± 0.31	0.874 ± 0.40	0.389 ± 0.01
R^2	0.999 ± 0.00	0.999 ± 0.00	0.999 ± 0.00	0.999 ± 0.00
MPSD	9.354 ± 4.46	6.640 ± 5.01	13.31 ± 7.47	19.72 ± 22.5

Note: q_m and $q_{m,I}$ are monolayer adsorption capacity for single and i component (mg/g); K_L and $K_{L,I}$ are the Langmuir constants for single and i component, respectively (L/mg); R_L is the separation constant (dimensionless); $\eta_{L,i}$ is the interaction factor for modified Langmuir equation; K_F and $K_{f,I}$ are the Freundlich constants for single and i component, respectively (L/g), n and $n_{,i}$ are the Freundlich exponents for single and i component, respectively (unitless-ranging from 0 to 1); $x_{,I}$, $y_{,I}$, and $z_{,I}$ are the parameters of extended Freundlich model for i component; R^2 is the coefficient of correlation; X^2 is the nonlinear chi-square; and MPSD is an abbreviation for Marquardt's percent standard deviation used for minimising of error in nonlinear modelling. Each value represents mean ± standard deviation of three (3) different samples (n = 3). R_L values are range between the lowest and highest value, and were calculated based on K_L and initial Pb (II) concentration, (C_O) ranging from 10 − 500 mg/L

6.3.3. Desorption studies

The results for the desorption (recovery) of adsorbed Pb(II) and Cu(II) ions by different EDTA concentrations i.e., from 0.1 to 5.0 x 10^2 mmol/L (corresponding to 0.1 to 5.0 x 10^2 mEq/L, respectively) are shown in Figure 6.9. As can be seen, the optimal recovery of both Pb(II) and Cu(II) ions was achieved with 1.0 x 10^1 mmol/L (corresponding to 1.0 x 10^1 mEq/L) EDTA aqueous solutions. Subsequently, the desorption of adsorbed Pb(II) and Cu(II) ions (from Bt-Ch composites/beads) was carried out using 1.0 x 10^1 mEq/L EDTA aqueous solutions.

The adsorption and desorption percentages of both Pb(II) and Cu(II) ions recovered from 70%Bt-30%Ch composites/beads are shown in Figure 6.10. For beads (Figure 6.10-A), the desorption percentages (for both metal ions) in the 1st cycle was above 80%. This value, though slightly lower compared to adsorption percentages (about 90 to 99%), still portrayed good recoveries. Serial adsorption-desorption steps were conducted up to five times, and the observed percentages obtained for both adsorption and desorption of both Pb(II) and Cu ions remained similar as those obtained for the first initial adsorption-desorption cycle. This indicates that beads were stable without apparent loss of the adsorption capacity up to at least 5 cycles. On the other hand, for composites (Figure 6.10-B), about 80% and 60% adsorption was achieved in the 1st cycle for Pb(II) and Cu(II), respectively. For subsequent adsorption-desorption cycles, the adsorption percentages (for both Pb and Cu ions) decreased significantly after the second cycle Overall, the results indicated that the Bt-Ch composites/beads exhibited good reusability for simultaneous removal of both Pb(II) and Cu(II) ions from water. A notable physical observation was that after subjecting both adsorbents (i.e., composites and beads) to aqueous binary solutions containing Pb(II)-Cu(II) ions during the adsorption procedures, the beads become pale-blue, while the colour of the composites remained unchanged (as demonstrated in Figure 6.11).
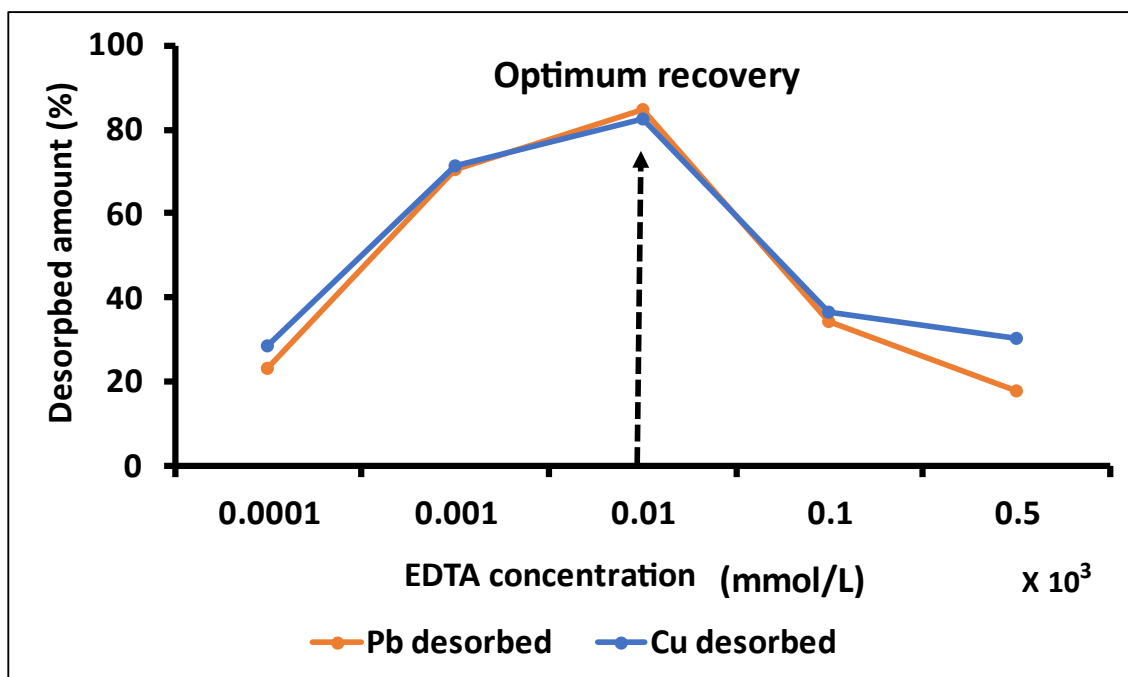
Figure 6.9: Simultaneous desorption of Pb(II) and Cu(II) from Bt-Ch composites/beads by different EDTA concentrations
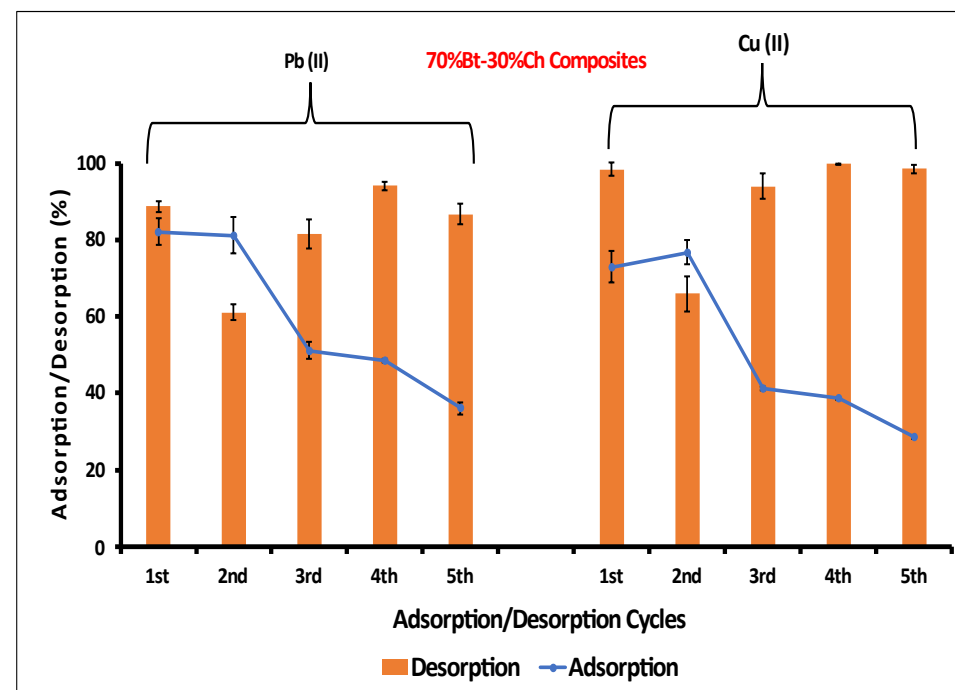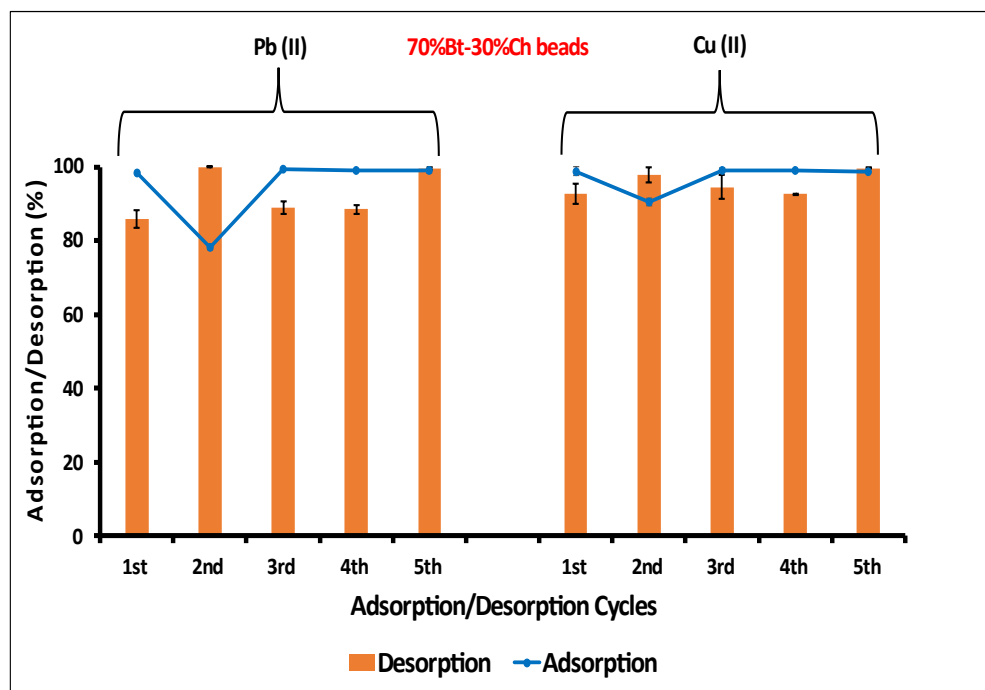
Figure 6.10: Charts showing the serial % Adsorption/Desorption of Pb (II) and Cu(II) ions adsorbed onto (A) 70%Bt-30%Ch beads and (B) 70%Bt-30%Ch composites.

Note: Initial Pb and Cu concentrations 100 mg/L (corresponding to 0.96 and 3.14 mEq/L of Pb and Cu ions respectively); pH = 4.5; adsorbent amount = 0.2 g; adsorption agitation time (at 230 rpm) = 10 minutes; desorbing agent = EDTA (1.0 x 10^1 mEq/L); desorption agitation time (at 230 rpm) = 120 minutes. Each bar represents mean ± standard deviation of three (3) different samples (n = 3).
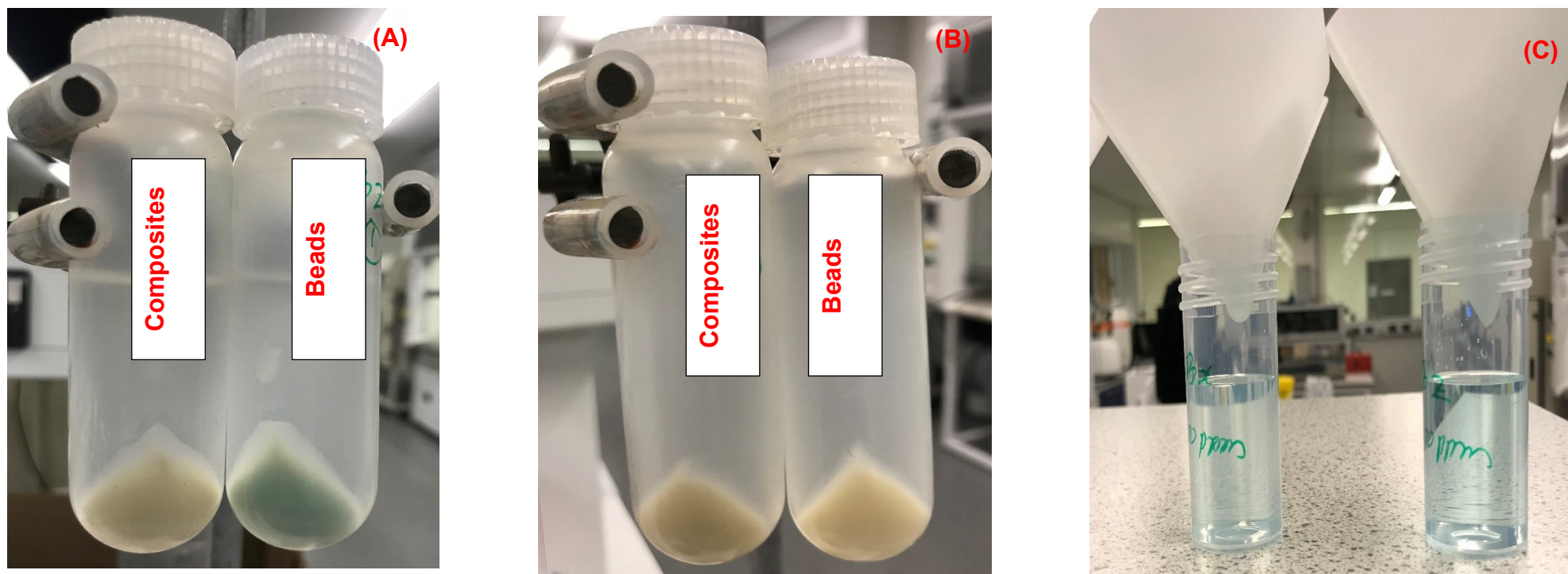
Figure 6.11: Pictures showing (A) adsorbent samples loaded with Pb(II) and Cu(II) ions after adsorption-procedure (B) adsorbent samples recovered after desorption-procedure and (C) filtrate solutions containing Pb(II) and Cu(II) ions desorbed with EDTA solutions

6.4. Conclusion

The simultaneous adsorption of Pb(II) and Cu(II) ions onto 70%Bt-30%Ch composites/beads from binary solution were investigated via a statistical design of experiments approach. It was observed that co-adsorption of Pb(II) and Cu(II) ions were affected by pH, adsorbent dose, and initial concentration. With respect to each analysed metal ions (and the adsorbent used), the optimum adsorption capacities were determined, and accuracy (precision) of the design space is within 95% for both prediction and confidence intervals. The adsorption equilibrium data correlated well with single-component Langmuir and Freundlich models. Also, the same equilibrium adsorption data fitted well with multi-component non-modified Langmuir, modified Langmuir and extended Freundlich model equations. The maximum adsorption capacities, Q_{max} (mg/g) of both Pb (II) and Cu (II) ions estimated for Bt-Ch composites were lower than the values obtained for Bt-Ch beads. When Bt-Ch composite was used as an adsorbent, the Q_{max} values obtained for Pb(II) ions were about 60% higher compared to values obtained for Cu(II) ions. However, the Q_{max} value of Cu(II) ions obtained (compared to values obtained for Pb(II) ions) were higher when the Bt-Ch bead was used as adsorbent. Overall, both composites and beads exhibited good potential for re-use after five cycles of regeneration, thus, indicating their potential as cost-effective adsorbents for simultaneous removal of Pb (II) and Cu (II) ions from wastewater.

Chapter 7

As(III) adsorption onto 70%Bt-30%Ch composites and beads: optimisation, equilibrium, kinetic, and thermodynamic modelling

7.1. Introduction

The health of some individuals, primarily in developing countries with inadequate sanitation and infrastructure, has been affected by elevated levels of arsenic in water [8]. Arsenic is present in both organic and inorganic forms in natural waters, with the latter being more toxic and prevalent in the form of arsenate (AsO_4^{3-}) and arsenite (AsO_3^{3-}) species with oxidation states of As(V) and As(III), respectively [8,26]. As(III), in particular, is highly toxic and difficult to eliminate through conventional methods. To safeguard the environment and promote public health, the World Health Organisation has emphasised the need to limit arsenic levels in drinking water to less than 0.01 mg/L, necessitating the removal of As(III) from various water sources, including groundwater [8]. To date, there are very few reports (or none) on using Bentonite-Chitosan composites/beads(Bt-Ch) for the removal of As(III) ions from aqueous solution.

In our previous experimental work, Bt-Ch composites or beads has been used as an adsorbent to effectively remove Pb(II) and combinations of Pb(II)-Cu(II) ions from aqueous solutions (chapter 5 and 6, respectively). This study was aimed at using Bt-Ch composites or beads as an adsorbent for the removal of As(III) ions from aqueous solutions. The optimisation and influence of multiple adsorption parameters with three adsorbent samples (70%Bt-30%Ch composites, beads-A and beads-B) were investigated simultaneously using the statistical design of the experiment (DoE). The equilibrium, kinetics, and thermodynamics studies were carried out. Also, the effects of coexisting ions on the adsorption behaviour of As(III) was investigated. A non-linear modelling method was employed to analyse the adsorption equilibrium and kinetic process, and optimisation was done using the "Solver add-in" in Excel Microsoft 365 (Latest Version).

7.2. Experimental

7.2.1. Materials

In this study, only three adsorbents were tested for adsorption of As(III) ions; 70%Bt-30%Ch-1 composites, beads-A and beads-B, these were prepared as described in Chapter 4. The sodium meta arsenite salt (NaAsO$_2$; ≥ 90.0%), sodium nitrate (NaNO$_3$; ≥ 99.0%),), sodium bicarbonate (NaHCO$_3$; ≥ 99.7%), sodium chloride (NaCl; ≥ 99.0%), potassium phosphate monobasic (KH$_2$PO$_4$ ≥ 99.0%), and the stock standard solutions (for ICP) of As (III) were obtained from Sigma-Aldrich (now Merck). Sodium hydroxide (reagent grade, 97%, pellets) and nitric acid (5%) were used to prepare aqueous basic and acidic solutions, respectively. All chemicals used, unless otherwise stated, were of analytical grade purity and preparations were made using deionised water.

7.2.2. Adsorption experiments

The batch adsorption procedure as described in Section 5.2.2 was used. The batch adsorption experiment was designed based on Optimal-I designs (Section 7.2.2.1). Five quantitative factors; pH, adsorbent dosage, Initial concentration, agitation time and temperature were investigated for their significant effect on the adsorption of As(III) onto Bt-Ch composites/beads. According to the literature [218], As(III) is primarily in the form of neutral H$_3$AsO$_3$ when the pH of a solution is below 9.2 (the pK$_{a1}$ of H$_3$AsO$_3$). Some of these neutral molecules will be in the anionic form (H$_2$AsO$_3^-$) as the pH of the solution approaches 9.0, but it was not confirmed since a speciation experiment was not conducted in this study. When the pH is 9.2 or above, As(III) is highly dissociated to H$_2$AsO$_3^-$ [218]. As a result, the experiments for adsorption were conducted within a pH range of 2 to 9 since most natural waters have a pH value below 9.2.

The quantitative measurement of As(III) ions was carried out using a Agilent 5110 ICP-OES using wavelength (As-278.022 nm).

The amounts of As(III) ions per unit mass of Bt-Ch composites/beads and percent adsorption performance (%) were calculated Equations 5.1 and 5.2, respectively as shown in Section 5.2.2.

7.2.2.1 *Surface Response Methodology - Optimal-I designs*

In this study, a set of 43 experiments/runs based on five numeric factors (as mentioned above), plus one categoric factor, was created, which included five replicates, using Design-Expert 13 software (Table 7.1 and Appendix D1). Each factor level combination was used in a randomised order. This design enabled to fit for a second-order polynomial model, which has main effects, two-factor interactions, and quadratic terms. The equation model was defined as:

$$Y = \alpha + aA + bB + cC + dD + eE + fF + abAB + acAC + adAD + aeAE + afAF +$$
$$bcBC + bdBD + beBE + bfBF + cdCD + ceCE + cfCF + deDE + dfDF + efEF + \quad (7.1)$$
$$aaA^2 + bbB^2 + ccC^2 + ddD^2 + eeE^2$$

where Y is the measured response (e.g., As-adsorption efficiency, %) associated with every variable level combination, α is the intercept (mean value), A, B, C, D, E and F are the main factors (representing pH, adsorbent dosage, initial concentration, agitation time, temperature, and adsorbent type, respectively); AB, AC, AD, AE, AF, BC, BD, BE, BF, CD, CE, CF, DE, DF, and EF are the two-factor (binary) interactions; A^2, B^2, C^2, D^2, and E^2, are the quadratic numerical (quantitative) factors; a, b, c, d, e, f or ab, ac, ad, ae, af, bc, bd, be, bf, cd, ce, cf, de, df, ef or aa, bb, cc, dd and ee are the coefficients of the main factors, interaction factors, and quadratic numerical factors, respectively.

Table 7.1: Factors and their levels investigated during optimal stage in the batch adsorption experiments of As (III) ions onto Bt-Ch composites/beads

Levels	Numeric continuous factors					Categoric nominal factor
	A-pH	B-Adsorbent dosage (g)	C-Initial concentration (mg/L)	D-Agitation time (min)	E-Temperature (^{O}C)	F-Adsorbent type
Low (-1)	1	0.05	50	10	25	X
Centre point (0)	varied	varied	varied	varied	varied	Y
High (+1)	9	0.5	250	300	55	Z

Note: The centre points (0) maybe slightly different due the algorithms of the optimal-I design; X = Bt-Ch composites; Y = Bt-Ch beads-A; Z = Bt-Ch beads-B

7.2.2.2 *Adsorption equilibrium and Isotherm*

To determine the equilibrium adsorption capacity of Bt-Ch composites/beads to absorb As(III) ions from aqueous solutions, a wider range of As(III) concentrations (i.e., from 10 to 500 mg L^{-1}) that differs from the one used in the optimal experiment (50 to 250 mg L^{-1}; Table 7.1). The experiment was performed based on the optimal experimental conditions obtained from the surface response-optimal designs of the previous section. Thus, 0.2 g of each adsorbent was exposed to 25 mL of As(III) solutions with varying concentrations (as stated above) at pH 8.0, agitation time of 180 minutes (with the speed of 230 rpm) and at room temperature (25°C). The experiment was repeated with the same conditions at the temperatures of 40 and 55°C. The equilibrium adsorption capacities, qe (mg/g) were calculated and then plotted against the corresponding respective equilibrium concentrations, Ce (mg/L) for adsorption isotherm modelling. In this study, three well known adsorption isotherm models namely Langmuir, Freundlich, and Dubinin-Radushkevich were used to fits the equilibrium data. The non-linear equations of these models are shown in Equations 2.9, 2.11 and 2.13, respectively, presented in Table 2.5.

Based on the Langmuir model, the separation factor (R$_L$) was calculated from Equation 2.14 (Section 2.5.4.1).

The adsorption potential (Ɛ) parameter (from the Dubinin-Radushkevich equation) and the mean free energy, E, per molecule of adsorbate were calculated from Equations 2.15 and 2.16, respectively (Section 2.5.4.3).

7.2.2.3 *Adsorption Kinetics*

To investigate the adsorption kinetics, the batch adsorption procedure (as described above) was carried out within the different time range of 10 – 300 minutes, with constant 0.2 g of adsorbent dosage, initial As(III) solution concentration (50 mg/L), pH 8 and at room temperature (25°C). The adsorption capacities (qt) were calculated at the different times of agitation and then plotted against the corresponding individual times to determine the equilibrium time for the adsorption to occur. In this study, the three kinetic models; pseudo-first order (PFO) [122,124], pseudo-second order (PSO) [124] and Elovich models [132] were used to analyse the experimental data. The linear

equations of PFO, PSO and Elovich are shown in Equations 2.2, 2.4, and 2.6, respectively. While the non-linear equations of these models are shown in Equations 2.3, 2.5 and 2.7, respectively, presented in Table 2.4.

7.2.2.4 *Adsorption thermodynamics*

The equilibrium adsorption of As (III) onto Bt-Ch composites/beads was carried out at different temperatures; 25°C (298.15K), 40°C (313.15K) and 55°C (328.15), and were used to calculate the thermodynamic parameters for the adsorption system. The three thermodynamic parameters were calculated by using a Van't Hoff approach from the equations shown below [116,219]:

$$\Delta G° = -RT \ln K_C \tag{7.2}$$

$$\Delta G° = \Delta H° - T\Delta S° \tag{7.3}$$

Where R is the universal gas constant (8.314 J mol^{-1} K^{-1}), T is the temperature (K), and K_C is the equilibrium constant. If the unit of $\Delta G°$ is J mol^{-1}, and that of term "RT" is also J mol^{-1}, then, the equilibrium constant K_C in Equation 7.2 must be dimensionless [116,219]. Based on the estimated Langmuir equilibrium constant K_L (L/g), the dimensionless value of the equilibrium constant Kc can be obtained by using the relationship shown below [116,219];

$$K_C = K_L \times M_W \times 55.5 \times 1000 \tag{7.4}$$

Where M_W is the molecular weight of adsorbate (i.e., Arsenic), the factor 55.5 (dm^{3}mol^{-1}moldm^{-3}) is dimensionless and it is the number of moles of pure water per litre of solution. It is obtained by dividing 1000 g/L by 18 g/mol (assuming the solution density is ≈ 1 g ml^{-1}). From Equations 7.2 and 7.3, the equilibrium constant K_C may be expressed in terms of $\Delta H°$ and $\Delta S°$ as a function of temperature as shown below:

$$\ln K_C = -\frac{\Delta H°}{R} \times \frac{1}{T} + \frac{\Delta S°}{R} \tag{7.5}$$

A plot of $\ln K_C$ against $1/T$ should give a straight line in the form of $Y = mx + c$, and the slope and intercept obtained can be used to calculate the values of $\Delta H°$ and $\Delta S°$, respectively.

7.3. Results

7.3.1. Surface Response: I-optimal designs

Although the investigated adsorbents (i.e., 70%Bt-30%Ch-1 composites, beads-A and beads-B) employed in this study were observed to be very poor towards As(III) uptake, the batch adsorption experiments were still carried out to generate data for the understanding of As adsorption with similar adsorbents. In this study, adsorption efficiency, % (instead of adsorption capacity, mg/g) was used as a response. Unlike adsorption efficiency, the adsorption capacity values were small and not adequately responsive to the model. The experimental adsorption efficiency results from the 43 experimental runs, alongside the corresponding predicted values obtained from the Design Expert software, are presented in Appendix D1. The mathematical relationships between the five studied independent factors (i.e., pH, adsorbent dose, initial concentration, agitation time and temperature) and the response (adsorption efficiency) were also provided by Design Expert 13 software. The equation in terms of actual factors (with regards to respective adsorbent (composites, beads-A & beads-B) which describes the various parameters regarding the As(III) adsorption onto Bt-Ch composites are all shown in Equation 7.6, 7.7, and 7.8, respectively.

Log_{10}(Adsorption efficiency)$X = -0.6845 - 0.2869A + 4.9868B - 0.0102C + 0.0052D + 0.0691E + 0.1943AB + 0.0001AD + 0.0020AE - 0.0380BE + 0.00006CE - 0.00003DE + 0.0103A^2 - 3.5460B^2 + 0.00002C^2 - 0.00001D^2 - 0.0008E^2$ (7.6)

Log_{10}(Adsorption efficiency)$Y = -0.3507 - 0.2709A + 4.2737B - 0.007C + 0.0052D + 0.0582E + 0.1943AB + 0.0001AD + 0.0020AE - 0.0380BE + 0.00006CE - 0.00003DE + 0.0103A^2 - 3.5460B^2 + 0.00002C^2 - 0.00001D^2 - 0.0008E^2$ (7.7)

Log_{10}(Adsorption efficiency)$Z = -0.1058 - 0.3492A + 3.9161B - 0.0061C + 0.0052D + 0.0642E + 0.1943AB + 0.0001AD + 0.0020AE - 0.0380BE + 0.00006CE - 0.00003DE + 0.0103A^2 - 3.5460B^2 + 0.0002C^2 - 0.00001D^2 - 0.0008E^2$ (7.8)

7.3.1.1 *Analysis of variance (ANOVA)*

The summary of ANOVA results for the adsorption efficiency (% removal) of As (III) ions by 70%Bt-30%Ch composites/beads are presented in Appendix D2. After data-fitting was carried out, the modified quadratic model concerning the response was deemed significant (Coefficient = 0.86; F = 31.78; P<0.0001) for adsorption efficiency (%). The non-significant "lack-of-fit" for adsorption efficiency (F = 0.771; P = 0.6368 > 0.05) suggest the adequacy of the model to explain data in the experimental region. This implies that there is a 85.15% chance that the F-value (for Lack of Fit) could be due to noise concerning adsorption efficiency. The R^2 value for this model was found to be 0.99 which indicates that about 99% of the experimental data could be matched with the predicted value, and only 1% of it was not explained by the model. The predicted R^2 (0.95) was in reasonable agreement with adjusted R^2 (0.99). The small value of coefficient of variance (CV = 1.81) implies that deviation between the predicted and experimental data values were minimal. Adequate precision measures the signal to noise ratio, and a ratio greater than 4 is desirable [195]. For this model, the ratio value was found to be 104.77 for adsorption efficiency, which indicates an adequate signal for Pb adsorption. P-values less than 0.05 indicate model terms are significant, and therefore, A, B, C, D, AB, AD, BC, BD, CD, A², B², and C² are significant terms in the modified quadratic model related to adsorption efficiency. However, p-values greater than 0.10 indicate model terms are not significant and so, they were completely removed or deleted from the model. The estimated coefficients for these significant terms, as obtained by coded equation, are useful for identifying their relative impact. When comparing the factor coefficients (second column shown in Appendix II) a positive and negative coefficient signifies increasing and decreasing effects, respectively.

The adsorption efficiency (%) of As (III) by 70%Bt-30%Ch composites/beads, was affected by linear effects of pH (A), adsorbent dosage (B), initial concentration (C), agitation time (D), temperature (E), and categorical factor-D (adsorbent type). Interaction effects of AB, AD, AE, AF, BE, BF, CE, CF, DE, EF were also observed concerning the absorption efficiency of As (III) by 70%Bt-30%Ch composites/beads. In addition, a quadratic effect of A², B², C², D² and E² are all significant in the model.

With respect to diagnostic statistics, both the normal probability plot and the correlation graph (between actual and predicted values) for adsorption efficiency, are shown in Figure 7.1 (a & b). Figure 7.1a represents the normal probability plot of studentised residuals for adsorption efficiency. This plot indicates whether residuals follow a normal distribution, i.e., the points should lay on an approximately straight line without any apparent deviation. However, when the distribution is not normal, it signifies a nonlinear pattern, which may be corrected by a proper transformation [202]. As can be seen in Figure 7.1a, almost all data are on a straight line for both responses, and therefore, it can be assumed that they are normally distributed. Figure 7.1b represents the correlation (relationship) between actual and predicted values of adsorption efficiency. The actual values are the measured values of the adsorption efficiency (%) obtained for 70%Bt-30%Ch composites/beads, which were determined experimentally using Equations 5.2. While, predicted values were generated using Equations 7.6 – 7.8. The predicted values of adsorption efficiency of 70%Bt-30%Ch composites/beads for As(III) adsorption, obtained from the model, are in good agreement with the actual experimental data. Please take note that these models tend to exhibit inherent bias as they make predictions based on the data that was utilised in their development.
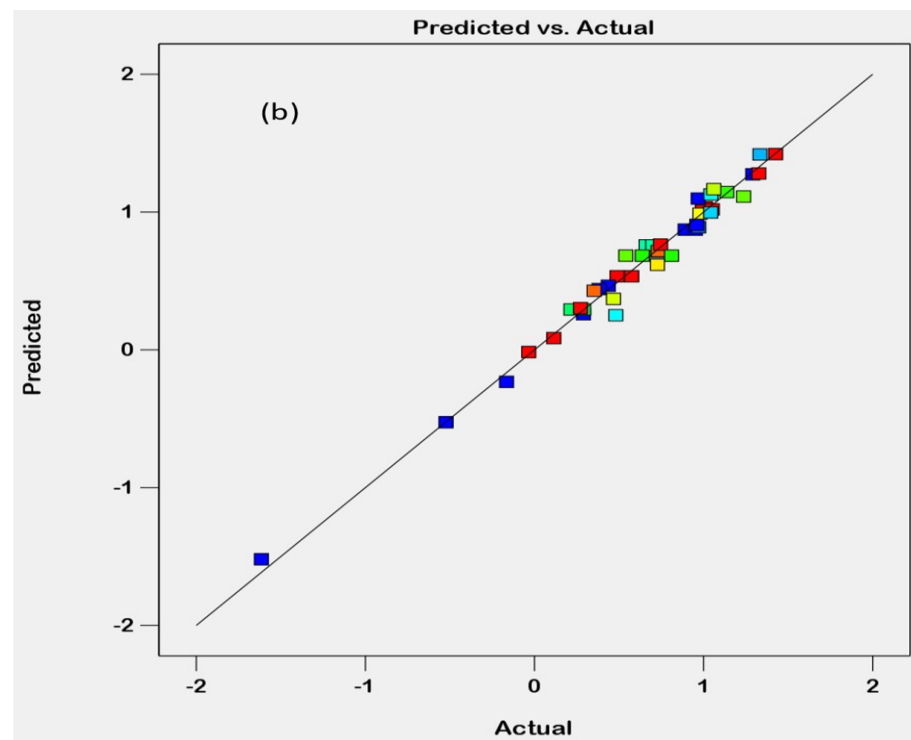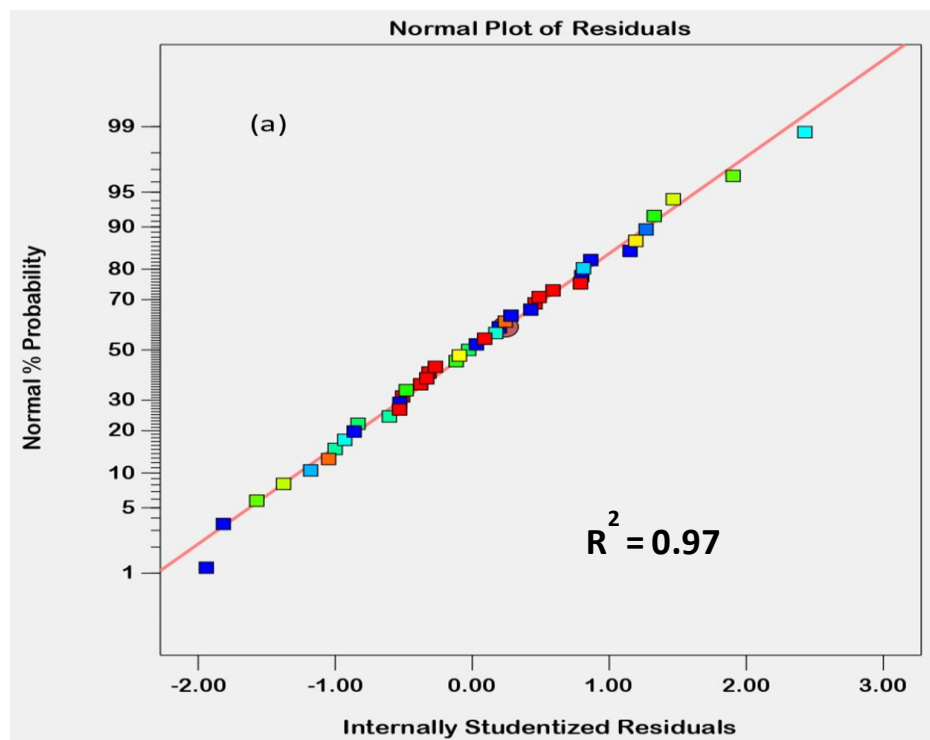
Figure 7.1: Normal probability plot of studentised residuals (a) and correlation between actual and predicted values (b) of As (III) ion adsorption efficiency for 70%Bt-30%Ch composites/beads

Note: these graphs were plotted and obtained from Design-Expert®13

7.3.1.2 *Effects of main factors and their interactions*

The model-graphs showing the effect of each quantitative factor on the adsorption efficiency (%) of As(III) by 70%Bt-30%Ch composites (adsorbent X) are shown in Figure 7.2. The model-graphs (concerning the main effect on the As(III) adsorption) obtained for the remaining two adsorbent samples (70%Bt-30%Ch beads-A and beads-B) show a similar trends and are not presented herein. As can be seen, when the pH (A; from 1 to 9) and initial concentration (C; 50 to 250 mg/L) of the solution increases, the As (III) adsorption efficiency of the Bt-Ch composites decreases initially and then increases. For adsorbent dosage (B), the adsorption efficiency of As(III) increases with increasing adsorbent dose from 0.05 to 0.5 g. Concerning agitation time (D), As (III) adsorption efficiency increases steadily from 10 to 180 min, maintains a higher % removal (between 180 to 240 min) and then slightly decreases for the remaining part of agitation time (240 to 300 min). When the temperature (E) of the adsorption system increases from 25 to 55 ^{O}C, the As (III) adsorption efficiency of the Bt-Ch composites/beads first increases and then decreases.

The model-graphs showing 2-way interaction effects of these factors are presented in Figure 7.3. Based on these plots, the interactive effects can be easily visualised and interpreted. When the effects of two factors appear as two non-parallel lines, it indicates that the effect of one factor depends on the level of another factor, and vice versa [202,203]. Therefore, the interactive effects were observed for pH-temperature (AE), adsorbent dosage-temperature (BE), initial concentration-temperature (CE), and agitation time-temperature (DE). Even though the lines are almost parallel, interactive effects were also observed for pH-adsorbent (AB) and pH-agitation time (AD) because from ANOVA table presented in Appendix D2, it was confirmed that the interactions of pH-adsorbent and pH-agitation time have significant effect.

7.3.1.3 *The 3D surface response plots and combined effects of significant factors*

Figure 7.4 show the 3D surface response plots regarding the combined effects of the significant factors on the As(III) adsorption efficiency (%) by Bt-Ch composites. The 3D plots (concerning the combined effects on the As(III) adsorption) obtained for the

remaining two adsorbent samples (70%Bt-30%Ch beads-A and beads-B) show a similar trends and are not presented herein.

(A) Combined effects of the solution pH and adsorbent dosage

Figure 7.4(a) shows the 3D response surface plot for the interaction effect of pH and adsorbent dosage, while the initial As(III) concentration, agitation time, and temperature of the system were kept constant at 50 mg/l, 180 minutes and $40^{\circ}C$, respectively. It was observed that the As(III) adsorption efficiency of the Bt-Ch composites/beads decreases initially (from pH 1 to 4), and then steadily increases (with an increase in pH level from 5 to 9). According to report [218], neutral H_3AsO_3 is the main form of As(III) in a solution at lower pH level. However, as the pH level gets close to 9.0, these neutral molecules will transform into the anionic form ($H_2AsO_3^-$) encouraging electrostatic force of attractions. This account for the rise in As(III) adsorption efficiency as the pH level increases from 5 to 9, despite the deprotonation of the adsorbents (Bt-Ch composites/beads) as the pH approaches 9.0. Previous work carried out by Boddu et al. [220] observed that pH does not have strong effects on the removal of arsenic(III) ions by chitosan-coated bio-sorbent. However, Manning et al. [221] reports that maximum sorption of As(III) ions by Goethite (adsorbent) was achieved in the pH range of 5 to 9. In this study, the influence of solution pH was more pronounced at the higher value of adsorbent dosage (0.5g). Also, it was noticed that the pH has a positive effect on the As(III) adsorption efficiency in a non-linear manner (A^2, check the coefficient in Appendix D2). The quadratic effect of pH (A^2) was observed to have a similar strength (but opposing sign) in comparison to the linear effect of pH (A), and this has accounted for the characteristic curve-shape of the 3D surface plot.

In terms of adsorbent dosage, it was observed that, the adsorption efficiency of As(III) ions increases with an increase in adsorbent dose from 0.05 to 0.5 g. The observed higher removal efficiency with increase in adsorbent dosage, was due to the fact that at high adsorbent dose, more adsorbent surface and exchangeable sites for adsorption are available for the As (III) ions adsorption [206]. The influence of adsorbent dosage may have a slightly negative effect on the As (III) adsorption efficiency in a non-linear manner (B^2, check the coefficient in Appendix D2). Even though this quadratic effect of adsorbent dosage (B^2) is less (in comparison to the linear effect of adsorbent dosage

(B)), this could be the reason for slight curved-shape of the 3D Surface plot in the direction of adsorbent dosage.

(B) Agitation time and temperature

Figure 7.4 (b) shows the 3D response surface plot for the interaction effect of agitation time and temperature, while the pH of the As (III) solution, adsorbent dose, and initial As (III) concentration were kept constant at 8.0, 0.5 g, and 50 mg/l, respectively. It was observed that the adsorption efficiency of As(III) ions increases with agitation time from 10 to 180 min, which remains constant with higher % removal (between 180 to 240 min) and then decreases for the remaining part of agitation time (240 to 300 min). The influence of agitation time has a strong negative effect on the As(III) adsorption in a non-linear manner (D^2, check the coefficient in Appendix L). This quadratic effect of adsorbent dose (D^2) is greater in comparison to the linear effect of adsorbent dosage (D, check the coefficient in Appendix L), and this contributed to curve-shape of the 3D surface plot.

Concerning temperature (E), it was observed that As (III) adsorption efficiency (%) increases when the temperature of the system increases from 25 to about 35 ^{O}C, maintains a constant (between 35 to about 40 ^{O}C) and then slightly decreases (between 43 to 55 ^{O}C). Like other significant factors, temperature has a strong negative effect on the As(III) adsorption in a non-linear manner (E^2, check the coefficient in Appendix L).

(C) Initial concentration and temperature

Figure 7.4(c) shows the 3D response surface plot for the interaction effect of initial concentration and temperature, while the pH of the As (III) solution, adsorbent dose, and agitation time were kept constant at 8.0, 0.5 g, 180 minutes, respectively. As can be seen, As(III) adsorption efficiency (%) of the Bt-Ch composites decreases initially and then slightly increases, when the initial As(III) concentration of the solution was increased from 50 to 250 mg/L. Based on general trends, adsorption efficiency (%) should decrease with increasing initial concentration of adsorbate (e.g. heavy metals). This may be due to increase in the number of heavy metal ions (such as As (III) ions) at higher concentration with the limited available binding sites on the adsorbent (Bt-Ch composites). At lowest initial As (III) concentrations (50 mg/L), the ratio of initial number of As (III) ions to the available adsorption active sites is low, and therefore, this

185

account for observed highest removal efficiency [206]. The effect of temperature on the influence of initial concentration effects was not clear or fully understood. However, the initial concentration has a strong negative effect on the As (III) adsorption efficiency with respect to temperature in a non-linear manner (C^2, check the coefficient in Appendix L). Since the strength of this quadratic effect (C^2) is greater in comparison to the linear effect (C, check the coefficient in Appendix II), and this contributed to curve-shape of the 3D surface plot.

7.3.1.4 *Optimisation of parameters for As (III) adsorption by Bt-Ch composites/beads*

The obtained optimal conditions (selected by the model) estimated for the adsorption of As (III) by 70%Bt-30%Ch composites, beads-A, and beads-B were pH of 8.0, adsorbent dose of 0.5, initial As (III) concentrations of 50 mg/l, agitation time of 180 minutes, and temperature of 40°C. The linear effect (Figure 7.2e) showed an increase in As adsorption as the temperature rose from 25 to 50°C. However, the presence of other quantitative factors had interactive effects (Figure 7.4b), resulting in the highest As adsorption efficiency (%) at 40°C. Under these conditions, the adsorption of As(III) ions was tested with only one of the adsorbents (sample Z; beads-B), which was selected randomly (by model) to confirm the robustness of the predicted model. As shown in Table 7.2, the experimental value (adsorption efficiency) obtained from confirmation runs was found to be 15.24 ± 0.37 %, which agrees well with the predicted value of 17.08 ± 4.96 *%* (desirability = 0.99) within the accuracy and precision of the design space (95% for both prediction and confidence intervals).
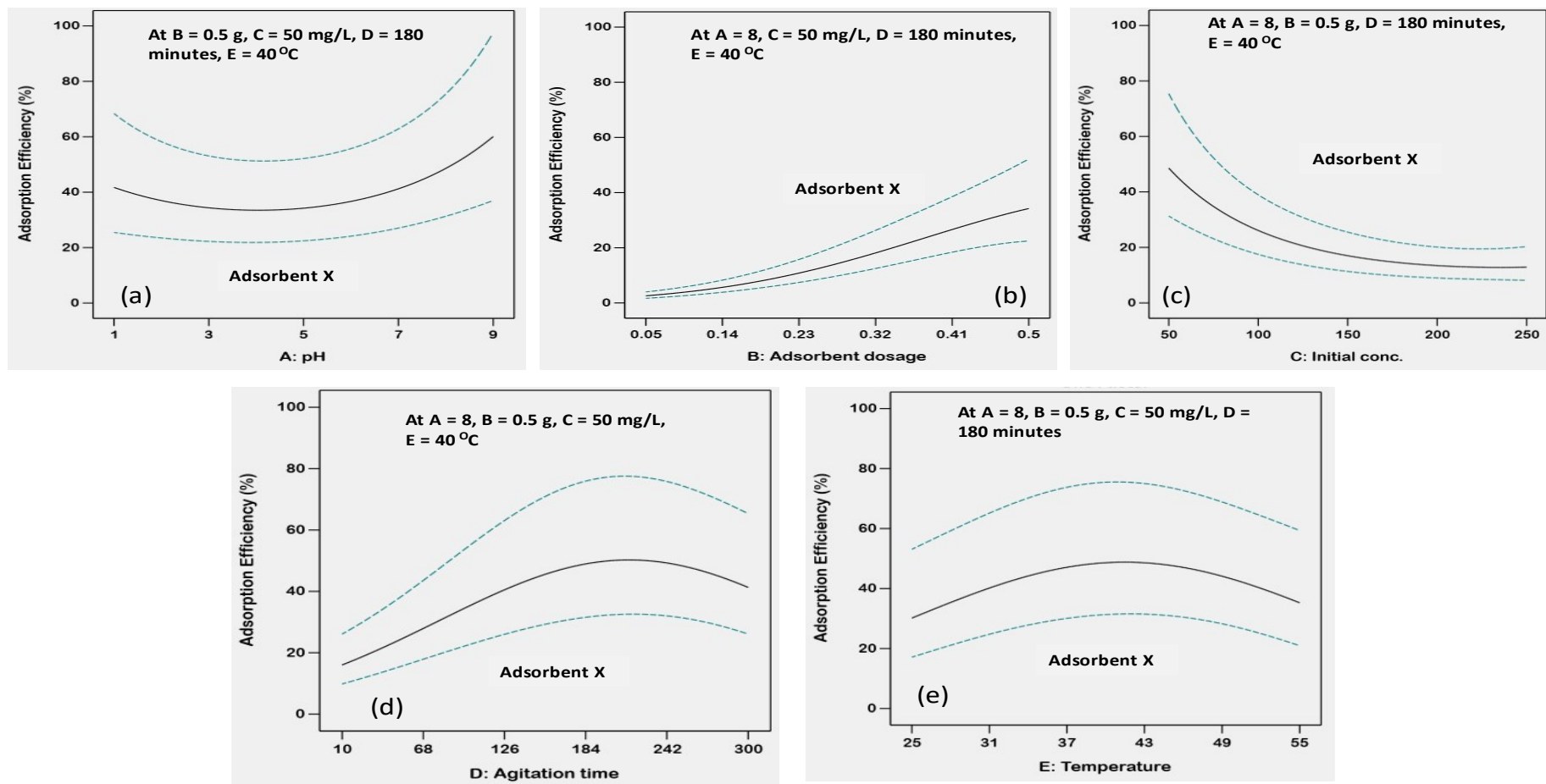
Figure 7.2: Graphs showing the effect of each factor on the As (III) adsorption efficiency (%)

Note: Dashed lines represent 95% confidence interval bands of the experimental data; (a) A-pH; (b) B-Adsorbent dose; (c) C-Initial concentration; (d) D-Agitation time; (e) E-Temperature; Adsorbent X = Bt-Ch composites.
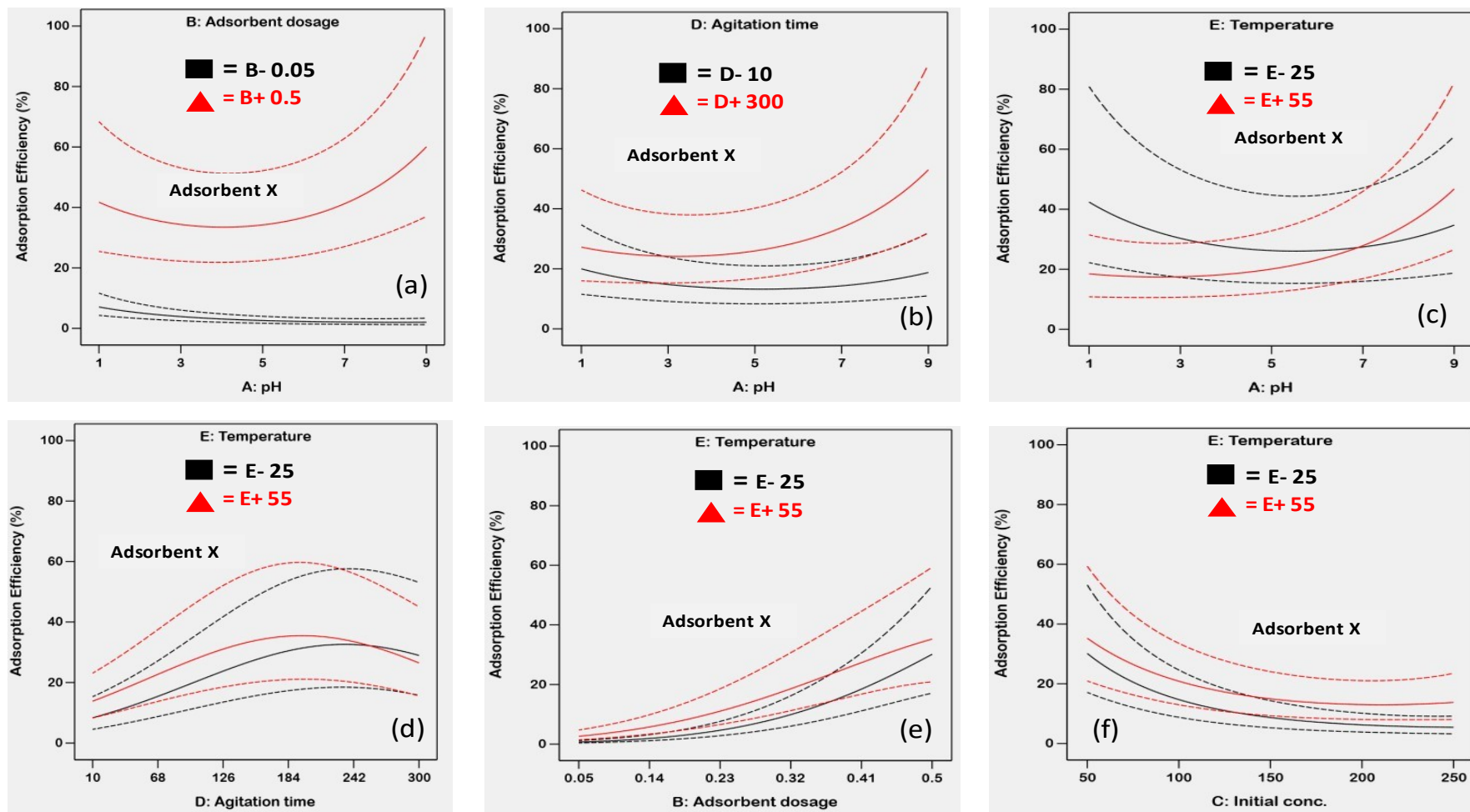
Figure 7.3: Graphs showing two-factor interactions and their effects on the As (III) adsorption efficiency (%)

Note: Dashed lines represent 95% confidence interval bands of the experimental data; (a) pH-Adsorbent dosage; (b) pH-Agitation time; (c) pH-Temperature; (d) Agitation time-Temperature; (e) Adsorbent dosage-Temperature; (f) Initial conc.-Temperature; Adsorbent X = Bt-Ch composites.
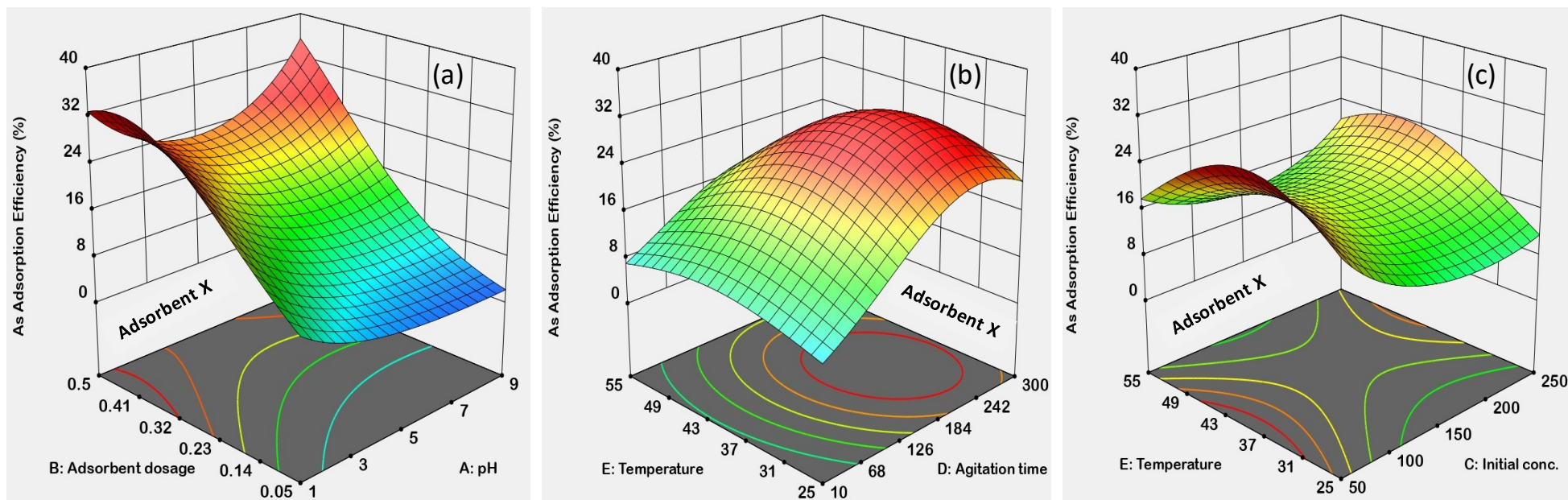
Figure 7.4: 3D surface response plots showing the combined effect of significant factors on the As (III) adsorption efficiency (%) by Bt-Ch composites

Note: these 3D surface plots were plotted and obtained from Design-Expert®13; (a) pH and adsorbent dosage (at constant initial conc. Of 50 mg/L, agitation time of 180 minute, and temperature of 40°C*)*; (b) agitation time and temperature (at constant pH of 8, adsorbent dose of 0.5 g, and initial conc. of 50 mg/L); (c) initial conc. and temperature (at constant pH of 8, adsorbent dose of 0.5 g, and agitation time of 180 minute).

Table 7.2: Confirmation of experimental runs for analysed Optimal-I design model

Response	Adsorbent type	Target	Predicted Mean	Desirability	Confirmation experiment	Confidence Interval (95%)	
						Low	High
As-Adsorption efficiency (%)	Z	Maximize	17.08 ± 4.96	0.99	15.24 ± 0.37	9.20	29.29

Adsorbent uesd = 70%Bt-30%Ch beads-B (Z); pH = 8.0; adsorbent dose = 0.5 g; Initial As (III) concentration = 50.0 mg/L; agitation time = 180 minutes; temperature = 40°C. For confirmation experiment, each value represents mean ± standard deviation of three (3) different samples (n = 3)

7.3.2. Adsorption Isotherm studies

Modelling equilibrium data with isotherm equations can provide qualitative and quantitative information about the adsorption process, which could contribute to understanding the adsorption mechanisms [24,48,116].

Figure 7.5 show the non-linear plots illustrating Langmuir/Freundlich and Dubinin-Radushkevich isotherm models, respectively, for As (III) adsorption by 70%Bt-30%Ch composites at 25, 40 and 55°C. The isotherm plots for other adsorbent samples (70%Bt-30%Ch beads-A and 70%Bt-30%Ch beads-B) are presented in Appendix D3 and D4 , respectively), but the calculated values (or constants) obtained for the three adsorbents (Bt-Ch composites, beads-A and beads-B) are presented in Table 7.3. The experimental data correlated well with both the Langmuir and Freundlich isotherm models, which indicates that both monolayer and heterogeneous adsorption processes may coexist under these experimental conditions.

The maximum adsorption capacity, Q_{max} (mg/g) of As (III) ions as determined through the Langmuir isotherm, does not show significant differences between the three adsorbents (Bt-Ch composites, beads-A and beads-B), but slightly increases with increasing temperature (25 to 55°C). The Q_{max} values obtained from this study were compared with other adsorbents reported in the literature (Table 7.4), although the values are small they are comparable (or even better) than most adsorbents previously reported.

Generally, low values for the Langmuir equilibrium constant (K_L) was observed for all the adsorbents used. A low value of K_L suggests poor affinity for the adsorbate-adsorbent

interaction and vice-versa [32,199]. The K_L values slightly decrease with increasing temperature for Bt-Ch beads-A and beads-B. This is similar to a previous study involving adsorption of chromium ions onto chitosan [175]. For Bt-Ch composite, it was observed that the value of K_L decreased slightly when the temperature increased from 25 to 40°C, and then slightly increased with temperature at 55°C. The calculated R_L values were all found within the range of 0 to 1 indicating that the adsorption of As (III) ions onto all the adsorbents (Bt-Ch composites/beads) were favourable.

Like the Langmuir equilibrium constant (K_L) values, the Freundlich constant (K_F) values are generally low for all the Bt-Ch composites/beads concerning As (III) adsorption. A very low K_F value indicates that only minimal loading of adsorbate onto adsorbent could be achieved and vice-versa [48]. The Freundlich exponent (n value) was also estimated and fall within the range of 0 to 1, indicating favourable adsorption.

To distinguish between the physical and chemical adsorption nature of As (III) adsorption by Bt-Ch composites/beads, both Langmuir and Freundlich isotherms are insufficient, and therefore, D–R isotherm was used for this purpose. As calculated from the D–R parameters, the mean free energy (E) of As (III) adsorption for all the analysed Bt-Ch composites/beads were found within the range from 0.022 to 0.038 kJ mol^{-1}, and these increase with temperature. Since the calculated E values were substantially lower than 8 kJmol^{-1}, therefore, the adsorption of As(III) ions onto Bt-Ch composites/beads occurs by a physical process, possibly by via ion-exchange or weak van der Waals forces [7,175].
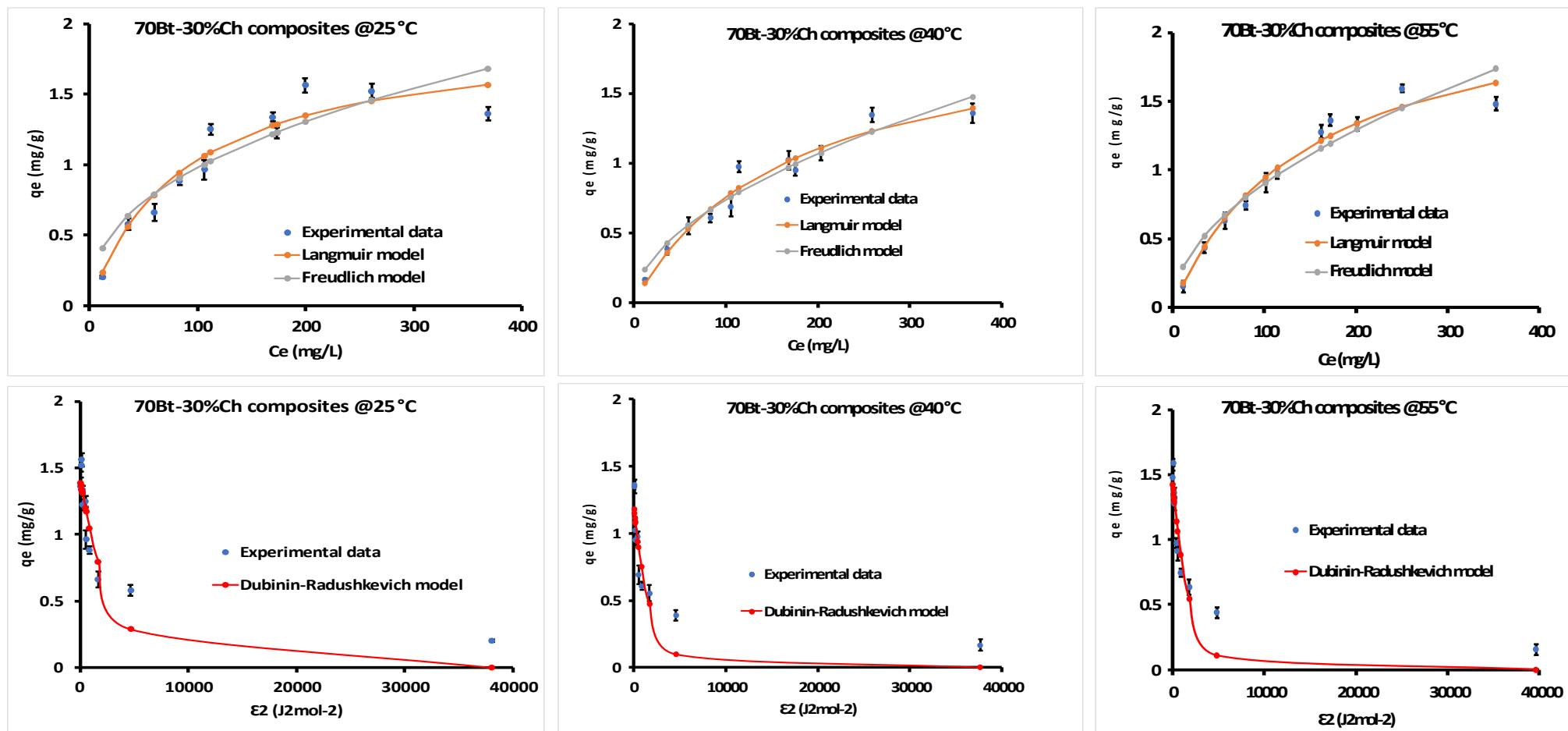
Figure 7.5: The non-linear Langmuir/Freundlich (top) and Dubinin-Radushkevich (bottom) isotherms for adsorption of As(III) by 70%Bt-30%Ch composites

Note: at 25, 40 and 55 ^{O}C. pH = 8.0; adsorbent amount = 0.2 g; agitation time (at 230 rpm) = 180 minutes; Initial As(III) concentrations = 10 - 350 mg/L; Each data-point represents mean ± standard deviation of three (3) different experiments (n = 3).

Table 7.3: The fitting parameters of Langmuir, Freundlich and Dubinin-Radushkevich isotherms for the adsorption of As(III) onto Bt-Ch composites/beads

Isotherm Model	70%Bt-30%Ch composites			70%Bt-30%Ch beads-A			70%Bt-30%Ch beads-B		
	25°C	40°C	55°C	25°C	40°C	55°C	25°C	40°C	55°C
Langmuir									
Q_{max}	1.940 ± 0.90	2.029 ± 0.14	2.316 ± 0.24	2.054 ± 0.11	2.660 ± 0.25	3.31 ± 0.74	1.711 ± 0.24	2.859 ± 0.24	2.937 ± 0.21
K_L	0.011 ± 0.01	0.006 ± 0.10	0.007 ± 0.00	0.007 ± 0.00	0.006 ± 0.00	0.004 ± 0.00	0.007 ± 0.00	0.004 ± 0.00	0.0038 ± 0.00
R_L	$0.21 - 0.88$	$0.27 - 0.91$	$0.27 - 0.91$	$0.27 - 0.91$	$0.26 - 0.90$	$0.40 - 0.95$	$0.26 - 0.91$	$0.42 - 0.95$	$0.35 - 0.94$
R^2	0.999 ± 0.00	0.999 ± 0.00	0.999 ± 0.00	0.999 ± 0.00	0.999 ± 0.00	0.999 ± 0.00	0.999 ± 0.00	0.999 ± 0.00	0.999 ± 0.00
X^2	0.014 ± 0.01	0.007 ± 0.00	0.006 ± 0.00	0.021 ± 0.00	0.026 ± 0.00	0.016 ± 0.00	0.032 ± 0.00	0.022 ± 0.02	0.046 ± 0.00
Freundlich									
K_F	0.144 ± 0.11	0.063 ± 0.02	0.082 ± 0.04	0.085 ± 0.04	0.072 ± 0.03	0.045 ± 0.03	0.082 ± 0.03	0.042 ± 0.01	0.039 ± 0.02
n	0.416 ± 0.24	0.534 ± 0.05	0.521 ± 0.08	0.497 ± 0.08	0.556 ± 0.08	0.648 ± 0.06	0.462 ± 0.12	0.042 ± 0.05	0.649 ± 0.06
R^2	0.999 ± 0.00	0.999 ± 0.00	0.999 ± 0.00	0.999 ± 0.00	0.999 ± 0.00	0.999 ± 0.00	0.999 ± 0.00	0.999 ± 0.00	0.999 ± 0.00
X^2	0.026 ± 0.01	0.009 ± 0.00	0.015 ± 0.01	0.030 ± 0.01	0.037 ± 0.00	0.026 ± 0.01	0.043 ± 0.00	0.034 ± 0.03	0.058 ± 0.00
D-R									
Q_{DR}	1.411 ± 0.11	1.210 ± 0.04	1.464 ± 0.14	1.329 ± 0.07	1.637 ± 0.03	1.747 ± 0.07	1.285 ± 0.07	1.473 ± 0.07	1.600 ± 0.02
K_{DR}	0.0003 ± 0.0	0.0005 ± 0.0	0.0005 ± 0.0	0.0005 ± 0.0	0.0007 ± 0.0	0.0009 ± 0.0	0.0008 ± 0.0	0.0009 ± 0.0	0.0010 ± 0.0
R^2	0.999 ± 0.00	0.999 ± 0.00	0.999 ± 0.00	0.999 ± 0.00	0.999 ± 0.00	0.999 ± 0.00	0.999 ± 0.00	0.999 ± 0.00	0.999 ± 0.00
X^2	0.027 ± 0.00	0.032 ± 0.00	0.025 ± 0.00	0.036 ± 0.00	0.040 ± 0.00	0.027 ± 0.00	0.068 ± 0.00	0.021 ± 0.00	0.041 ± 0.00
E	0.038 ± 0.00	0.034 ± 0.00	0.030 ± 0.00	0.032 ± 0.00	0.024 ± 0.00	0.022 ± 0.00	0.025 ± 0.00	0.0234 ± 0.00	0.022 ± 0.00

Note: D-R = Dubinin-Radushkevich; Qmax (mg/g) is the maximum saturated monolayer adsorption capacity of an adsorbent, K_L is the Langmuir constant called solute absorptivity (L/mg), R_L is the separation constant (dimensionless), K_F is the adsorbent capacity (L/g), n is the heterogeneity factor (unitless-ranging from 0 to 1), q_{RD} is the Dubinin-Radushkevich adsorption capacity (mg/g), K_{RD} is the Dubinin-Radushkevich constant related to the sorption energy (mol^2/kJ^2), E is the mean free energy of adsorption (KJ/mol), R^2 is the coefficient of correlation, and X^2 is nonlinear chi-square. Each value represents mean ± standard deviation of three (3) different samples (n = 3). R_L values are range between the lowest and highest value, and were calculated based on K_L and initial Pb (II) concentration, (C_0) ranging from 10 − 350 mg/L

Table 7.4: Comparisons of As(II) adsorption capacity by Bt-Ch composites/beads with other adsorbents reported in the literature

Adsorbents	Maximum adsorption capacity, Q_{max} (mg/g); (pH)			Ref.
	20°C /25°C	40°C	55°C	
Activated alumina	3.5; (7.0)	---	---	[26]
Gibbsite	3.3; (5.5)	---	---	[27]
Ferrihydrites	0.58; (4.2)	---	---	[28]
C-mVMT	72.2; (5.0)	---	---	[24]
HDTMA-modified kaolinite	0.32; (7.0)	---	---	[29]
Polymetallic sea nodule	0.69; (2.0 -9.0)	---	---	[30,31]
P-Al/Fe-mMont .	19.11; (7.0 − 9.0)	---	---	[30]
SMB3	0.82; (9.0)	---	---	[32]
Natural laterite	0.20; (7.2)	---	---	[24,33]
70%Bt-30%Ch composites	1.940 ± 0.90; (8.0)	2.029 ± 0.14; (8.0)	2.316 ± 0.24; (8.0)	this study
70%Bt-30%Ch beads-A	2.054 ± 0.11; (8.0)	2.660 ± 0.25; (8.0)	3.31 ± 0.74; (8.0)	this study
70%Bt-30%Ch beads-B	1.711 ± 0.24; (8.0)	2.859 ± 0.24; (8.0)	2.937 ± 0.21; (8.0)	this study

C-mVMT = chitosan-modified vermiculite; HDTMA = hexadecyltrimethylammonium ; P-Al/Fe-mMont = Polymeric Al/Fe modified montmorillonite ; SMB = surfactant-modified bentonite

7.3.3. Kinetic studies

To determine the controlling mechanism and the rate of adsorption between As (III) ions and Bt-Ch beads/composites, various kinetic models were applied. The pseudo-first order (PFO) usually depends on the initial solute concentration and may not fit well for the full-length of agitation time [72,115,124]. While, Pseudo-second order (PSO) is based on the sorption equilibrium capacity and depends on the number of adsorption sites and the number of adsorbate ions in the solid/liquid system [72,124,130]. The Elovich model assumes that the actual solid adsorbent surfaces are energetically heterogeneous, and no interactions occur among the adsorbed species.

In this study, both linear and non-linear equations of PFO, PSO and Elovich were used. Figure 7.6 and Figure 7.7 show the non-linear and linear-regression plots (illustrating PFO, PSO and Elovich kinetic models), respectively, for As (III) adsorption by 70%Bt-30%Ch composites at 25℃. The kinetic plots (both non-linear and linear) for other adsorbent samples (70%Bt-30%Ch beads-A and 70%Bt-30%Ch beads-B) are presented Appendix D5 – D8), but the calculated values (or constants) obtained for all the adsorbents are presented in Table 7.5. Based on non-linear models, it can be seen that the correlation coefficient (R^2) values for all the models were found to be the same (0.999), and the chi-square (X^2) values obtained were quite similar. Therefore, linear regression analysis of the linear forms of the kinetic equations were further employed to access the quality of the fits concerning the adsorption of As(III) onto Bt-Ch composites/beads. Based on linear models, higher correlation coefficient (R^2) values were observed for PSO (compared to PFO and Elovich models). In addition, based on both linear and non-linear equations, the calculated adsorption capacities, $q_{e(cal.)}$ for PSO (compared to PFO) were closer to the experimental adsorption capacities, $q_{e(exp.)}$, and this indicates that PSO model fitted better to the kinetic adsorption data. Also, the parameters obtained from the linear equations of these kinetic models were computed into their original corresponding equations, which then represent the calculated kinetic adsorption data. Both experimental and calculated kinetic adsorption data were plotted against time to observe the biases and confirm the best-fit kinetic system. Since the PSO model correlates better (with kinetic adsorption data), this suggests that the adsorption of As(III) adsorption onto Bt-Ch composites/beads occurs by a chemical process, which

contradicts our previous assertion of physical adsorption (as evidenced by Dubinin-Radushkevich isotherm modelling). A similar result was observed by Tawfik *et. al* [100], when they carried out a study using Chitosan-modified vermiculite for As(III) adsorption. Concerning the Elovich kinetic parameters (considering the non-linear equation), higher values of α were observed (compared to the β values) for Bt-Ch beads, and this suggests that the rate of adsorption is greater than the rate of desorption, which showed more feasibility towards As(III) adsorption. Similar results were found for cadmium (II) ion adsorption onto iron-oxide-activated-red-mud [130]. However, for Bt-Ch composites, the values of β obtained were higher than the α values.

7.3.4. Thermodynamic study

The spontaneousness and feasibility of any adsorption process is usually examined by thermodynamic parameters such as free energy change ($\Delta G°$), enthalpy change ($\Delta H°$), and entropy change ($\Delta S°$) [116,201,219,222]. The thermodynamic plots for all three adsorbent samples (70%Bt-30%Ch composites, beads-A and beads-B) are shown in shown in Figure 7.8, and the calculated values (or constants) obtained are presented in Table 7.6. As can be seen, the negative values of $\Delta G°$ observed at all the temperatures studied indicates that the adsorption of As (III) onto Bt-Ch composites/beads occurred spontaneously. Also, the negative values of $\Delta H°$ suggests that adsorption process proceeded exothermically. It has been reported that an exothermic process is usually associated to physical adsorption coupled with relatively weak interactions (i.e., van der Waal forces) [7,222]. Moreover, the positive values of $\Delta S°$ obtained signifies an increased randomness at the adsorbent-adsorbate (i.e., solid-solution) interface during the adsorption interaction [222].
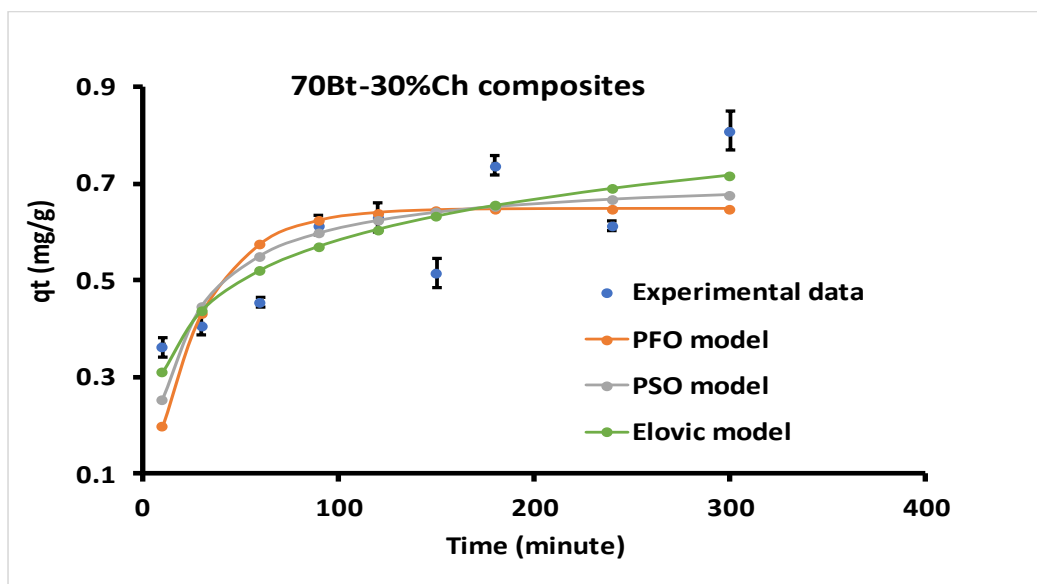
Figure 7.6: The non-linear PFO, PSO and Elovich kinetic models for adsorption of As(III) by 70%Bt-30%Ch composites

Note: at 25 ^{O}C. pH = 8.0; adsorbent amount = 0.2 g; Initial As(III) concentrations = 50 mg/L; agitation time (at 230 rpm) = 10 - 300 minutes; PFO = Pseudo-first order; PSO = Pseudo-second order. Each data-point represents mean ± standard deviation of three (3) different experiments (n = 3).
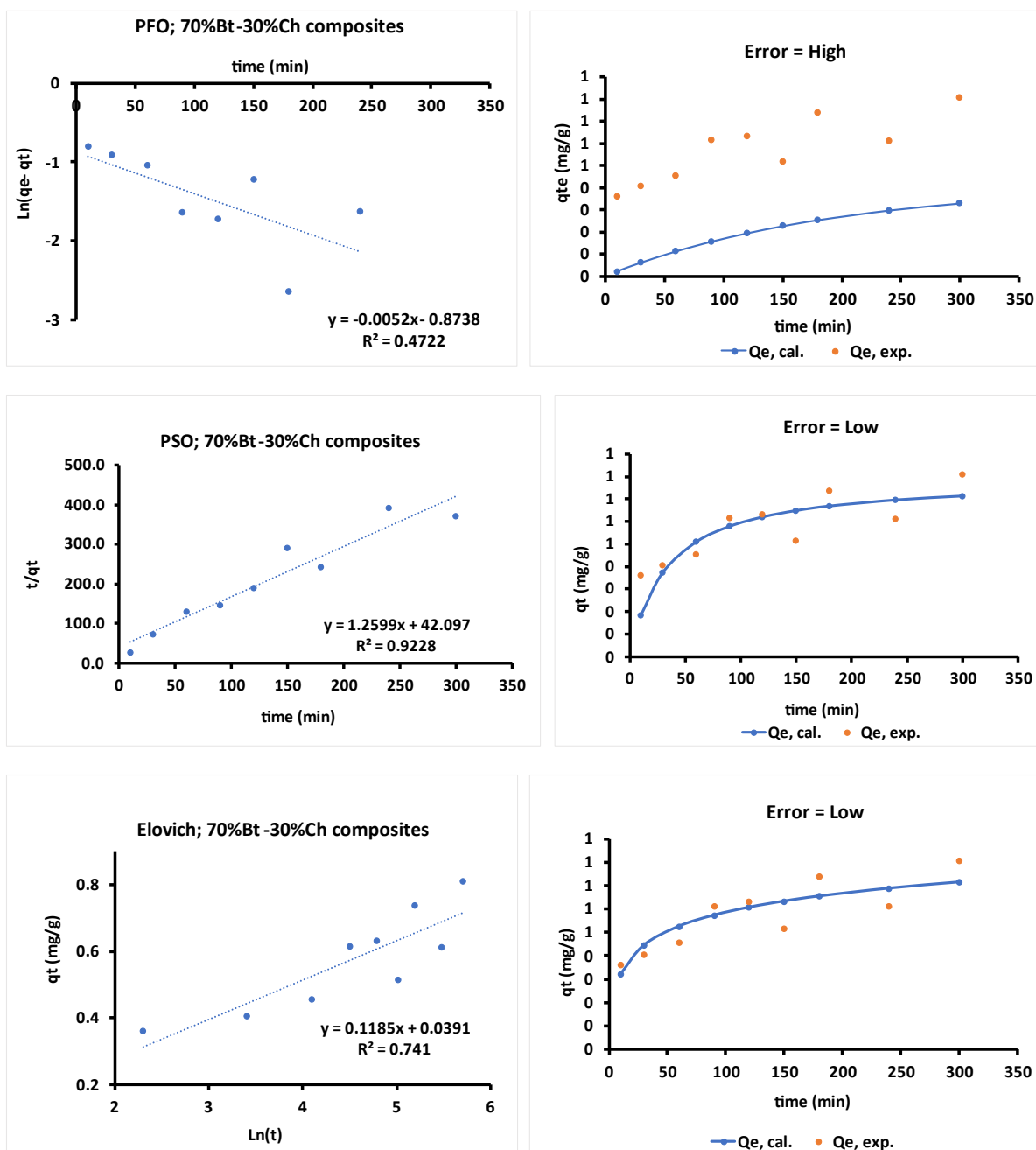
Figure 7.7: The linear regression analysis of PFO, PSO and Elovich kinetic models for adsorption of As(III) by 70%Bt-30%Ch composites

Note: at 25 ^{O}C. pH = 8.0; adsorbent amount = 0.2 g; Initial As(III) concentrations = 50 mg/L; agitation time (at 230 rpm) = 10 - 300 minutes; PFO = Pseudo-first order; PSO = Pseudo-second order. The average of the kinetic adsorption data was used to plot the linear regression graph.

Table 7.5: The fitting parameters of kinetic models for the adsorption of As(III) onto Bt-Ch composites/beads

Kinetic Models	70%Bt-30%Ch composites		70%Bt-30%Ch beads-A		70%Bt-30%Ch beads-B	
	Non-linear	linear	Non-linear	linear	Non-linear	linear
PFO						
K_1	0.043 ± 0.01	0.005 ± 0.00	0.135 ± 0.05	0.014 ± 0.00	0.100 ± 0.04	0.005 ± 0.00
$q_{e,exp}$	0.810 ± 0.02	0.810 ± 0.02	0.978 ± 0.07	0.978 ± 0.07	0.628 ± 0.06	0.628 ± 0.06
$q_{e,cal}$	0.615 ± 0.06	0.420 ± 0.00	0.830 ± 0.05	0.300 ± 0.01	0.574 ± 0.05	0.190 ± 0.02
R^2	0.999 ± 0.00	0.472 ± 0.00	0.999 ± 0.00	0.458 ± 0.00	0.999 ± 0.00	0.844 ± 0.00
X^2	0.021 ± 0.00	---	0.008 ± 0.00	---	0.009 ± 0.00	---
PSO						
K_2	0.079 ± 0.00	0.038 ± 0.00	0.707 ± 0.10	0.101 ± 0.01	0.308 ± 0.16	0.111 ± 0.04
$q_{e,exp}$	0.810 ± 0.02	0.810 ± 0.02	0.978 ± 0.07	0.978 ± 0.07	0.628 ± 0.06	0.628 ± 0.06
$q_{e,cal}$	0.691 ± 0.05	0.790 ± 0.01	0.872 ± 0.06	0.990 ± 0.01	0.605 ± 0.01	0.620 ± 0.01
R^2	0.999 ± 0.00	0.923 ± 0.00	0.999 ± 0.00	0.995 ± 0.00	0.999 ± 0.00	0.990 ± 0.00
X^2	0.015 ± 0.00	---	0.013 ± 0.00	---	0.008 ± 0.00	---
Elovich						
β	8.384 ± 0.41	8.440 ± 0.19	65.070 ± 13.64	8.750 ± 1.13	17.301 ± 5.14	17.560 ± 1.18
α	0.130 ± 0.02	0.165 ± 0.05	37932 ± 241.0	2.334 ± 0.34	36.384 ± 16.95	6.029 ± 0.30
R^2	0.999 ± 0.00	0.741 ± 0.00	0.999 ± 0.00	0.904 ± 0.00	0.999 ± 0.00	0.915 ± 0.00
X^2	0.010 ± 0.00	---	0.014 ± 0.00	---	0.009 ± 0.00	---

Note: PFO = Pseudo-first order; PSO = Pseudo-second order; $q_{e,\,exp}$ is the experimental adsorption capacity at equilibrium (mg/g); $q_{e,\,cal}$ is the calculated adsorption capacity at equilibrium (mg/g); k_1 is the PFO rate constant (min^{-1}); k_2 is the PSO rate constant (g/mg min); β is the Elovich desorption coefficient (g/mg min); α is the Elovich initial sorption rate (mg/g min); R^2 is the coefficient of correlation, and X^2 is nonlinear chi-square. Each value represents mean $\pm$ standard deviation of three (3) different samples (n = 3).

Table 7.6: The fitting of thermodynamic parameters for the adsorption of As(III) onto Bt-Ch composites/beads

Adsorbent	Temperature (K)	K_c	$\Delta G°$ (KJ mol^{-1})	$\Delta H°$ (KJ mol^{-1})	$\Delta S°$ (J mol^{-1} K^{-1})	Van't Hoff equation	R^2
X	298.15	45738.66	-26.59	-12.57	46.07	Y = 1512.5x + 5.5407	0.5422
	313.15	24948.36	-26.36				
	328.15	29106.42	-28.04				
Y	298.15	29106.42	-25.48	-15.05	35.34	Y = 1810.6x + 4.2501	0.9229
	313.15	24948.36	-26.36				
	328.15	16632.24	-26.52				
Z	298.15	29106.42	-25.48	-16.77	28.57	Y = 2017.3x + 3.4368	0.8336
	313.15	16632.24	-25.30				
	328.15	15800.63	-26.38				

X = 70%Bt-30%Ch composites; Y = 70%Bt-30%Ch beads-A; Z = 70%Bt-30%Ch beads-B; K_c = equilibrium constant; $\Delta G°$ = free energy change; $\Delta H°$ = enthalpy change; $\Delta S°$ = entropy change; R^2 = correlation coefficient; $K_c = K_L \times 74.92 \times 55.5 \times 1000$; K_L is the Langmuir constant (L/mg) obtained from Table 7.5.
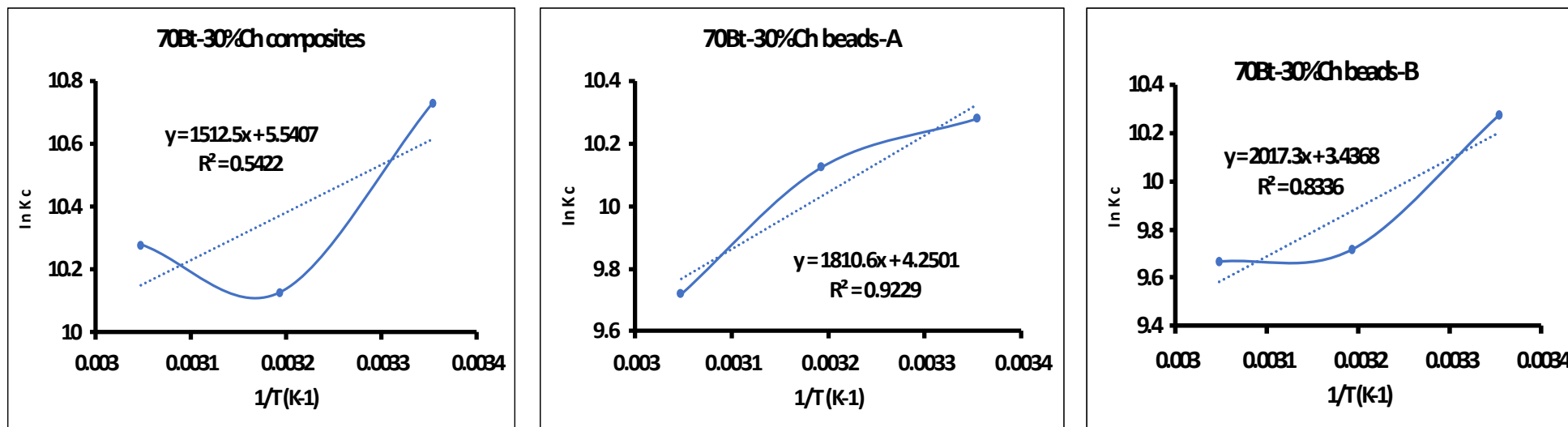
Figure 7.8: A line graph to determine the thermodynamic parameters for the adsorption of As(III) onto Bt-Ch composites/beads

7.3.5. Adsorption efficiency of As(III) ions

To investigate the efficiency of the absorption process in a single component system, a batch adsorption with different concentrations *of A*s(III) solutions (at pH of 8.0) were exposed to 0.2 g of Bt-Ch composites/beads, bentonite, and chitosan. After 180 minutes of agitation and even with lowest As(III) concentration (5 mg/L), the amount of As(III) ions removed were less than 10% for all the Bt-Ch composites/beads (as shown in Figure 7.9). A similar trend (but slightly higher) for As(III) efficiency (%) was observed for pristine bentonite. However, only less than 1% removal of As(III) ions were observed for pure chitosan. It is interesting to note that the bentonite performed better towards As(III) compared to chitosan. This suggests that the chitosan present in the Bt-Ch composites/beads does not contribute much towards As(III) ion adsorption. These very low adsorption efficiencies, indicate the need for modification of Bt-Ch beads/composites for effective removal of As(III) ions.
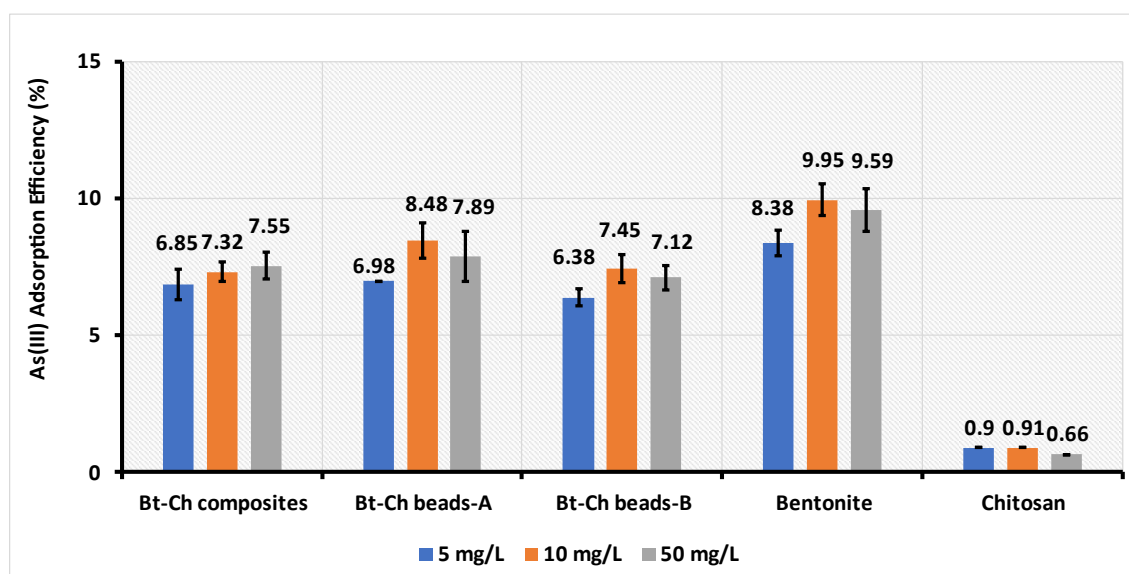
Figure 7.9: Charts showing the As(III) adsorption efficiencies (%) of Bt-Ch composites, beads, chitosan, and Na-bentonite.

Note: Initial As(III) concentrations = 5, 10 and 50 mg/L; pH = 8.0; adsorbent amount = 0.2 g; agitation time (at 230 rpm) = 180 minutes. Each bar represents mean ± standard deviation of three (3) different samples (n = 3).

7.3.6. Effect of coexisting ions on As(III) ion removal

Various anionic species might exist in natural water sources (e.g., groundwater) which could compete with arsenic for the available adsorption sites. Common co-existing anions present in the natural water includes carbonates, phosphates, sulphates, chlorides, and nitrates, and these could inhibit arsenic removal. In this study, the effects of nitrates (NO_3^-), dihydrogen phosphates (H_2PO^-), bicarbonates (HCO_3^-) and Chlorides (Cl^-) on removal of As (III) ions by Bt-Ch composites/beads were investigated at pH 8.0 with competing anion concentrations of 20 and 200 mg/L. As can be seen (Figure 7.10), the presence of NO_3^-, HCO_3^- and Cl^- ions (even at high concentrations of 200 mg/L) have no inhibition effects on the removal of As (III) by Bt-Ch composites/beads. However, H_2PO^- ions (at concentrations of 20 and 200 mg/L) are an obvious interference and significantly decrease the removal of As(III) ions by Bt-Ch composites/beads. A similar result was observed by Ramesh *et al*. [223], where the presence of phosphates (PO_4^{3-}) significantly affected the adsorption of As(III), As(V) and dimethylarsinate (DMA) by polymeric Al/Fe modified montmorillonite. The noticeable decrease in arsenic adsorption in the presence of phosphates ions may be due to competition for the binding sites of the adsorbent between the phosphate and arsenic, since both phosphate and arsenic have similar chemical features [223,224]. Even though Bt-Ch composites/beads were poor towards As adsorption, this result has demonstrated that the use of these adsorbents to remove As(III) from aqueous solution exhibited good anti-interference ability towards co-existing ions.
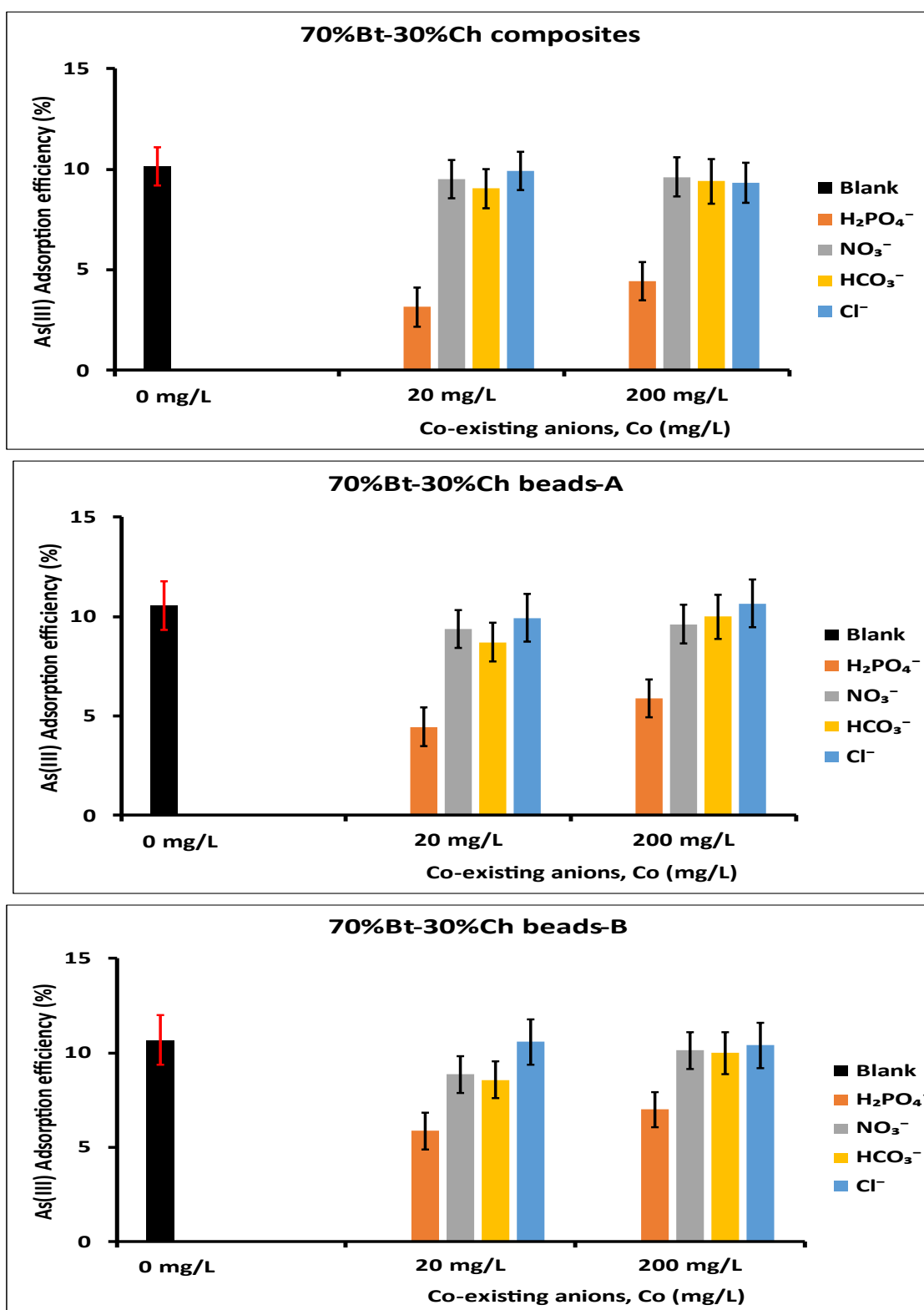
Figure 7.10: Charts showing the effect of anions on removal efficiencies (%) of As(III) ions from binary solutions by Bt-Ch composites/beads

Note: Initial concentrations of As(III) solution = 10 mg/L; pH = 8.0; adsorbent amount = 0.2 g; agitation time (at 230 rpm) = 180 minutes. Each bar represents mean ± standard deviation of three (3) different samples (n = 3).

7.4. Conclusion

The capability of 70%Bt-%Ch composites/beads to remove As(III) ions have been investigated. It was observed that adsorption efficiency (%) of As(III) ions were affected by pH, adsorbent dose, initial concentration, agitation time and temperature. The adsorption equilibrium data correlated well with Langmuir, Freundlich and Dubinin-Radushkevich isotherm models. Low values of maximum As(III) adsorption capacities (Qmax) were recorded for all Bt-Ch composites/beads. Both equilibrium isotherm (by Dubinin-Radushkevich modelling) and thermodynamic analysis indicate that the adsorption of As(III) adsorption onto Bt-Ch composites/beads occurs by physical process. However, kinetic investigations suggest that the adsorption of As(III) onto Bt-Ch composites/beads may occur via a chemical process. With exception of phosphates (PO_4^{3-}), other anions investigated have no inhibition effects on the removal of As (III) by Bt-Ch composites/beads. Overall, the poor loading capacity and very low adsorption efficiencies of these adsorbents indicates the need for modification of Bt-Ch beads/composites for effective removal of As(III) ions from aqueous solution.

Chapter 8

Preparation and characterisation of iron-based bentonite-chitosan composites for As(III) adsorption

8.1. Introduction

Contamination of natural waters with toxic arsenic, especially in developing nations, has been documented, and long-term exposure to elevated arsenic concentrations has been reported to cause cancer in humans [24]. Arsenic occurs in environmental media (e.g., water) both in organic and inorganic forms. The inorganic form of arsenic which dominates natural waters and more hazardous usually occurs as arsenite (AsO_3^{3-}) and arsenate (AsO_4^{3-}) species with different oxidation states of trivalent-As (III) and pentavalent-As(V), respectively [24]. As(III) is significantly more toxic and more mobile than As (V), which is also more difficult to remove by conventional treatment procedures [24]. In regard to that, most purification techniques require pre-oxidation of As (III) to As(V) for effective arsenic removal, thus causing more complexity and no longer being cost-effective [24].

Clays such as bentonite (mainly montmorillonite) has been widely studied for metal sorption processes [49,57]. However, previous studies demonstrated that clay materials have been very poor adsorbents towards anion species (e.g., nitrates, arsenites) [225,226]. Since clay mineral surfaces are negatively charged, thus, their low-loading capacity is attributed to coulombic repulsion between the negatively charged smectite surface and the anion species [225,227]. To overcome this problem, Su et al [225], carried out modification work by exchanging smectite with poly-diallyl-dimethylammonium (poly-DADMAC) cations which creates positively charged smectite surfaces and improves the nitrate uptake significantly (Figure 8.1) [225]. Charge reversal on the surface of smectites has been reported to enhance the anion exchange-adsorption capacity [75,94,225,227].

In our previous study, a positively charged biopolymers (chitosan) was intercalated into layered silicates (bentonite) to reverse the charge on the clay surface from negative to positive. However, we observed that the biggest drawback of these prepared Bt-Ch

composites as an adsorbent, is their extremely poor performance towards As (III) uptake (as demonstrated in chapter 7). This justifies the modification by introduction of Fe (III) cation into chitosan prior to combination with bentonite clay. The free hydroxyl groups (and perhaps, amine groups) on the chitosan backbone structure interacted with Fe (III) to produce a clay-polymer composite with Fe(III) oxide surfaces. The prepared Fe-modified composite could be a potential adsorbent to remove toxic anionic pollutant, such as As (III) ions from water [228,229]. Many types of Fe(III)-bearing materials such as hydrous-ferric-oxide [230], goethite and hematite [221,231], iron oxide-coated sand [232], iron-chitosan composites[233], ferrihydrite[234], and iron-oxide-coated polymers [235] has been researched and used as an adsorbents for effective removal inorganic arsenic species from water. Although some of these materials have been efficient for arsenic adsorption, but their application might be limited due to cost. Thus, the use of iron-modified Bentonite-Chitosan composite for As (III) adsorption could be a viable option.

The aim of this study was to synthesise positively charged composites by modifying bentonite clay with chitosan and Fe(III) cations. The iron-modified composites were characterised by thermogravimetric analysis, X-ray diffraction, and Fourier transform infrared spectroscopy. The prepared composites were applied (as an adsorbent) by using batch adsorption procedures and assessed via statistical design of experiments, to abstract As (III) ions from aqueous solutions. As (III) ion concentrations were analysed by using inductively coupled plasma optical emission spectrometry (ICP-OES). A non-linear modelling method was employed to analyse the kinetics and adsorption equilibrium process and optimisation was done using the "Solver add-in" in Excel Microsoft 365 (Latest Version). Regeneration of adsorbents and selectivity towards As (III) adsorption was also carried out.

8.2. Experimental

8.2.1. Materials

The bentonite, Cloisite® Na$^+$ and medium molecular weight chitosan as previously stated in Section 4.2.1 were used. The sodium meta arsenite salt (NaAsO$_2$; ≥ 90.0%), iron (III)

nitrate nona-hydrate (≥ 99.95%), and the stock standard solutions (for ICP) of As (III) were obtained from Sigma-Aldrich (now Merck). All chemicals used, unless otherwise stated, were of analytical grade purity and preparations were made using deionised water.
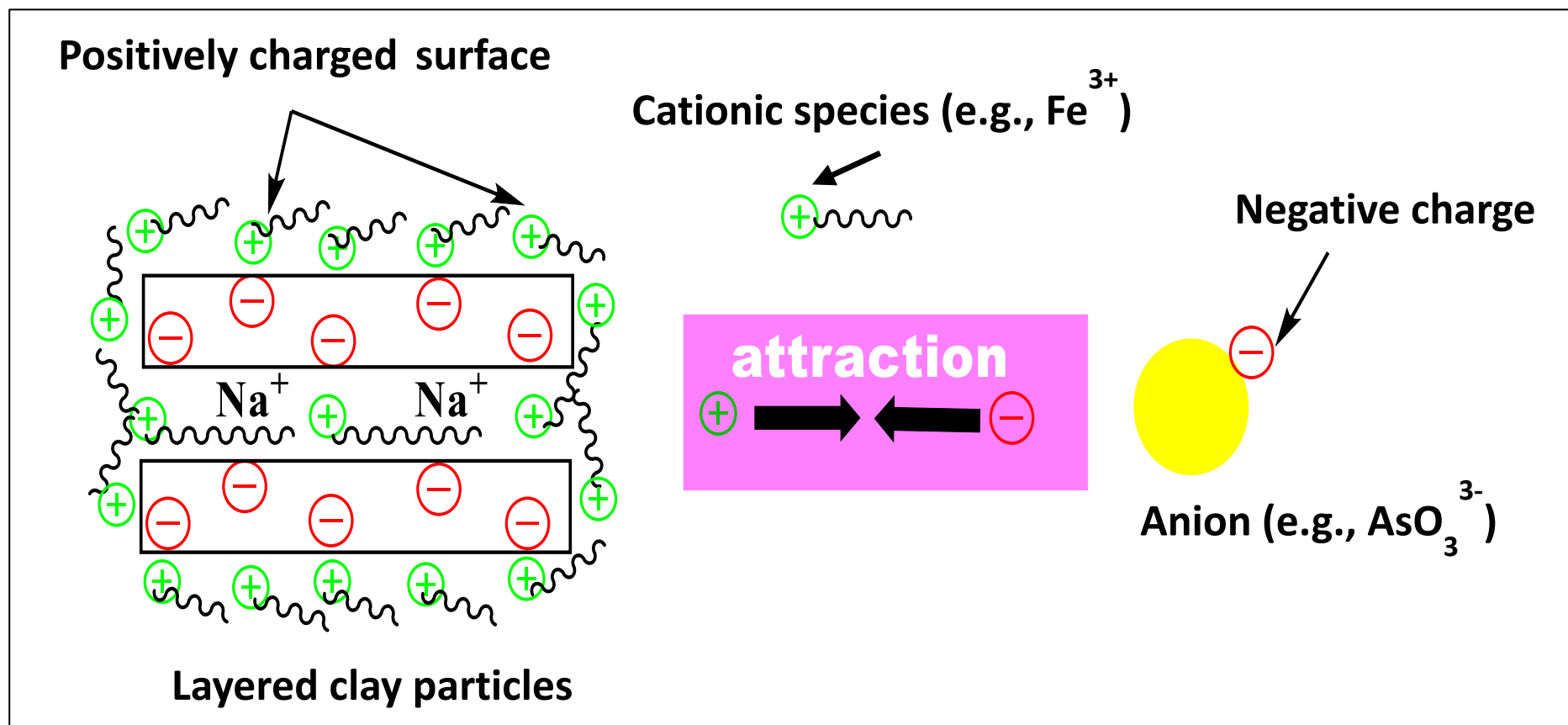
Figure 8.1: Scheme illustrating the coulombic attraction between the positively charged clay surface and the anion species

8.2.2. Preparation of Iron-modified Bentonite-Chitosan (Fe-Bt-Ch) composites

The precipitation method which involves addition of NaOH until neutralisation as described in Section 4.2.2.2 was used for making of Fe-Bt-Ch composites (Figure 8.2). Here, the chitosan was initially dissolved in aqueous Fe(III) solution (pH ~ 1.35; 350 ml capacity) before mixing it with bentonite suspension. Two forms of composites were made depending on the concentration of Fe(III) solution (0.01 M and 0.02 M), and both were prepared in the weight ratios of 70% Bt. Clay and 30% chitosan biopolymer. The modified composites were identified as "Fe-Bt-Ch 1" and "Fe-Bt-Ch 2" and were formed by dissolving chitosan in either 0.01 M or 0.02 M Fe(III) solution, respectively. The composites were characterised by thermogravimetric analysis, X-ray diffraction, and Fourier transform infrared spectroscopy.

8.2.1. Adsorption experiments

The batch adsorption procedures as described in Section 5.2.2 and 7.2.2 were used. The batch adsorption experiment was designed based on Optimal-I designs (Table 8.1 and Appendix E1). The quantitative measurement of As(III) ions was carried out as described in Section 7.2.2

The amounts of As(III) ions per unit mass of Fe-Bt-Ch composites and percent adsorption performance (%) were calculated Equations 5.1 and 5.2, respectively as shown in Section 5.2.2.

Fe(III) solution (0.02 or 0.01 M)

Chitosan-Fe solution

Bentonite suspension

Fe-Bt-Ch mixture 70%Bt-30%Ch

Neutralisation

Dried in the oven at 7 0 °C, 24 hours and pulverised

Powdered Fe-Bt-Ch composite

Freshly prepared Fe-Bt-Ch composite

Separation of Fe-Bt-Ch ppt.

Fe-Bt-Ch ppt formed after neutralisation with 1M NaOH
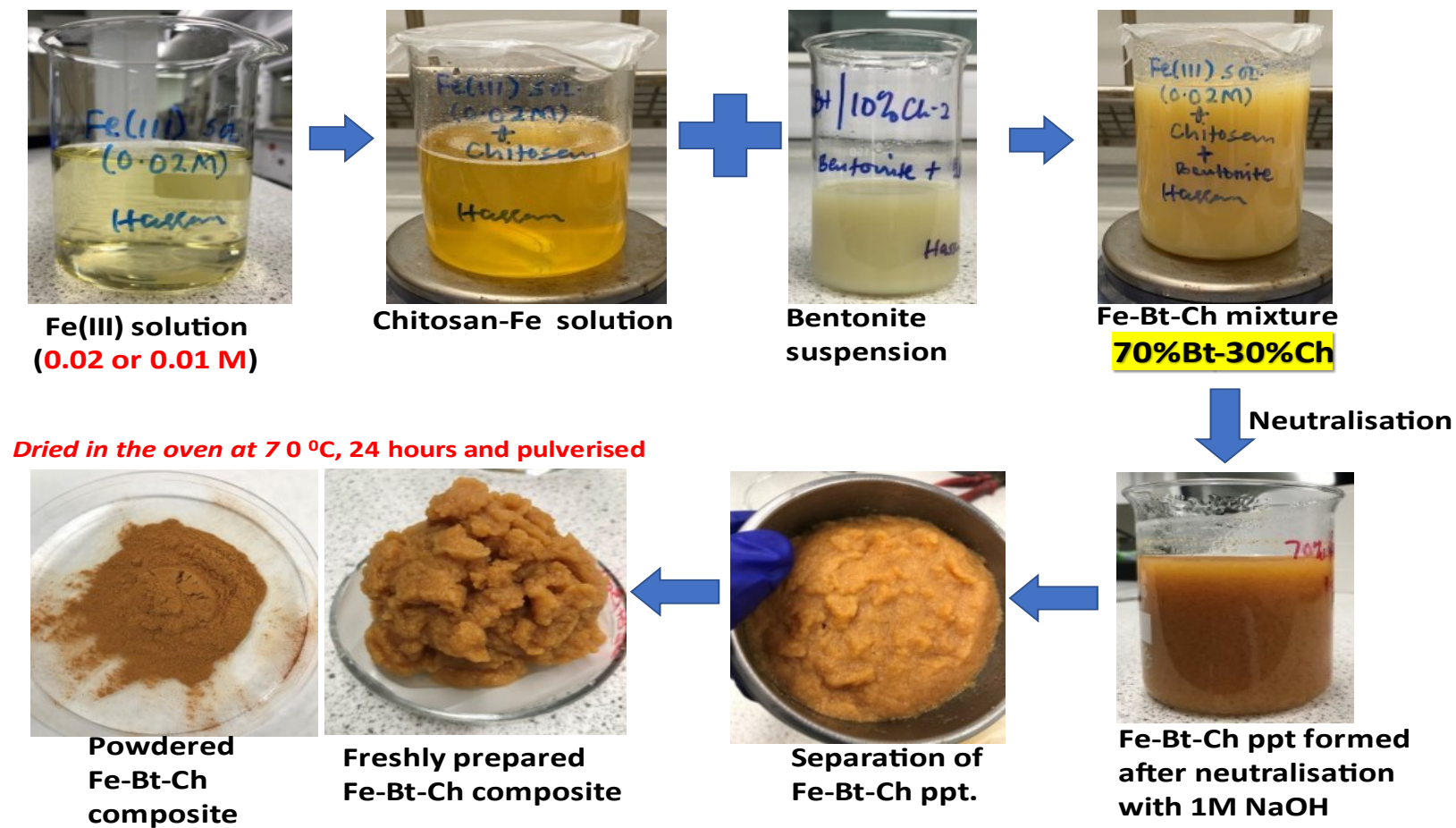
Figure 8.2: Images and schemes showing the making of Fe-Bt-Ch composites

8.2.1.1 *Surface Response Methodology - Optimal-I designs*

In this study, four factors; pH, adsorbent dosage, initial concentration, agitation time and temperature were identified to have a significant effect on the adsorption of As(III) ions from aqueous solutions. These quantitative factors were tested simultaneously with only one adsorbent sample (i.e., Fe-Bt-Ch-1), therefore, no categorical factor. To reduce the number of experimental runs, the other composite sample (Fe-Bt-Ch-2) was not used during the surface response experiment, since the information obtained from one would be sufficient to explain the adsorption behaviour of As(III) ions onto Fe-Bt-Ch composites. Therefore, a set of 25 experiments/runs was created, which included five replicates, using Design-Expert 13 software (Table 8.1 and Appendix E1). Each factor level combination was used in a randomised order. This design enabled fit for a second-order polynomial model, which has main effects, two-factor interactions, and quadratic terms. The equation model was defined as:

$$Y = \alpha + aA + bB + cC + dD + abAB + acAC + adAD + bcBC + bdBD + cdCD + aaA^2 + bbB^2 + ccC^2 + ddD^2 \tag{8.1}$$

where Y is the measured response (e.g., As-adsorption capacity, mg/g) associated with every variable level combination, **α** is the intercept (mean value), A, B, C, and D are the main factors (representing pH, adsorbent dosage, initial concentration, and agitation time, respectively); AB, AC, AD, BC, BD, and CD are the two-factor interactions; A^2, B^2, C^2, and D^2 are the quadratic numerical (quantitative) factors; a, b, c, d, or ab, ac, ad, bc, bd, cd, or aa, bb, cc, and dd are the coefficients of the main factors, interaction factors, and quadratic numerical factors, respectively.

Table 8.1: Factors and their levels investigated during optimal stage in the batch adsorption experiments of As (III) ions onto Fe-Bt-Ch-1 composites

Levels	Numeric continuous factors			
	A-pH	B-Adsorbent dosage (g)	C-Initial concentration (mg/L)	D-Agitation time (min)
Low (-1)	1	0.05	50	10
Centre point (0)	varied	varied	varied	varied
High (+1)	9	0.5	250	300

Note: The centre points (0) maybe slightly different due the algorithms of the optimal-I design

8.2.1.2 *Adsorption equilibrium and Isotherm*

The two adsorbent samples (i.e., Fe-Bt-Ch-1 and Fe-Bt-Ch-2 composites) were used for the adsorption equilibrium study. To determine the equilibrium adsorption capacity of these adsorbents to absorb As(III) ions from aqueous solutions, a wider range of As(III) concentrations (i.e., from 10 to 350 mg L^{-1}) that differs from the one used in the optimal experiment (50 to 250 mg L^{-1}; Table 8.1). The experiment was performed based on the optimal experimental conditions obtained from the surface response-optimal designs of the previous section. Thus, 0.1 g of each adsorbent was exposed to 25 mL of As(III) solutions with varying concentrations (as stated above) at pH 8.0, agitation time of 180 minutes (with the speed of 230 rpm) and at room temperature (25°C). The equilibrium adsorption experiment and the isotherm modelling were all carried out as described in Section 7.2.2.2.

8.2.1.3 *Adsorption Kinetics*

Exactly 0.1 g of each adsorbent (i.e., Fe-Bt-Ch-1 and Fe-Bt-Ch-2 composites) was exposed to 25 mL of As(III) solutions (50 mg L^{-1}) at pH 8.0 and room temperature (25°C) with varying agitation times from 10 to 300 minutes (with the mixing speed of 230 rpm). The kinetic adsorption experiment and the kinetic modelling were all carried out as described in Section 7.2.2.3.

8.2.1.4 *Adsorption thermodynamics*

The equilibrium adsorption of As(III) onto Fe-Bt-Ch composites was carried out at different temperatures; 25°C (298.15K), 40°C (313.15K) and 55°C (328.15), and were used to calculate the thermodynamic parameters for the adsorption system. The three thermodynamic parameters were calculated by using a Van't Hoff approach as described in Section 7.2.2.4.

8.2.1.5 *Desorption studies*

Strong alkali solutions such as sodium hydroxide (NaOH) are widely used in desorption of arsenic ions adsorbed onto different kinds of adsorbent [197]. Therefore, dilute aqueous solutions of NaOH were used as a stripping (desorbing) agent to recover As(III) ions adsorbed onto Fe-Bt-Ch composites. The batch desorption procedure as described in section 5.2.2.4 was used.

8.3. Results and discussion

8.3.1. Characterisation of prepared Fe-Bt-Ch composites

The prepared Fe-Bt-Ch-1 and Fe-Bt-Ch-2 composites were characterised by thermogravimetric analysis, X-ray diffraction, and Fourier transform infrared spectroscopy.

8.3.1.1 *Thermogravimetric Analysis*

TGA curves for bentonite, unmodified Bt-Ch composite, Fe-modified Bt-Ch composite, and chitosan are shown in Figure 8.3A. The unmodified Bt-Ch composite represent 70%Bt-30%Ch beads-A which was formed via precipitation method as described in Section 4.2.2.2. While Fe-modified composite represent Fe-Bt-Ch-1 and Fe-Bt-Ch-2 composites which were prepared using the same precipitation procedure in the weight ratio 70%/30 of bentonite to chitosan, respectively. The TGA curves of bentonite, unmodified Bt-Ch composite, and that of chitosan show exactly as previously described in Section 4.3.2. Like unmodified Bt-Ch composite, the TGA curves of Fe-modified Bt-Ch

composite exhibited three stages of weight loss. In the first stage, slight weight loss is observed between 100-120 °C, and no significant difference between the weight loss of unmodified Bt-Ch and Fe-modified samples. In the second stage, a major weight loss is observed between approximately 200-450 °C for Fe-modified Bt-Ch composites, which is higher compared to that of the modified Bt-Ch composite sample (Table 8.2). The higher weight loss for Fe-modified composites within this temperature region might be due to complexation of Fe(III) ion onto chitosan, which makes the composites less thermally stable compared to the unmodified sample [236]. In the third stage a subsequent small weight loss was observed for Fe-modified Bt-Ch composites between approximately 600-700 °C, which is lower compared to the weight loss observed for unmodified Bt-Ch composites in this temperature region (Table 8.2).

The amount of chitosan in each of the i.e., Fe-Bt-Ch-1 and Fe-Bt-Ch-2 composites and unmodified Bt-Ch composites were all calculated as described in Section 4.3.2 and are shown in Figure 8.3B. As can be seen, similar amounts of chitosan are present in both prepared Fe-modified and unmodified Bt-Ch composites.
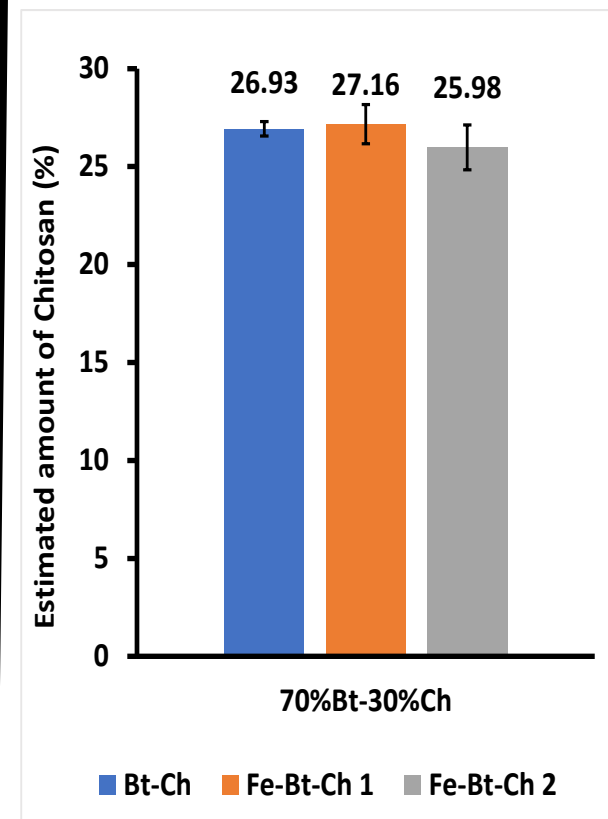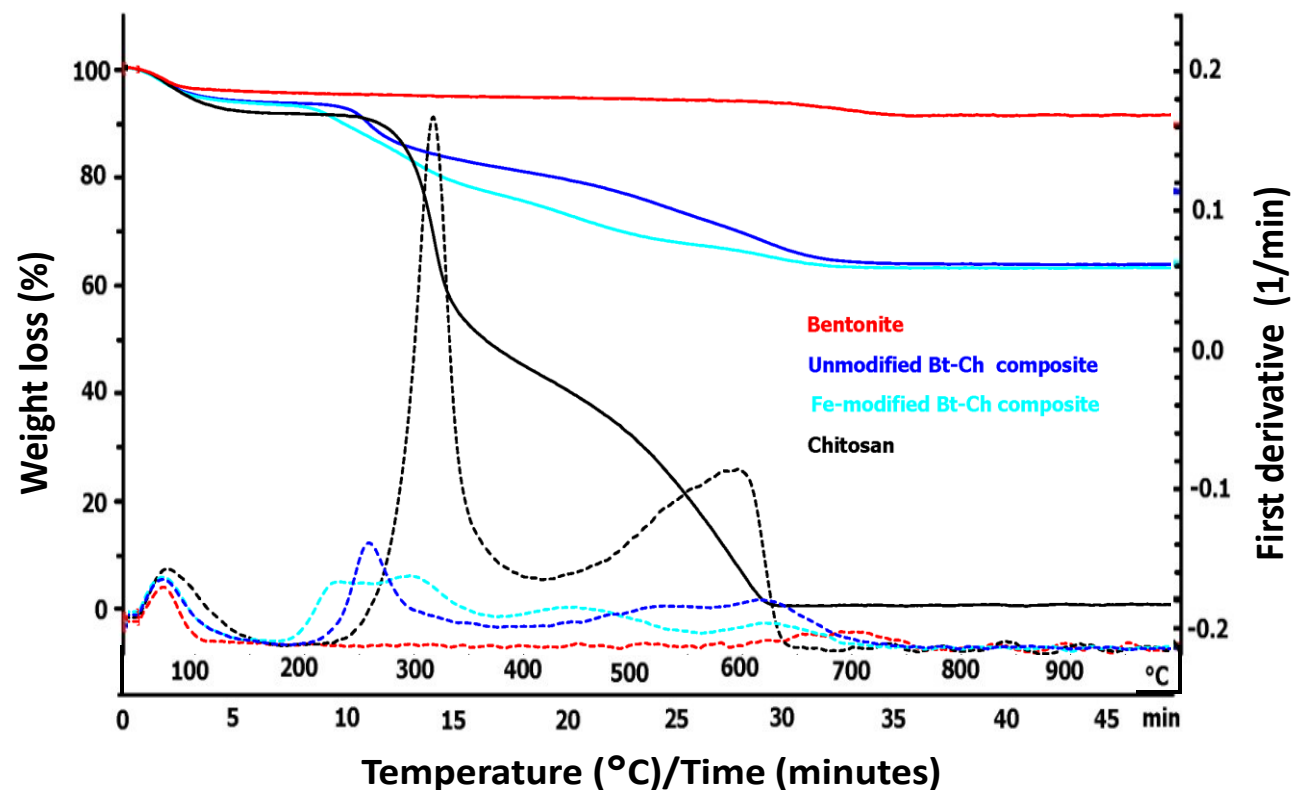
Figure 8.3: (A) TGA curves and first derivatives of bentonite, unmodified Bt-Ch composite, Fe-modified composites, and chitosan (B) Charts showing the amount of chitosan estimated from weight loss values (TGA) of Bt-Ch (unmodified), and Fe-modified composites

Note: smooth lines represent weight loss; break line represent first derivatives; each bar represents mean ± standard error of three (3) different samples (n = 3). The unmodified Bt-Ch composite represent 70%Bt-30%Ch beads-A. While Fe-modified Bt-Ch composite represent Fe-Bt-Ch-1 and Fe-Bt-Ch-2 composites formed in the weight ratio 70%/30% of bentonite/chitosan.

Table 8.2: Calculated weight loss (%) for unmodified Bt-Ch composite and Fe-modified composites

composite sample	Weight loss (%) at;		
	90 - 120 °C	200 - 450 °C	600 - 700 °C
Unmodified Bt-Ch	6.52 ± 0.7	13.43 ± 1.1	16.92 ± 1.1
Fe-Bt-Ch-1	5.29 ± 0.6	21.27 ± 1.2	9.31 ± 0.9
Fe-Bt-Ch-2	5.48 ± 0.8	21.74 ± 1.4	7.66 ± 0.7

Note: unmodified Bt-Ch composite = 70%Bt-30%Ch beads-A; Fe-Bt-Ch-1 = Bt-Ch modified with Fe^{3+} (0.01 M); Fe-Bt-Ch-2 = Bt-Ch modified with Fe^{3+} (0.02 M)

8.3.1.2 *XRD Analysis*

The XRD patterns of bentonite, unmodified Bt-Ch, and Fe-modified Bt-Ch composites (I.e., Fe-Bt-Ch-1 and Fe-Bt-Ch-2) are shown in Figure 8.4. As previously described in Section 4.3.3, higher d-spacing was observed for unmodified Bt-Ch sample, which suggests that more chitosan was intercalated into the interlayers of the clay for unmodified Bt-Ch composites. Similar reflection shifts may have been expected for Fe-modified Bt-Ch composites in comparison to unmodified Bt-Ch because similar amounts of chitosan are present (as evidenced by TGA; Figure 8.3B), however this was not the case. The shifts are less for Fe-modified Bt-Ch composites, which suggests that the amount of chitosan present in the clay interlayers are considerably less. This data suggests that solubilising of chitosan with Fe(III) solution before mixing with bentonite suspension significantly affects (i.e. lowers) the penetration of chitosan within the interlayer space of the clay.
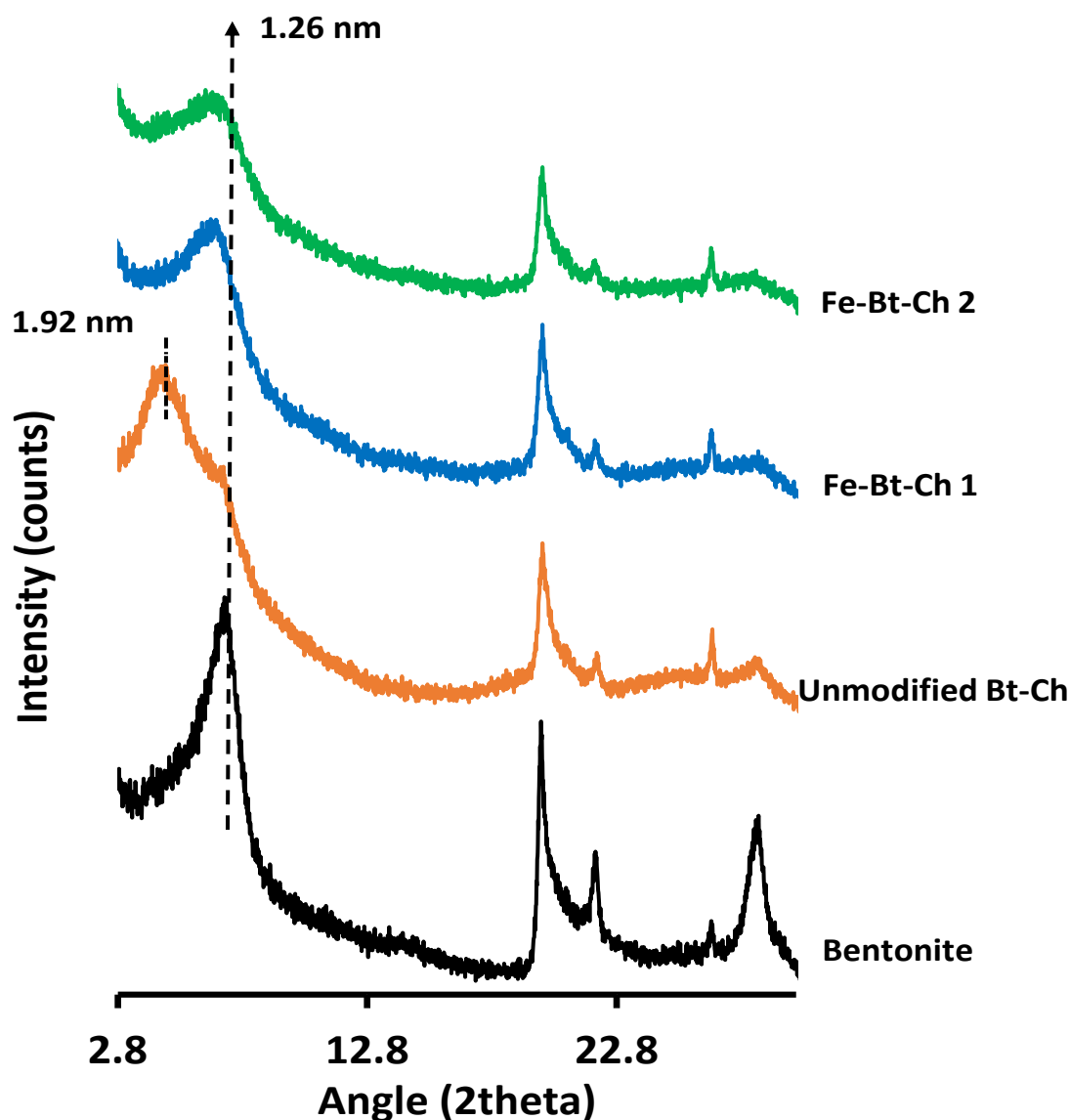
Figure 8.4: XRD patterns of bentonite, unmodified Bt-Ch, Fe-Bt-Ch-1 and Fe-Bt-Ch-2 composites

Note: Fe-Bt-Ch-1 = Bt-Ch modified with Fe^{3+} (0.01 M); Fe-Bt-Ch-2 = Bt-Ch modified with Fe^{3+} (0.02 M)

8.3.1.3 *FTIR Analysis*

Figure 8.5 shows the FTIR spectra of bentonite, unmodified Bt-Ch, Fe-Bt-Ch-1, Fe-Bt-Ch-2 and chitosan. The spectra of bentonite, unmodified Bt-Ch (i.e., 70%Bt-30%Ch-1 beads-A) and chitosan has previously been described in Section 4.3.4. The spectra of Fe-Bt-Ch-1 and Fe-Bt-Ch-2 composites shows similar bands to that of unmodified Bt-Ch. In addition, higher intensity bands at around 1420 cm^{-1} were observed for Fe-modified composites, which increases with the concentration of Fe(III) ions used during the preparation stage. This is not yet fully understood, but further characterisation will be

carried out to ascertain the type of Fe molecules formed on the surface of the composite.
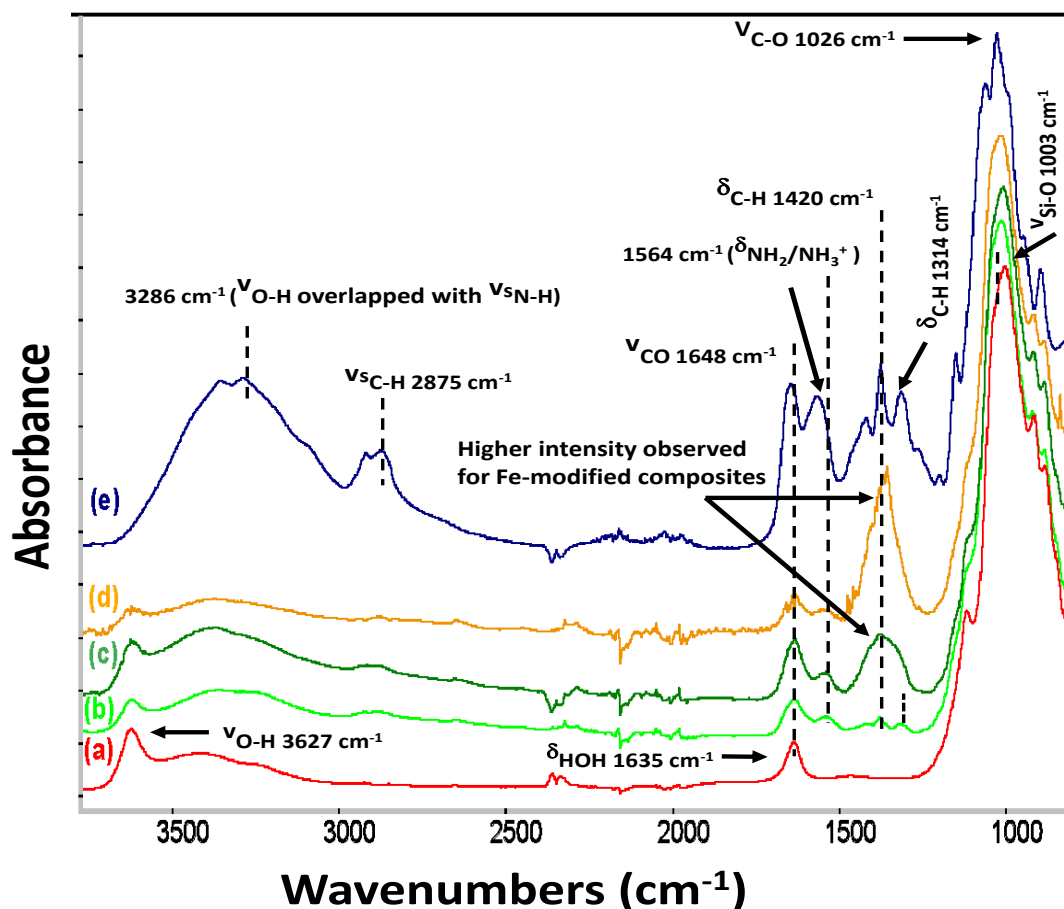
Figure 8.5: FTIR spectra of (a) pristine bentonite (b) unmodified Bt-Ch composites (c) Fe-Bt-Ch-1 composites (d) Fe-Bt-Ch-2 composites and (e) pure chitosan.
Note: Fe-Bt-Ch-1 = Bt-Ch modified with Fe^{3+} (0.01 M); Fe-Bt-Ch-2 = Bt-Ch modified with Fe^{3+} (0.02 M); V = stretching vibration; δ = bending vibration; v_s = symmetric stretching vibration

8.3.2. Surface Response: I-optimal designs

In this study, only one response (i.e., adsorption capacity, mg/g) was used for analysis of the optimal model related to adsorption of As(III) onto Fe-Bt-Ch-1 composites. The experimental adsorption capacity results from the 25 experimental runs, alongside the corresponding predicted values obtained from the Design Expert software, are presented in Appendix E1. The mathematical relationships between the four studied independent factors (i.e., pH, adsorbent dose, initial concentration, and agitation time) and the response (adsorption capacity) were also provided by Design Expert 13

software. The equation in terms of actual factors which describes the various parameters regarding the adsorption of As(III) onto Fe-Bt-Ch-1 composites is shown in Equation 8.2.

$$Log_{10}(\text{Adsorption capacity})X = -0.6845 - 0.2869A + 4.9868B - 0.0102C + 0.0052D + 0.0691E + 0.1943AB + 0.0001AD + 0.0020AE - 0.0380BE + 0.00006CE - 0.00003DE + 0.0103A^2 - 3.5460B^2 + 0.00002C^2 - 0.00001D^2 - 0.0008E^2$$

(8.2)

8.3.2.1 *Analysis of variance (ANOVA)*

The summary of ANOVA results for the adsorption capacity (mg/g) of As (III) ions by Fe-Bt-Ch-1 composites are presented in Appendix E2. After data-fitting was carried out, the modified quadratic model concerning the response was deemed significant (Coefficient = 1.05; F = 78.21; P<0.0001) for adsorption capacity (mg/g). The non-significant "lack-of-fit" for adsorption capacity response (F = 1.23; P = 0.41 > 0.05) suggest the adequacy of the model to explain data in the experimental region. The R^2 value (Appendix E2) for this model was found to be 0.99 which indicates that about 99% of the experimental data could be matched with the predicted value, and only 1% of it was not explained by the model. The predicted R^2 (0.95) was in reasonable agreement with adjusted R^2 (0.95). The small value of coefficient of variance (CV = 2.07) implies that deviation between the predicted and experimental data values were minimal. P-values less than 0.05 indicate model terms are significant, and therefore, A, B, C, D, AB, AC, BC, CD, A^2, C^2, and D^2 are significant terms in the modified quadratic model related to adsorption capacity. However, p-values greater than 0.10 indicate model terms are not significant and so, they were completely removed or deleted from the model. Though, we have a few exceptions, where the P-values of the three model terms (which includes AD, BD, and B^2) estimated are slightly greater than 0.10, this does not mean the term should be removed from the model, because they are important terms which supports other significant terms.

The estimated coefficients for these significant terms, as obtained by coded equation, are useful for identifying their relative impact. When comparing the factor coefficients

(second column shown in Appendix E2) a positive and negative coefficient signifies increasing and decreasing effects, respectively.

The adsorption capacity (mg) of As(III) by Fe-Bt-Ch-1 composites, was affected by linear effects of pH (A), adsorbent dosage (B), initial concentration (C), and agitation time (D). Interaction effects of pH-adsorbent dosage (AB), pH-initial concentration (AC), adsorbent dosage- initial concentration (BC), and initial concentration-agitation time (CD), were also observed concerning the absorption capacity of As(III) by Fe-Bt-Ch-1 composites. In addition, a quadratic effect of A^2, C^2, and D^2 are all significant in the model. From coefficients values in Appendix E2, it indicates that adsorption capacity of As(III) increases with pH (A), initial concentration (C) and agitation time (D), but decreases with the adsorbent dosage (B). Also, As(III) adsorption capacity may increase with these significant model terms; BC, CD, but decrease with AB, AC, A^2, C^2 and D^2. In addition, these insignificant terms: adsorbent dosage-agitation time (BD), may have favourable effect, while pH-agitation time (AD) and B^2 may have an antagonistic effect towards As(III) adsorption capacity (mg/g).

With respect to diagnostic statistics, both the normal probability plot and the correlation graph (between actual and predicted values) for adsorption capacity, are shown in Figure 8.6 . Figure 8.6a represents the normal probability plot of studentised residuals for adsorption efficiency. This plot indicates whether residuals follow a normal distribution, i.e., the points should lie on an approximately straight line without any apparent deviation. However, when the distribution is not normal, it signifies a nonlinear pattern, which may be corrected by a proper transformation [202]. As can be seen, almost all data are on a straight line for both responses, and therefore, it can be assumed that they are normally distributed. Figure 8.6b represents the correlation (relationship) between actual and predicted values of adsorption capacity. The actual values are the measured values of the adsorption capacity obtained for Fe-Bt-Ch-1 composites, which were determined. While predicted values were generated using Equations 8.2. The predicted values of adsorption capacity of Fe-Bt-Ch-1 composites for As(III) adsorption, obtained from the model, are in good agreement with the actual experimental data. It is worth mentioning that these models make predictions based on data used in their development, which may give them some inherent bias.
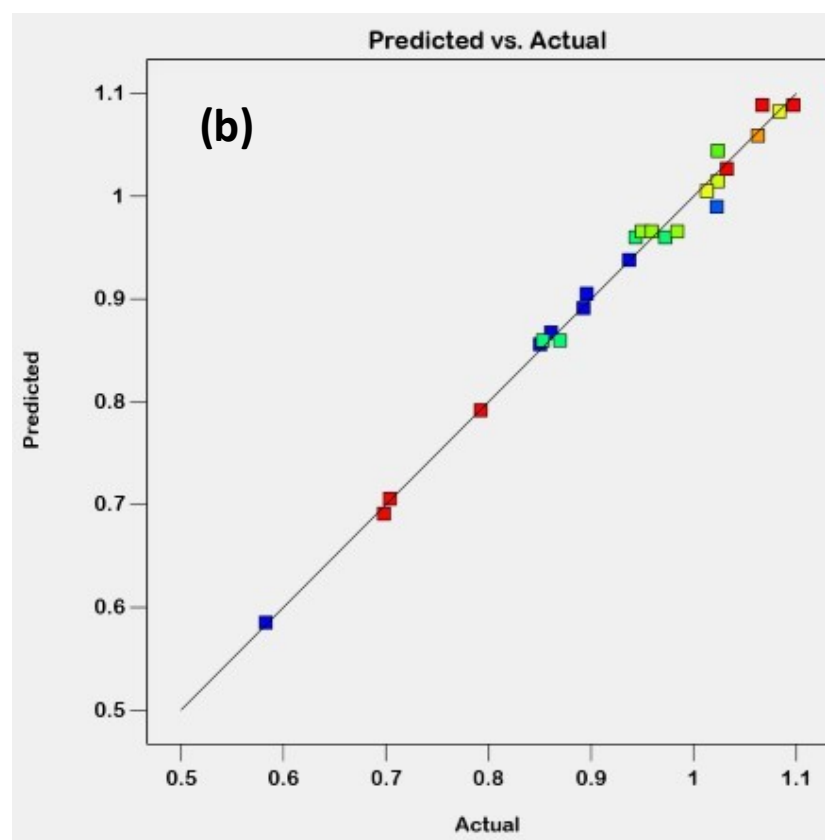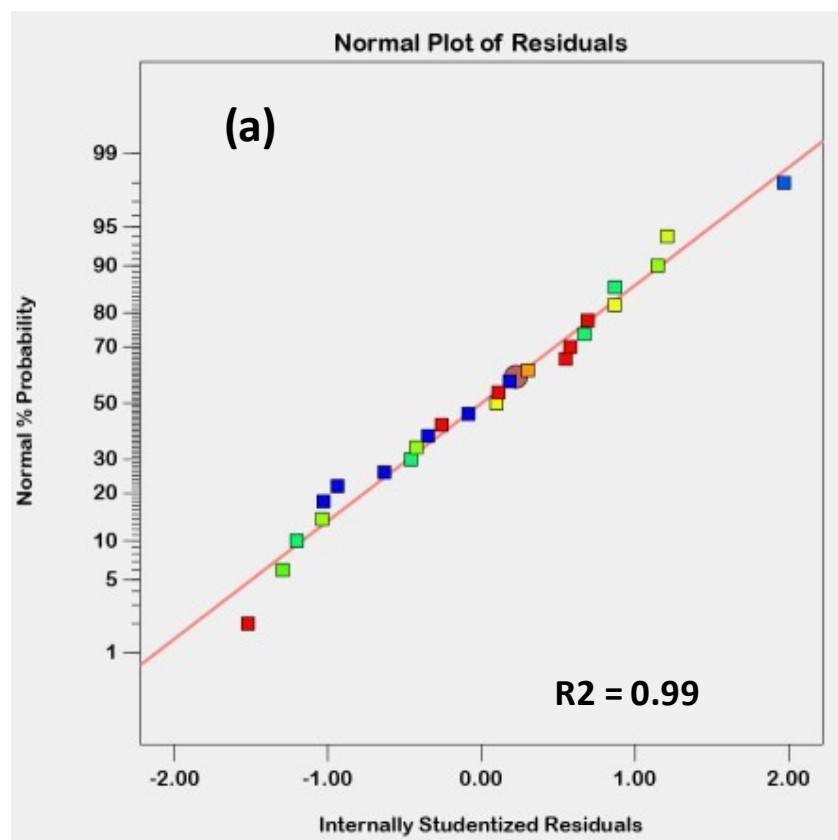
Figure 8.6: (a) normal probability plot of studentised residuals and (b) correlation between actual and predicted values (experimental data) of As (III) ion adsorption capacity for Fe-Bt-Ch-1 composites

8.3.2.2 *Effects of main factors and their interactions*

The effect of each quantitative factor (and their two-factors interactions) concerning As (III) adsorption capacity (mg/g) were separately visualised with model graphs which are shown in Figure 8.7. When the pH is varied (from 1 to 9), adsorption capacity (mg/g) of As(III) ions slightly increases with pH from 1 to 8, and then maintains the same adsorption capacity value from pH of 8 to 9 (Figure 8.7a). For adsorbent dosage, the adsorption capacity of As(III) slightly decreases with increasing adsorbent dose from 0.05 to 0.2 g (Figure 8.7.b). When the initial concentration of the solution is varied from 50 to 250 mg/L, the As(III) adsorption capacity of the Fe-Bt-Ch-1 composites increases initially and then decreases (Figure 8.7c). Concerning the agitation time, the As(III) adsorption capacity increases slightly from 10 to 180 min, maintains a higher adsorption capacity between 180 to 240 min and then slightly decreases for the remaining part of agitation time (240 to 300 min; Figure 8.7.d).

The model-graphs showing 2-way interaction effects on the As(III) adsorption capacity are presented in Figure 8.8. When the effects of two factors appear as two non-parallel lines, it indicates that the effect of one factor depends on the level of another factor, and vice versa [202,203]. Therefore, the major interactive effects were only observed for pH-adsorbent dosage (AB), as the two lines slightly crossed each other at lower pH; Figure 8.8a). However, parallel lines were generally observed for pH-initial conc. (AC), adsorbent dosage-initial conc. (BC;), initial conc.-agitation time (CD) indicating that these 2-way interaction have less effect during the adsorption of As(III) ions onto Fe-Bt-Ch composites.

8.3.2.3 *The 3D response surface plots and combined effects of significant factors*

The three-dimensional response (3D) surface plots concerning the combined effects of the significant factors affecting the As(III) adsorption (by Fe-Bt-Ch-1 composites) are shown in Figure 8.9. The 3D response surface plots are graphical representations of the regression equation showing the simultaneous interaction effect of two variables (on response), while maintaining the other variables constant [192,201].

(A) Combined effects of the solution pH and adsorbent dosage

223

Figure 8.9a shows the 3D response surface plot for the interaction effect of pH and adsorbent dosage (at constant initial conc. of 150 mg/L and agitation time of 60 minutes) on As(III) adsorption capacity (mg/g) for Fe-Bt-Ch composites. At lower adsorbent dosage, the adsorption capacity (mg/g) of As(III) ions increases with an increase in pH from 1 to 9. As(III) ions exist as uncharged species (i.e., $H_3AsO_3^0$) at low pH (2.0 – 6.0). However, between the pH of 7.5 – 9.0, they predominantly exist as a negative anionic species ($H_2AsO_3^-$ or $HAsO_3^{2-}$), which are readily attracted to the positively charged adsorbent surface (such as Fe-Bt-Ch-1 composites), and thus, resulting to higher adsorption capacity of As(III) ions [167,237]. At higher adsorbent dose, the adsorption capacity of As(III) ions slightly increases, and then slightly decreases (with insignificant trend) as pH of the solution increases from 2 to 9. It was observed that the pH has a negative effect on the As(III) adsorption capacity in a non-linear manner (A^2, check the coefficient in Appendix E2). The observed quadratic effect of pH (A^2) has less strength (but opposing sign) in comparison to the linear effect of pH (A).

In terms of adsorbent dosage: at lower pH, the adsorption capacity (mg/g) of As(III) ions slightly increases with an increase in adsorbent dose from 0.05 to 0.2 g. However, at higher pH, the adsorption capacity (mg/g) of As(III) ions decreases significantly more as adsorbent dose increases from 0.05 to 0.2 g. The influence of adsorbent dosage may have negative effect on the adsorption capacity (mg/g) in a non-linear manner (B^2, check the coefficient in Appendix E2). The quadratic effect of adsorbent dosage (B^2) is minimal, but less strength (and same sign) in comparison to the linear effect of adsorbent dosage (B).

(B) Combined effects of the solution pH and initial concentration

Figure 8.9b shows the 3D response surface plot for the interaction effect of pH and initial concentration (at constant adsorbent dosage of 0.1 g and agitation time of 180 minutes) on As(III) adsorption capacity (mg/g) for Fe-Bt-Ch-1 composites. At lower initial concentration, the adsorption capacity (mg/g) of As(III) ions steadily increases as pH of the solution increases from 2 to 9. At higher initial concentration, the adsorption capacity (mg/g) of As(III) ions only slightly increases as pH varies from 2 to 9.

In terms of initial concentration: at lower pH, the adsorption capacity (mg/g) of As(III) ions steadily increases as initial concentration varies from 50 to 200 mg/L, and the absorption capacity values remained the same with initial concentration from 200 to

250 mg/L. However, at higher pH, the adsorption capacity (mg/g) of As(III) ions increases (with initial concentration from 50 to 150 mg/L), and then, decreases as initial concentration varies from 150 to 250 mg/L. Overall, the influence of initial concentration may have a negative effect on the adsorption capacity (mg/g) in a non-linear manner (C^2, check the coefficient in Appendix II). The quadratic effect of initial concentration (C^2) has a stronger strength (but opposing sign) in comparison to the linear effect of initial concentration (C).

(C) Combined effects of the adsorbent dosage and initial concentration

Figure 8.9c shows the 3D response surface plot for the interaction effect of adsorbent dosage and initial concentration (at constant pH of 8.0 and agitation time of 180 minutes) on As(III) adsorption capacity (mg/g). At both lower and higher initial concentration, the adsorption capacity (mg/g) of As(III) ions slightly decreases as adsorbent dose increases from 0.05 to 0.2 g. The quadratic effect of adsorbent dosage (B^2) has been previously discussed.

In terms of initial concentration: at both lower and higher adsorbent dosage, the adsorption capacity (mg/g) of As(III) ions increases, and then decreases as initial concentration varies from 50 to 250 mg/L. The quadratic effect of initial concentration (C^2) has been previously discussed.

(D) Initial concentration and Agitation time

Figure 8.9d shows the 3D response surface plot for the interaction effect of initial concentration and agitation time, while the pH of the As (III) solution and adsorbent dose were kept constant at 8.0 and 0.1 g, respectively. At both lower and higher agitation time, the adsorption capacity (mg/g) of As(III) ions increases, and then decreases as initial concentration varies from 50 to 250 mg/L. The quadratic effect of initial concentration (C^2) has been previously discussed.

In terms of agitation time: at lower initial concentration, the adsorption capacity (mg/g) of As(III) ions increases when the agitation time increases from 10 to 180 min, reaches equilibrium between 180 to 240 min, and then slightly decreases for the remaining part of agitation time (240 to 300 min). A similar trend of agitation time was observed at higher initial concentration. The influence of agitation time has a negative effect on the As(III) adsorption capacity in a non-linear manner (D^2, check the coefficient in in

225

Appendix II). This quadratic effect of adsorbent dose (D^2) has lesser strength (but opposing sign) in comparison to the linear effect of agitation time, and this might have contributed to curve-shape of the 3D surface plot.

8.3.2.4 *Optimisation of parameters for As (III) adsorption by Fe-Bt-Ch composites*

The obtained optimal conditions (selected by the model) estimated for the adsorption of As (III) by Fe-Bt-Ch-1 composites were pH of 8.0, adsorbent dose of 0.1, initial As (III) concentrations of 150 mg/l, and agitation time of 180 minutes. At these conditions, the predicted adsorption capacity (mg/g) of As(III) ions by Fe-Bt-Ch composites is found to be 12.59 mg/g (Figure 8.10).

Under these conditions, the adsorption of As (III) ions was tested to confirm the robustness of the predicted model. As shown in Table 8.3, the experimental value (adsorption capacity) obtained from confirmation runs was found to be 12.07 ± 0.35 mg/g, which agrees well with the predicted value of 12.59 ± 0.56 mg/g (desirability = 0.72) within the accuracy and precision of the design space (95% for both prediction and confidence intervals).
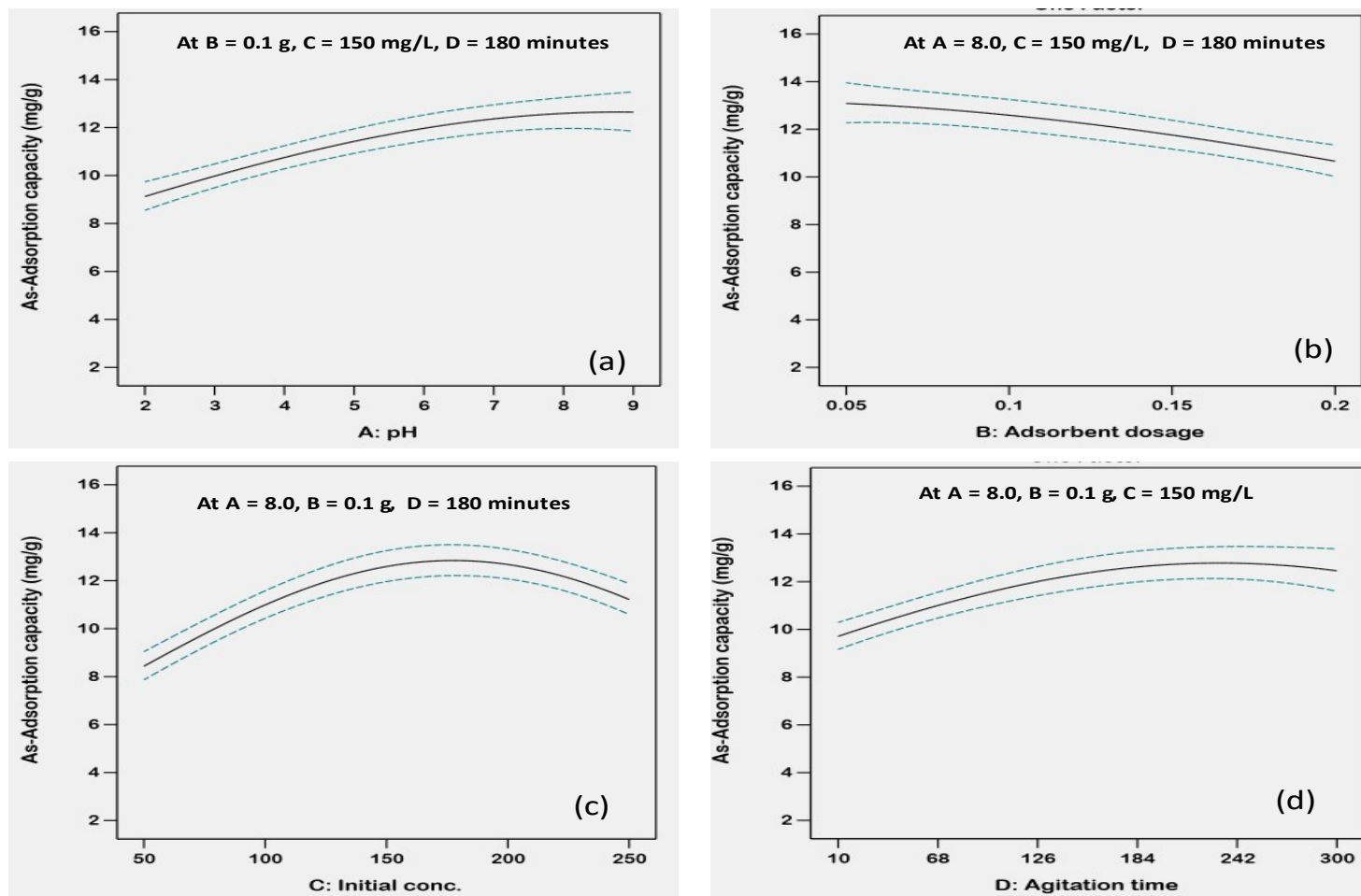
Figure 8.7: Graphs showing the effect of each factor on the As (III) adsorption capacity (mg/g)

Note: these graphs were plotted and obtained from Design-Expert®13; dashed lines represent 95% confidence interval bands of the experimental data; (a) A-pH; (b) B-Adsorbent dose; (c) C-Initial concentration; (d) D-Agitation time
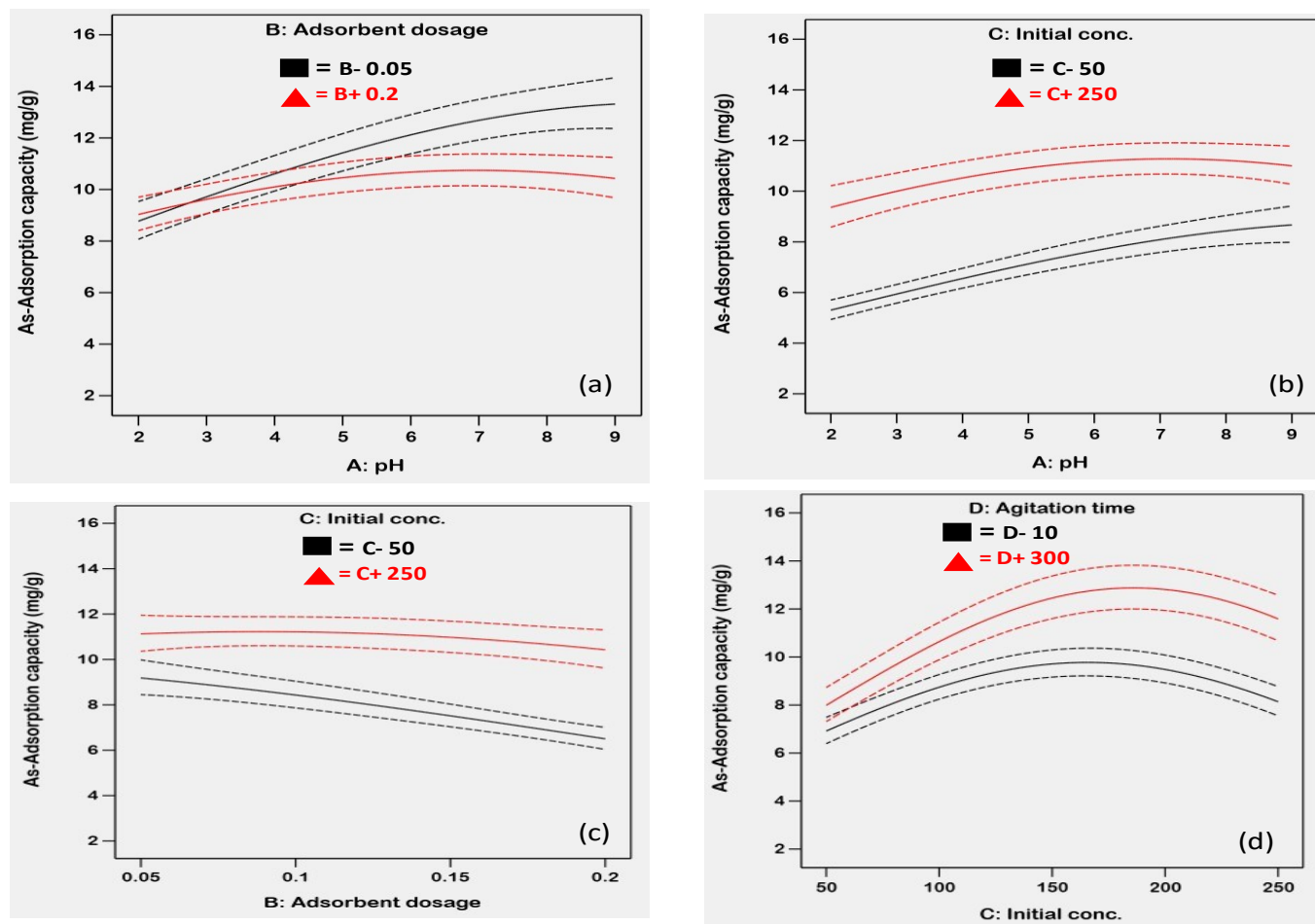
Figure 8.8: Figure Graphs showing two-factor interactions and their effects on the As(III) adsorption capacity (mg/g)

Note: these graphs were plotted and obtained from Design-Expert®13; dashed lines represent 95% confidence interval bands of the experimental data; (a) pH-Adsorbent dosage; (b) pH-Initial conc.; (c) Adsorbent-Initial conc.; (d) Initial conc.-Agitation time

228
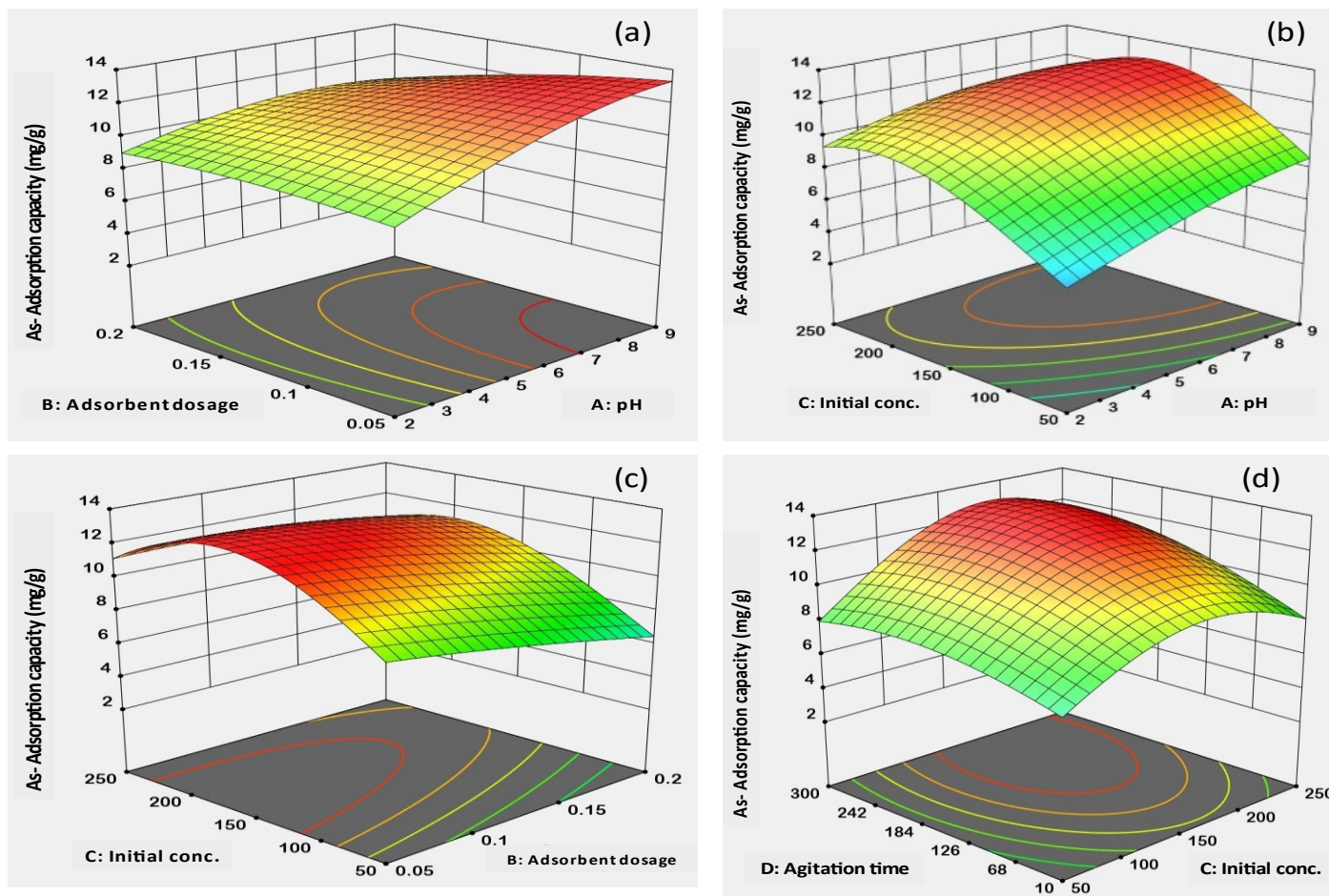
Figure 8.9: 3D response surface plots showing the combined effect of significant factors on the As (III) adsorption capacity (mg/g)

Note: these 3D surface plots were plotted and obtained from Design-Expert®13; (a) pH and adsorbent dosage (at constant initial conc. of 150 mg/L and agitation time of 180 minute; (b) pH and initial conc. (at constant adsorbent dosage of 0.1 g and agitation time of 180 minute); (c) adsorbent dosage and initial conc. (at constant pH of 8.0 and agitation time of 180 minute); (d) initial conc. and agitation time (at constant pH of 8.0 and adsorbent dosage of 0.1 g)
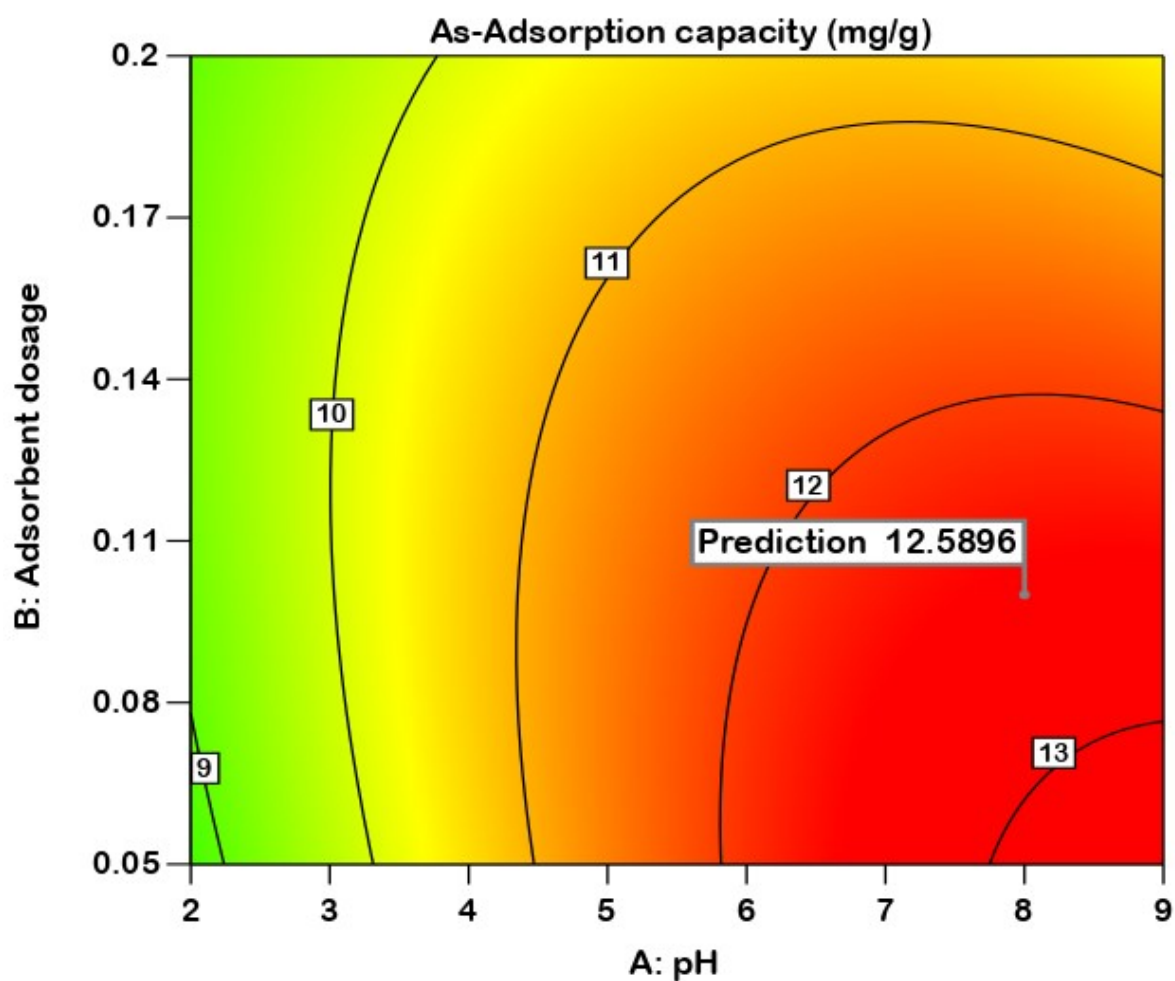
Figure 8.10: Contour graphs showing optimised conditions with respect to As(III) ion adsorption capacity for Fe-Bt-Ch composites. Note: this contour plot was plotted and obtained from Design-Expert®13

Table 8.3: Confirmation of experimental runs for analysed Optimal-I design model

Response	Adsorbent used	Target	Predicted Mean	Desirability	Confirmation experiment	Confidence Interval (95%)	
						Low	High
As-Adsorption capacity (mg/g)	Fe-Bt-Ch-1	Maximize	12.59 ± 0.56	0.72	12.07 ± 0.35	11.65	13.58

pH = 8.0; adsorbent dose = 0.1 g; Initial As (III) concentration = 150.0 mg/L; agitation time = 180 minutes. For confirmation experiment, each value represents mean ± standard deviation of three (3) different samples (n = 3)

8.3.3. Adsorption Isotherm studies

Figure 8.11 shows non-linear plots illustrating Langmuir/Freundlich and Dubinin-Radushkevich isotherm models, respectively, for As(III) adsorption by Fe-Bt-Ch-1 composites at 25, 40 and 55°C. The isotherm plots for the other adsorbent sample (Fe-

Bt-Ch-2 composites) are presented in Appendix E3, but the calculated values (or constants) obtained for the two adsorbents are presented in Table 8.4. In terms of correlation coefficient (R^2), both the Langmuir and Freundlich isotherm models correlated well with the experimental data. However, from the lower chi-square (X^2) value obtained with the Langmuir isotherm, this model fitted better compared to Freundlich isotherm model concerning the adsorption of As(III) ions by both adsorbents. This indicates that both monolayer and heterogeneous adsorption processes may coexist, but monolayer seems to be more dominant under these experimental conditions.

The maximum adsorption capacity, Q_{max} (mg/g) of As(III) ions, as determined through the Langmuir isotherm for Fe-Bt-Ch-2 composites, was significantly higher compared to the values obtained for Fe-Bt-Ch-1 composites and slightly increased with increasing temperature (25 to 55℃). During the preparation stage, a higher concentration of Fe(III) cation was used for Fe-Bt-Ch-2 composites, and this accounts for the higher Q_{max} values. The Q_{max} values obtained in this study (for both Fe-Bt-Ch-1 and Fe-Bt-Ch-2 at 25℃) were about six or eight times higher compared to the Q_{max} values obtained from the previous studies of As(III) adsorption for unmodified Bt-Ch composite (70%Bt-30%Ch bead-A) as shown in Table 7.3 of Section 7.3.2. This result demonstrates that the two prepared Fe-modified composites have significantly improved As(III) removal from aqueous solutions. In addition, the Q_{max} value (12.26 ± 0.12 mg/g) obtained for Fe-Bt-Ch-1 composite was similar to the predicted optimum value (12.59 mg/g; Figure 8.10) obtained for the same adsorbent. Overall, the Q_{max} values obtained from adsorption of As(III) with both Fe-Bt-Ch-1 and Fe-Bt-Ch-2 composites were compared with other adsorbents reported in the literature (Table 8.5), and the higher adsorption capacities indicates that these Fe-modified composites could serve as potential and better adsorbent.

Generally, low values for the Langmuir equilibrium constant (K_L) were observed for the two adsorbents used, but the values of K_L obtained in this study were higher compared to the values obtained for As(III) adsorption by unmodified Bt-Ch composite (Table 7.3 of Section 7.3.2). This accounts for better As(III) adsorption by Fe-modified composites. In this study, the values of R_L obtained for both adsorbents has been found to be below

1.0, showing that the adsorption of As(III) by Fe-Bt-Ch-1 and Fe-Bt-Ch-2 is favourable under the current experimental conditions.

The Freundlich constant (K_F) values obtained for both Fe-Bt-Ch-1 and Fe-Bt-Ch-2 composites are generally higher compared to values obtained for unmodified Bt-Ch composite (Table 7.3 of Section 7.3.2) concerning As(III) adsorption. A higher K_F value suggests greater loading of adsorbate (e.g., As(III) ions) onto an adsorbent [48]. The observed Freundlich exponent (n) values fall within the range of 0 to 1, and since it is closer to zero, this implies that the surfaces of these adsorbents (I.e., Fe-Bt-Ch-1 and Fe-Bt-Ch-2 composites) in contact with As(III) ions are heterogeneous, and also suggests a chemisorption process [138].

Concerning Dubinin-Radushkevich (D-R) isotherms, and as calculated from the D–R parameters, the mean free energy (E) of As(III) adsorption for both adsorbents were found within the range from 0.116 to 0.199 kJ mol^{-1}. Since the calculated E values were substantially lower than 8 kJmol^{-1}, the adsorption of As(III) adsorption onto Fe-Bt-Ch-1/ Fe-Bt-Ch-1 composites may also occur by a physical process, possibly by weak van der Waals forces [7,175].
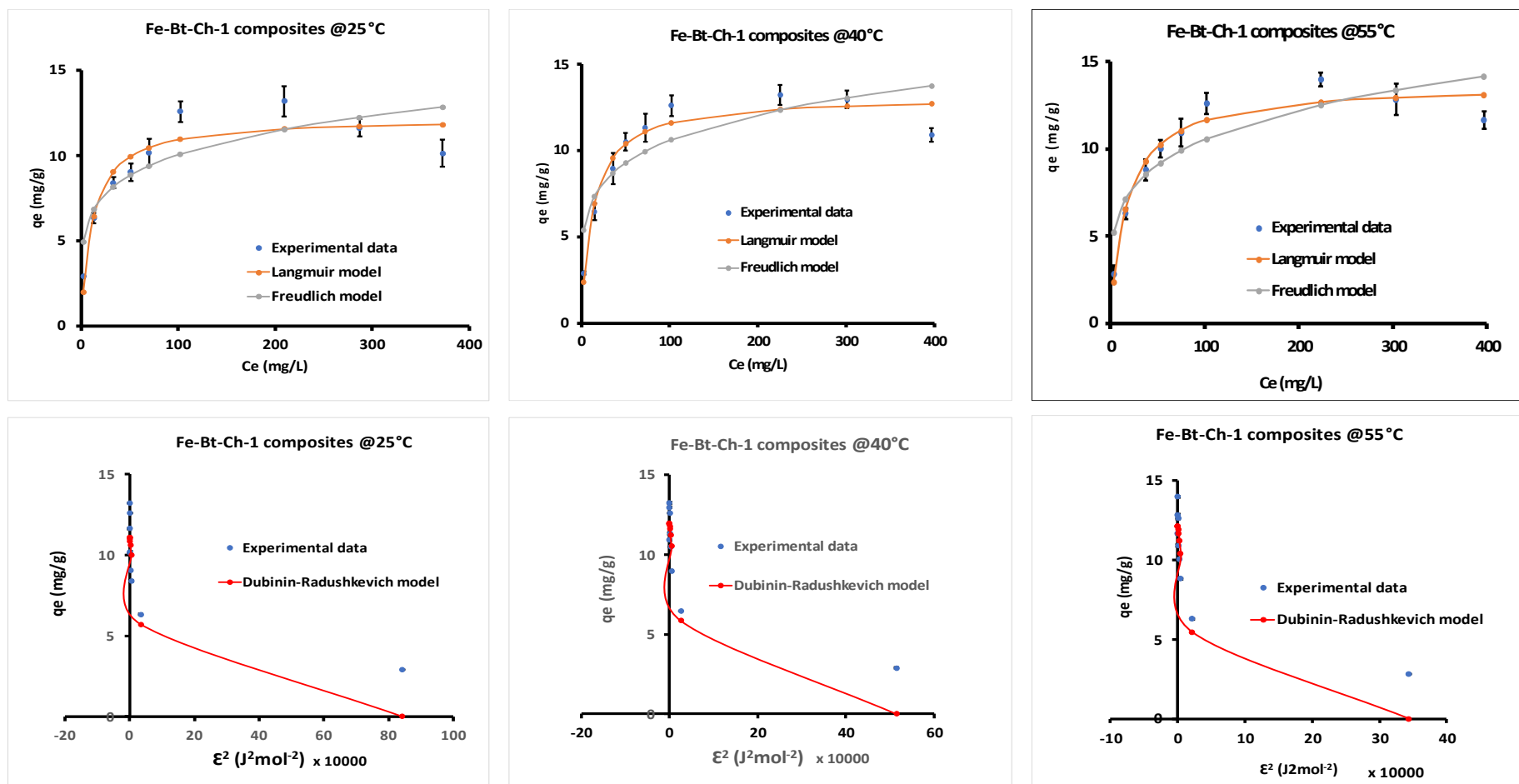
Figure 8.11: The non-linear Langmuir/Freundlich (top) and Dubinin-Radushkevich (bottom) isotherms for adsorption of As(III) by Fe-Bt-Ch-1 composites

Note: At 25, 40 and 55 ^{O}C. pH = 8.0; adsorbent amount = 0.1 g; agitation time (at 230 rpm) = 180 minutes; Initial As(III) concentrations = 10 - 500 mg/L; Each data-point represents mean ± standard deviation of three (3) different experiments (n = 3).

Table 8.4: The fitting parameters of isotherms for the adsorption of As(III) onto Fe-modified composites

Isotherm Model	Fe-Bt-Ch-1 composites			Fe-Bt-Ch-2 composites		
	25°C	40°C	55°C	25°C	40°C	55°C
Langmuir						
Q_{max}	12.26 ± 0.12	13.23 ± 0.17	13.74 ± 0.12	16.37 ± 0.12	17.22 ± 0.06	17.70 ± 0.17
K_L	0.089 ± 0.01	0.078 ± 0.01	0.059 ± 0.01	0.137 ± 0.06	0.138 ± 0.06	0.089 ± 0.01
R_L	0.03 – 0.45	0.03 – 0.48	0.04– 0.55	0.02 – 0.35	0.02 – 0.34	0.03 – 0.45
R^2	0.999 ± 0.00	0.999 ± 0.00	0.999 ± 0.00	0.999 ± 0.00	0.999 ± 0.00	0.999 ± 0.00
X^2	0.158 ± 0.06	0.069 ± 0.01	0.061 ± 0.01	0.277 ± 0.06	0.174 ± 0.06	0.168 ± 0.01
Freundlich						
K_F	4.227 ± 0.00	4.481 ± 0.17	3.931 ± 0.06	6.292 ± 0.06	6.616 ± 0.06	6.181 ± 0.06
n	0.188 ± 0.00	0.194 ± 0.01	0.219 ± 0.01	0.171 ± 0.01	0.172± 0.01	0.186 ± 0.01
R^2	0.999 ± 0.00	0.999 ± 0.00	0.999 ± 0.00	0.999 ± 0.00	0.999 ± 0.00	0.999 ± 0.00
X^2	0.261 ± 0.01	0.262 ± 0.01	0.235 ± 0.01	0.479 ± 0.01	0.424 ± 0.01	0.421 ± 0.01
D-R						
Q_{DR}	11.14 ± 0.06	11.97 ± 0.01	12.17 ± 0.06	14.99 ± 0.00	15.83 ± 0.04	15.94 ± 0.04
K_{DR}	0.00002 ± 0.0	0.00003 ± 0.0	0.00004 ± 0.0	0.00001 ± 0.0	0.00001 ± 0.0	0.00002 ± 0.0
R^2	0.999 ± 0.00	0.999 ± 0.00	0.999 ± 0.00	0.999 ± 0.00	0.999 ± 0.00	0.999 ± 0.00
X^2	0.281 ± 0.01	0.190 ± 0.01	0.205 ± 0.00	0.470 ± 0.01	0.349 ± 0.01	0.398 ± 0.00
E	0.161 ± 0.00	0.135 ± 0.00	0.116 ± 0.00	0.198 ± 0.00	0.199 ± 0.00	0.180 ± 0.00

Note: D-R = Dubinin-Radushkevich; Qmax (mg/g) is the maximum saturated monolayer adsorption capacity of an adsorbent, K_L is the Langmuir constant called solute absorptivity (L/mg), R_L is the separation constant (dimensionless), K_F is the adsorbent capacity (L/g), n is the heterogeneity factor (unitless-ranging from 0 to 1), q_{RD} is the Dubinin-Radushkevich adsorption capacity (mg/g), K_{RD} is the Dubinin-Radushkevich constant related to the sorption energy (mol²/kJ²), E is the mean free energy of adsorption (KJ/mol), R^2 is the coefficient of correlation, and X^2 is nonlinear chi-square. Each value represents mean ± standard deviation of three (3) different samples (n = 3). R_L values are range between the lowest and highest value, and were calculated based on K_L and initial Pb (II) concentration, (C_O) ranging from 10 – 350 mg/L

Table 8.5: Comparisons of As(II) adsorption capacity by Bt-Ch composites/beads with other adsorbents reported in the literature

Adsorbents	Maximum adsorption capacity, Q_{max} (mg/g); (pH)			Ref.
	20°C /25°C	40°C	55°C	
Fe-TiO$_2$ nanoparticles	3.08; (7.0)	---	---	[238]
Ag-TiO$_2$ nanoparticles	1.71; (7.0)	---	---	[238]
TiO$_2$ nanoparticles	1.60; (7.0)	---	---	[238]
Activated alumina	3.5; (7.0)	---	---	[239]
Modified blast furnace slag	0.82; (7.0)	---	---	[240]
Gibbsite	3.3; (5.5)	---	---	[241]
Fe$_3$O$_4$ nanoparticles coated sand	2.14; (7.0)	---	---	[237]
Ferrihydrites	0.58; (4.2)	---	---	[234]
Iron oxide impregnated activated alumina	0.73; (12)	---	---	[242]
C-mVMT	72.2; (5.0)	---	---	[100]
HDTMA-modified kaolinite	0.32; (7.0)	---	---	[229]
Polymetallic sea nodule	0.69; (2.0 -9.0)	---	---	[223,243]
Iron acetate coated activated alumina	0.09; (7.4)			[244]
P-Al/Fe-mMont.	19.11; (7.0 – 9.0)	---	---	[223]
SMB3	0.82; (9.0)	---	---	[228]
Natural laterite	0.20; (7.2)	---	---	[100,226]
70%Bt-30%Ch beads-A	2.054 ± 0.11; (8.0)	2.660 ± 0.25; (8.0)	3.31 ± 0.74; (8.0)	previous study (Section 7.3.2)
Fe-Bt-Ch1 composite	**12.26 ± 0.12; (8.0)**	**13.23 ± 0.17; (8.0)**	**13.74 ± 0.12; (8.0)**	this study
Fe-Bt-Ch-2 composite	**16.37 ± 0.12; (8.0)**	**17.22 ± 0.06; (8.0)**	**17.70 ± 0.17; (8.0)**	this study

C-mVMT = chitosan-modified vermiculite; HDTMA = hexadecyltrimethylammonium; P-Al/Fe-mMont = Polymeric Al/Fe modified montmorillonite; SMB = surfactant-modified bentonite; 70%Bt-30%Ch beads-A = unmodified Bt-Ch; Fe-Bt-Ch-1 = Bt-Ch modified with Fe^{3+} (0.01 M); Fe-Bt-Ch-2 = Bt-Ch modified with Fe^{3+} (0.02 M)

8.3.4. Kinetic studies

In this study, both linear and non-linear equations of Pseudo-first order (PFO), Pseudo-second order (PSO) and Elovich were used. Figure 8.12 and Figure 8.13 shows the non-linear and linear-regression plot (illustrating PFO, PSO and Elovich kinetic models), respectively, for As (III) adsorption by Fe-Bt-Ch-1 composites at 25°C. The kinetic plots (both non-linear and linear) for the second adsorbent sample (Fe-Bt-Ch-2 composites) are presented Appendix E4 and E5, respectively, though the calculated values (or constants) obtained for the two adsorbents are presented in Table 8.6. Based on non-linear models, the correlation coefficient (R^2) values for all the models were found to be the same (0.999), and the chi-square (X^2) values obtained for PSO (compared to PFO model) were quite lower, indicating that PSO fitted better to the experimental data. Based on linear models, higher correlation coefficient (R^2) values were observed for PSO (compared to PFO model). In addition, based on both linear and non-linear equations, the calculated adsorption capacities, $q_{e(cal.)}$ for PSO (compared to PFO) were closer to the experimental adsorption capacities, $q_{e(exp.)}$, and this indicates that PSO model fitted better to the kinetic adsorption data. Also, the parameters obtained from the linear equations of these kinetic models were computed into their original corresponding equations, which then represent the calculated kinetic adsorption data. Both experimental and calculated kinetic adsorption data were plotted against time to observe the biases and confirm the best-fit kinetic system. Since the PSO model correlates better (with kinetic adsorption data), this suggests that the adsorption of As(III) adsorption onto Fe-Bt-Ch-1/Fe-Bt-Ch-2 composites occurs by a chemical process, which contradicts our previous assertion of physical adsorption (as evidenced by Dubinin-Radushkevich isotherm modelling). A similar result was observed from our previous study as reported in Section 7.3.4.

Concerning the Elovich kinetic model, both non-linear and linear equations fitted well, and higher values of α were observed (compared to the β values) for the adsorption of As(III) ions by Fe-Bt-Ch-1/Fe-Bt-Ch-2 composites. This suggests that the rate of adsorption is greater than the rate of desorption, which showed more feasibility towards As(III) adsorption. A similar result was observed from our previous study as reported in Section 7.3.4.

8.3.5. Thermodynamic study

The spontaneousness and feasibility of any adsorption process is usually examined by thermodynamic parameters such as free energy change (ΔG°), enthalpy change (ΔH°), and entropy change (ΔS°) [116,201,219,222]. The thermodynamic plots for the two adsorbent samples (Fe-Bt-Ch-1 and Fe-Bt-Ch-2 composites) are shown in shown in Figure 8.14, and the calculated values (or constants) obtained are presented in Table 8.7. As can be seen, the negative values of free energy change (ΔG°) observed at all the temperatures studied indicates that the adsorption of As(III) onto Fe-Bt-Ch-1 and Fe-Bt-Ch-2 composites occurred spontaneously. Also, the negative values of enthalpy change (ΔH°) suggests that adsorption process proceeded exothermically. It has been reported that an exothermic process is usually associated to physisorption coupled with relatively weak interactions (i.e., van der Waal forces) [7,222]. Moreover, the positive values of ΔS° obtained signifies an increased randomness at the adsorbent-adsorbate (i.e., solid-solution) interface during the adsorption interaction [222].
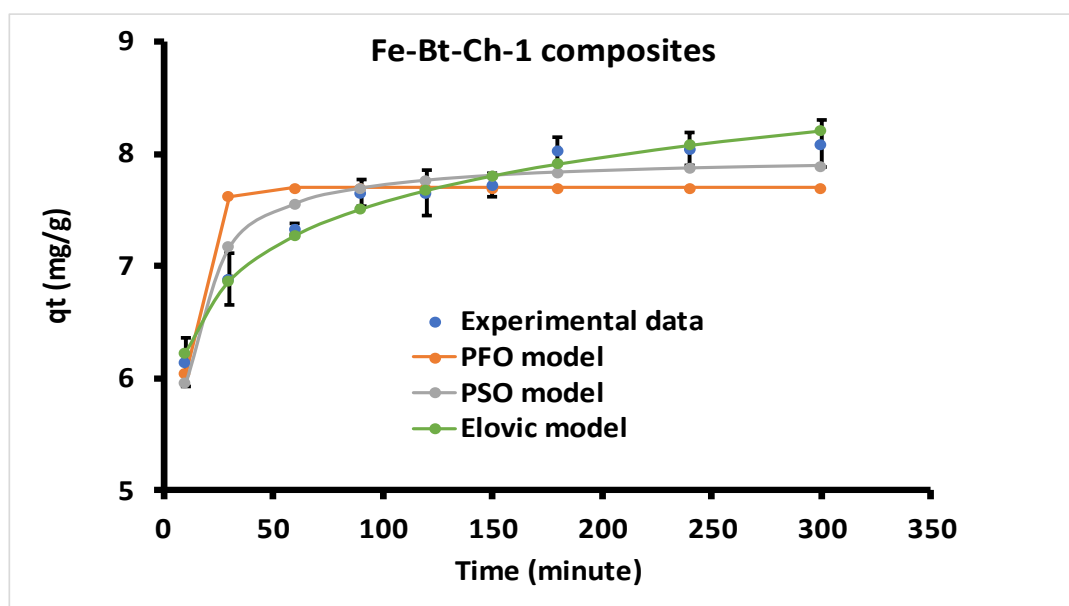
Figure 8.12: The non-linear PFO , PSO and Elovich kinetic models for adsorption of As(III) by Fe-Bt-Ch-1 composites

Note: At 25 °C. pH = 8.0; adsorbent amount = 0.1 g; Initial As(III) concentrations = 50 mg/L; agitation time (at 230 rpm) = 10 - 300 minutes. Note: PFO = Pseudo-first order; PSO = Pseudo-second order. Each data-point represents mean ± standard deviation of three (3) different experiments (n = 3).
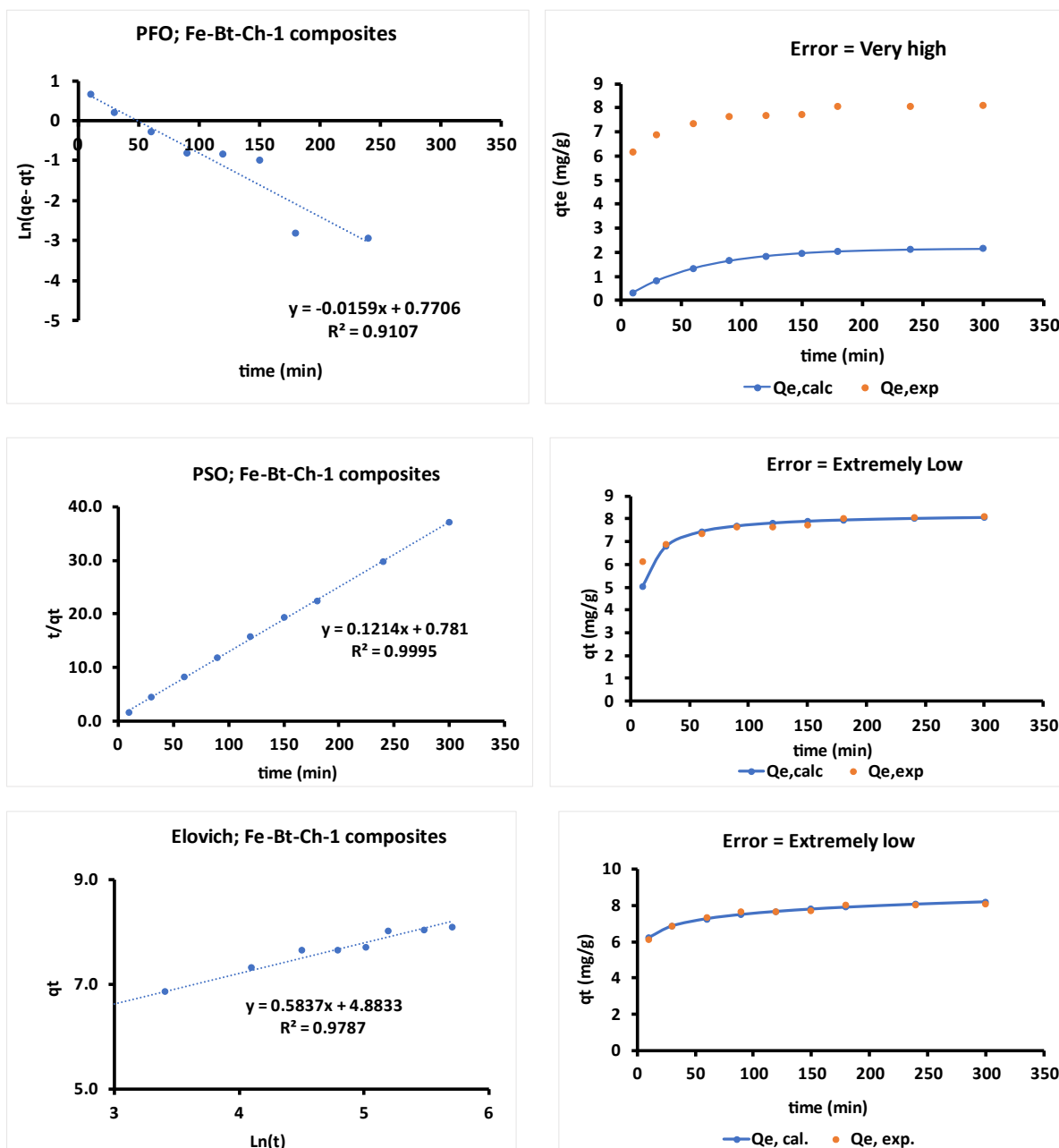
Figure 8.13: The linear regression analysis of PFO, PSO and Elovich kinetic models for adsorption of As(III) by 70%Bt-30%Ch composites

Note: At 25 $^\circ$C. pH = 8.0; adsorbent amount = 0.2 g; Initial As(III) concentrations = 50 mg/L; agitation time (at 230 rpm) = 10 - 300 minutes. Note: PFO = Pseudo-first order; PSO = Pseudo-second order. The average of the kinetic adsorption data was used to plot the linear regression graph.

Table 8.6: The fitting parameters of kinetic models for the adsorption of As(III) onto Bt-Ch composites/beads

Kinetic Models	Fe-Bt-Ch-1 composites		Fe-Bt-Ch-2 composites	
	Non-linear	linear	Non-linear	linear
PFO				
K_1	0.154 ± 0.00	0.016 ± 0.00	0.197 ± 0.00	0.016 ± 0.00
$q_{e,exp}$	8.148 ± 0.09	8.148 ± 0.09	11.86 ± 0.11	11.86 ± 0.11
$q_{e,cal}$	7.752 ± 0.09	2.160 ± 0.00	11.39 ± 0.12	2.160 ± 0.00
R^2	0.999 ± 0.00	0.917 ± 0.00	0.999 ± 0.00	0.917 ± 0.00
X^2	0.016 ± 0.00	---	0.011 ± 0.00	---
PSO				
K_2	0.037 ± 0.00	0.019 ± 0.00	0.042 ± 0.00	0.020 ± 0.00
$q_{e,exp}$	8.148 ± 0.09	8.148 ± 0.09	11.86 ± 0.11	11.86 ± 0.11
$q_{e,cal}$	8.039 ± 0.09	8.290 ± 0.09	11.66 ± 0.12	11.99 ± 0.12
R^2	0.999 ± 0.00	0.999 ± 0.00	0.999 ± 0.00	0.999 ± 0.00
X^2	0.004 ± 0.00	---	0.003 ± 0.00	---
Elovich				
β	1.713 ± 0.00	1.710 ± 0.00	1.667 ± 0.03	1.710 ± 0.00
α	2769.1 ± 448.5	2769.6 ± 449.0	876245.6 ± 137.8	1445270.0 ± 300.1
R^2	0.999 ± 0.00	0.979 ± 0.00	0.999 ± 0.00	0.979 ± 0.00
X^2	0.001 ± 0.00	---	0.001 ± 0.00	---

Note: PFO = Pseudo-first order; PSO = Pseudo-second order; $q_{e,exp.}$ is the experimental adsorption capacity at equilibrium (mg/g); $q_{e,cal.}$ is the calculated adsorption capacity at equilibrium (mg/g); k_1 is the PFO rate constant (min^{-1}); k_2 is the PSO rate constant (g/mg min); β is the Elovich desorption coefficient (g/mg min); α is the Elovich initial sorption rate (mg/g min); *R^2 is the coefficient of correlation, and X^2 is nonlinear chi-square. Each value represents mean ± standard deviation of three (3) different samples (n = 3).*

Table 8.7: The fitting of thermodynamic parameters for the adsorption of As(III) onto Fe-Bt-Ch composites

Adsorbent	Temperature (K)	K_c	$\Delta G°$ (KJ mol^{-1})	$\Delta H°$ (KJ mol^{-1})	$\Delta S°$ (J mol^{-1} K^{-1})	Van't Hoff equation	R^2
Fe-Bt-Ch-1	298.15	369721.04	-31.78	-11.09	69.62	Y = 1333.7x + 8.3735	0.9483
	313.15	323717.69	-33.03				
	328.15	244974.57	-33.85				
Fe-Bt-Ch-2	298.15	571124.18	-32.86	-11.61	71.97	Y = 1396.3x + 8.6463	0.7157
	313.15	574362.32	-34.53				
	328.15	369441.48	-34.98				

Note: K_c = equilibrium constant; $\Delta G°$ = free energy change; $\Delta H°$ = enthalpy change; $\Delta S°$ = entropy change; R^2 = correlation coefficient; $K_c = K_L \times 74.92 \times 55.5 \times 1000$; K_L is the Langmuir constant (L/mg) obtained from Table 8.4
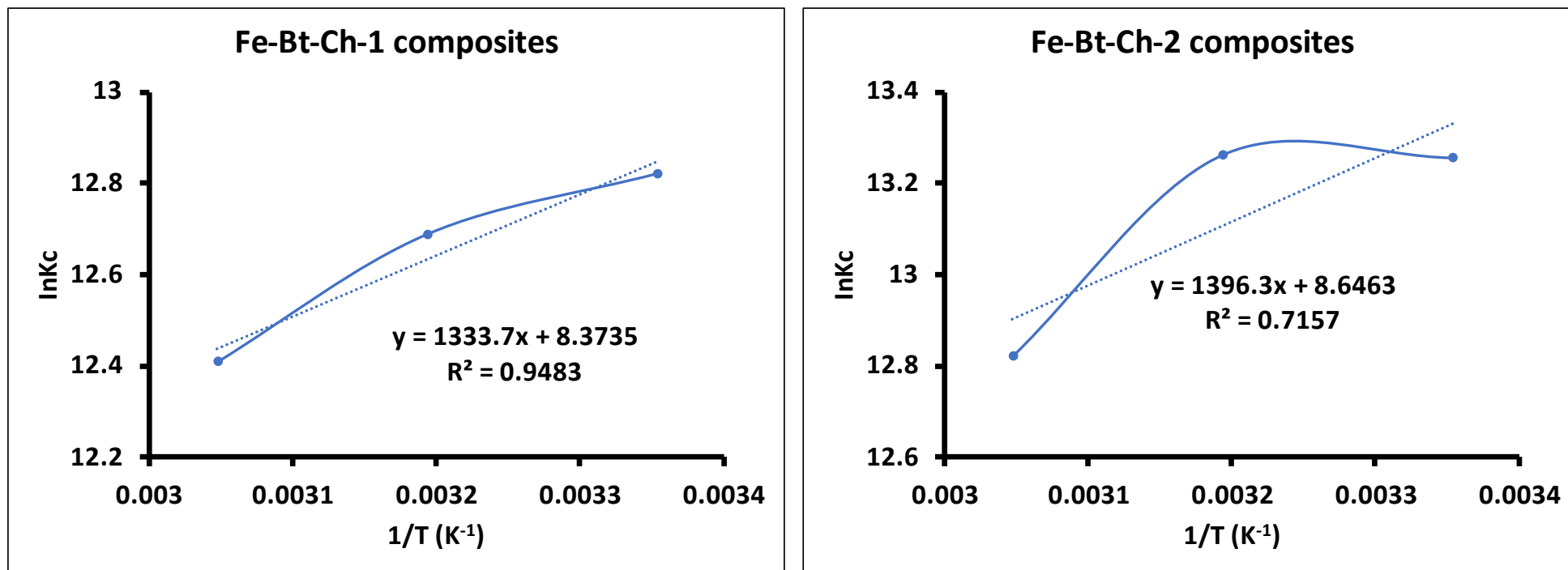
Figure 8.14: A line graph to determine the thermodynamic parameters for the adsorption of As(III) onto Fe-Bt-Ch-1/ Fe-Bt-Ch-2 composites

8.3.6. Adsorption efficiency of As(III) ions

To investigate the efficiency of the absorption process in a single component system, batch adsorption experiments with 0.2 g of Fe-Bt-Ch-1/Fe-Bt-Ch-2 composites, unmodified Bt-Ch composites, bentonite, and chitosan were exposed to different concentrations of As*(III)* solutions (5, 10, and 50 mg/L; at pH of 8.0). As can be seen, better As(III) adsorption efficiency was observed with Fe-modified composites compared to unmodified Bt-Ch, pristine bentonite, and pure chitosan (Figure 8.15). A complete removal (100%) of As(III) ions was achieved when 0.1 g of Fe-Bt-Ch-2 composite sample was exposed to 5 mg/L of As(III) solution. Overall these high adsorption efficiencies support the potential use of Fe-Bt-Ch-1/ Fe-Bt-Ch-2 composites as cost-effective adsorbents for removal of As(III) ions from both drinking and wastewater to the safe level.
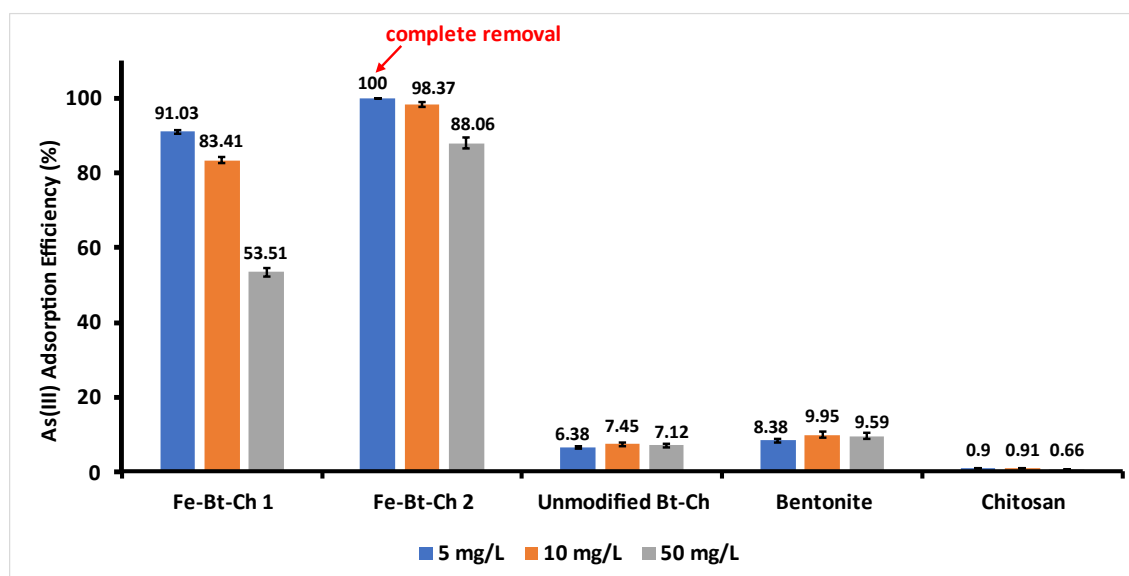
Figure 8.15: Charts showing the As(III) adsorption efficiencies (%) of Fe-Bt-Ch-1/Fe-Bt-Ch-2 composites, bentonite and chitosan

Note: Initial As(III) concentrations = 5, 10 and 50 mg/L; pH = 8.0; adsorbent amount = 0.2 g; agitation time (at 230 rpm) = 180 minutes. Each bar represents mean ± standard deviation of three (3) different samples (n = 3).

8.3.7. Desorption studies

In this study, aqueous NaOH solution was used as the stripping (desorbing) agent. The optimal recovery of As(III) ions was achieved with a 1.0×10^2 mmol/L (or mEq/L)

concentration of aqueous NaOH solution. The adsorption and desorption percentages of both As(III) ions recovered from Fe-Bt-Ch-1 and Fe-Bt-Ch-2 composites are shown in Figure 8.16. About 80% and 98% adsorption was achieved in the 1st cycle for Fe-Bt-Ch-1 and Fe-Bt-Ch-2 composites, respectively. However, only about 70% (for Fe-Bt-Ch-1) and 60% (Fe-Bt-Ch-2) of adsorbed As(III) ions were recovered with dilute NaOH solution (0.1 M) in the 1st cycle. Serial adsorption-desorption steps were conducted up to five times for both adsorbents. The observed adsorption percentage obtained for Fe-Bt-Ch-2 composites (in 2nd cycle) is like the value obtained for the first initial cycle (i.e., 98%), but decreases to about 90% for the subsequent cycles (i.e., 3rd, 4th and 5th cycles). Concerning Fe-Bt-Ch-1, the adsorption percentages in the 2nd cycle were observed to be about 80% (like 1st cycle), but about 70% were observed for subsequent cycles (i.e., 3rd, 4th and 5th cycles). On the other hand, the desorption percentages (for both adsorbents) decrease slightly (to about 60% and 50% for Fe-Bt-Ch-1 and Fe-Bt-Ch-2, respectively) at the second stage, maintain similar value at third stage, and then, slightly increases at fourth and the fifth cycles. Overall, the results indicated that the Fe-Bt-Ch composites exhibited good reusability for removal of both As(III) ions from water. One interesting observation is that these Fe-modified composites are very stable, and the concentration of Fe(III) ions in the filtrate solution was measured through ICP-OES. Results show that the values range from 0.03 to 0.12 mg/L (corresponding to 5.33×10^{-2} - 2.14×10^{-1} mmol/L). This suggests that the composite formation does not leach Fe or causes a change in the color of the filtrate solution (as shown in Figure 8.17).
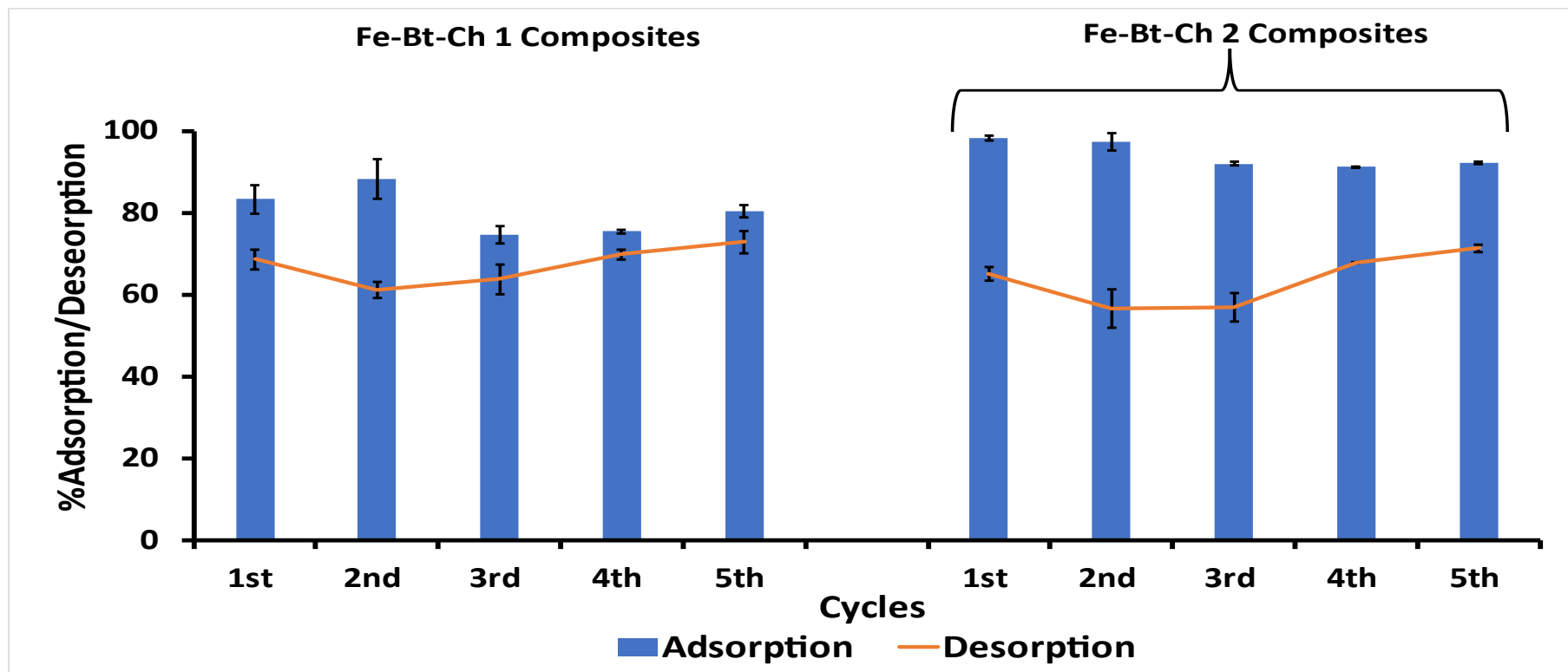
Figure 8.16: Charts showing the serial % Adsorption/Desorption of As(III) ions adsorbed onto Fe-Bt-Ch-1/Fe-Bt-Ch-2 composites

Note: Initial As(III) concentrations = 0.13 mmol/L or 0.39 mEq/L (corresponding to 10 mg/L); pH = 8.0; adsorbent amount = 0.2 g; adsorption agitation time (at 230 rpm) = 180 minutes; desorbing agent = NaOH (0.1 M); desorption agitation time (at 230 rpm) = 180 minutes. Each bar represents mean ± standard deviation of three (3) different samples (n = 3).

After 3 hours of agitation (Adsorption)
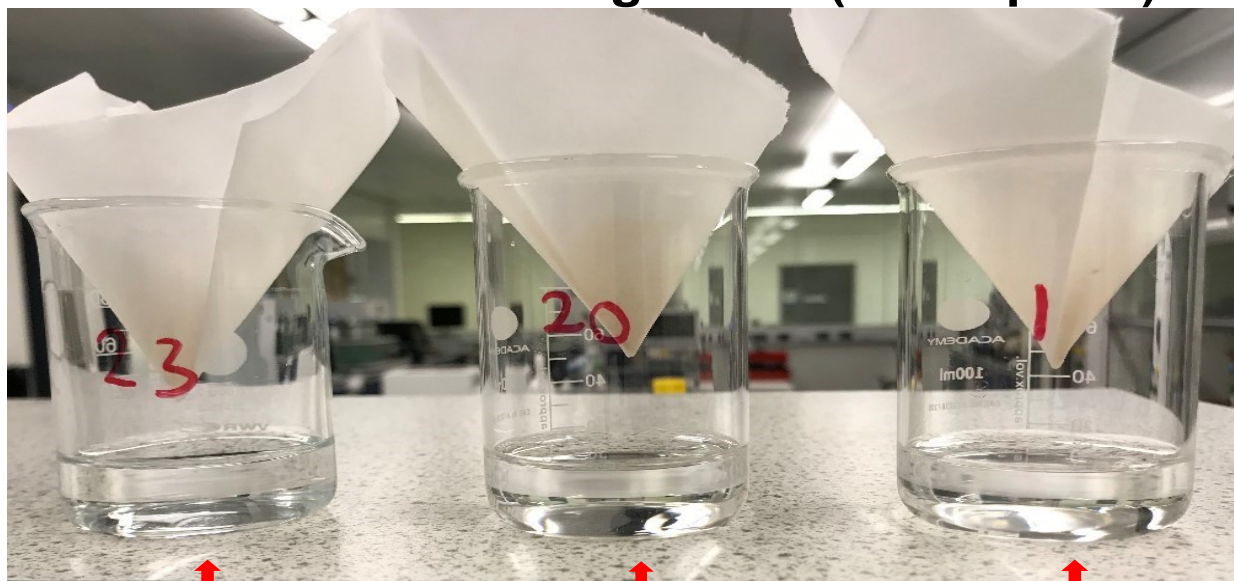
Fe(III) ions (ppm) = 0.03 ± 0.00   0.12 ± 0.00   0.08   ± 0.00

Figure 8.17: Pictures showing filtrate solutions containing As(III) ions after adsorption experiments

8.3.8. Effect of coexisting ions on As(III) ion removal

In this study, the effects of nitrate (NO_3^-), dihydrogen phosphate (H_2PO^-), bicarbonate (HCO_3^-) and chloride (Cl^-) anions on removal of As(III) ions by Fe-Bt-Ch-1/Fe-Bt-2 composites were investigated at pH 8.0 with competing anion concentrations of 20 and 200 mg/L. As can be seen (Figure 8.18), the presence of NO_3^-, HCO_3^- and Cl^- ions (even at high concentrations of 200 mg/L) have no inhibition effects on the removal of As(III) by both adsorbents. However, H_2PO^- ions (at concentrations of 20 and 200 mg/L) are an obvious interference and significantly decrease the removal of As(III) ions. A similar result was observed in our previous study, where the presence of phosphates (PO_4^{3-}) significantly affected the adsorption of As(III) ion by 70%Bt-30%Ch beads-A. The noticeable decrease in arsenic adsorption in the presence of phosphates ions is due to competition for the binding sites of the adsorbent between the phosphate and arsenic, since both phosphate and arsenic have similar chemical features [223,224]. Overall, the result demonstrates that Bt-Ch composites or beads can be utilised as an adsorbent for the selective removal of As(III) from a solution containing other ions.
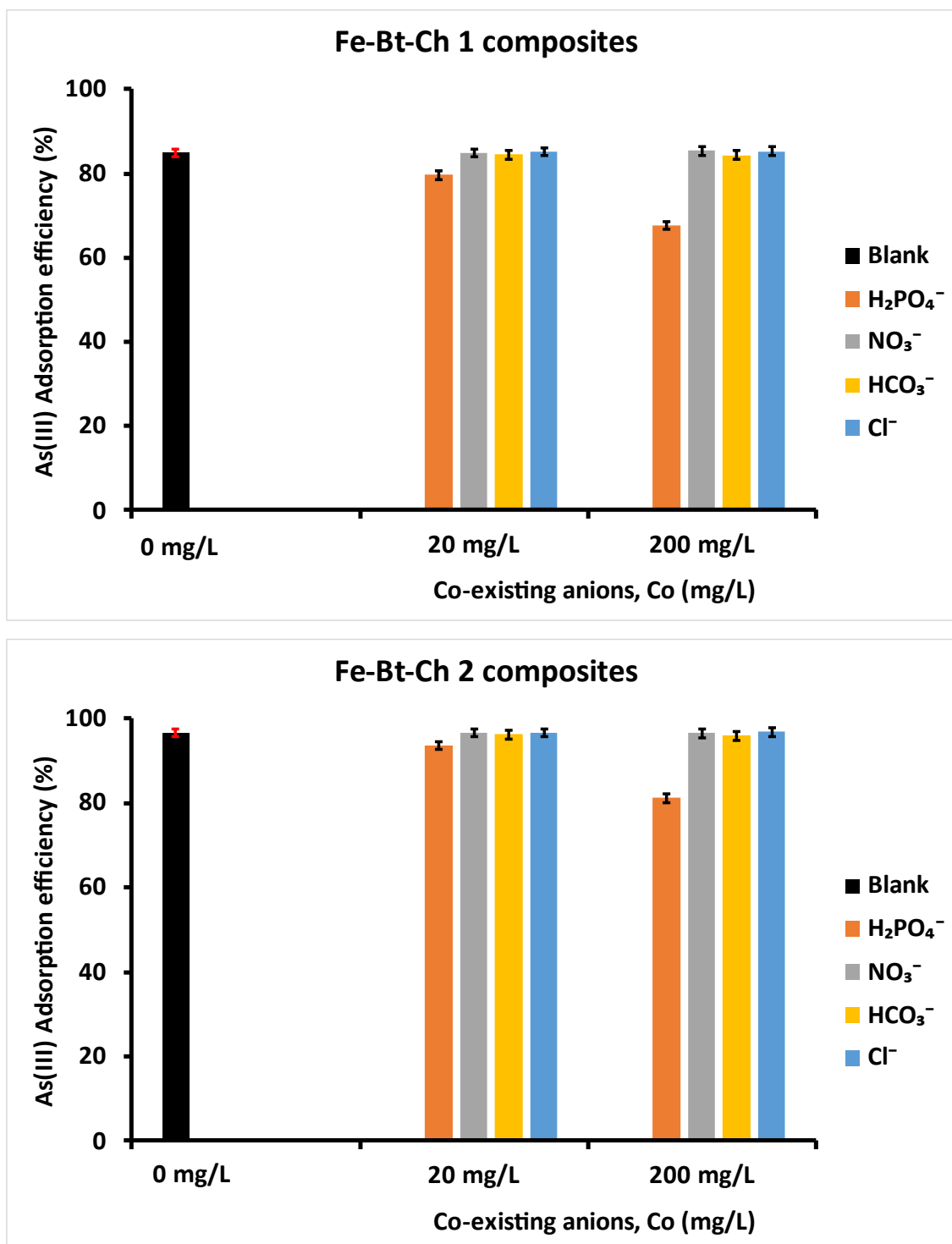
Figure 8.18: Charts showing the effect of anions on removal efficiencies (%) of As(III) ions from binary solutions by Fe-Bt-Ch-1 (top) and Fe-Bt-Ch-2 (bottom)

Note: Initial concentrations of As(III) solution = 10 mg/L; pH = 8.0; adsorbent amount = 0.2 g; agitation time (at 230 rpm) = 180 minutes. Each bar represents mean ± standard deviation of three (3) different samples (n = 3).

8.3.9. Conclusion

An iron-modified composite based on low-cost and sustainable resources was successfully synthesised. Two forms of composites were made depending on the concentration of Fe(III) solution, and both were prepared in the weight ratios of 70% Bt. Clay and 30% chitosan biopolymer. The composites were characterised by TGA, XRD, and FTIR. TGA results confirmed that similar amount of chitosan were observed for all the prepared composites. According to XRD results, less chitosan was intercalated into the interlayers of the clay for Fe-Bt-Ch composites compared to unmodified Bt-Ch composites. From FTIR results, higher intensity bands at 1420 cm^{-1} were observed for Fe-modified composites compared to unmodified Bt-Ch composites. From the adsorption results (via design of experiment), it was observed that that adsorption capacity of As(III) increases with pH, initial concentration and agitation time, but decreases with the adsorbent dosage. The adsorption equilibrium data correlated well with Langmuir, Freundlich and Dubinin-Radushkevich isotherm models. Significantly higher values of maximum As(III) adsorption capacities (Qmax) were recorded for Fe-Bt-Ch composites compared to unmodified Bt-Ch composites. Both Freundlich isotherm and kinetic investigations suggest that the adsorption of As(III) onto Fe-Bt-Ch composites occur via a chemical process. However, the Dubinin-Radushkevich isotherm and thermodynamic analysis indicates that the adsorption of As(III) adsorption onto Fe-Bt-Ch composites may occur by physical process. Better As(III) adsorption efficiency was observed by Fe-modified composites compared to unmodified Bt-Ch, pristine bentonite, and pure chitosan. The prepared Fe-modified composites exhibited good potential for re-use after many cycles of regeneration up to the fifth cycle. With exception of phosphates (PO_4^{3-}), other anions investigated have no inhibition effects on the removal of As (III) by Fe-Bt-Ch composites.

Chapter 9

Column adsorption studies for effective removal of Pb(II) ions from aqueous solution by using Wet-Bentonite-Chitosan beads

9.1. Introduction

To assess the performance of adsorbent materials for large-scale adsorption systems, the typical approach is to utilize the continuous adsorption method or column technique [156]. Having achieved the main objectives set for batch adsorption in the previous chapters, another aspect to explore in this thesis (research project) is the feasibility of using the column adsorption procedure. This will mimic industrial applications to see if the developed material can act as a medium to abstract metal ions from wastewater during the treatment stage of water contaminated with heavy metals and their potential use in filter systems and faucets. The principles and modes of operation of column adsorption (especially the fixed-bed technique) have been briefly reviewed in Section 2.5.6.

In this study, the wet-Bt-Ch beads were tested as an adsorbent to access the removal of Pb(II) ions from aqueous solution via column adsorption. Our previous studies demonstrated that the prepared Bt-Ch composites and beads offers excellent potential for removal of Pb(II) ions using batch sorption experiments. It was not possible to use dried-powder Bt-Ch beads/composites (as previously used for batch adsorption) for column adsorption because there is difficulty in passing the fluid or liquid through the powdered adsorbent (down the column), causing flow resistance. The influence of operating parameters of the fixed-bed column such as inlet initial concentration and bed height were determined for fixed-bed columns packed with wet-Bt-Ch beads used for the dynamic adsorption of Pb(II) ions from aqueous solutions. The breakthrough and other relevant parameters were determined by non-linear modelling of column adsorption equations.

9.2. Experimental

9.2.1. Materials

In this study, only one sample of the wet-Bt-Ch beads (i.e., freshly prepared 70%Bt-30Ch-1 beads-B as described in Chapter 4, picture shown in Figure 9.1) was used and tested as an adsorbent for column adsorption of Pb(II) ions. Lead (II) nitrate ($\geq$ 99.95%), nitric acid (70% w/v), and sodium hydroxide (reagent grade, 97%, pellets) as previously stated in Section 5.2.1, were used to prepared Pb(II), acidic and basic solutions, respectively.

9.2.2. Fixed-bed column adsorption experiment

Figure 9.2 shows a photograph of the experimental set up used for column studies. The fixed-bed column adsorption studies were carried out like procedures reported in the literature [245,246] with modifications. Basically, the fixed-bed column adsorption was conducted in a glass column of 1.75 cm internal diameter and 14 cm height. The column was packed with the adsorbent (wet-Bt-Ch beads). At the bottom of the column is packed glass beads used as a support and to prevent loss of the adsorbent. A peristaltic pump (Colepalmer/Masterflex) was used to pump the aqueous Pb(II) solution (pH 5.0) downward through the column at a constant flow rate of 2 mL min^{-1}. The effluent samples were collected at specified times and the quantitative measurements of Pb(II) ions remaining in the effluent were carried out using the Agilent 5110 ICP-OES instrument using wavelength of 220.353 nm. The operating conditions of the ICP-OES instrument are as stated in Section 3.2.1.

9.2.2.1 *Effects of column operating parameters*

The experiments to determine effects of the operating parameters are described below;

(A) Effect of influent concentration: the effect of inlet concentration on the column performance was studied by varying Pb (II) concentration of 50 and 70 mg/L, while maintaining a constant bed volume of 2.4 cm^3 (2.5 g) and flow rate of 2 min^{-1}.

(B) Effect of bed volume: the effect of bed volume on the adsorption of Pb (II) on Bt-Ch beads-B was investigated by varying the bed volume of 2.4 and 3.4 cm^3 (equivalent to

2.5 and 3.5 g, respectively) while maintaining a constant flow rate of 2 mlmin^{-1} and influent concentration of 50 mg/L. These bed volumes were calculated from the bed height of the adsorbent packed in the (1.0 and 1.4 cm, respectively) and the internal diameter of the glass column. It is important to acknowledge that the cross-sectional area of the bed volume may be influenced by the way the adsorbent is packed into the glass column.

9.2.2.2 *Calculations regarding the performance of the adsorption column*

As described in the literature [164], the performance of the packed bed column was evaluated from the breakthrough curves, which are plotted as ratios of effluent concentration (C_f) to influent concentration (C_i) versus process time (t, min.).

So, the amount of Pb(II) ions loaded in the column (X, mg) up to time t is the influent concentration (C_i, mg/L) multiplied by flow rate (Q, ml/min) and time (t, min). That is,

$$X \ (\text{mg}) = C_i Q t \tag{9.1}$$

The amount of unabsorbed Pb(II) ions (Y, mg) at time t can be obtained from the area under the breakthrough curve up to time t multiplied by inlet concentration (C_i, mg/L) and flow rate (Q, mL/min). That is,

$$Y \ (\text{mg}) = C_i Q \int_0^t \left(\frac{C_f}{C_i}\right) dt \tag{9.2}$$

The amount of Pb(II) ions adsorbed in the column at time t (Z, mg) can be given as;

$$Z \ (\text{mg}) = X - Y \tag{9.3}$$

The maximum equilibrium adsorption capacity (q_e, mg/g) was calculated as the total amount of Pb(II) ions adsorbed at equilibrium time (saturation) to the mass of adsorbent in column (M, g): That is;

$$q_e \ (\text{mg/g}) = \frac{Z \ (\text{mg})}{M \ (\text{g})} \tag{9.4}$$

9.2.2.3 *Modelling of Analytical results*

The dynamic behavior of the columns was predicted using Thomas, Adams-Bohart, Yoon-Nelson and Dose-Response models. The non-linear equations of these models are shown in Equations 2.21, 2.22, 2.23, 2.24 and 2.25, respectively, presented in Table 2.8. These models are important when designing an efficient fixed-bed adsorption system with the optimum required conditions. A plot of C_f/C_i against time (min) will be used for all the modelling. Where C_i and C_f (mg L^{-1}) are the influent and effluent concentrations of the Pb(II) ions before and after the column adsorption experiment, respectively.

Figure 9.1: Photograph of the freshly prepared wet-bentonite-chitosan composites used as an adsorbent packed in a fixed-bed column for Pb(II) adsorption
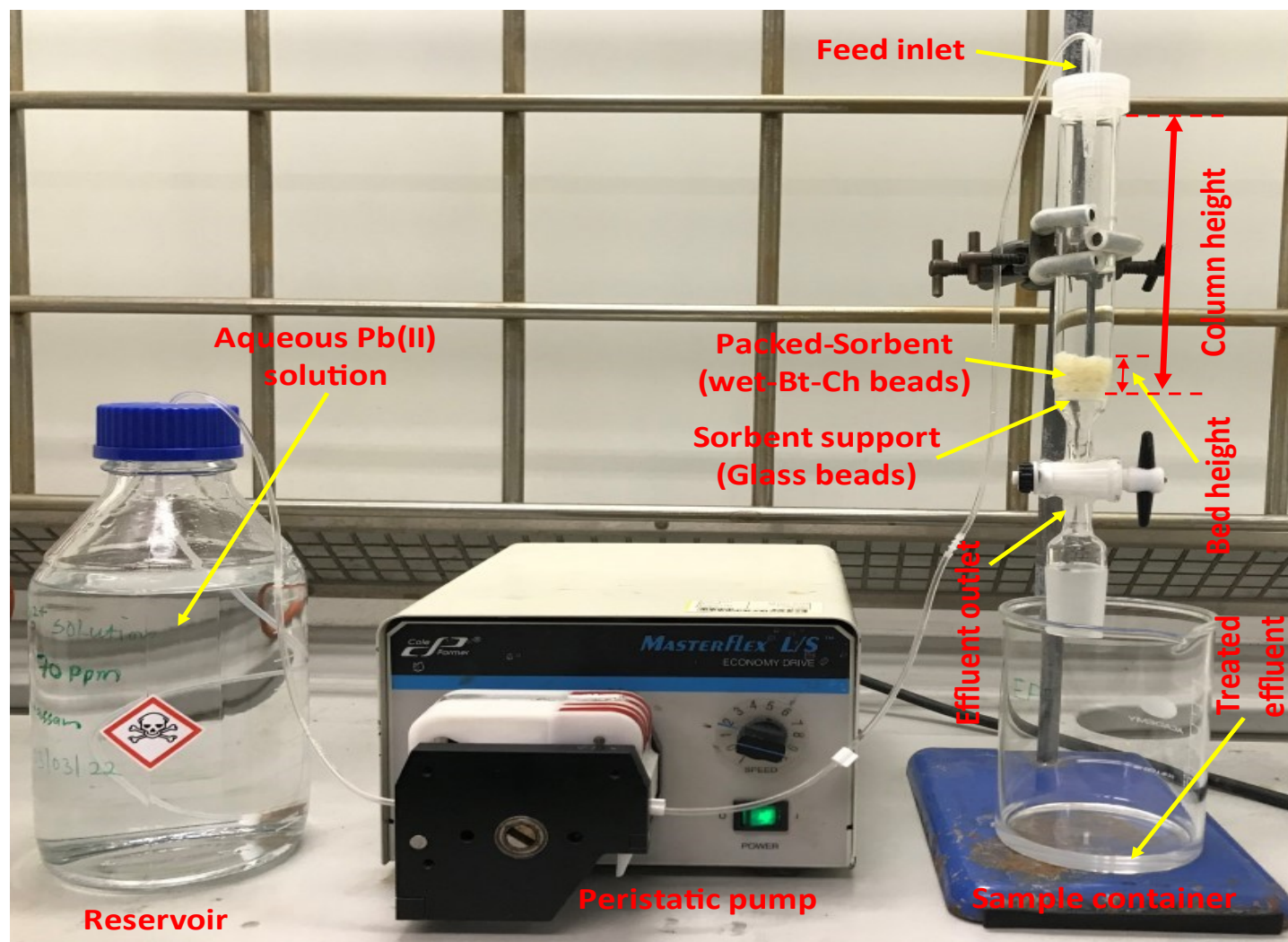
Figure 9.2: Photograph of the experimental set-up for the fixed-bed column adsorption of Pb(II) onto wet-Bt-Ch composites

9.3. Results and discussion

9.3.1. Effects of the operating parameters on breakthrough curve

(A) Effect of influent Pb(II) concentration

Figure 9(A) shows the breakthrough curves illustrating the effect of the influent Pb(II) concentration (50 and 70 mg/L) on the breakthrough curves at constant pH 5.0, bed volume of 2.4 cm^3 (which correspond to bed height of 1.0 cm or 2.5 g of adsorbent) and flow rate of 2 mL min^{-1}. As can be seen, the graph does not look like the typical S-shaped breakthrough curves obtained for most fixed-bed column adsorption. This might be since the adsorption Pb(II) onto wet-Bt-Ch composite was very fast and reached equilibrium within the short time as evidenced from the previous batch adsorption experiments conducted in Chapter 5. Thus, it will be difficult to determine the breakthrough point (t_b) experimentally. This situation happens sometimes, and similar shapes of the breakthrough curve were previously observed for various fixed-bed sorption systems reported in the literatures [247,248]. The value of C_f/C_i increases steadily with time and the times required for 50 % adsorbate breakthrough (t_{50}) were 20 and 35 minutes when the influent Pb(II) concentrations were 50 and 70 mg/L, respectively. This illustrates that the breakthrough time increases with increasing influent Pb(II) concentration. This result (in terms of breakthrough time) is in contrast to those found by most researchers for different adsorbate and using different sorbent materials [164,165,245–247,249–252]. However, from regression analysis, a slightly higher slope (0.1455) was observed for the breakthrough curve of the higher concentration (70 mg/L) compared that of the lower concentration (50 mg/L; slope = 0.1433). This implies that when the influent Pb(II) concentration increases, the column containing the adsorbent becomes saturated quickly, and this accounts for the steeper slope (higher slope) of the breakthrough curve. This in turns, increases the metal loading rate as shown in Table 9, where the maximum column adsorption capacity calculated for breakthrough curve of 70 mg/L influent concentration is significantly higher compared to that of the 50 mg/L influent concentration. Similar results (in terms of steeper slope) are reported in the literature [247,249,253].

(B) Effect of bed volume

Figure 9(B) shows the breakthrough curves illustrating the effect of the bed volume of 2.4 and 3.4 cm^3 (corresponding to 1.0 and 1.4 cm or 2.5 and 3.5 g of the adsorbent, respectively) on the breakthrough curves at constant pH 5.0, influent Pb(II) concentration of 50 mg/L, and flow rate of 2 mL min^{-1}. The shape of the breakthrough curve (for different bed height) looks like that of the breakthrough curve obtained for different influent Pb(II) concentration. The time required for 50% adsorbate breakthrough (t_{50}) were observed to be 20 and 30 minutes when the bed heights were 2.4 and 3.4 cm^3, respectively (equivalent to 1.0 and 1.4 cm, respectively). This indicates that as the bed volume or bed height increases, the length of the bed through which the effluent passes increase, and thus longer breakthrough time elongated. The result is similar to those found by most researchers in the literature for the fixed-bed systems [245,246,252,253].

In terms of the slope of the breakthrough curve, a slightly lower slope (0.1392) was observed for the breakthrough curve when the bed volume was 3.4 cm^3 (or bed height 1.4 cm), compared to when the bed volume was 3.4 cm^3 or bed height of 1.0 cm (slope = 0.1433). This is like a previous fixed-bed column study conducted by Han et al. (2007)[247], they observed that the slope of breakthrough curve decreased with increasing bed height, which resulted in a broadened mass transfer zone. Concerning the column adsorption capacity (mg/g), lower Pb(II) uptake was observed with a bigger bed height, which is in contrast to what has been previously reported in the literature [246,252,253].
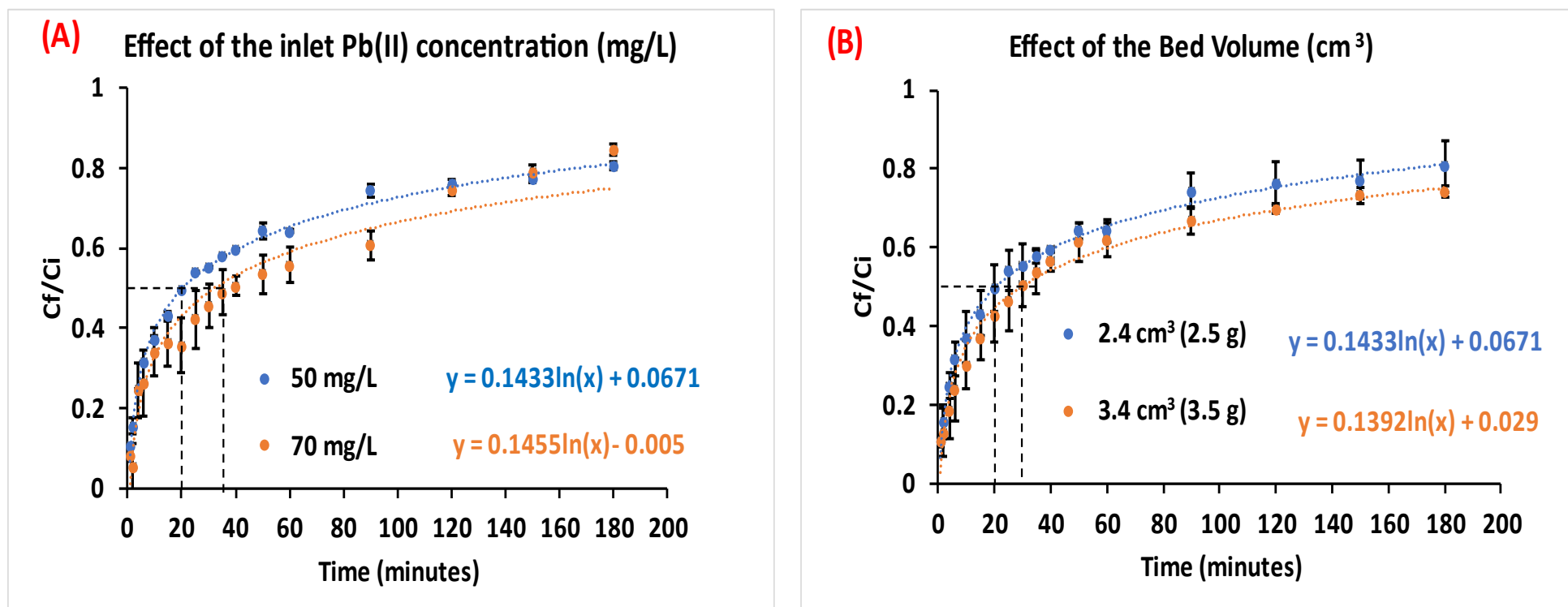
Figure 9.3: Breakthrough curve showing the effect of column operating parameters on the Pb(II) adsorption

Note: (A) effect of the influent Pb(II) concentration (50 and 70 mg/L) at constant pH 5.0, bed volume of 2.4 cm^3 (bed height of 1.0 cm or 2.5 g of adsorbent) and flow rate of 2 mL min^{-1}., (B) effect of the bed volume of 2.4 and 3.4 cm^3 (corresponding to bed height of 1.0 and 1.4 cm or 2.5 and 3.5 g of the adsorbent, respectively) at constant pH 5.0, influent (P(II) concentration of 50 mg/L, and flow rate of 2 mL min^{-1}.

Table 9.1: The $t_{0.5}$ and $q_{e\ (exp.)}$ values obtained for different parameters

	Influent Pb(II) concentration			Bed volume	
	50 mg/L	70 mg/L		2.4 cm^3 (2.5 g)	3.4 cm^3 (3.5 g)
$t_{0.5}$ (minutes)	20.00	35.00		20.00	30.00
$q_{e\ (exp.)}$ (mg/g)	2108.5 ± 190.2	5071.3 ± 8.037		2108.5 ± 190.2	1644.1 ± 104.3

Note: $t_{0.5}$ is the breakthrough time at 50% (i.e., $C_f/C_i = 0.5$); $q_{e\ (exp.)}$ is the maximum column adsorption capacity calculated from experimental data; $t_{0.5}$ values were obtained from extrapolation as indicated with dash-lines of the respective graphs in Figure 9; For $q_{e\ (exp.)}$, each value represents mean ± standard deviation of three (3) different experiments (n = 3)

9.3.2. Modelling of column experimental data

In this study, the Thomas, Adams-Bohart, Dose-Response, Yoon-Nelson, and Bed Depth Service Time (BDST) models were applied to the experimental data with respect to influent Pb(II) concentration and bed height (Figure 9(A/B) and 9(C/D)). A non-linear modelling method was employed to analyse the behaviour of the breakthrough curve for the fixed-bed column adsorption of the Pb(II) by wet-Bt-Ch composites, and optimisation was done using the "Solver add-in" in Excel Microsoft 365. The values (or constants) obtained from these models are presented in Table 9.2.

Generally, the correlation coefficient (R^2) values for all the models were found to be equal or greater than 0.99, indicating that experimental data correlated well with all the column adsorption models studied. Also, the chi-square (X^2) values obtained for all the models were extremely low, indicating a good agreement between the experimental data and the column data generated using the models.

(A) Thomas model

The Thomas model was applied to investigate the breakthrough behaviour of Pb(II) ions on wet-Bt-Ch composites. Usually, it has been applied between the breakthrough time and the saturation time in the column [249]. The values of the kinetic rate constant (K_{Th}) and the column equilibrium Pb(II) uptake (q_{Th}) were both calculated from Thomas model. As can be seen, the value of K_{Th} decreases (from 0.0005 ± 0.00 to 0.0003 ± 0.00 L/mg/min), while the value of q_{Th} increases significantly (from 1141.9 ± 123.6 to 2846.8 ± 214.7 mg/g) as influent Pb(II) concentration increases from 50 mg/L to 70 mg/L. These results agree with what was obtained by other researchers studying different solute−sorbent systems. Calero et al. (2009) [249] found that when the influent concentration increases (from 10 to 100 mg/L), the values of K_{th} and q_{Th} varies from 0.683 to 0.415 L/mg/min and from 0.286 to 0.451 mg/g, respectively, for the study of Cr(III) biosorption in a fixed-bed column by using olive-stone as an adsorbent; Saad et al. (2015)[246], studying the removal of uranium (U) from aqueous solutions by phosphonated cross-linked polyethylenimine, showed that the K_{th} value decreases from 0.0058 to 0.00043 L/mg/min when the influent concentration increases from 40 to 100 mg/L, whereas the value of q_{Th} increases from 1.0862 to 4.1860 mg/g, in the same range of concentrations.

The increased q_{Th} value with concentration gradient suggest that higher Pb(II) concentration is a key driving force which resulted in better column performance [247].

In terms of the bed height, as bed volume varies from 2.4 to 3.4 cm^3 (i.e., from 2.5 to 3.5 g), the value of q_{Th} increases (from 1141.9 ± 123.6 to 1390.8 ± 100.9 mg/g), whereas the value of K_{Th} decreases (from 0.0005 ± 0.00 to 0.0004 ± 0.00 L/mg/min). This is in contrast to the few results reported in the literatures [245,246].

(B) Adams-Bohart model

Adam-Bohart model is usually applied to column adsorption experimental data to describe the initial part of the breakthrough curve [156]. The values of the Adams–Bohart rate constant (K_{AB}) and the column saturation concentration (N_0) were both estimated. As both influent Pb(II) concentration and bed volume increases (i.e., 50 to 70 mg/L and 2.4 to 3.4 cm^3, respectively) the value of K_{AB} slightly decreases (from 0.0005 ± 0.00 to 0.0003 ± 0.00 L/mg/min and from 0.0005 ± 0.00 to 0.0004 ± 0.00 L/mg/min, respectively), while the value of N_0 increases (from 1952.5 ± 90.39 to 3831.9 ± 65.08 mg/L and from 1952.5 ± 90.39 to 1962.2 ± 214.9 mg/L, respectively). This is similar to a previous study conducted by Saad et al. (2015) [246], they observed that when both the influent concentration and bed height increases (from 40 to 100 mg/L and 2.5 to 4.5 cm, respectively), the values of K_{AB} decrease from 0.00015 to 0.00002 L/mg min and increase from 0.000045 to 0.00015 L/mg min, respectively. While the values of N_0 increases from 678.3 to 1,616.9 mg/L and from 663.8 to 733.3 mg/L with respect to influent concentration and bed height, respectively. In addition, Calero et al. (2009) [249] observed that when the influent concentration increases from 10 to 100 mg/L (for the column biosorption of Cr(III) onto olive-stone), the values of K_{AB} and N_0 varies from 0.0083 to 0.0011 L/mg min and from 65.7 to 197.4 mg/L, respectively. Overall, these results suggest that the kinetics of the fixed-bed column system studied were dominated by external mass transfer, because the sorption capacity (N_0) increases with increase in influent concentration and bed height [246].

(C) Dose-Response model

The Dose-Response model is usually applied to column adsorption experimental data to analyse the entire breakthrough curve [164,165]. The parameter determined from Dose-Response model equations are q_{DR} (mg/g) and α (dimensionless) which are referred to as the Pb(II) concentration in the solid phase (i.e., column adsorption capacity in mg/g)

and Dose-Response constant. As both influent Pb(II) concentration and bed volume increases (i.e., 50 to 70 mg/L and 2.4 to 3.4 cm^3, respectively) the value of q_{DR} significantly increases (from 4229.0 ± 712.4 to 11171 ± 28.13 mg/g and from 4229.0 ± 712.4 to 9883.7 ± 882.6 mg/g, respectively). This is similar to a previous study conducted Calero et al. (2009) [249], they reported that when the influent concentration increases (from 10 to 100 mg/L), the value of q_{DR} varies from 0.263 to 0.406 mg/g, for the biosorption study of Cr(III) with olive-stone packed in a fixed-bed column. However, a contrasted result was reported by Cruz-Olivares et al. (2013)[165], they observed that the value of q_{DR} decreases from 14.6 to 13.0 mg/g as influent concentration increases (from 15 to 25 mg/L), for their biosorption study of Pb(II) by allspice-residue packed in a fixed-bed column. The major observation from these two cited literature is that the calculated column adsorption capacity (mg/g) from Dose-Response equation (q_{DR}) were similar to the corresponding q_{TH} values obtained from the Thomas model[165,249]. In this study, however, the values of q_{DR} were significantly different from the corresponding q_{TH} values obtained from the Thomas model (check Table 9.2 for comparison).

(C) Yoon-Nelson model

Like the Thomas model, the Yoon-Nelson model is usually applied for a range of concentrations in the effluent describing the column behaviour between the breakthrough time and the saturation time[249]. The values of the Yoon-Nelson rate constant (K_{YN}) and the time required for the 50% breakthrough (τ) of Pb (II) retention were both estimated. As both influent Pb(II) concentration and bed volume increases (i.e., 50 to 70 mg/L and 2.4 to 3.4 cm^3, respectively) the value of K_{YN} slightly decreases (from 0.02215 ± 0.003 to 0.0186 ± 0.001 min^{-1} and from 0.02215 ± 0.003 to 0.0177 ± 0.003 min^{-1}, respectively), while the value of τ increases (from 30.838 ± 3.338 to 55.542 ± 0.614 min and from 30.838 ± 3.338 to 51.752 ± 6.022 min, respectively). With respect to K_{YN}, these results agree with the previous study by Cruz-Olivares et al. (2013)[165], they observed that the value of K_{YN} decreases from 0.089 to 0.075 min^{-1} as influent concentration increases (from 15 to 25 mg/L). However, with regards to 50% breakthrough time (τ values), their results contrasted with findings of this study as they observed that the value of τ decreases from 295.1 to 166.4 min with the influent concentration gradient. In sum, the values of the τ calculated from the model are

different to those obtained experimentally, but the trends with respect to both influent Pb(II) concentration and bed height remain the same.
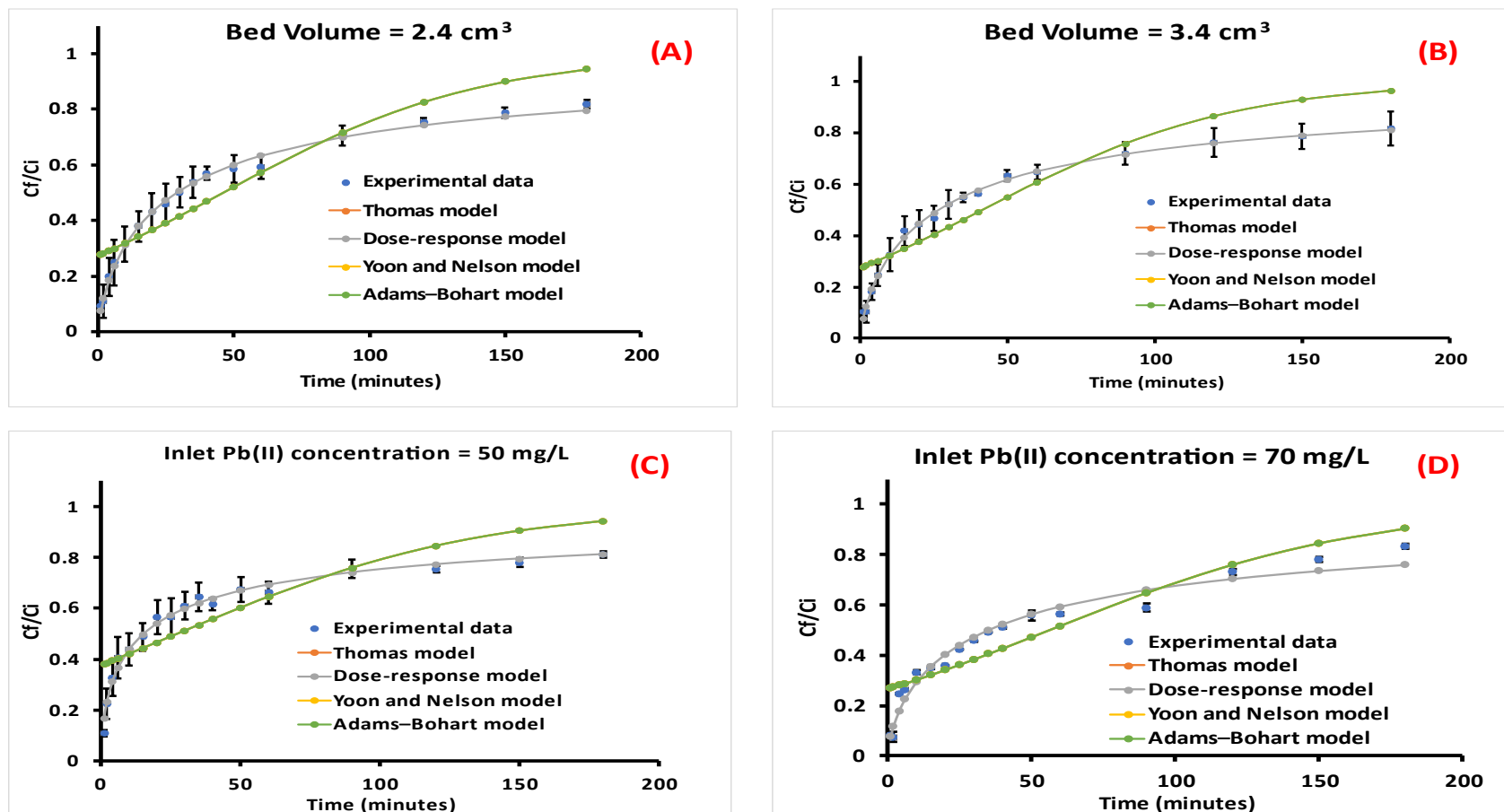
Figure 9.4: The non-linear modelling of the breakthrough curve for Thomas, Adams-Bohart, Dose-Response, and Yoon-Nelson models

Note: The non-linear modelling of the breakthrough curve for Thomas, Adams-Bohart, Dose-Response, and Yoon-Nelson regarding the column adsorption of Pb(II) by wet-Bt-Ch composites with respect to (A/B) bed volume (2.4 and 3.4 cm^3) at constant pH 5.0, influent (P(II) concentration of 50 mg/L, and flow rate of 2 mL min^{-1}, (C/D) influent Pb(II) concentration (50 and 70 mg/L) at constant pH 5.0, bed volume of 2.4 cm^3 and flow rate of 2 mL min^{-1}. Each data-point represents mean ± standard deviation of three (3) different experiments (n = 3)

Table 9.2: The fitting parameters of the column adsorption models for the removal of Pb(II) wet-Bt-Ch composites

Column models	Parameters	Inlet Pb(II) concentration (C)		Bed Volume	
		50 ppm	70 ppm	2.4 cm³ (2.5 g)	3.4 cm³ (3.5 g)
Thomas	K_{th}	0.0005±0.000	0.0003±0.000	0.0005±0.000	0.0004±0.000
	q_{th}	1141.9±123.6	2846.8±214.7	1141.9±123.6	1390.8±100.9
	R^2	0.9998±0.000	0.9999±0.000	0.9998±0.000	0.9998±0.000
	X^2	0.0217±0.002	0.0159±0.006	0.0217±0.002	0.0243±0.003
Adams–Bohart	K_{AB}	0.0005±0.000	0.0003±0.000	0.0005±0.000	0.0004±0.000
	N_0	1952.5±90.39	3831.9±65.08	1952.5±90.39	1962.2±214.9
	R^2	0.9996±0.000	0.9999±0.000	0.9996±0.000	0.9996±0.000
	X^2	0.0261±0.000	0.0051±0.000	0.0261±0.000	0.0262±0.005
Dose–Response	q_{DR}	4229.0±712.4	11171±28.13	4229.0±712.4	9883.7±882.6
	α	0.6480±0.058	0.7129±0.012	0.6480±0.058	0.6828±0.057
	R^2	0.9999±0.000	0.9999±0.000	0.9999±0.000	0.9999±0.000
	X^2	0.0000±0.000	0.0000±0.000	0.0000±0.000	0.0000±0.000
Yoon and Nelson	K_{YN}	0.0215±0.003	0.0186±0.001	0.0215±0.003	0.0177±0.003
	τ	30.838±3.338	55.542±0.614	30.838±3.338	51.752±6.022
	R^2	0.9998±0.000	0.9999±0.000	0.9998±0.000	0.9998±0.000
	X^2	0.0002±0.000	0.0001±0.000	0.0002±0.000	0.0002±0.000

Note: K_{Th} is the Thomas rate constant (L/min/mg), q_{th} is the maximum concentration of the Pb(II) in the solid phase in (mg/g), K_{AB} is the Adams–Bohart rate constant (ml/ min/ mg), N_0 is the maximum volumetric sorption capacity (saturation concentration) (mg/L), q_{DR} is the Pb(II) concentration in the solid phase (i.e., column adsorption capacity in mg/g), α is the constant of the Dose–Response model (dimensionless), K_{YN} is the Yoon and Nelson rate constant (min^{-1}) and τ the time required for 50% adsorbate breakthrough (min), K_{BDST} is the BDST rate constant that describes the mass transfer from the liquid to the solid phase (L/mg min), and N_{BDST} is the sorption capacity of the bed (mg/L)

9.4. Conclusion

The removal of Pb(II) ions from aqueous solution by wet-Bt-Ch composites packed in a fixed bed column mode was investigated. The results of the breakthrough curve obtained showed that the sorption of Pb(II) is dependent on the influent concentration and bed height. Unfortunately, the effect of flow rate was not tested at the time of this study. An increase in the influent concentration of Pb(II) ions at constant flow rate which leads to an increase in the slope of the breakthrough curve, thereby reducing the volume treated (throughput) before adsorbent regeneration. This may be cause by high Pb concentration saturating the adsorbent more quickly, thereby decreasing the breakthrough time. On the other hand, when the bed volume or height was increased, the number of available sites for adsorption and contact time between the Pb(II) ions and Bt-Ch composite also increased which should resulted in higher loading of Pb(II) ions in the column. Unfortunately, lower column loading was obtained for higher bed height. The various column adsorption models including Thomas, Adams-Bohart, Dose-Response, and Yoon-Nelson models were applied to the experimental data with respect to influent Pb(II) concentration and bed height. All the applied models correlated well and coupled with a good agreement with the experimental data. The constants evaluated from these models can be employed for the designing of the fixed-bed adsorption columns (for removal of Pb) over a range of feasible flow rates, bed height and influent concentrations. Even though more work needs to be done, the overall performance of the column study demonstrated that wet-Bt-Ch composite can be used in fixed-bed columns for removal of Pb(II) ions.

Chapter 10

General Conclusion, Limitation, Future work

10.1. General Conclusion

The synthesis of layered silicate-polymer composites has been researched extensively and for many applications including potential adsorbents for purification of water contaminated with heavy metals. Among the different clays, bentonite (mainly montmorillonite) is good for composite formation in many applications, it is also very abundant in nature and widely used for metal sorption processes as a raw material. Clays alone have some limitations for most applications and to overcome these deficiencies clays are combined with other materials, the most attractive of all being polymers. The use of traditional non-biodegradable polymers (produced from fossil fuels) for composite formation is becoming less attractive due to their damaging effect on the health of the ecosystem[76]. There is therefore a need to develop novel polymer composites which are non-toxic and biodegradable such as to allow degradation via natural composting processes[76]. The intercalation of positively charged biopolymers (e.g. chitosan) into layered silicates (e.g. bentonite) has only gained attention in recent decades. These alternative materials are interesting from a sustainability and environmental aspect, but also have potential to offer a cost-benefit.

The removal of toxic metals from contaminated water sources are of fundamental importance to protect the environment and ensure the wellbeing of the populations. The conventional methods used in remediating metal-contaminated waters are very expensive, and sometimes, they may not be effective for very low concentrations. Under this framework, this study focuses on the preparation of functional composites (or beads) from bentonite clay (and chitosan biopolymer) and their employment as adsorbent to achieve a sustainable, affordable, and efficient water treatment platform. This present study investigated the efficiency of mixing bentonite with chitosan via two different preparation methods (i.e., solution and precipitation), subsequently the different forms were investigated for their ability to remove heavy metals (Pb, Cu and As ions) from solution.

This research project contributes to a better understanding about interaction of bentonite clays and the chitosan biopolymers, which are highlighted in detail in the following section.

10.1.1. Specific findings and major contributions

(A) The making of Bt-Ch composites and beads

Chapter 4 was devoted to the making of composites and beads by combination of bentonite clay and chitosan biopolymer. This is the chapter where the first phase of the experimental work carried out in this thesis was reported. In this chapter, we investigated the efficiency of mixing bentonite with two different chitosans via two different preparation methods. The different forms of bentonite-chitosan (Bt-Ch), composites and beads, were prepared in the weight ratios of 90%/10%, 70%/30% and 50%/50%, and via solution blending and precipitation methods, respectively. The beads were further subdivided, identified as "beads-A" and "beads-B", and were formed by adding either bentonite suspension or bentonite powder, respectively, to solubilised chitosan solution. The composites and beads were characterised by thermogravimetric analysis, X-ray diffraction, and Fourier transform infrared spectroscopy. From our results, it was observed that higher product yield (%) was recovered for beads samples synthesised via the precipitation method, compared to the composite samples recovered through the solution blending method. This is attributed to loss of solubilised chitosan during the washing step of the products recovered via the solution blending method. TGA showed the beads contained more chitosan than the composites whilst XRD show that less chitosan could be intercalated into the interlayers of the clay when the bentonite was added to the chitosan solution as a powder (beads B) rather than as an aqueous dispersion (composites and beads A). When intercalated, the interlayer spacings increased from mono-layers to bi-layers structures as chitosan loading increased.

Although few works have already been done in the synthesis of clay-polymer composites; even less is that of the Bt-Ch composites in order to establish inexpensive adsorbent for the removal of heavy metals from wastewaters or drinking water. But interaction of bentonite clay and chitosan biopolymer has never been investigated

systematically based on different synthetic procedures. The findings shown that the yield (%) depends on; 1) the synthetic method used, (2) weight ratio (especially for composite formation via solution method), (3) state of the bentonite clay before mixing with chitosan solution (i.e., suspension or powdered) as well as the type of chitosan. For the first time TGA technique was used to quantify the quantity of chitosan in the final Bt-Ch composites and beads.

(B) Evaluation of the adsorption capabilities of Bt-Ch composites and beads

The applicability and evaluation of Bt-Ch composites or beads as an adsorbent for the removal of metal ions from aqueous solutions was done by batch procedure and systematic approach, beginning with Pb(II) adsorption from single-component solution (Chapter 5), followed by co-adsorption from binary solution containing Pb(II) and Cu(II) ions (Chapter 6), and eventually with adsorption of As(III) from single-component solution (Chapter 7). Further, statistical design of experiments (DoE) has been applied as the methodology in all the batch adsorption experiments carried out in this thesis to gain a better understanding of the systems (effect of factors) and process optimisation. DoE reduces the time (spent to carried out the adsorptions experiments) and reduces the consumptions of adsorbents and chemical reagents.

Results showed that Pb (or Pb-Cu) ions can be removed from aqueous solutions effectively. It was noted that the adsorption of Pb(II) ions with these adsorbents from the aqueous solutions was independent of time, but influenced by solution pH, adsorbent dose, initial Pb(II) concentration, and significantly affected by the presence of other multi-competing ions. Further results shown that higher Pb(II) adsorption capacity (mg/g) was observed for beads compared to their corresponding composites. In addition, it was observed that higher Pb(II) loading capacity (mg/g) was obtained for beads-B compared to their corresponding beads-A, even though they both contains similar amount of chitosan as evidenced from TGA. Therefore, it was confirmed that the amount of chitosan present in the adsorbent and its distribution within or outside the interlayer space of the bentonite clay (as evidenced from TGA and XRD results) was shown to have pronounced effects on the Pb(II) uptake by Bt-Ch composites/beads. In terms of chitosan type, higher Pb(II) adsorption capacity (mg/g) was observed for Bt-Ch-2 samples (compared to Bt-Ch-1), and this may be due to a higher degree of deacetylation (DD) of Chitosan-2 used for composite/beads formation. The results from

the equilibrium isotherm and ion-exchange experiments suggest that both chemisorption (complexation) and physisorption (ion-exchange process) played crucial roles during adsorption of Pb(II) ions by all Bt-Ch composites/beads. Finally, it was concluded that from the desorption results, the developed Bt-Ch composites/beads exhibited good potential for re-use after five cycles of regeneration, thus, indicating their potential as cost-effective adsorbents for removal of Pb(II) ions from both drinking and wastewater.

In terms of Pb-Cu; It was observed that the simultaneous removal of these metal ions from binary aqueous solutions by Bt-Ch composites/beads was independent of time, but influenced by solution pH, adsorbent dose, and initial Pb(II) concentration. From equilibrium studies, it was found that the adsorption capacity (mg/g) of both Pb (II) and Cu (II) ions estimated for Bt-Ch composites was lower than the values obtained for Bt-Ch beads. When Bt-Ch composite was used as an adsorbent, the Pb(II) loading capacity (mg/g) was about 60% higher compared to values obtained for Cu (II) ions. However, no significant difference was observed between the uptake (mg/g) of the two analysed ions when the Bt-Ch bead was used as adsorbent. In terms of adsorption efficiencies, about 90 to 99% removal (of both Pb(II) and Cu(II) ions) was observed for beads, and the desorption percentages (for both metal ions) in the 1st cycle were above 80%. Similar trends were observed for subsequent adsorption-desorption cycles up to five times. For composites, about 80% and 60% adsorption was achieved in the 1st cycle for Pb(II) and Cu(II), respectively. For subsequent adsorption-desorption cycles, the adsorption percentages (for both Pb and Cu ions) decreased significantly after the second cycle. This indicates that composites are less stable (compared to beads) with apparent loss of the active sites for multiple adsorption cycles. It was concluded that the prepared Bt-Ch composites and beads are a low-cost, sustainable alternative to expensive adsorbents (e.g., activated carbon), which can be employ for simultaneous removal of Pb(II) and Cu (II) ions from aqueous solution.

However, these Bt-Ch composites (and beads) showed a poor loading capacity (very low removal efficiencies) towards As ions but the study produced some informative results. It was observed that the removal of As(III) ions from aqueous solution were affected by pH, adsorbent dose, initial concentration, agitation time and temperature. Both equilibrium isotherm and thermodynamic analysis indicated that the adsorption of As(III) adsorption onto Bt-Ch composites/beads occurred by physisorption. The kinetic investigations suggest otherwise (i.e., chemisorption). It was concluded that these studied adsorbents need further modification for effective removal of As(III) ions from water.

(C) Development of Fe-modified composites for effective removal of As(III) ions

A novel positively charged Fe-modified composite was developed via precipitation method by modifying bentonite clay with chitosan and Fe(III) cations as demonstrated in Chapter 8, which was employed as an adsorbent for effective removal of As(III) ions from aqueous solution. In this study, two forms of composites were made depending on the concentration of Fe(III) solution, and both were prepared in the weight ratios of 70% Bt. Clay and 30% chitosan biopolymer. The Fe-modified composites were characterised by TGA, XRD and FTIR. It was demonstrated that the two samples of the Fe-modified composites are effective for removal of As(III) ions from aqueous solution, and were influenced by pH, adsorbent dose, initial concentration, agitation time and temperature. One exciting finding was that there is no need for pre-oxidation before the removal of typically challenging As(III) from aqueous solutions as usually done in the case of conventional methods. It was noted that the amount of Fe(III) cation present in the adsorbent was shown to have significant effects on the As(III) uptake by Fe-modified composites. Both equilibrium isotherm and thermodynamic analysis indicated that the adsorption of As(III) adsorption onto Fe-modified composites occurred by physisorption. While kinetic investigations suggested that chemisorption could also contribute to As(III) adsorption. Better As(III) adsorption efficiency was observed by Fe-modified composites compared to unmodified Bt-Ch, pristine bentonite, and pure chitosan. From desorption results, the prepared Fe-modified composites exhibited good potential for re-use after many times to remove arsenic both from natural waters and wastewaters.

(D) Fixed-bed column adsorption studies of Pb(II) ions

Finally in Chapter 9 it was reported for the first time the use of wet sample of freshly prepared 70%Bt-30%Ch composite (wet-Bt-Ch) packed in a fixed bed column for effective removal of Pb(II) ions from aqueous solutions. According to the obtained breakthrough curve results, the column sorption of Pb(II) depends on both the influent concentration and bed volume (or height); however, the impact of flow rate was not investigated in this study. It was shown that adsorbent bed was exhausted faster at higher Pb(II) influent concentrations because the column become quickly saturated in the column. Even though higher Pb(II) loading was obtained for the higher Pb(II) concentration; nevertheless, quick exhaustion of the bed is not desirable, thus a compromised should be reach while choosing operating concentration in order to obtain the best column performance (i.e., best loading and breakthrough time). In terms of bed height, higher bed height was expected to result in higher Pb(II) loading, but instead, lower loading was observed. Studies has demonstrated that slow exhaustion of the adsorbent bed is more desirable, higher bed height of the column is preferable for the column operation. The good performance of wet-Bt-Ch composites in fixed-bed mode to abstract Pb(II) ions from aqueous solutions gave insight on the potential use of this material in purification of metal-contaminated water such as household filter systems. Although more work needs to be done, we are optimistic that the wet-Bt-Ch composites can easily be packed in small columns which can be placed in local containers such as household water jars, and when in contact with metal-contaminated water will allow mass transfer of the toxic metals to the adsorbent in the column.

Overall, the series of work carried out in this study has demonstrated that the prepared Bt-Ch composites/beads and Fe-modified Bt-Ch composites could be a low-cost, sustainable alternative to expensive adsorbents (e.g., activated carbon) and a feasible technology for the effective removal toxic metals from water.

10.2. Limitations of this study

In general, one of the main limitations of this study was that it focused only on prepared metal solutions (i.e., synthetic metal-contaminated water), which limits the realistic evaluation of the Bt-Ch composites/beads (and Fe-modified composites) performance

in removing these metals. Real or natural metal-contaminated wastewaters (or drinking waters) were not available to be tested with these developed composites at the time of this study.

Secondly, the performance of Bt-Ch composites/beads towards the removal Pb and Cu from aqueous solutions is highly pH dependent (i.e., lower removal efficiency was observed at pH below 4.5). This will limit the application of Bt-Ch composites/beads for purification of water contaminated with these metals at low pH, for instance, acid-mine-drainage impacted waters which are mostly found in mining areas can have pHs lower than 3. In addition, the chitosan present in the Bt-Ch composites/beads is highly likely to be soluble in an acidic medium (e.g., pH 2 to 3), and therefore a high portion of chitosan can be washed away during the adsorption process in low pH.

10.3. Recommendation and future work

1. To fully evaluate the feasibility of using Bt-Ch composites/beads and Fe-modified Bt-Ch composites, more research effort is needed towards applying these adsorbents for purification of natural waters (contaminated with toxic metals) with a wide variety of other interfering pollutants (including microbes, ions, and organic matters).

2. There is a need to assess chemical modification (e.g., cross-linking) of Bt-Ch composites/beads to further stabilise the chitosan present in the composites (or beads) and make the adsorbents independent of pH during the removal of toxic metals from low pH waters.

3. Characterisation of regenerated Bt-Ch composites/beads and Fe-modified composites with more analytical techniques (e.g., SEM, EDS and NMR) to obtain more information about adsorption mechanisms of the analysed metals (Pb, Cu and As) adsorbed onto these adsorbents.

4. Large scale column experiments to mimic industrial application use to see if the materials developed can act as a medium to effectively abstract metal ions (Pb and As) for their potential use in filter systems and faucets.

5. Production of composites (or beads) using the same procedures (as described in this thesis) with other type of bentonites (instead of Na-bentonites).

6. There is a need to study the optimisation of Fe concentration present in the modified composites and investigate how Fe interact with both chitosan and bentonite clay.

References

[1]   D.M. Saad, E.M. Cukrowska, H. Tutu, Functionalisation of cross-linked polyethylenimine for the removal of As from mining wastewater, *WATER SA*, Vol.   39 (2), Pp. 257-263, (2013).

[2]   S. Ahuja, Chemistry and Water: The Science Behind Sustaining the World's Most Crucial Resource, Elsevier, Amsterdam, (2017).

[3]   S.N. Kulshreshtha, A Global Outlook for Water Resources to the Year 2025, *Water Resources Management*, Vol. 12, Pp. 167–184, (1998)

[4]   M. Momina, M. Shahadat, S. Isamil, Regeneration performance of clay-based adsorbents for the removal of industrial dyes: a review, *RSC Adv.* Vol. 8, Pp. 24571–24587, (2018).

[5]   F. Fu, Q. Wang, Removal of heavy metal ions from wastewaters: A review, *J. Environ. Manage.*, Vol. 92, Pp. 407–418, (2011).

[6]   J.H. Duffus, "heavy metals" - A meaningless term? (IUPAC technical report), *Pure Appl. Chem.,* Vol. 74 (5), Pp. 793–807, (2002).

[7]   M. Zbair, Z. Anfar, H.A. Ahsaine, Reusable bentonite clay: modelling and optimization of hazardous lead and p-nitrophenol adsorption using a response surface methodology approach, *RSC Adv.*, Vol. 9, Pp. 5756–5769, (2019).

[8]   A.C. Dias, M.P.F. Fontes, Arsenic (V) removal from water using hydrotalcites as adsorbents: A critical review, *Appl. Clay Sci.,* Vol. 191, Pp. 105615, (2020).

[9]   P. Miretzky, A.F. Cirelli, Hg(II) removal from water by chitosan and chitosan derivatives: A review, *J. Hazard. Mater.,* Vol. 167, Pp. 10–23, (2009).

[10]   P. Jarvis, J. Fawell, Lead in drinking water – An ongoing public health concern?, *Curr. Opin. Environ. Sci. Heal.,* Vol. 20, Pp. 100239, (2021).

[11]   M. Sallau, M. Majiya, A. Nuhu, Mercury, Cadmium and Nickel Contamination Levels in Water Samples of Bagega Artisanal Gold Mining Communities: The Environmental Health Importance, *RJPBCS*, Vol. 5(6) Pp. 531-536, (2014).

[12]   World Health Organization, Guidelines for Drinking-Water Quality, 4th editio, WHO Press, Geneva, 2022.

[13]   M. Jaishankar, T. Tseten, N. Anbalagan, B.B. Mathew, K.N. Beeregowda, Toxicity, mechanism and health effects of some heavy metals., *Interdiscip. Toxicol.,* Vol. 7, Pp. 60–72, (2014).

[14]   S. Babel, T. Agustiono Kurniawan, Low-cost adsorbents for heavy metals uptake from contaminated water: a review, *J. Hazard. Mater.,* Vol. B97, Pp. 219-243, (2003).

[15]   G. Crini, Recent developments in polysaccharide-based materials used as adsorbents in wastewater treatment, *Prog. Polym. Sci.,* Vol. 30, Pp. 38–70, (2005).

[16]   R. Das, C.D. Vecitis, A. Schulze, B. Cao, A.F. Ismail, X. Lu, J. Chen, S.Ramakrishna, Recent advances in nanomaterials for water protection and monitoring, *Chem. Soc. Rev.,* Vol. 46, Pp. 6946, (2017).

[17]   I. Ali, New Generation Adsorbents for Water Treatment, *Chem. Rev.,* Vol. 112, Pp. 5073–5091, (2012)

[18]   R. Deng, D. Huang, G. Zeng, J. Wan, W. Xue, X. Wen, X. Liu, S. Chen, J. Li, C. Liu, Q. Zhang, Decontamination of lead and tetracycline from aqueous solution by a promising carbonaceous nanocomposite: Interaction and mechanisms insight, *Bioresour. Technol.,* Vol. 283, (2019) Pp. 277–285, (2019).

[19]   H. Yang, M. Lu, D. Chen, R. Chen, L. Li, W. Han, Efficient and rapid removal of Pb^{2+} from water by magnetic $Fe_3O_4@MnO_2$ core-shell nanoflower attached to carbon microtube: Adsorption behavior and process study, *J. Colloid Interface Sci.,* Vol. 563, Pp. 218–228, (2020).

[20]   L. Chen, P. Wu, M. Chen, X. Lai, Z. Ahmed, N. Zhu, Z. Dang, Y. Bi, T. Liu, Preparation and characterization of the eco-friendly chitosan/vermiculite biocomposite with excellent removal capacity for cadmium and lead, *Appl. Clay Sci.* Vol., 159, Pp. 74–82, (2018).

[21]   S.E. Bailey, T.J. Olin, R.M. Bricka, D.D. Adrian, A review of potentially low-cost sorbents for heavy metals, *Water Res.,* Vol. 33, Pp. 2469–2479 (1999).

[22]   Q.U. Jiuhui, Research progress of novel adsorption processes in water purification: a review., *J. Environ. Sci. (China).,* Vol., 20, Pp. 1–13 (2008).

[23]   A. Demirbas, Heavy metal adsorption onto agro-based waste materials: A review, *J. Hazard. Mater.,* Vol. 157, Pp. 220–229 (2008).

[24]   M. Pirilä, Adsorption and Photocatalysis in Water Treatment- Active, abundant and inexpensive materials and methods, PhD thesis, Graduate School, Faculty of Technology, University of Oulu, Finland, Pp. 1-143, (2015).

[25]   UNICEF Current Issues, Arsenic contamination in groundwater, No. 2, (2013).

[26]   A. Basu, D. Saha, R. Saha, T. Ghosh, B. Saha, A review on sources, toxicity and remediation technologies for removing arsenic from drinking water, *Res. Chem. Intermed.,* Vol. 40, Pp. 447–485, (2015).

[27]   M.M. Hassan, A.A. Nuhu, M.S. Sallau, H.M. Majiya, A.K. Mohammed, Zamfara lead poisoning saga: Comparison of lead contamination level of water samples and lead poisoning in Bagega Artisanal gold mining district, Nigeria, *J. Chem. Pharm. Res.,* Vol. 7, Pp. 7–12, (2015).

[28]   A.A. Nuhu, M.M. Hassan, Heavy Metal Pollution: The Environmental Impact of Artisanal Gold Mining on Bagega Village of Zamfara State, Nigeria, *RJPBCS,* Vol. 5(6) Pp. 306-313, (2014).

[29]   The Presidency, Federal republic of Nigeria; Everything You Need To Know About The Presidential Artisanal Gold Mining Development Initiative (PAGMI), The State House, Press Release, Abuja, (2020).

[30]   R. Olurounbi, Nigeria dangerously exposed to oil crash, Petroleum Economist, (2020).

[31]   D.M. Saad, E.M. Cukrowska, H. Tutu, Selective removal of mercury from aqueous solutions using thiolated cross-linked polyethylenimine, *Appl. Water Sci.,* Vol. 3, Pp. 527–534, (2013).

[32]   E. Guibal, A. Larkin, T. Vincent, J.M. Tobin, Chitosan sorbents for platinum sorption from dilute solutions, *Ind. Eng. Chem. Res.,* Vol. 38, Pp. 4011–4022 (1999).

[33]   R.O. Afolabi, O.D. Orodu, V.E. Efeovbokhan, Properties and application of Nigerian bentonite clay deposits for drilling mud formulation: Recent advances and future prospects, *Appl. Clay Sci.,* Vol. 143, Pp. 39–49, (2017).

[34]   K.C. Igwilo, N. Uwaezuoke, N. Okoli, F.T. Obasi, E.E. Okoro, Beneficiation of Nigerian bentonite using local materials, *J. Pet. Explor. Prod. Technol.,* Vol. 10, Pp. 3399–3407, (2020).

[35]   R.P. Schwarzenbach, T. Egli, T.B. Hofstetter, U. Von Gunten, B. Wehrli, Global water pollution and human health, *Annu. Rev. Environ. Resour.,* Vol. 35, Pp. 109–136 (2010).

[36]   J. Landdaburu-Aguirre, Micellar-enhanced ultrafiltration for the removal of heavy metals from phosphorous-rich wastewaters : From end-of-pipe to clean technology, PhD thesis, Graduate School, Faculty of Technology, University of Oulu, Finland, Pp. 1-112, (2012)

[37]   European Commission, Directive 2006/11/EC of the European Parliament and of the Council of 15 February 2006 on pollution caused by certain dangerous substances discharged into the aquatic environment of the Community., *Off. J. Eur. Union.,* Vol. L64, Pp. 52–59 (2006).

[38]   European Commission, Directive 2008/105/EC of the European Parliament and of the Council of 16 December 2008 on environmental quality standards in the field of water policy, *Off. J. Eur. Union.*, Pp. L348/84-L348/97 (2008).

[39]   European Commission, Directive 2010/75/EU of the European Parliament and of the Council of 24 November 2010 on industrial emissions (integrated pollution prevention and control), *Off. J. Eur. Union.*, Vol. L334 (2010) Pp. 17–119 (2010).

[40]   Helcom recommendation 23/11 (2002) Requirements for discharging of waste from the chemical industry., (2002).

[41]   T. Brinkmann, G. Giner Santonja, H. Yükseler, S. Roudier, L. Delgado Sancho, Best Available Techniques (BAT) Reference Document for Common Waste Water and Waste Gas Treatment/Management Systems in the Chemical Sector (BREF 2016) - Industrial Emissions Directive 2010/75/EU (Integrated Pollution Prevention and Control), EUR 28112, European Union, Luxembourg, (2016).

[42]   A. Baysal, N. Ozbek, S. Akman, Determination of Trace Metals in Waste Water and Their Removal Processes, in: Waste Water - Treat. Technol. Recent Anal. Dev., IntechOpen, (2013).

[43]   World Health Organization, The International Network to Promote Household Water Treatment and Safe Storage, (2007).

[44]   B. Ehdaie, C. Krause, J.A. Smith, Porous ceramic tablet embedded with silver nanopatches for low-cost point-of-use water purification, *Environ. Sci. Technol.*, Vol. 48 (2014) Pp. 13901–13908, (2014).

[45]   M.M. Ahammed, V. Meera, Metal oxide/hydroxide-coated dual-media filter for simultaneous removal of bacteria and heavy metals from natural waters, J. Hazard. Mater., Vol. 181, Pp.788–793, (2010).

[46]   T.K. Sen, C. Khoo, Adsorption Characteristics of Zinc (Zn 2+) from Aqueous Solution by Natural Bentonite and Kaolin Clay Minerals: A Comparative Study, Comput. Water, Energy, Environ. Eng., Vol.2, Pp. 1–6, (2013).

[47]   V. Masindi, W.M. Gitari, Simultaneous removal of metal species from acidic aqueous solutions using cryptocrystalline magnesite/bentonite clay composite: an experimental and modelling approach, *J. Clean. Prod.,* Vol. 112, Pp. 1077–1085 (2016).

[48]   E. Worch, Adsorption Technology in Water Treatment: Fundamentals, Processes, and Modeling, De Gruyter, Inc., 01062 Dresden Germany, (2012).

[49]   K. Gopal Bhattacharyya, S. Sen Gupta, Adsorption of a few heavy metals on natural and modified kaolinite and montmorillonite: A review, *Advances in Colloid and Interface Sci.,* Vol. 140, Pp. 114–131, (2008).

[50]   F. Clegg, Thermo-Analytical and Spectroscopic Characterisation of Pore Lining Minerals in Reservoir Rocks, Doctoral thesis, Sheffield Hallam University, England, (1998).

[51]   C.R.T. J.M. Thomas, Modern Synthetic Methods, in: I. Scheffold (Ed.), Springer-Verlag, Berlin Heidelberg, Pp. 249 (1989).

[52]   V. Vimonses, Development of Multifunctional Nanomaterials and Adsorption - Photocatalysis Hybrid System for Wastewater Reclamation, PhD Thesis, Sch. Chem. Eng. Univ. Adelaide, Ausralia, (2011).

[53]   S.R. Chitnis, M.M. Sharma, Industrial applications of acid-treated clays as catalysts, *React. Funct. Polym.*, Vol.32, Pp. 93–115, (1997).

[54]   M.K. Uddin, A review on the adsorption of heavy metals by clay minerals, with special focus on the past decade, *Chem. Eng. J.,* Vol. 308, Pp. 438–462, (2017).

[55]   J. Konta, Clay and man: clay raw materials in the service of man, *Appl. Clay Sci.*, Vol. 10, Pp. 275–335, (1995).

[56]   H.H. Murray, Traditional and new applications for kaolin, smectite, and palygorskite: A general overview, *Appl. Clay Sci.,* Vol. 17, Pp. 207–221, (2000).

[57]   M. Kotal, A.K. Bhowmick, Polymer nanocomposites from modified clays: Recent advances and challenges, *Prog. Polym. Sci.*, Vol. 51, Pp. 127–187, (2015).

[58]   R. Srinivasan, Advances in application of natural clay and its composites in removal of biological, organic, and inorganic contaminants from drinking water, *Adv. Mater. Sci. Eng.,* Vol. 2011, Pp. 1-17, (2011).

[59]   M. ROZÏC, S CERJAN-STEFANOVIC, S. KURAJICA, V. VANCÏ INA and E. HODZÏ IC, Ammoniacal nitrogen removal from water by treatment with clays and zeolites, *Wat. Res.,* Vol 34, Pp. 3675–3681, (2000).

[60]   F. Ayari, E. Srasra, M. Trabelsi-Ayadi, Characterization of bentonitic clays and their use as adsorbent, *Desalination*, Vol. 185 (2005) Pp. 391–397, (2005).

[61]   G. Jozefaciuk, D. Matyka-Sarzynska, Effect of acid treatment and alkali treatment on nanopore properties of selected minerals, *Clays and Clay Miner.*, Vol. 54, Pp. 220–229, (2006).

[62]   B. Sarkar, Y. Xi, M. Megharaj, G.S.R. Krishnamurti, D. Rajarathnam, R. Naidu, Remediation of hexavalent chromium through adsorption by bentonite based Arquad® 2HT-75 organoclays, *J. Hazard. Mater.*, Vol. 183, Pp. 87–97, (2010).

[63]   T.S. Anirudhan, S. Rijith, A.R. Tharun, Adsorptive removal of thorium(IV) from aqueous solutions using poly(methacrylic acid)-grafted chitosan/bentonite composite matrix: Process design and equilibrium studies, *Colloids Surfaces A Physicochem. Eng. Asp.,* Vol. 368, Pp. 13–22, (2010).

[64]   B. Alexandre, D. Langevin, P. Médéric, T. Aubry, H. Couderc, Q.T. Nguyen, A. Saiter, S. Marais, Water barrier properties of polyamide 12/montmorillonite nanocomposite membranes: Structure and volume fraction effects, *J. Memb. Sci.,* Vol. 328, Pp. 186–204, (2009).

[65]   B. Hu, H. Luo, Adsorption of hexavalent chromium onto montmorillonite modified with hydroxyaluminum and cetyltrimethylammonium bromide, *Appl. Surf. Sci*., Vol. 257, Pp. 769–775, (2010).

[66]   S. Yang, D. Zhao, H. Zhang, S. Lu, L. Chen, X. Yu, Impact of environmental conditions on the sorption behavior of Pb(II) in Na-bentonite suspensions, *J. Hazard. Mater.,* Vol. 183, Pp. 632–640, (2010).

[67]   Ö. Yavuz, Y. Altunkaynak, F. Güzel, Removal of copper, nickel, cobalt and manganese from aqueous solution by kaolinite, *Water Res.,* Vol. 37, Pp. 948–952, (2003).

[68]   K.G. Akpomie, F.A. Dawodu, K.O. Adebowale, Mechanism on the sorption of heavy metals from binary-solution by a low cost montmorillonite and its desorption potential, *Alexandria Engineering Journal*, Vol. 54, Pp. 757- 767, (2015).

[69]   T. Phothitontimongkol, N. Siebers, N. Sukpirom, F. Unob, Preparation and characterization of novel organo-clay minerals for Hg(II) ions adsorption from aqueous solution, *Appl. Clay Sci.,* Vol. 43, Pp. 343–349, (2008).

[70]   O. Abollino, M. Aceto, M. Malandrino, C. Sarzanini, E. Mentasti, Adsorption of heavy metals on Na-montmorillonite. Effect of pH and organic substances, *Water Res.,* Vol. 37, Pp. 1619–1627, (2003).

[71]   S. Aytas, M. Yurtlu, R. Donat, Adsorption characteristic of U(VI) ion onto thermally activated bentonite, *J. Hazard. Mater.,* Vol. 172, (2009) Pp. 667–674 (2009).

[72] O. Zlem Etci, N. Bektas, B. Bektas¸ M. Salim, Single and binary adsorption of lead and cadmium ions from aqueous solution using the clay mineral beidellite, *Env. Earth Sci.,* Vol. 61, Pp. 231–240, (2010).

[73] E.I. Unuabonah, A. Taubert, Clay-polymer nanocomposites (CPNs): Adsorbents of the future for water treatment, *Appl. Clay Sci.,* Vol. 99, Pp. 83–92, (2014).

[74] R.S. Hebbar, A.M. Isloor, A.F. Ismail, Preparation and evaluation of heavy metal rejection properties of polyetherimide/porous activated bentonite clay nanocomposite membrane, *RSC Adv.* Vol. 4, Pp. 47240–47248, (2014).

[75] C. Breen, The characterisation and use of polycation-exchanged bentonites, *Appl. Clay Sci.,* Vol. 15, Pp. 187–219, (1999).

[76] S.F. Wang, L. Shen, Y.J. Tong, L. Chen, I.Y. Phang, P.Q. Lim, T.X. Liu, Biopolymer chitosan/montmorillonite nanocomposites: Preparation and characterization, *Polymer Degradation and Stability*, Vol. 90, Pp. 123-131, (2005).

[77] C.K.S. Pillai, W. Paul, C.P. Sharma, Chitin and chitosan polymers: Chemistry, solubility and fiber formation, *Prog. Polym. Sci.,* Vol. 34, Pp. 641–678 (2009).

[78] M. Rinaudo, Chitin and chitosan: Properties and applications, *Prog. Polym. Sci.*, Vol. 31, Pp. 603–632, (2006).

[79]   K. Kurita, Chitin and Chitosan: Functional Biopolymers from Marine

Crustaceans, Mini-Review, *Marine Biotechnology*, Vol. 8, Pp. 203- 226, (2006).

[80] E. Guibal, Interactions of metal ions with chitosan-based sorbents: a review, *Sep. Purif. Technol.,* Vol. 38, Pp. 43–74, (2004).

[81]   M. Darder, M. Colilla, E. Ruiz-Hitzky, Biopolymer-Clay Nanocomposites Based on Chitosan Intercalated in Montmorillonite, *Chem. Mater*., Vol. 15, Pp. 3774-3780, (2003).

[82] H. Majiya, K.F. Chowdhury, N.J. Stonehouse, P. Millner, TMPyP functionalised chitosan membrane for efficient sunlight driven water disinfection, *J. Water Process Eng*., Pp. 1-8, (2017).

[83]   M. Darder, M. Colilla, E. Ruiz-Hitzky, Chitosan-clay nanocomposites: application as electrochemical sensors, *Appl. Clay Sci.,* Vol. 28, Pp. 199–208, (2005).

[84] A. and P.M. Giannakas, Chitosan/Bentonite Nanocomposites for Wastewater Treatment : A Review, *J. Nanochemistry Nanotechnol.,* Vol. 1, Pp. 1–17, (2018).

[85]   E. Ruiz-Hitzky, M. Darder, P. Aranda, Functional biopolymer nanocomposites based on layered solids, *J. Mater. Chem*., Vol. 15, Pp. 3650–3662, (2005).

[86]   A. Alemdar, O.I. Ece, O. Atici, The rheological properties and characterization of bentonite dispersions in the presence of non-ionic polymer PEG, *J. Mater. Sci.,* Vol. 40, Pp. 171– 177, (2005).

[87]   P. Lertsutthiwong, K. Noomun, S. Khunthon, S. Limpanart, Influence of chitosan characteristics on the properties of biopolymeric chitosan-montmorillonite, *Prog. Nat. Sci. Mater. Int*. Vol. 22, Pp. 502–508, (2012).

[88]   C. W. Chiu, T. K. Huang, Y. C. Wang, B.G. Alamani, J. J. Lin, Intercalation strategies in clay/polymer hybrids, *Prog. Polym. Sci*. Vol. 39, Pp. 443–485, (2014).

[89]   C. Morales Futalan, C. C. Kan, M. Lourdes Dalida, K. J. Hsien, C. Pascua, M. W. Wan, Comparative and competitive adsorption of copper, lead, and nickel using chitosan immobilized on bentonite, *Carbohydr. Polym.,* Vol. 83, Pp. 528–536, (2010).

[90]   M.P. Lourdes Dalida, A. V Francia Mariano, C.M. Futalan, C.-C. Kan, W.-C. Tsai, M.-W. Wan, Adsorptive removal of Cu(II) from aqueous solutions using non-crosslinked and crosslinked chitosan-coated bentonite beads, *DES.*, Vol. 275, Pp. 154–159 (2011).

[91]   C. Hu, P. Zhu, M. Cai, H. Hu, Q. Fu, Comparative adsorption of Pb(II), Cu(II) and Cd(II) on chitosan saturated montmorillonite: Kinetic, thermodynamic and equilibrium studies, *Appl. Clay Sci.,* Vol. 143, Pp. 320–326 (2017).

[92]   V.N. Tirtom, A. ße Dinçer, S. Becerik, T. Aydemir, A. Çelik, Comparative adsorption of Ni(II) and Cd(II) ions on epichlorohydrin crosslinked chitosan-clay composite beads in aqueous solution, *Chem. Eng. J.*, Vol. 197, Pp. 379–386, (2012).

[93]   H. Wang, H. Tang, Z.Z. Liu, X. Zhang, Z. Hao, Z.Z. Liu, Removal of cobalt(II) ion from aqueous solution by chitosan-montmorillonite, *J. Environ. Sci. (China).*, Vol. 26, Pp. 1879–1884, (2014).

[94]   N. Bleiman, Y.G. Mishael, Selenium removal from drinking water by adsorption to chitosan-clay composites and oxides: Batch and columns tests, *J. Hazard. Mater.*, Vol. 183, Pp. 590–595, (2010).

[95]   H. Moussout, H. Ahlafi, M. Aazza, C. El Akili, Performances of local chitosan and its nanocomposite 5%Bentonite/Chitosan in the removal of chromium ions (Cr(VI)) from wastewater, *Int. J. Biol. Macromol.,* Vol. 108, Pp. 1063–1073, (2018).

[96]   P. Gogoi, A.J. Thakur, R. Devi, B. Das, T.K. Maji, A comparative study on sorption of arsenate ions from water by crosslinked chitosan and crosslinked chitosan/MMT nanocomposite, *Biochem. Pharmacol.*, Vol. 4, Pp. 4248–4257 (2016).

[97]   S. Pandey, S.B. Mishra, Organic-inorganic hybrid of chitosan/organoclay bionanocomposites for hexavalent chromium uptake, *J. Colloid Interface Sci.,* Vol. 361, Pp. 509–520, (2011).

[98]   M.C. Jane Calagui, D.B. Senoro, C.-C. Kan, J.W. Salvacion, C. Morales Futalan, M.-W. Wan, Adsorption of indium(III) ions from aqueous solution using chitosan-coated bentonite beads, *J. Hazard. Mater.*, Vol. 277, Pp. 120–126 (2014).

[99]   R. Rusmin, B. Sarkar, Y. Liu, S. Mcclure, R. Naidu, Structural evolution of chitosan-palygorskite composites and removal of aqueous lead by composite beads, *Appl. Surf. Sci.*, Vol. 353, Pp. 363–375, (2015).

[100] T. A. Saleh, A. Sarı, M. Tuzen, Chitosan-modified vermiculite for As(III) adsorption from aqueous solution: Equilibrium, thermodynamic and kinetic studies, *J. Mol. Liq.*, Vol. 219, Pp. 937–945, (2016).

[101] C.W. Scheele, Chemische Abhandlung von der Luft und dem Feuer, 1773, See: Ostwald's Klassiker Der Exakten Wiss., Pp. 1-58, (1894).

[102] F. Fontana, *Mem. Mat., Fis. Soc. Ital.,* Vol.1, Pp. 679, (1777).

[103] A. Dabroswski, Adsorption from theory to practice, *Adv. Colloid Interface Sci.,* Vol. 93, Pp. 135–224 (2001).

[104] T. Lowitz, Crell's Chem., Ann., Vol. 1, Pp. 211, (1786).

[105] T. Lowitz, Crell's Chem., Ann., Vol. 2, (1788) Pp. 36, (1788).

[106] T. de Saussure, Gilbert's Ann., *Phys.,* Vol. 47, Pp. 113, (1814).

[107] T. de Saussure, Ann., *Phil.,* Vol. 6, Pp. 241, (1915).

[108] P. Chappuis, Wied. Ann., Vol. 8, Pp. 1 (1879).

[109] P. Chappuis, Wied. Ann., Vol. 12, Pp. 161, (1881).

[110] P. Chappuis, Wied. Ann., Vol. 19, Pp. 21, (1883).

[111] L. Joulian, Ann. Chim., *Phys.,* Vol. 22, Pp. 398, (1881).

[112] H. Kayser, Wied. Ann., *Phys.* Vol. 12, Pp.526, (1881).

[113] H. Kayser, Wied. Ann., *Phys.,* Vol. 14, Pp. 450, (1881).

[114] M.S. Tswett, Chromatographic Adsorption Analysis: Selected Works, Elis Horwood Ltd, (1990).

[115] H.K.Ö. and S.A. George William Kajjumba, Serkan Emik, Atakan Öngen, Modelling of Adsorption Kinetic Processes—Errors, Theory and Application, in: Adv. Sorption Process Appl., IntechOpen: pp. 1–19, (2018).

[116] H.N. Tran, S.J. You, A. Hosseini-Bandegharaei, H.P. Chao, Mistakes and inconsistencies regarding adsorption of contaminants from aqueous solutions: A critical review, *Water Res.* Vol. 120, Pp. 88–116, (2017).

[117] S. Azizian, Kinetic models of sorption: a theoretical analysis, *J. Colloid Interface Sci*. Vol. 276, Pp. 47–52, (2004).

[118] S. Azizian, A novel and simple method for finding the heterogeneity of adsorbents on the basis of adsorption kinetic data, *J. Colloid Interface Sci*., Vol. 302, Pp. 76–81, (2006).

[119] H.N. Tran, S.J. You, H.P. Chao, Effect of pyrolysis temperatures and times on the adsorption of cadmium onto orange peel derived biochar, *Waste Manag. Res*., Vol. 34, Pp. 129–138, (2016).

[120] H. Guo, S. Zhang, Z. Kou, S. Zhai, W. Ma, Y. Yang, Removal of cadmium(II) from aqueous solutions by chemically modified maize straw, *Carbohydr. Polym.,* Vol. 115, 177–185, (2015).

[121] S. Canzano, P. Iovino, S. Salvestrini, S. Capasso, Comment on "Removal of anionic dye Congo red from aqueous solution by raw pine and acid-treated pine cone powder as adsorbent: Equilibrium, thermodynamic, kinetics, mechanism and process design," *Water Res.*, Vol. 46, Pp. 4314–4315, (2012).

[122] S. Lagergren, About the theory of so-called adsorption of soluble substances, K. Sven. Vetensk. Handl., Vol. 24, Pp. 1–39, (1898).

[123] W. Plazinski, W. Rudzinski, A. Plazinska, Theoretical models of sorption kinetics including a surface reaction mechanism: A review, *Adv. Colloid Interface Sci.*, Vol. 152, Pp. 2–13, (2009).

[124] Y.S. Ho, G. McKay, Pseudo-second order model for sorption processes, *Proc. Biochem.,* Vol. 34, Pp. 451–465, (1999).

[125] J. P. Simonin, On the comparison of pseudo-first order and pseudo-second order rate laws in the modeling of adsorption kinetics, *Chem. Eng. J.*, Vol. 300, Pp. 254–263, (2016).

[126] Y.S. Ho, G. McKay, A Comparison of chemisorption kinetic models applied to pollutant removal on various sorbents, *Process Saf. Environ. Prot.*, Vol. 76, Pp. 332–340, (1998).

[127] G. McKay, Y.S. Ho, J.C.Y. Ng, Biosorption of copper from waste waters: A review, *Sep. Purif. Methods.*, Vol. 28, Pp. 87–125, (1999).

[128] J. Febrianto, A.N. Kosasih, J. Sunarso, Y.H. Ju, N. Indraswati, S. Ismadji, Equilibrium and kinetic studies in adsorption of heavy metals using biosorbent: A summary of recent studies, *J. Hazard. Mater.*, Vol. 162, Pp. 616–645, (2009).

[129] G. Blanchard, G. Maunaye, M. Martin, Removal of heavy metals from waters by means of natural zeolites, *Water Res.,* Vol. 18, Pp. 1501–1507, (1984).

[130] T.A. Khan, S.A. Chaudhry, I. Ali, Equilibrium uptake , isotherm and kinetic studies of Cd (II) adsorption onto iron oxide activated red mud from aqueous solution, *J. Mol. Liq.,* Vol. 202, Pp. 165–175, (2015).

[131] Y.S. Ho, D.A.J. Wase, C.F. Forster, Kinetic studies of competitive heavy metal adsorption by sphagnum moss peat, *Environ. Technol. (United Kingdom)*, Vol. 17, Pp. 71–77 (1996).

[132] Z.Y.B. Roginsky S., The catalytic oxidation of carbon monoxide on manganese dioxide, *Acta Phys. Chem. (USSR),* Vol. 1, Pp. 554, (1934).

[133] M.K. Hans-Jürgen Butt, Karlheinz Graf, The Physics and Chemistry of Interfaces, WILEY-VCH GmbH & Co. KGaA, (2013).

[134] S.K. Milonjić, Comments on "factors influencing the removal of divalent cations by hydroxyapatite," *J. Hazard. Mater.*, Vol. 162, Pp. 1588–1589, (2009).

[135] S.K. Milonjić, Comments on the authors' response to the comments on "Factors influencing the removal of divalent cations by hydroxyapatite", by Smiciklas et al., *J. Hazard. Mater.*, Vol. 176, Pp. 1126–1127, (2010).

[136] K.V. Kumar, K. Porkodi, Relation between some two- and three-parameter isotherm models for the sorption of methylene blue onto lemon peel, *J. Hazard. Mater.*, Vol. 138, Pp. 633–635, (2006).

[137] O. Hamdaoui, E. Naffrechoux, Modeling of adsorption isotherms of phenol and chlorophenols onto granular activated carbon. Part I. Two-parameter models and equations allowing determination of thermodynamic parameters, *J. Hazard. Mater.,* Vol. 147, 381–394, (2007).

[138] K.Y. Foo, B.H. Hameed, Insights into the modeling of adsorption isotherm systems, *Chem. Eng. J.,* Vol. 156, Pp. 2–10, (2010).

[139] I. Langmuir, The constitution and fundamental properties of solids and liquids, *J. Am. Chem. Soc.,* Vol. 38, Pp. 2221–2295, (1916).

[140] K. Vijayaraghavan, T.V.N. Padmesh, K. Palanivelu, M. Velan, Biosorption of nickel(II) ions onto Sargassum wightii: Application of two-parameter and three-parameter isotherm models, *J. Hazard. Mater.*, Vol. 133, Pp. 304–308, (2006).

[141] E. Demirbas, M. Kobya, A.E.S. Konukman, Error analysis of equilibrium studies for the almond shell activated carbon adsorption of Cr(VI) from aqueous solutions, *J. Hazard. Mater.*, Vol. 154, Pp. 787–794, (2008).

[142] S.J. Allen, G. Mckay, J.F. Porter, Adsorption isotherm models for basic dye adsorption by peat in single and binary component systems, *J. Colloid Interface Sci.,* Vol. 280, Pp. 322–333 (2004).

[143] K.R. Hall, L.C. Eagleton, A. Acrivos, T. Vermeulen, Pore- and solid-diffusion kinetics in fixed-bed adsorption under constant-pattern conditions, *Ind. Eng. Chem. Fundam.*, Vol. 5, Pp. 212–223, (1966).

[144] T.W. Webi, Ranjit K. Chakravort, Pore and Solid Diffusion Models for Fixed-Bed Adsorbers, *AIChE J.,* Vol. 20, Pp. 228–238, (1974).

[145] H. Freundlich, Über die Adsorption in Lösungen, *Z Phys. Chem*. Vol. 57, Pp. 385–471, (1906).

[146] L.V. Dubinin, M.M. and Radushkevich, The Equation of the Characteristic Curve of Activated Charcoal, in: Proc. Acad. Sci. Phys. Chem. Sect. 55: pp. 331–337, (1947).

[147] A. Günay, E. Arslankaya, I. Tosun, Lead removal from aqueous solution by natural and pretreated clinoptilolite: Adsorption equilibrium and kinetics, *J. Hazard. Mater.*, Vol. 146, Pp. 362–371, (2007).

[148] M.M. Dubinin, The potential theory of adsorption of gases and vapors for adsorbents with energetically nonuniform surfaces, *Chem. Rev.*, Vol. 60, Pp. 235–266, (1960).

[149] C.R. Girish, Various isotherm models for multicomponent adsorption: A review, *Int. J. Civ. Eng. Technol.*, Vol. 8, Pp. 80–86, (2017).

[150] B. Noroozi, G.A. Sorial, Applicable models for multi-component adsorption of dyes: A review, *J. Environ. Sci. (China).*, Vol. 25, Pp. 419–429, (2013).

[151] V.C. Srivastava, I.D. Mall, I.M. Mishra, Competitive adsorption of cadmium(II) and nickel(II) metal ions from aqueous solution onto rice husk ash, *Chem. Eng. Process. Process Intensif.*, Vol. 48, Pp. 370–379, (2009).

[152] C. Leodopoulos, D. Doulia, K. Gimouhopoulos, T.M. Triantis, Single and simultaneous adsorption of methyl orange and humic acid onto bentonite, *Appl. Clay Sci.*, Vol. 70, Pp. 84–90, (2012).

[153] V.K. Rathore, D.K. Dohare, P. Mondal, Competitive adsorption between arsenic and fluoride from binary mixture on chemically treated laterite, *J. Environ. Chem. Eng.*, Vol. 4, 2417–2430, (2016).

[154] A. Gupta, C. Balomajumder, Simultaneous adsorption of Cr(VI) and phenol from binary mixture using iron incorporated rice husk: Insight to multicomponent equilibrium isotherm, *Int. J. Chem. Eng.* Vol. 2016, Pp. 1-11, (2016).

[155] X. Luo, Z. Zhang, P. Zhou, Y. Liu, G. Ma, Z. Lei, Synergic adsorption of acid blue 80 and heavy metal ions (Cu^{2+}/Ni^{2+}) onto activated carbon and its mechanisms, *J. Ind. Eng. Chem.*, Vol. 27, Pp. 164–174, (2015).

[156] H. Patel, Fixed-bed column adsorption study: a comprehensive review, *Appl. Water Sci.*, Vol. 9, Pp. 1–17, (2019). doi:10.1007/s13201-019-0927-7.

[157] V.C. Taty-Costodes, H. Fauduet, C. Porte, Y.S. Ho, Removal of lead (II) ions from synthetic and real effluents using immobilized Pinus sylvestris sawdust: Adsorption on a fixed-bed column, *J. Hazard. Mater.,* Vol. 123, Pp. 135–144, (2005).

[158] K.H. Chu, Improved fixed bed models for metal biosorption, *Chem. Eng. J.*, Vol. 97, 233–239, (2004).

[159] Z. Xu, J.G. Cai, B.C. Pan, Mathematically modeling fixed-bed adsorption in aqueous systems, *J. Zhejiang Univ. Sci. A.*, Vol. 14, Pp. 155–176, (2013).

[160] H.C. Thomas, Heterogeneous ion exchange in a flowing system, *J. Am. Chem. Soc.* Vol. 66, Pp. 1664–1466, (1944).

[161] G.B. and E.Q. Adams, Some aspects of the behaviour of charcoal with respect to chlorine, *J. Am. Chem. Soc.*, Vol. 42, 523–544, (1920).

[162] J.H. Yoon, Y.H. and Nelson, Application of Gas Adsorption Kinetics 1. A Theoretical Model for Respirator Cartridge Service Time, *Am. Ind. Hyg. Assoc. J.,* Vol. 45, Pp. 509–516, (1984).

[163] M. Hanbali, H. Holail, H. Hammud, Remediation of lead by pretreated red algae: adsorption isotherm, kinetic, column modeling and simulation studies, *Green Chem. Lett. Rev.* Vol. 7, Pp. 342–358, (2014).

[164] A. Chatterjee, S. Schiewer, Biosorption of Cadmium(II) Ions by Citrus Peels in a Packed Bed Column: Effect of Process Parameters and Comparison of Different Breakthrough Curve Models, *Clean - Soil, Air, Water.*, Vol. 39, Pp. 874–881, (2011).

[165] J. Cruz-Olivares, C. Pérez-Alonso, C. Barrera-Díaz, F. Ureña-Nuñez, M.C. Chaparro-Mercado, B. Bilyeu, Modeling of lead (II) biosorption by residue of allspice in a fixed-bed column, *Chem. Eng. J.*, Vol. 228, Pp. 21–27, (2013).

[166] M.T. Runping Han, Yu Wang, Xin Zhao, Yuanfeng Wang, Fuling Xie, Junmei Cheng, Adsorption of methylene blue by phoenix tree leaf powder in a fixed-bed column: experiments and prediction of breakthrough curves, *Desalination*, Vol. 238, Pp. 333–346 (2009).

[167] S. Kundu, A.K. Gupta, Arsenic adsorption onto iron oxide-coated cement (IOCC): Regression analysis of equilibrium data with several isotherm models and their optimization, *Chem. Eng. J.*, Vol. 122, Pp. 93–106, (2006).

[168] F.J. Rivas, F.J. Beltrán, O. Gimeno, J. Frades, F. Carvalho, Adsorption of landfill leachates onto activated carbon. Equilibrium and kinetics, *J. Hazard. Mater.,* Vol. 131, Pp. 170–178 (2006).

[169] S. Ayoob, A.K. Gupta, Insights into isotherm making in the sorptive removal of fluoride from drinking water, *J. Hazard. Mater*., Vol. 152 (2008) Pp. 976–985, (2008).

[170] F.M. Lima, E.C., Adebayo, M.A., Machado, Kinetic and Equilibrium Models of Adsorption, in: Carbon Nanomaterials as Adsorbents, Environ. Biol. Appl., Springer: Pp. 33–69, (2015).

[171] R. Krishna Prasad, S.N. Srivastava, Sorption of distillery spent wash onto fly ash: Kinetics and mass transfer studies, *Chem. Eng. J.*, Vol. 146, Pp. 90–97, (2009).

[172] Y.S. Ho, Selection of optimum sorption isotherm, *Carbon N. Y.*, Vol. 42, Pp. 2115–2116, (2004).

[173] Y.S. Ho, W.T. Chiu, C.C. Wang, Regression analysis for the sorption isotherms of basic dyes on sugarcane dust, *Bioresour. Technol*., Vol. 96 (2005) Pp. 1285–1291, (2005).

[174] C.H. Bolster, G.M. Hornberger, On the Use of Linearized Langmuir Equations, *Soil Sci. Soc. Am. J.,* Vol. 71, Pp. 1796–1806 (2007).

[175] Y.A. Aydin, N.D. Aksoy, Adsorption of chromium on chitosan: Optimization, kinetics and thermodynamics, *Chem. Eng. J.*, Vol. 151, Pp. 188–194, (2009).

[176] K. Anupam, S. Dutta, C. Bhattacharjee, S. Datta, Adsorptive removal of chromium (VI) from aqueous solution over powdered activated carbon: Optimisation through response surface methodology, *Chem. Eng. J.*, Vol. 173, Pp. 135–143, (2011).

[177] E. Morgan, Chemometrics: experimental design (analytical chemistry by open learning), John Wiley & Sons, Chichester, (1991).

[178] D.C. Montgomery, Design and Analysis of Experiments, Ninth, John Wiley & Sons, Inc., (2013).

[179] L. Goupy Jacques, Methods for experimental design: principles and applications for physicist and chemists, Elsevier, Amsterdam, Netherlands, (1993).

[180] B. Dejaegher, Y. Vander Heyden, Experimental designs and their recent advances in set-up, data interpretation, and analytical applications, *J. Pharm. Biomed. Anal*., Vol. 56, 141–158, (2011).

[181] Laboratory Solutions from METTLER TOLEDO, Thermogravimetry Analysis (TGA) – online training course, https://youtu.be/qaUAJ1RJqMU, (2012).

[182] J.R. Dean, A.M. Jones, D. Holmes, R. Reed, J. Weyers, A. Jones, Practical Skills in Chemistry, Third, Pearson Education Limited, Harlow, England, (2017).

[183] N. D'MELLO, Spectroscopic and thermal analysis of clay mineral-organic composites, Doctoral thesis, Sheffield Hallam University, United Kindom, (2003).

[184] B.C. Smith, Fundamentals of fourier transform infrared spectroscopy, second edition, (2011).

[185] Xiandeng Hou and Bradley T. Jones, Inductively Coupled Plasma-Optical Emission Spectroscopy, *Anal. Chem.,* Vol. 46, Pp. 1110A-1120A, (1974).

[186] Charles B. Boss and Kenneth J. Fredeen, Concepts,Instrumentation and Techniques in Inductively Coupled Plasma Optical Emission Spectroscopy, Third, Perkin Elmer, (2004).

[187] M.-W. Wan, I.G. Petrisor, H.-T. Lai, D. Kim, T. Fu Yen, Copper adsorption through chitosan immobilized on sand to demonstrate the feasibility for in situ soil decontamination, *Carbohydr. Polym*., Vol. 55, Pp. 249–254, (2004).

[188] J. Liu, L. Zheng, Y. Li, M. Free, M. Yang, Adsorptive recovery of palladium(II) from aqueous solution onto cross-linked chitosan/montmorillonite membrane, *RSC Adv*., Vol. 6, Pp. 51757–51767, (2016).

[189] M.F.Z. Kadir, Z. Aspanut, S.R. Majid, A.K. Arof, FTIR studies of plasticized poly(vinyl alcohol)-chitosan blend doped with NH4NO3 polymer electrolyte membrane, *Spectrochim. Acta - Part A Mol. Biomol. Spectrosc*., Vol. 78, Pp. 1068–1074, (2011).

[190] A.R. Nesic, S.J. Velickovic, D.G. Antonovic, Characterization of chitosan/ montmorillonite membranes as adsorbents for Bezactiv Orange V-3R dye, *J. Hazard. Mater.,* Vol. 209, Pp. 256–263, (2012).

[191] D. Gusain, F. Bux, Y.C. Sharma, Abatement of chromium by adsorption on nanocrystalline zirconia using response surface methodology, *J. Mol. Liq.*, Vol. 197, Pp. 131–141, (2014).

[192] R. Ahmad, I. Hasan, Optimization of the adsorption of Pb (II) from aqueous solution onto PAB nanocomposite using response surface methodology, *Environ. Nanotechnology, Monit. Manag.* Vol. 6, Pp. 116–129, (2016).

[193] W.A. Jensen, Open problems and issues in optimal design, *Qual. Eng.,* Vol. 30, Pp. 583–593, (2018).

[194] J. Sall, A. Lehman, M. Stephens, L. Creighton, JMP Start Statistics: A Guide to Statistics and Data Analysis Using JMP, (2017).

[195] Design Expert, "Version 13.0 Stat-Ease," Design Expert Inc., Minneapolis, (2020).

[196] C.M. Myers, R.H., Montgomery, D.C., Anderson-Cook, Response Surface Methodology: Process and Product Optimization Using Designed Experiments, 4th Editio, Wiley & Sons Inc., (2016).

[197] M. Vakili, S. Deng, G. Cagnetta, W. Wang, P. Meng, D. Liu, G. Yu, Regeneration of chitosan-based adsorbents used in heavy metal adsorption: A review, *Sep. Purif. Technol.*, Vol. 224, Pp. 373–387, (2019).

[198] M. Šćiban, M. Klašnja, B. Škrbić, Modified softwood sawdust as adsorbent of heavy metal ions from water, *J. Hazard. Mater.,* Vol. 136, Pp. 266–271, (2006).

[199] W.S.W. Ngah, S. Fatinathan, Adsorption characterization of Pb(II) and Cu(II) ions onto chitosan-tripolyphosphate beads: Kinetic, equilibrium and thermodynamic studies, *J. Environ. Managem.*, Vol. 91, Pp. 958–969, (2010).

[200] W.S.W. Ngah, S. Fatinathan, Pb(II) biosorption using chitosan and chitosan derivatives beads: Equilibrium, ion exchange and mechanism studies, *J. Environ. Sci.*, Vol. 22, Pp. 338–346, (2010).

[201] Ayushi Verma, K.S. Kumar Shashi, Statistical modeling, equilibrium and kinetic studies of cadmium ions biosorption from aqueous solution using S. filipendula, *J. Environ. Chem. Eng.*, Vol. 5, Pp. 2290–2304, (2017).

[202] S. Maleki, A. Karimi-Jashni, Optimization of Ni(II) adsorption onto Cloisite Na$^+$ clay using response surface methodology, *Chemosphere.*, Vol. 246 , Pp. 125710, (2020).

[203] H. Sereshti, M. Karimi, S. Samadi, Application of response surface method for optimization of dispersive liquid-liquid microextraction of water-soluble components of Rosa damascena Mill. essential oil, *J. Chromatogr. A.*, Vol. 1216, Pp. 198–204, (2009).

[204] S. Wang, Y. Dong, M. He, L. Chen, X. Yu, Characterization of GMZ bentonite and its application in the adsorption of Pb(II) from aqueous solutions, *Appl. Clay Sci.* Vol. 43, Pp. 164–171, (2008).

[205] C. Jeon, H.P. Kwang, Adsorption and desorption characteristics of mercury(II) ions using aminated chitosan bead, *Water Res.*, Vol. 39, Pp. 3938–3944, (2005).

[206] H. Radnia, A.A. Ghoreyshi, H. Younesi, G.D. Najafpour, Adsorption of Fe(II) ions from aqueous phase by chitosan adsorbent: Equilibrium, kinetic, and thermodynamic studies, *Desalin. Water Treat.* Vol. 50, Pp. 348–359, (2012).

[207] F. Ghorbani, H. Younesi, S.M. Ghasempouri, A.A. Zinatizadeh, M. Amini, A. Daneshi, Application of response surface methodology for optimization of cadmium biosorption in an aqueous solution by Saccharomyces cerevisiae, *Chem. Eng. J.* Vol. 145, Pp. 267–275, (2008).

[208] A.M. Younis, M.A. Aly-Eldeen, E.M. Elkady, Effect of different molecular weights of chitosan on the removal efficiencies of heavy metals from contaminated water, *Egypt. J. Aquat. Biol. Fish.,* Vol. 23, Pp. 149–158, (2019).

[209] V.N. Tirtom, A. Dinçer, S. Becerik, T. Aydemir, A. Çelik, Removal of lead (II) ions from aqueous solution by using crosslinked chitosan-clay beads, *Desalin. Water Treat.,* Vol. 39, Pp. 76–82, (2012).

[210] R.A.A. Muzzarelli, Chitin, Pergamon Press, Oxford, (1977).

[211] D. Datta, H. Uslu, Adsorptive separation of lead (Pb2+) from aqueous solution using tri-n-octylamine supported montmorillonite, *J. Chem. Eng. Data.,* Vol. 62, Pp. 370–375, (2017).

[212] M. W. Wan, C. C. Kan, B.D. Rogel, M. Lourdes, P. Dalida, Adsorption of copper (II) and lead (II) ions from aqueous solution on chitosan-coated sand, *Carbohydr. Polym.*, Vol. 80, Pp. 891–899, (2010).

[213] G.L. Rorrer, T.Y. Hsien, J.D. Way, Synthesis of Porous-Magnetic Chitosan Beads for Removal of Cadmium Ions from Waste Water, *Ind. Eng. Chem. Res.*, Vol. 32, Pp. 2170–2178, (1993).

[214] M. Prasad, S. Saxena, Sorption Mechanism of Some Divalent Metal Ions onto Low-Cost Mineral Adsorbent, *Ind. Eng. Chem. Res.*, Vol. 43, Pp. 1512–1522, (2004).

[215] L. Jin, R. Bai, Mechanisms of lead adsorption on chitosan/PVA hydrogel beads, *Langmuir*. Vol. 18, Pp. 9765–9770, (2002).

[216] J.D. Cuppett, S.E. Duncan, A.M. Dietrich, Evaluation of copper speciation and water quality factors that affect aqueous copper tasting response, *Chem. Senses.*, Vol. 31, Pp. 689–697, (2006).

[217] V.C. Srivastava, I.D. Mall, I.M. Mishra, Equilibrium modelling of single and binary adsorption of cadmium and nickel onto bagasse fly ash, *Chem. Eng. J.*, Vol. 117, Pp. 79–91, (2006).

[218] L. Hao, M. Liu, N. Wang, G. Li, A critical review on arsenic removal from water using iron-based adsorbents, *RSC Adv.*, Vol. 8, Pp. 39545–39560, (2018).

[219] S.K. Milonjić, A consideration of the correct calculation of thermodynamic parameters of adsorption, *J. Serbian Chem. Soc.*, Vol. 72, Pp. 1363–1367, (2007).

[220] V.M. Boddu, K. Abburi, J.L. Talbott, E.D. Smith, R. Haasch, Removal of arsenic (III) and arsenic (V) from aqueous medium using chitosan-coated biosorbent, *Water Res.*, Vol. 42, Pp. 633–642, (2008).

[221] B.A. Manning, S.E. Fendorf, S. Goldberg, Surface structures and stability of arsenic(III) on goethite: Spectroscopic evidence for inner-sphere complexes, *Environ. Sci. Technol.*, Vol. 32, 2383–2388, (1998).

[222] H.N. Tran, S.J. You, H.P. Chao, Thermodynamic parameters of cadmium adsorption onto orange peel calculated from various methods: A comparison study, *J. Environ. Chem. Eng.*, Vol. 4, Pp 2671–2682, (2016).

[223] A. Ramesh, H. Hasegawa, T. Maki, K. Ueda, Adsorption of inorganic and organic arsenic from aqueous solutions by polymeric Al/Fe modified montmorillonite, *Sep. Purif. Technol.*, Vol. 56, Pp. 90–100, (2007).

[224] X. Luo, C. Wang, L. Wang, F. Deng, S. Luo, X. Tu, C. Au, Nanocomposites of graphene oxide-hydrated zirconium oxide for simultaneous removal of As(III) and As(V) from water, *Chem. Eng. J.*, Vol. 220, Pp. 98–106, (2013).

[225] K. Su, A. Radian, Y. Mishael, L. Yang, J.W. Stucki, Nitrate reduction by redox-activated, polydiallyldimethylammonium-exchanged ferruginous smectite, *Clays Clay Miner.*, Vol. 60, Pp. 464–472, (2012).

[226] A. Maiti, S. DasGupta, J.K. Basu, S. De, Adsorption of arsenite using natural laterite as adsorbent, *Sep. Purif. Technol.*, Vol. 55, Pp. 350–359, (2007).

[227] M. Pentrák, L. Pentráková, A. Radian, Y.G. Mishael, J.W. Stucki, Nitrate reduction by redox-modified smectites exchanged with chitosan, *Clays Clay Miner.*, Vol. 62, Pp. 403–414, (2014).

[228] J. Su, H.G. Huang, X.Y. Jin, X.Q. Lu, Z.L. Chen, Synthesis, characterization and kinetic of a surfactant-modified bentonite used to remove As(III) and As(V) from aqueous solution, *J. Hazard. Mater*. Vol. 185, Pp. 63–70, (2011).

[229] Z. Li, R. Beachner, Z. McManama, H. Hanlie, Sorption of arsenic by surfactant-modified zeolite and kaolinite, *Microporous Mesoporous Mater.,* Vol. 105, Pp. 291–297, (2007).

[230] J.A. Wilkie, J.G. Hering, Adsorption of arsenic onto hydrous ferric oxide: Effects of adsorbate/adsorbent ratios and co-occurring solutes, *Colloids Surfaces A Physicochem. Eng. Asp*. Vol. 107, Pp. 97–110, (1996).

[231] J. Giménez, M. Martínez, J. de Pablo, M. Rovira, L. Duro, Arsenic sorption onto natural hematite, magnetite, and goethite, *J. Hazard. Mater.,* Vol. 141, Pp. 575–580, (2007).

[232] O.S. Thirunavukkarasu, T. Viraraghavan, K.S. Subramanian, O. Chaalal, M.R. Islam, Arsenic removal in drinking water - Impacts and novel removal technologies, *Energy Sources.*, Vol. 27, Pp. 209–219, (2005).

[233] A. Gupta, V.S. Chauhan, N. Sankararamakrishnan, Preparation and evaluation of iron-chitosan composites for removal of As(III) and As(V) from arsenic contaminated real life groundwater, *Water Res.,* Vol. 43, Pp. 3862–3870, (2009).

[234] K.P. Raven, A. Jain, R.H. Loeppert, Arsenite and arsenate adsorption on ferrihydrite: Kinetics, equilibrium, and adsorption envelopes, *Environ. Sci. Technol.*, Vol. 32, Pp. 344–349, (1998).

[235] I.A. Katsoyiannis, A.I. Zouboulis, Removal of arsenic from contaminated water sources by sorption onto iron-oxide-coated polymeric materials, *Water Res.,* Vol. 36, Pp. 5141–5155, (2002).

[236] J.C.Y. Ng, W.H. Cheung, G. McKay, Equilibrium studies of the sorption of Cu(II) ions onto chitosan, *J. Colloid Interface Sci.*, Vol. 255, Pp. 64–74, (2002).

[237] S. Kango, R. Kumar, Low-cost magnetic adsorbent for As(III) removal from water: adsorption kinetics and isotherms, *Environ. Monit. Assess.*, Vol. 188, Pp. 1–14, (2016).

[238] M.I. Danish, I.A. Qazi, A. Zeb, A. Habib, M.A. Awan, Z. Khan, Arsenic removal from aqueous solution using pure and metal-doped Titania nanoparticles coated on glass beads: Adsorption and column studies, *J. Nanomater.*, Vol. 2013, Pp. 1-17, (2013).

[239] T.F. Lin, J.K. Wu, Adsorption of arsenite and arsenate within activated alumina grains: Equilibrium and kinetics, *Water Res.*, Vol. 35, Pp. 2049–2057, (2001).

[240] B.M. Lekić, D.D. Marković, V.N. Rajaković-Ognjanović, A.R. Dukić, L. V. Rajaković, Arsenic removal from water using industrial By-products, *J. Chem.,* Vol. 2013, Pp. 1-9, (2013).

[241] A.C.Q. Ladeira, V.S.T. Ciminelli, Adsorption and desorption of arsenic on an oxisol and its constituents, *Water Res.*, Vol. 38, Pp. 2087–2094, (2004).

[242] S. Kuriakose, T.S. Singh, K.K. Pant, Adsorption of As(III) from aqueous solution onto iron oxide impregnated activated alumina, *Water Qual. Res. J. (Canada).*, Vol. 39, 258–266, (2004).

[243] S. Maity, S. Chakravarty, S. Bhattacharjee, B.C. Roy, A study on arsenic adsorption on polymetallic sea nodule in aqueous medium, *Water Res.*, Vol. 39, Pp. 2579–2590, (2005).

[244] B. Das, R.R. Devi, I.M. Umlong, K. Borah, S. Banerjee, A.K. Talukdar, Arsenic (III) adsorption on iron acetate coated activated alumina: thermodynamic, kinetics and equilibrium approach, *J. Environ. Heal. Sci. Eng.,* Vol. 11, Pp. 1–10, (2013).

[245] S. Biswas, U. Mishra, Continuous Fixed-Bed Column Study and Adsorption Modeling: Removal of Lead Ion from Aqueous Solution by Charcoal Originated from Chemical Carbonization of Rubber Wood Sawdust, *J. Chem.,* Vol. 2015, Pp. 1-9, (2015).

[246] D.M. Saad, E. Cukrowska, H. Tutu, Column adsorption studies for the removal of U by phosphonated cross-linked polyethylenimine: modelling and optimization, *Appl. Water Sci.*, Vol. 5, Pp. 57–63, (2015).

[247] R. Han, Y. Wang, W. Yu, W. Zou, J. Shi, H. Liu, Biosorption of methylene blue from aqueous solution by rice husk in a fixed-bed column, *J. Hazard. Mater.*, Vol. 141, Pp. 713–718, (2007).

[248] H. Li, J. He, K. Chen, Z. Shi, M. Li, P. Guo, L. Wu, Dynamic adsorption of sulfamethoxazole from aqueous solution by lignite activated coke, *Materials*, Vol. 13, Pp. 16–20, (2020).

[249] M. Calero, F. Hernáinz, G. Blázquez, G. Tenorio, M.A. Martín-Lara, Study of Cr (III) biosorption in a fixed-bed column, *J. Hazard. Mater.*, Vol. 171, Pp. 886–893, (2009).

[250] M.C. De Hoces, G. Blázquez García, A.R. Gálvez, M.Á. Martín-Lara, Effect of the acid treatment of olive stone on the biosorption of lead in a packed-bed column, *Ind. Eng. Chem. Res.*, Vol. 49, Pp. 12587–12595, (2010).

[251] Z.Z. Chowdhury, S.B. Abd Hamid, S.M. Zain, Evaluating design parameters for

breakthrough curve analysis and kinetics of fixed bed columns for Cu(II) cations using lignocellulosic wastes, *BioResources*. Vol. 10, Pp. 732–749, (2015).

[252] X. Luo, Z. Deng, X. Lin, C. Zhang, Fixed-bed column study for Cu2+ removal from solution using expanding rice husk, *J. Hazard. Mater.* Vol. 187, Pp. 182–189, (2011).

[253] J. Goel, K. Kadirvelu, C. Rajagopal, V.K. Garg, Removal of lead(II) by adsorption using treated granular activated carbon: Batch and column studies, *J. Hazard. Mater.*, Vol. 125, Pp. 211–220, (2005).

Conference presentations undertaken during this PhD research project

1) **Hassan Majiya,** Francis Clegg, and Chris Sammon; Iron-modified Bentonite-Chitosan composites for effective and selective removal of arsenic ions from aqueous solutions, *Innovation Conference Green Future, organised by Industry and Innovation Research Institute, Sheffield Hallam university, United Kingdom,* 14th September 2022, **Poster Presentation (Physical)**

2) *Hassan Majiya,* Francis Clegg, and Chris Sammon; Preparation and characterisation of Iron-based Bentonite-Chitosan composites for arsenic(III) adsorption, *17th International Clay Conference, co-sponsored and co-organised by International Association for the Study of Clays (AIPEA), Clay Minerals Society (USA) and the Clay Science Society (Turkey), Istanbul, Turkey*, 25th to 29th July 2022, **Oral Presentation (Physical)**

3) *Hassan Majiya,* Francis Clegg, and Chris Sammon; Bentonite-Chitosan composites or beads: for co-adsorption of lead (Pb) and copper (Cu) from binary aqueous solutions, *75th Anniversary Jubilee Meeting, organised by Clay Minerals Group (CMG) of the Mineralogical Society, Natural History Museum, London, United Kingdom,* 25th - 26th May 2022, **Oral Presentation (Physical)**

   Award: Student Best Oral Presentation Award (1st place)

4) *Hassan Majiya,* Francis Clegg, and Chris Sammon; Experimental design as a chemometric tool to identify and optimise the significant parameters for adsorption of Pb(II) onto Bentonite-Chitosan composites/beads, *Analytical Research Forum (ARF) of the Royal Society of Chemistry, United Kingdom,* 15th – 16th June 2021, **Poster Presentation (Virtual)**

5) **Hassan Majiya,** Francis Clegg, and Chris Sammon; Bentonite-Chitosan composites and beads: for effective removal of lead (Pb) from water, *A research in progress meeting, co-organised by the Environmental Mineralogy Group (EMG) and Clay Minerals Group (CMG) of the Mineralogical Society, United Kingdom,* 14th June 2021, **Oral Presentation (Virtual)**

6) **Hassan Majiya,** Francis Clegg, and Chris Sammon; Bentonite-Chitosan composites or beads for heavy metal adsorption: design, preparation, and characterisation, *MERI Research Symposium, organised by Materials and Engineering Research Institute (MERI), Sheffield Hallam University,* 8th – 9th June 2021, **Oral Presentation (Virtual)**

7) *Hassan Majiya,* Francis Clegg, and Chris Sammon; Preparation and characterisation of bentonite-chitosan composites/beads, *Winter-Poster-Event co-organised by Biomolecular Sciences Research Centre (BMRC) & Materials and*

Engineering Research Institute (MERI), Sheffield Hallam University, 13th December 2019, **Poster Presentation (Physical)**

8) **Hassan Majiya,** Francis Clegg, and Chris Sammon; Bentonite-Chitosan beads: as a promising candidate for purification of metal-contaminated water, *MERI Research Symposium, organised by Materials and Engineering Research Institute (MERI), Sheffield Hallam University,* 20th – 21st May 2019, **Poster Presentation (Physical)**

9) **Hassan Majiya,** Francis Clegg, and Chris Sammon; Bentonite-Chitosan beads: as a promising candidate for purification of metal-contaminated water, *A trans-disciplinary research meeting, co-sponsored and co-organised by the Clay Minerals Group (CMG) of the Mineralogical Society and the Environmental Chemistry Group (ECG) of the Royal Society of Chemistry, Newcastle University*, 17th May 2019, **Poster Presentation (Physical)**

10) **Hassan Majiya,** Francis Clegg, and Chris Sammon; Monitoring, and removal of heavy metals from water using modified Clay-Polymer composites, *Winter-Poster-Event co-organised by Biomolecular Sciences Research Centre (BMRC) & Materials and Engineering Research Institute (MERI),* 14th December 2018, **Poster Presentation (Physical)**

Appendices

Appendix A1 to A2 (Chapter 4)

Appendix B1 to B22 (Chapter 5)

Appendix C1 to C4 (Chapter 6)

Appendix D1 to D8 (Chapter 7)

Appendix E1 to E5 (Chapter 8)

Appendix A1: FTIR spectra of (a) pristine bentonite (b) 90%Bt-10%Ch-1 beads-B (C) 70%Bt-30%Ch beads-B (d) 50%Bt-50%Ch beads-B and (e) pure chitosan
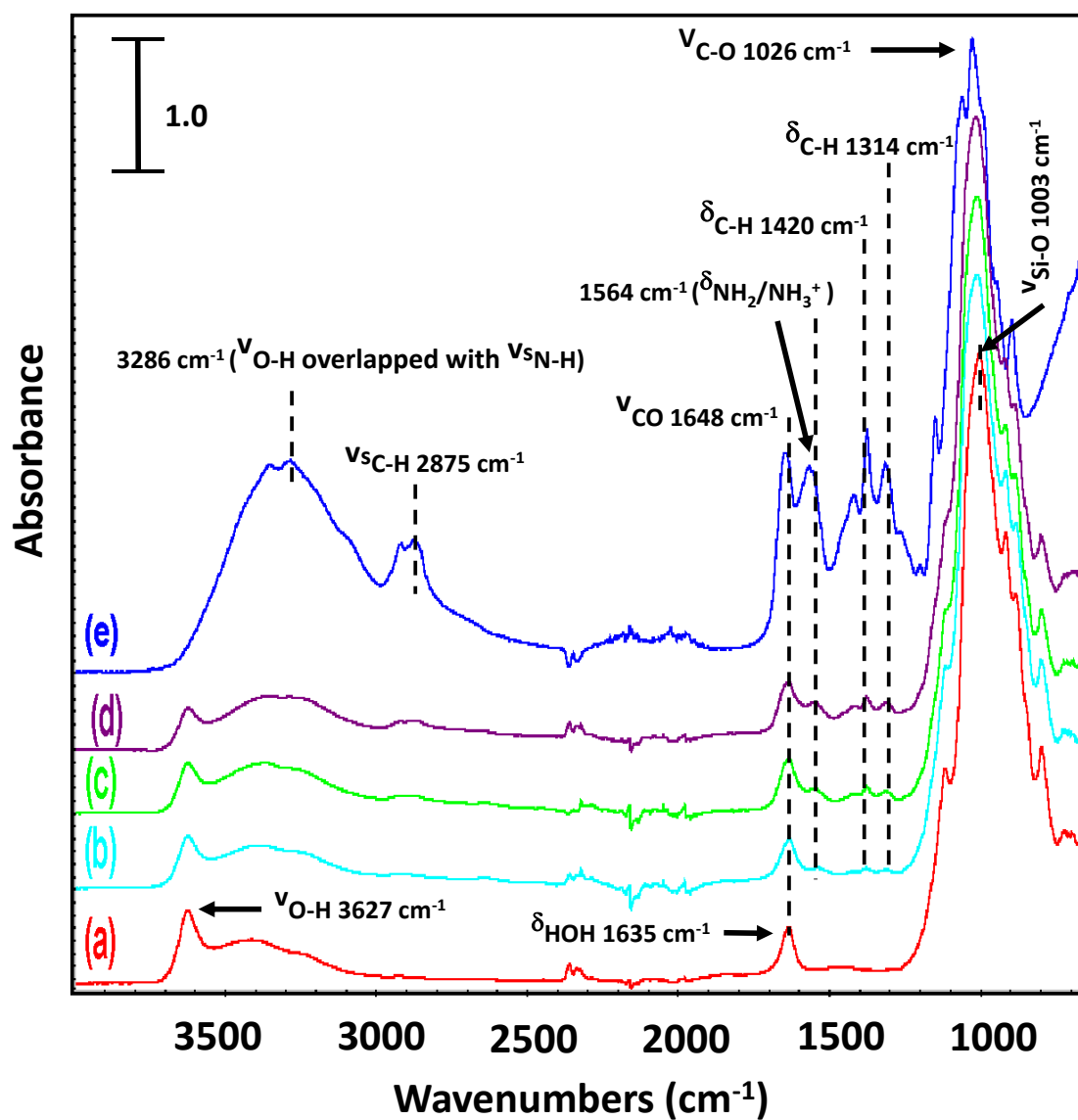
Appendix A2: FTIR spectra of (a) pristine bentonite (b) 90%Bt-10%Ch-1 composites (C) 70%Bt-30%Ch composites (d) 50%Bt-50%Ch composites and (e) pure chitosan
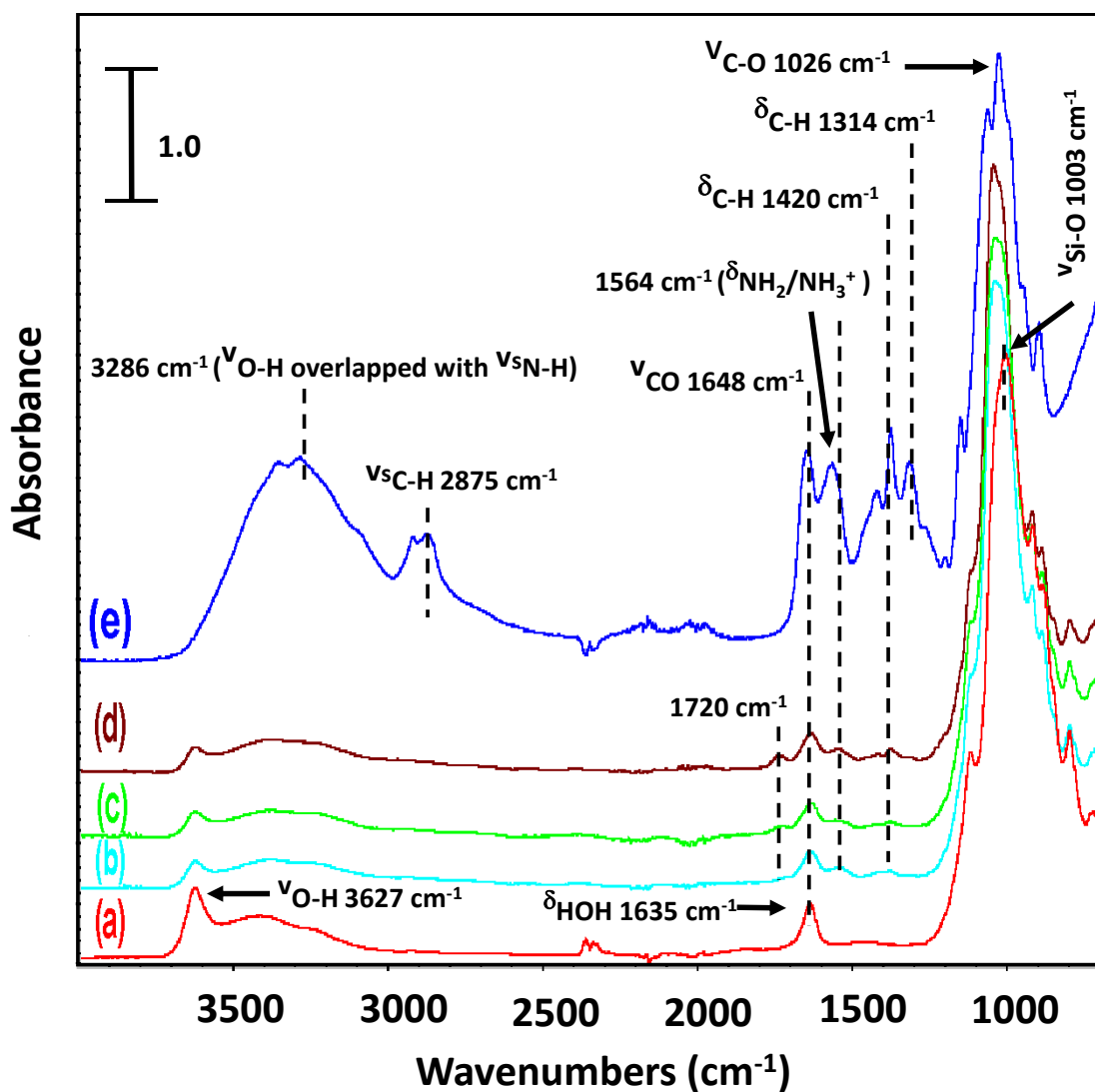
Appendix B1: Two-level fractional-factorial (Resolution IV) experimental design generated for batch adsorption of Pb (II) ions onto Bt-Ch composites/beads

Experiment (Standard order)	Factors						
	A	B	C	D	E	F	G
1	2	50	180	25	0.1	10	X
2	6	50	180	25	0.5	10	Y
3	2	250	180	25	0.5	60	Y
4	6	250	180	25	0.1	60	X
5	2	50	280	25	0.5	60	X
6	6	50	280	25	0.1	60	Y
7	2	250	280	25	0.1	10	Y
8	6	250	280	25	0.5	10	X
9	2	50	180	55	0.1	60	Y
10	6	50	180	55	0.5	60	X
11	2	250	180	55	0.5	10	X
12	6	250	180	55	0.1	10	Y
13	2	50	280	55	0.5	10	Y
14	6	50	280	55	0.1	10	X
15	2	250	280	55	0.1	60	X
16	6	250	280	55	0.5	60	Y

Note: A = pH; B = Initial concentration; C = agitation rate; D =Temperature; E = Adsorbent dosage; F = Agitation time; G = Adsorbent type; X = Bt-Ch Composites; Y = Bt-Ch Beads

Appendix B2: An I-optimal experimental design generated for batch adsorption of Pb (II) ions onto Bt-Ch composites/beads

Experimental Run	Factors			
	A	B	C	D
1	3.50	0.28	150.00	Y
2	3.50	0.50	50.00	Z
3	5.00	0.20	50.00	X
4	2.00	0.05	116.67	X
5*	3.50	0.28	150.00	Y
6	3.50	0.16	100.00	Z
7	2.00	0.05	50.00	Z
8	2.00	0.05	250.00	Y
9*	5.00	0.20	183.33	X
10	3.50	0.05	50.00	Y
11	5.00	0.05	116.67	Y
12*	3.50	0.28	150.00	Y
13	3.50	0.50	250.00	Y
14*	2.00	0.05	116.67	X
15*	2.00	0.20	250.00	X
16	3.50	0.05	250.00	Z
17	5.00	0.05	250.00	Y
18	2.00	0.20	250.00	X
19	5.00	0.35	116.67	Z
20	5.00	0.50	50.00	Y
21	3.00	0.50	50.00	X
22	5.00	0.05	50.00	Z
23	5.00	0.20	183.33	X
24	2.00	0.50	50.00	Y
25	5.00	0.35	250.00	Z
26	5.00	0.50	183.33	X
27	2.00	0.50	183.33	Z
28	2.00	0.28	50.00	X

A = pH; B = Adsorbent dosage; C = Initial concentration; D = Adsorbent type; X = Bt-Ch composites; Y = Bt-Ch beads-A; Z = Bt-Ch beads-B; * = replicates (experimental runs #5, #9, #12, #14 and #15 are the replicated experiments of run #1, #23, #5, #4, #18, respectively)

Appendix B3: Response for optimal experimental design (I-optimal) of Pb (II) ion adsorption onto Bt-Ch-1 composites/beads

Run	90%Bt-10%Ch-1 Adsorption capacity (mg/g)		70%Bt-30%Ch-1 Adsorption capacity (mg/g)		50%Bt-50%Ch-1 Adsorption capacity (mg/g)	
	Experimental	Predicted	Experimental	Predicted	Experimental	Predicted
1	15.73	15.67	15.57	15.80	15.09	14.43
2	2.70	2.67	2.81	2.93	2.79	2.69
3	6.79	6.96	6.98	7.08	6.88	6.33
4	18.53	17.22	13.73	14.65	8.77	10.36
5*	15.83	15.67	15.56	15.80	15.02	14.43
6	18.16	18.92	17.88	16.08	18.14	19.56
7	11.90	11.48	12.69	12.46	6.41	6.51
8	24.87	25.10	31.54	30.53	12.36	12.52
9*	23.26	21.93	23.29	22.19	21.32	22.84
10	23.39	23.58	26.95	27.37	12.38	13.09
11	54.84	53.96	47.52	46.17	26.76	28.34
12*	15.71	15.67	15.36	15.80	15.07	14.43
13	13.83	13.80	14.10	14.05	13.73	13.94
14*	16.07	17.22	15.89	14.65	12.70	10.36
15*	15.29	14.85	13.63	12.10	8.80	8.78
16	63.83	64.13	35.43	38.61	83.78	80.46
17	69.27	69.78	67.60	68.76	61.35	57.62
18	14.25	14.85	10.84	12.10	8.39	8.78
19	9.50	9.52	9.39	9.80	9.68	9.81
20	2.73	2.76	2.79	2.73	2.79	2.89
21	2.72	2.65	2.80	2.52	2.77	2.96
22	26.81	27.03	27.52	28.17	27.43	26.16
23	21.44	21.93	22.27	22.19	21.46	22.84
24	1.62	1.62	2.51	2.50	1.48	1.50
25	20.02	19.47	20.17	18.66	19.98	20.69
26	10.20	10.42	10.50	11.29	9.91	9.23
27	7.44	7.57	4.92	4.95	2.77	2.73
28	3.11	3.14	3.05	3.35	2.47	2.34

*= replicates (experimental-runs #5, #9, #12, #14 and #15 are the replicated experiments of run #1, #23, #5, #4, #18, respectively)

Appendix B4: Response for optimal experimental design (I-optimal) of Pb (II) ion adsorption onto Bt-Ch-2 composites/beads

Run	90%Bt-10%Ch-2		70%Bt-30%Ch-2		50%Bt-50%Ch-2	
	Adsorption capacity (mg/g)		Adsorption capacity (mg/g)		Adsorption capacity (mg/g)	
	Experimental	Predicted	Experimental	Predicted	Experimental	Predicted
1	13.41	14.06	22.16	24.38	16.08	15.92
2	2.74	3.03	3.23	2.87	2.80	2.87
3	6.92	7.61	7.56	8.71	6.73	7.44
4	19.76	21.56	13.68	17.11	21.42	22.62
5*	15.61	14.06	23.63	24.38	16.13	15.92
6	16.40	17.95	24.53	17.13	18.31	17.89
7	17.41	16.23	4.33	4.59	8.56	8.806
8	23.81	26.41	23.86	23.13	31.70	31.24
9*	21.96	25.17	32.47	30.22	24.90	24.86
10	26.37	30.43	26.94	29.87	23.03	22.69
11	55.85	46.44	49.52	49.15	39.66	42.39
12*	14.27	14.06	24.37	24.38	15.80	15.92
13	13.04	12.34	16.31	15.62	14.19	14.43
14*	21.99	21.56	20.99	17.11	22.95	22.62
15*	17.83	15.62	11.40	8.08	19.13	18.92
16	76.27	66.64	33.23	38.71	68.75	67.13
17	67.68	71.11	67.68	66.63	65.99	64.87
18	15.23	15.62	6.23	8.08	17.57	18.92
19	9.03	7.94	11.21	14.27	9.48	10.08
20	2.73	2.77	3.07	2.87	2.79	2.67
21	2.75	2.54	2.77	3.23	2.53	2.63
22	27.41	25.96	31.90	28.72	27.55	25.67
23	23.95	25.17	31.77	30.22	26.45	24.86
24	2.65	2.66	3.15	2.95	1.63	1.66
25	18.72	20.13	23.19	23.79	20.23	20.65
26	9.79	9.22	12.42	11.55	10.33	9.81
27	5.73	6.48	2.16	2.39	5.36	5.26
28	4.23	3.82	3.55	3.41	3.74	3.29

*= replicates (experimental-runs #5, #9, #12, #14 and #15 are the replicated experiments of run #1, #23, #5, #4, #18, respectively)

Appendix B5: The equations of modified quadratic model (in terms of actual or categorical factor) for Pb (II) adsorption onto Bt-Ch-2 composites/bead

90%Bt-10%Ch-2

Log_{10}(Adsorption capacity)$X = 0.538 + 0.3972A - 3.309B + 0.0031C - 0.1378AB + 0.00037AC + 0.0032BC - 0.0487A^2 + 2.8056B^2 - 0.000002C^2$

Log_{10}(Adsorption capacity)$Y = 0.714 + 0.3972A - 3.309B + 0.0021C - 0.1378AB + 0.00037AC + 0.0037BC - 0.0487A^2 + 2.8065B^2 - 0.000007C^2$

Log_{10}(Adsorption capacity)$Z = 0.618 + 0.3972A - 3.309B + 0.0028C - 0.1378AB + 0.00037AC + 0.0038BC - 0.0487A^2 + 2.8056B^2 - 0.000002C^2$

70%Bt-30%Ch-2

Log_{10}(Adsorption capacity)$X = -0.267 + 0.7297A - 2.541B + 0.0059C - 0.1319AB + 0.00049AC + 0.0022BC - 0.0908A^2 + 1.995B^2 - 0.000002C^2$

Log_{10}(Adsorption capacity)$Y = 0.042 + 0.6728A - 2.541B + 0.0059C - 0.1319AB + 0.00049AC + 0.0022BC - 0.0908A^2 + 1.995B^2 - 0.000002C^2$

Log_{10}(Adsorption capacity)$Z = -0.904 + 0.8831A - 2.541B + 0.0059C - 0.1319AB + 0.00049AC + 0.0022BC - 0.0908A^2 + 1.995B^2 - 0.000002C^2$

50%Bt-50%Ch-2

Log_{10}(Adsorption capacity)$X = 0.058 + 0.5711A - 3.216B + 0.0065C - 0.0824AB + 0.0025BC - 0.0695A^2 + 2.603B^2 - 0.00001C^2$

Log_{10}(Adsorption capacity)$Y = 0.009 + 0.5966A - 3.216B + 0.0061C - 0.0824AB + 0.0025BC - 0.0695A^2 + 2.603B^2 - 0.00001C^2$

Log_{10}(Adsorption capacity)$Z = -0.195 + 0.646A - 3.216B + 0.0063C - 0.0824AB + 0.0025BC - 0.0695A^2 + 2.603B^2 - 0.00001C^2$

Note: A = pH; B = Adsorbent dosage; C = Initial concentration; D = Adsorbent type; X = Bt-Ch composites; Y = Bt-Ch beads-A; Z = Bt-Ch beads-B

Appendix B6: Analysis of Variance (ANNOVA) of reduced quadratic model for the response (Pb adsorption capacity) obtained for 90%Bt-10%Ch-1 composites/beads

Source	Coefficient estimate	Sum of Squares	df	Mean Square	F-value	p-value	Remarks
Model	1.191605	4.62	16	0.2889	714.37	< 0.0001	significant
A-pH	0.131645	0.2327	1	0.2327	575.59	< 0.0001	
B-Adsorbent dosage	-0.3565	2.17	1	2.17	5367.79	< 0.0001	
C-Initial conc.	0.291027	1.18	1	1.18	2925.14	< 0.0001	
D-Adsorbent type	-0.03/0.003	0.0139	2	0.0070	17.19	0.0004	
AB	-0.05272	0.0275	1	0.0275	68.06	< 0.0001	
AD	-0.04/0.04	0.0175	2	0.0087	21.60	0.0002	
BC	0.082867	0.0653	1	0.0653	161.52	< 0.0001	
BD	0.05/0.03	0.0160	2	0.0080	19.82	0.0002	
CD	0.011/-0.03	0.0050	2	0.0025	6.21	0.0157	
A^2	-0.11711	0.0571	1	0.0571	141.29	< 0.0001	
B^2	0.127463	0.0653	1	0.0653	161.53	< 0.0001	
C^2	-0.14907	0.0887	1	0.0887	219.31	< 0.0001	
Residual	--	0.0044	11	0.0004	--	--	
Lack of Fit	--	0.0014	6	0.0002	0.4012	0.8515	not significant
Pure Error	--	0.0030	5	0.0006	--	--	
Cor Total	--	4.63	27	--	--	--	

Base 10 log transformation (k = 0); R^2 = 0.99; R^2_{adj}= 0.99; R^2_{pred} = 0.99; C.V (%) = 1.81; and Adequate precision = 104.37

Appendix B7: Analysis of Variance (ANNOVA) of reduced quadratic model for the response (Pb adsorption capacity) obtained for 70%Bt-30%Ch-1 composites/beads

Source	Coefficient estimate	Sum of Squares	df	Mean Square	F-value	p-value	Remarks
Model	1.129615	4.08	17	0.2400	128.95	< 0.0001	significant
A-pH	0.139231	0.2668	1	0.2668	143.32	< 0.0001	
B-Adsorbent dosage	-0.34209	2.03	1	2.03	1090.30	< 0.0001	
C-Initial conc.	0.243988	0.8094	1	0.8094	434.80	< 0.0001	
D-Adsorbent type	-0.05/0.07	0.0587	2	0.0294	15.77	0.0008	
AB	-0.0344	0.0117	1	0.0117	6.27	0.0313	
AC	0.044398	0.0201	1	0.0201	10.78	0.0083	
AD	-0.006/-0.04	0.0175	2	0.0087	4.69	0.0365	
BC	0.086587	0.0712	1	0.0712	38.27	0.0001	
BD	0.06/-0.04	0.0200	2	0.0100	5.37	0.0260	
CD	0.05/0.005	0.0173	2	0.0087	4.65	0.0374	
A^2	-0.08049	0.0269	1	0.0269	14.43	0.0035	
B^2	0.107495	0.0464	1	0.0464	24.95	0.0005	
C^2	-0.1002	0.0393	1	0.0393	21.09	0.0010	
Residual	--	0.0186	10	0.0019	--	--	
Lack of Fit	--	0.0114	5	0.0023	1.59	0.3120	not significant
Pure Error	--	0.0072	5	0.0014	--	--	
Cor Total	--	4.10	27	--	--	--	

Base 10 log transformation (k = 0); R^2 = 0.99; R^2_{adj}= 0.99; R^2_{pred} = 0.94; C.V (%) = 3.92; and Adequate precision = 41.61

Appendix B8: Analysis of Variance (ANNOVA) of reduced quadratic model for the response (Pb adsorption capacity) obtained for 50%Bt-50%Ch-1 composites/beads

Source	Coefficient estimate	Sum of Squares	df	Mean Square	F-value	p-value	Remarks
Model	1.183472	4.70	15	0.3134	153.90	< 0.0001	significant
A-pH	0.243461	0.7113	1	0.7113	349.25	< 0.0001	
B-Adsorbent dosage	-0.34634	1.87	1	1.87	918.38	< 0.0001	
C-Initial conc.	0.284541	1.21	1	1.21	592.86	< 0.0001	
D-Adsorbent type	-0.006/-0.02	0.0230	2	0.0115	5.65	0.0187	
AB	-0.0488	0.0236	1	0.0236	11.57	0.0053	
AC	0.045867	0.0238	1	0.0238	11.68	0.0051	
AD	-0.05/-0.007	0.0294	2	0.0147	7.22	0.0088	
BC	0.008997	0.0008	1	0.0008	0.3832	0.5475	
BD	0.03/0.08	0.0886	2	0.0443	21.74	0.0001	
A²	-0.23898	0.2452	1	0.2452	120.37	< 0.0001	
B²	0.097757	0.0388	1	0.0388	19.03	0.0009	
C²	-0.13537	0.0729	1	0.0729	35.78	< 0.0001	
Residual	--	0.0244	12	0.0020	--	--	
Lack of Fit	--	0.0113	7	0.0016	0.6116	0.7328	not significant
Pure Error	--	0.0132	5	0.0026	--	--	
Cor Total	--	4.73	27	--	--	--	

Base 10 log transformation (k = 0); R^2 = 0.99; R^2_{adj}= 0.99; R^2_{pred} = 0.97; C.V (%) = 4.43; and Adequate precision = 50.70

Appendix B9: Analysis of Variance (ANNOVA) of reduced quadratic model for the response (Pb adsorption capacity) obtained for 90%Bt-10%Ch-2 composites/beads

Source	Coefficient estimate	Sum of Squares	df	Mean Square	F-value	p-value	Remarks
Model	1.14	4.33	13	0.3334	102.02	< 0.0001	significant
A-pH	0.11	0.2011	1	0.2011	61.53	< 0.0001	
B-Adsorbent dosage	-0.40	2.63	1	2.63	804.38	< 0.0001	
C-Initial conc.	0.26	0.9499	1	0.9499	290.68	< 0.0001	
D-Adsorbent type	-0.02/0.003	0.0054	2	0.0027	0.8241	0.4588	
AB	-0.05	0.0223	1	0.0223	6.82	0.0205	
AC	0.06	0.0334	1	0.0334	10.23	0.0064	
BC	0.07	0.0496	1	0.0496	15.17	0.0016	
CD	0.05/-0.06	0.0304	2	0.0152	4.65	0.0282	
A²	-0.11	0.0546	1	0.0546	16.70	0.0011	
B²	0.14	0.0916	1	0.0916	28.04	0.0001	
C²	-0.07	0.0254	1	0.0254	7.77	0.0145	
Residual	--	0.0458	14	0.0033	--	--	
Lack of Fit	--	0.0394	9	0.0044	3.46	0.0927	not significant
Pure Error	--	0.0063	5	0.0013	--	--	
Cor Total	--	4.38	27	--	--	--	

Base 10 log transformation (k = 0); R^2 = 0.99; R^2_{adj}= 0.98; R^2_{pred} = 0.94; C.V (%) = 5.05; and Adequate precision = 35.81

Appendix B10: Analysis of Variance (ANNOVA) of reduced quadratic model for the response (Pb adsorption capacity) obtained for 70%Bt-30%Ch-2 composites/beads

| Source	Coefficient estimate	Sum of Squares	df	Mean Square	F-value	p-value	Remarks
Model	1.28	4.83	13	0.3713	44.59	< 0.0001	significant
A-pH	0.25	0.8528	1	0.8528	102.40	< 0.0001	
B-Adsorbent dosage	-0.35	2.04	1	2.04	244.56	< 0.0001	
C-Initial conc.	0.21	0.6484	1	0.6484	77.86	< 0.0001	
D-Adsorbent type	-0.003/0.11	0.1358	2	0.0679	8.15	0.0045	
AB	-0.04	0.0202	1	0.0202	2.42	0.1419	
AC	0.07	0.0622	1	0.0622	7.47	0.0162	
AD	-0.05/-0.13	0.2336	2	0.1168	14.03	0.0005	
BC	0.05	0.0252	1	0.0252	3.03	0.1038	
A^2	-0.20	0.1956	1	0.1956	23.49	0.0003	
B^2	0.10	0.0427	1	0.0427	5.12	0.0400	
C^2	-0.20	0.1858	1	0.1858	22.31	0.0003	
Residual	--	0.1166	14	0.0083	--		
Lack of Fit	--	0.0640	9	0.0071	0.6768	0.7126	not significant
Pure Error	--	0.0526	5	0.0105	--	--	
Cor Total	--	4.94	27	--	--	--	

Base 10 log transformation (k = 0); R^2 = 0.98; R^2_{adj}= 0.95; R^2_{pred} = 0.92; C.V (%) = 8.18; and Adequate precision = 22.40

Appendix B11: Analysis of Variance (ANNOVA) of reduced quadratic model for the response (Pb adsorption capacity) obtained for 50%Bt-50%Ch-2 composites/beads

Source	Coefficient estimate	Sum of Squares	df	Mean Square	F-value	p-value	Remarks
Model	1.21	4.77	14	0.3407	365.09	< 0.0001	significant
A-pH	0.14	0.2708	1	0.2708	290.18	< 0.0001	
B-Adsorbent dosage	-0.38	2.30	1	2.30	2463.87	< 0.0001	
C-Initial conc.	0.30	1.37	1	1.37	1471.49	< 0.0001	
D-Adsorbent type	0.01/-0.006	0.0004	2	0.0002	0.2345	0.7942	
AB	-0.03	0.0079	1	0.0079	8.42	0.0124	
AD	-0.05/-0.01	0.0345	2	0.0172	18.47	0.0002	
BC	0.06	0.0311	1	0.0311	33.32	< 0.0001	
CD	0.02/-0.02	0.0043	2	0.0022	2.33	0.1368	
A^2	-0.16	0.1109	1	0.1109	118.88	< 0.0001	
B^2	0.13	0.0718	1	0.0718	76.92	< 0.0001	
C^2	-0.13	0.0784	1	0.0784	84.01	< 0.0001	
Residual	--	0.0121	13	0.0009	--	--	
Lack of Fit	--	0.0106	8	0.0013	4.35	0.0610	not significant
Pure Error	--	0.0015	5	0.0003	--	--	
Cor Total	--	4.78	27	--	--	--	

Base 10 log transformation (k = 0); R^2 = 0.99; R^2_{adj}= 0.99; R^2_{pred} = 0.99; C.V (%) = 2.72; and Adequate precision = 71.87
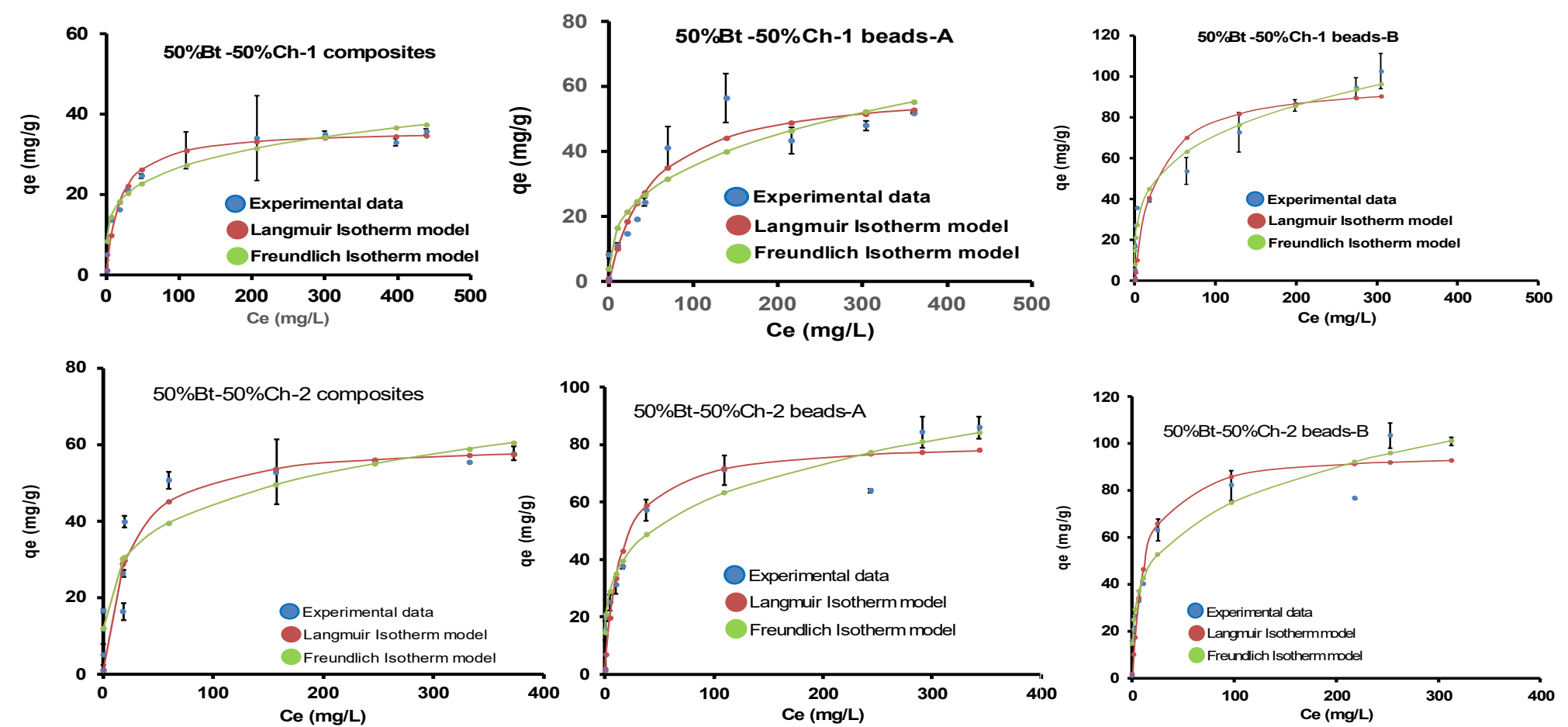
Appendix B12: The non-linear Langmuir and Freundlich isotherms for adsorption of Pb(II) by 90%Bt-10%Ch composites/beads
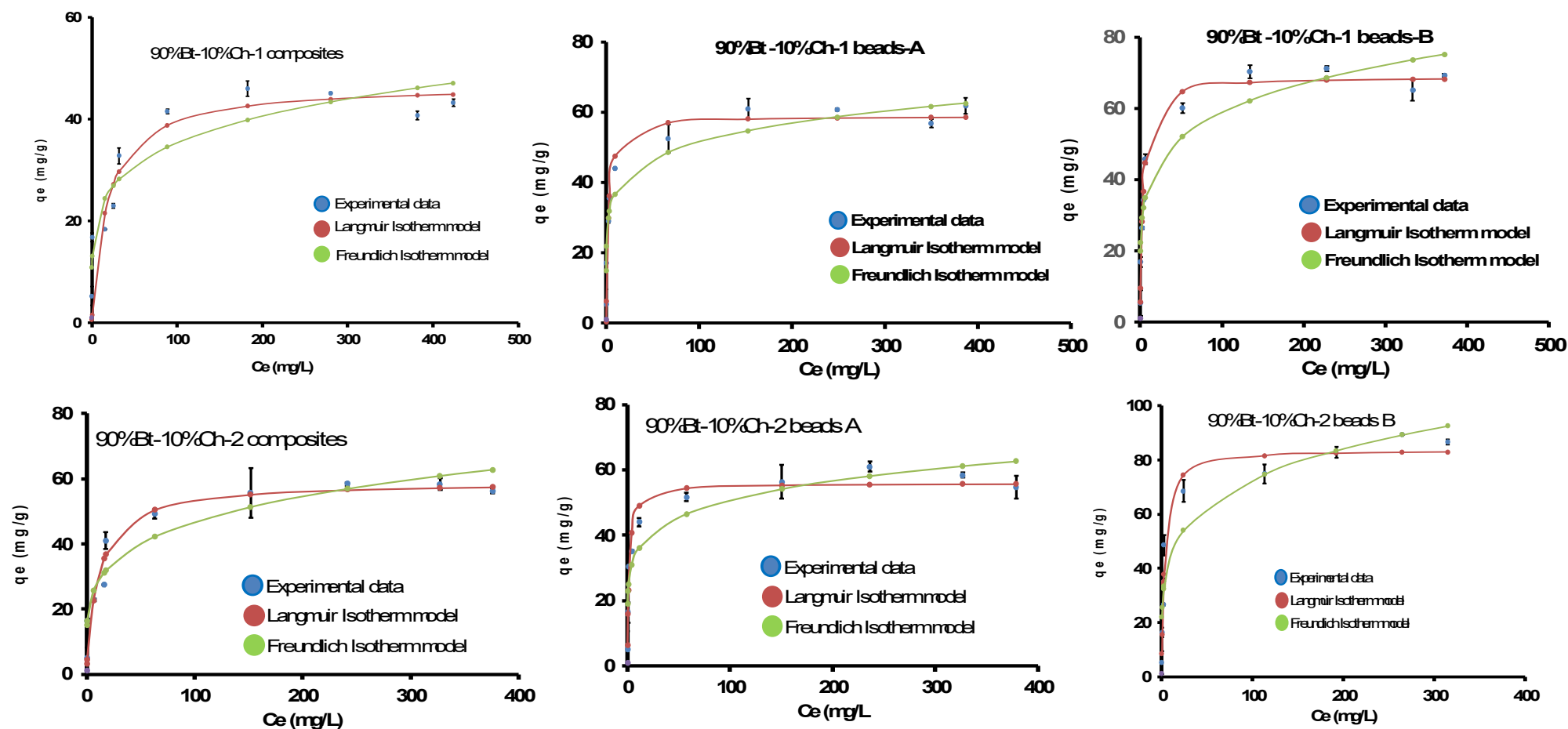
Appendix B13: The non-linear Langmuir and Freundlich isotherms for adsorption of Pb(II) by 70%Bt-30%Ch composites/beads
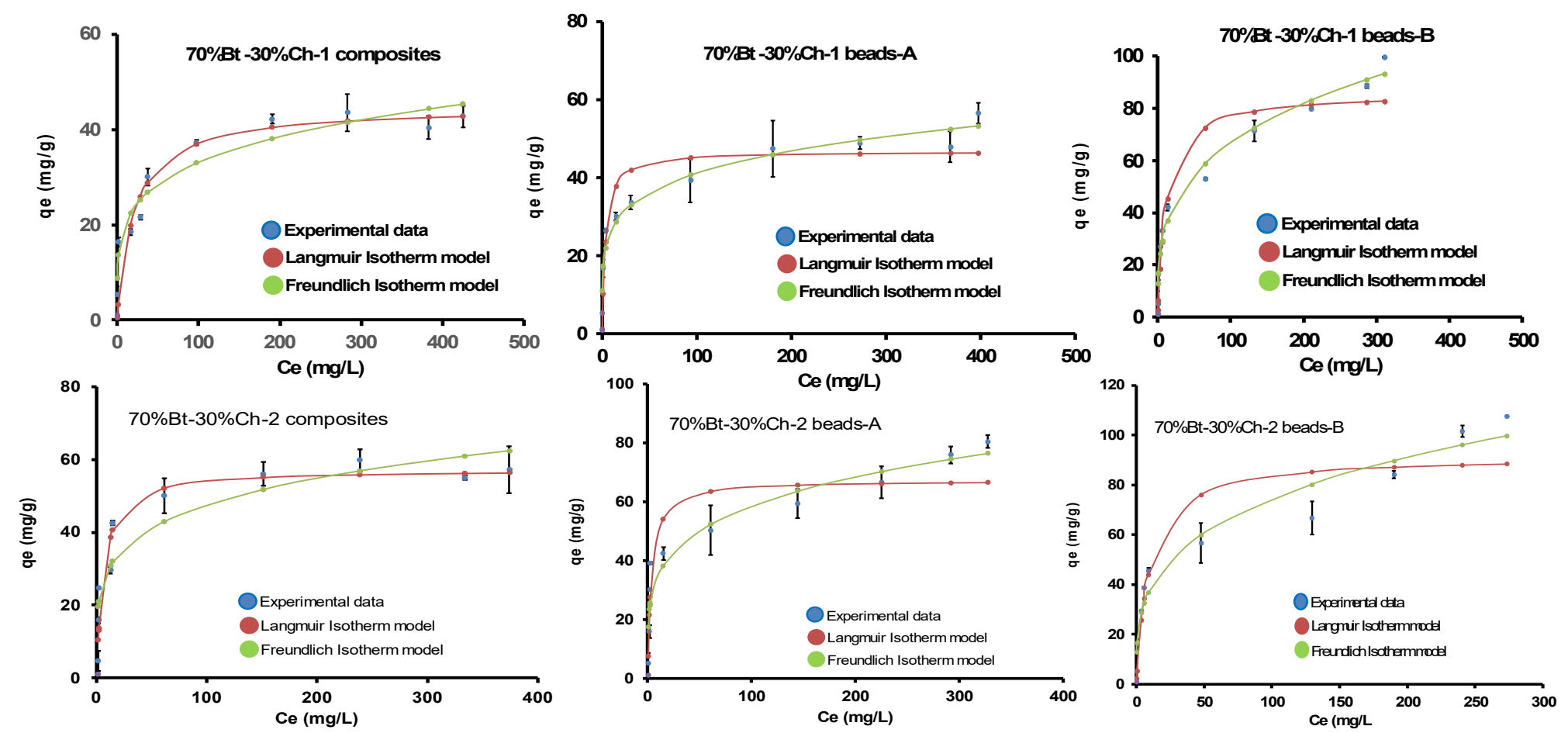
Appendix B14: The non-linear Langmuir and Freundlich isotherms for adsorption of Pb(II) by 50%Bt-50%Ch composites/beads

**Appendix B15:** The non-linear Langmuir for adsorption of Pb (II) by pure chitosan-1 and chitosan-2.

pH = 4.5; adsorbent amount = 0.05 g; agitation time (at 230 rpm) = 60 minutes; Initial Pb concentrations = 10 - 500 mg/L; Each data-point represents mean ± standard deviation of three (3) different experiments (n = 3).
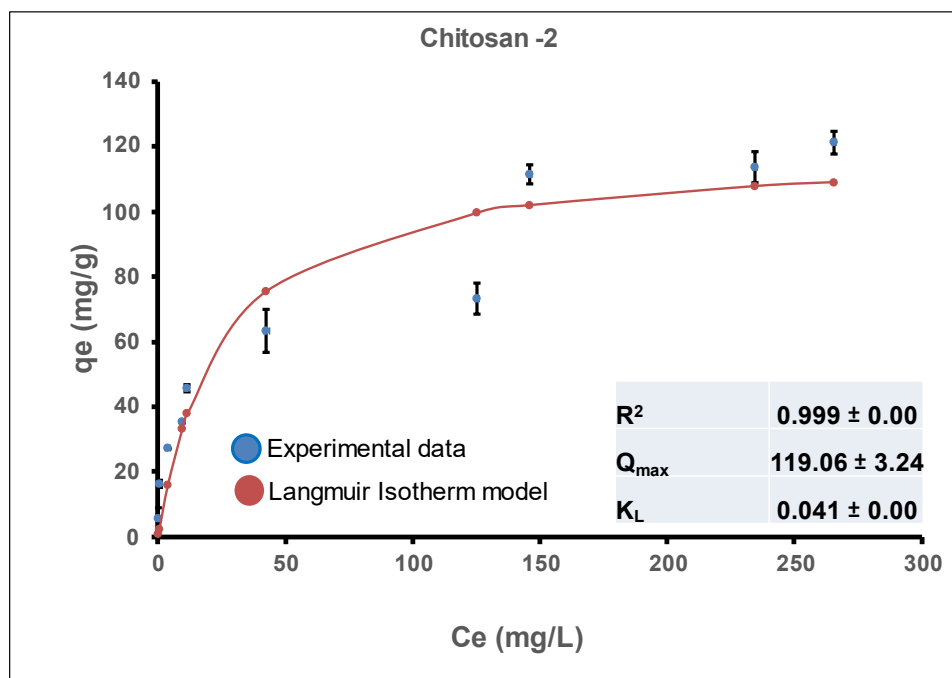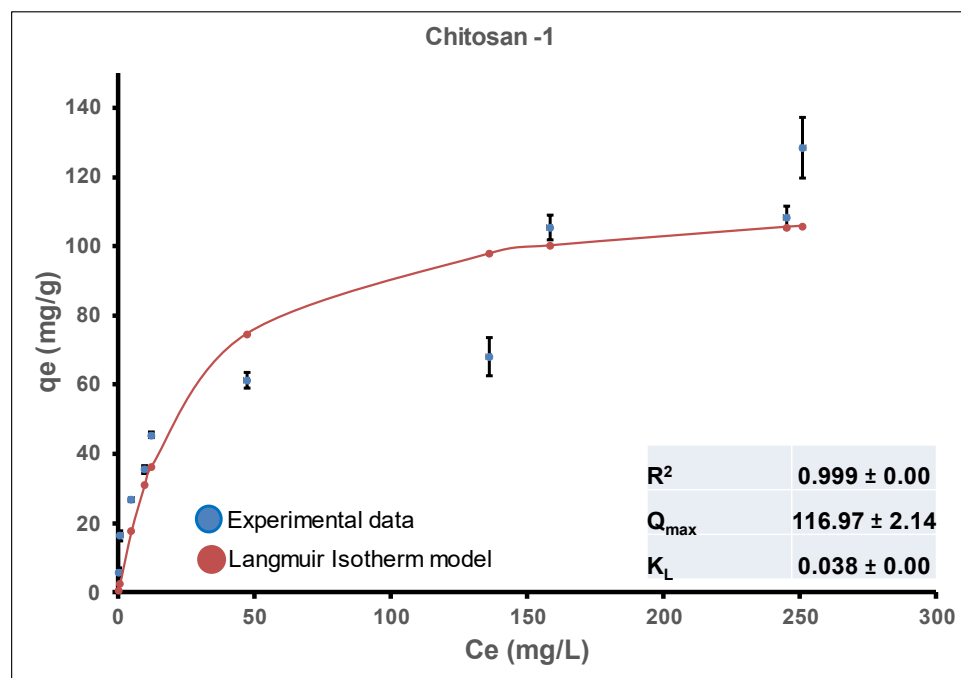
Appendix B16: Charts showing the comparative maximum adsorption capacity, Qmax (mg/g) due to fraction of chitosan (in the composites/beads) and due to whole Bt-Ch composites/beads.

Note: Expected Qmax values due to fraction of chitosan were calculated based on the experimental Qmax obtained from adsorption of Pb(II) ions by pure chitosan-1 (116.97 ± 2.14 mg/g) and chitosan-2 (119.06 ± 3.24 mg/g) for Bt-Ch-1 and Bt-Ch-2, respectively. Each bar represents mean ± standard deviation of three (3) different samples (n = 3).
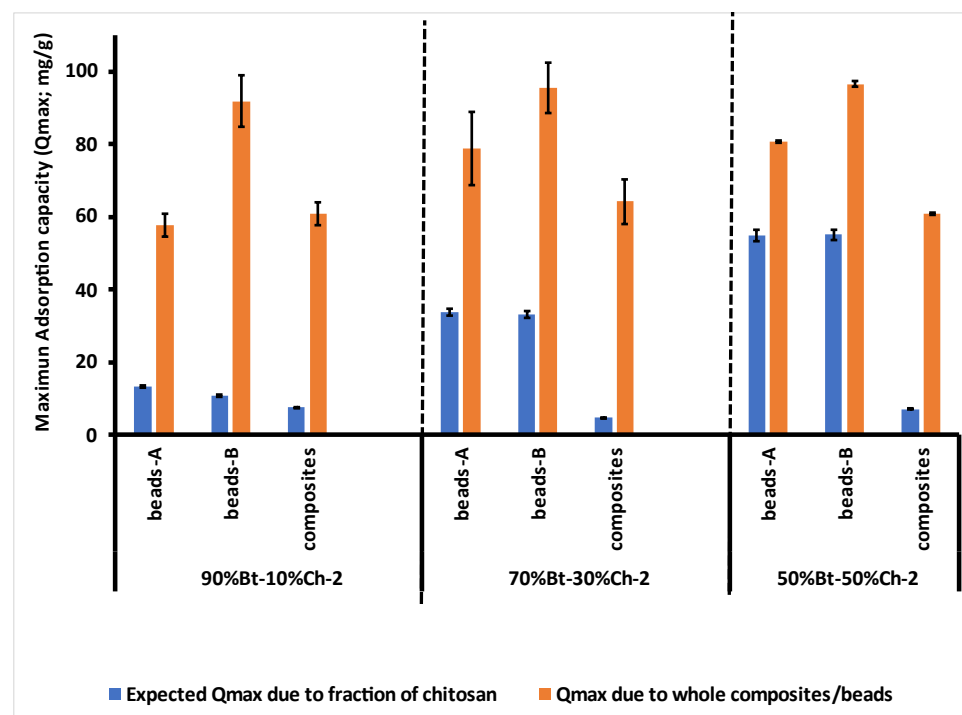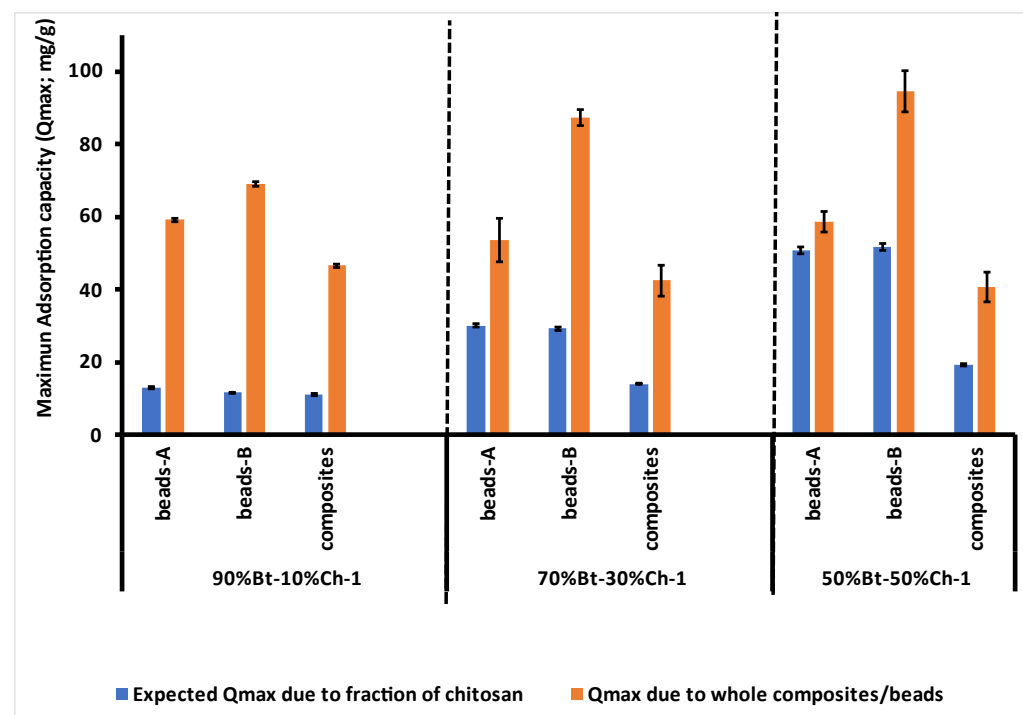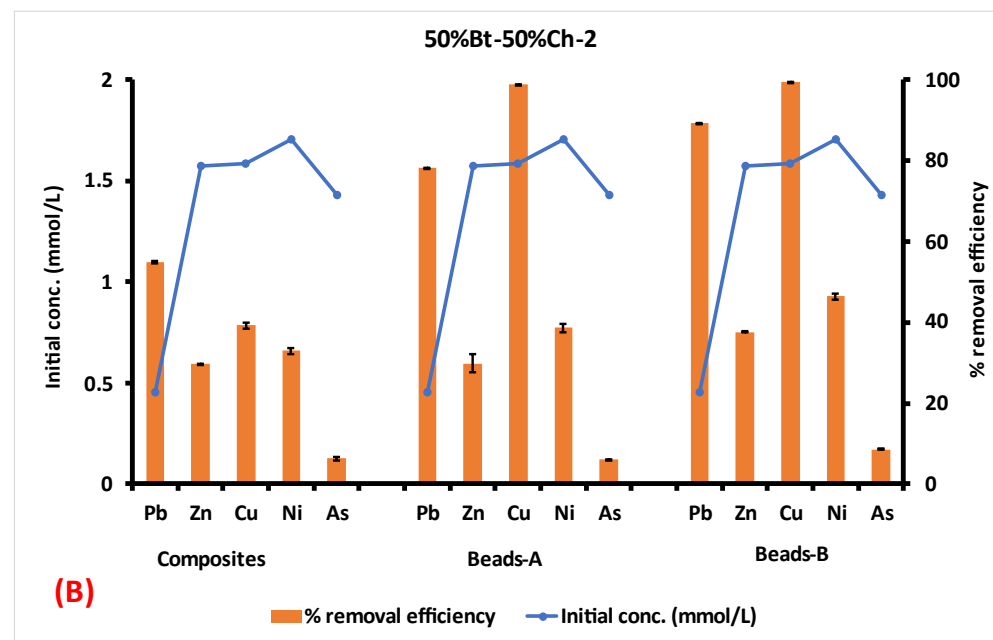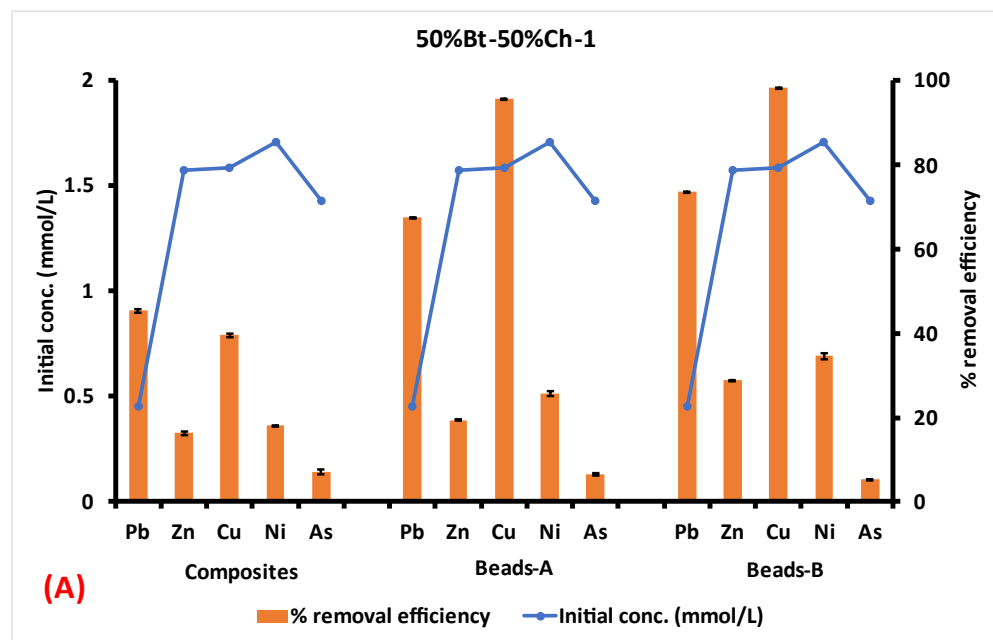
Appendix B17: Charts showing the % removal efficiency of various metal ions from multi-component solutions by (A) 70%Bt-30%Ch-1 and (B) 70%Bt-30%Ch-2 composites/beads

Note: In multi-component solution, the initial concentrations of Pb, Zn, Cu, Ni, and As were 0.45, 1.58, 1.59, 1.71 and 1.43 mmol/L respectively. These metal concentrations are actually the same in terms of mass concentration (i.e., 100 mg/L) but varies with molar concentration due to the molar mass of the respective metal ions; pH = 4.5; adsorbent amount = 0.2 g; agitation time (at 230 rpm) = 60 minutes. Each bar represents mean ± standard deviation of three (3) different samples (n = 3)
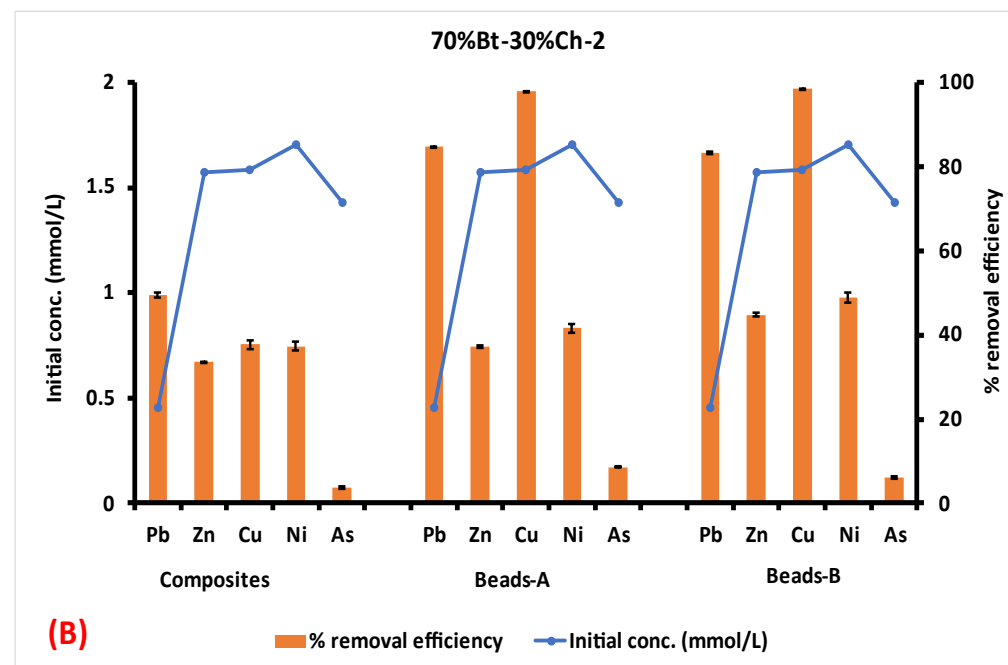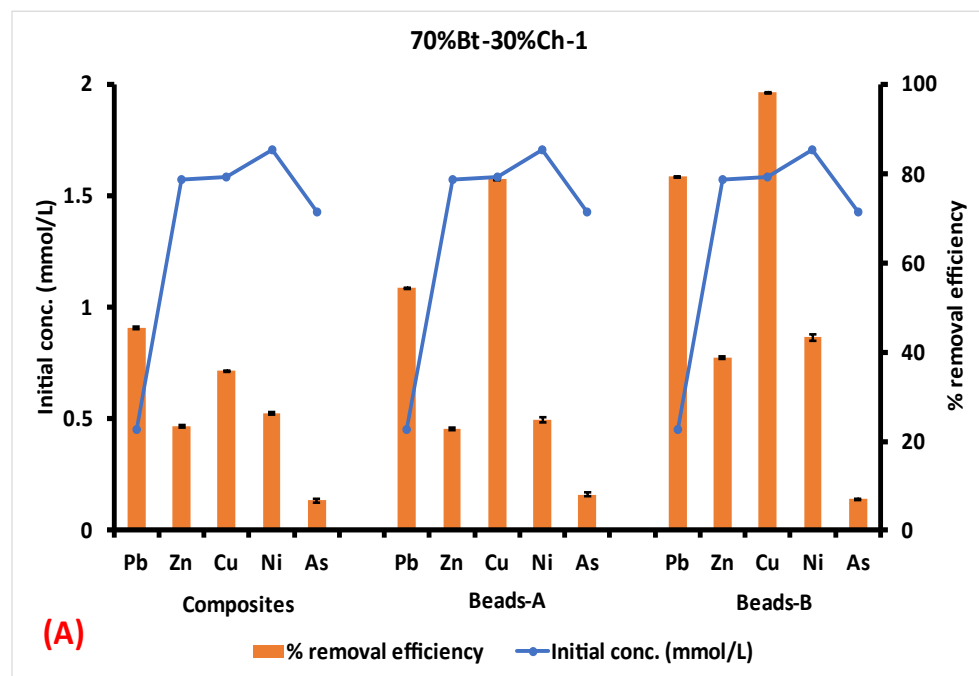
Appendix B18: Charts showing the % removal efficiency of various metal ions from multi-component solutions by (A) 50%Bt-30%Ch-1 and (B) 50%Bt-30%Ch-2 composites/beads

Note: In multi-component solution, the initial concentrations of Pb, Zn, Cu, Ni, and As were 0.45, 1.58, 1.59, 1.71 and 1.43 mmol/L respectively. These metal concentrations are actually the same in terms of mass concentration (i.e., 100 mg/L) but varies with molar concentration due to the molar mass of the respective metal ions; pH = 4.5; adsorbent amount = 0.2 g; agitation time (at 230 rpm) = 60 minutes. Each bar represents mean ± standard deviation of three (3) different samples (n = 3)
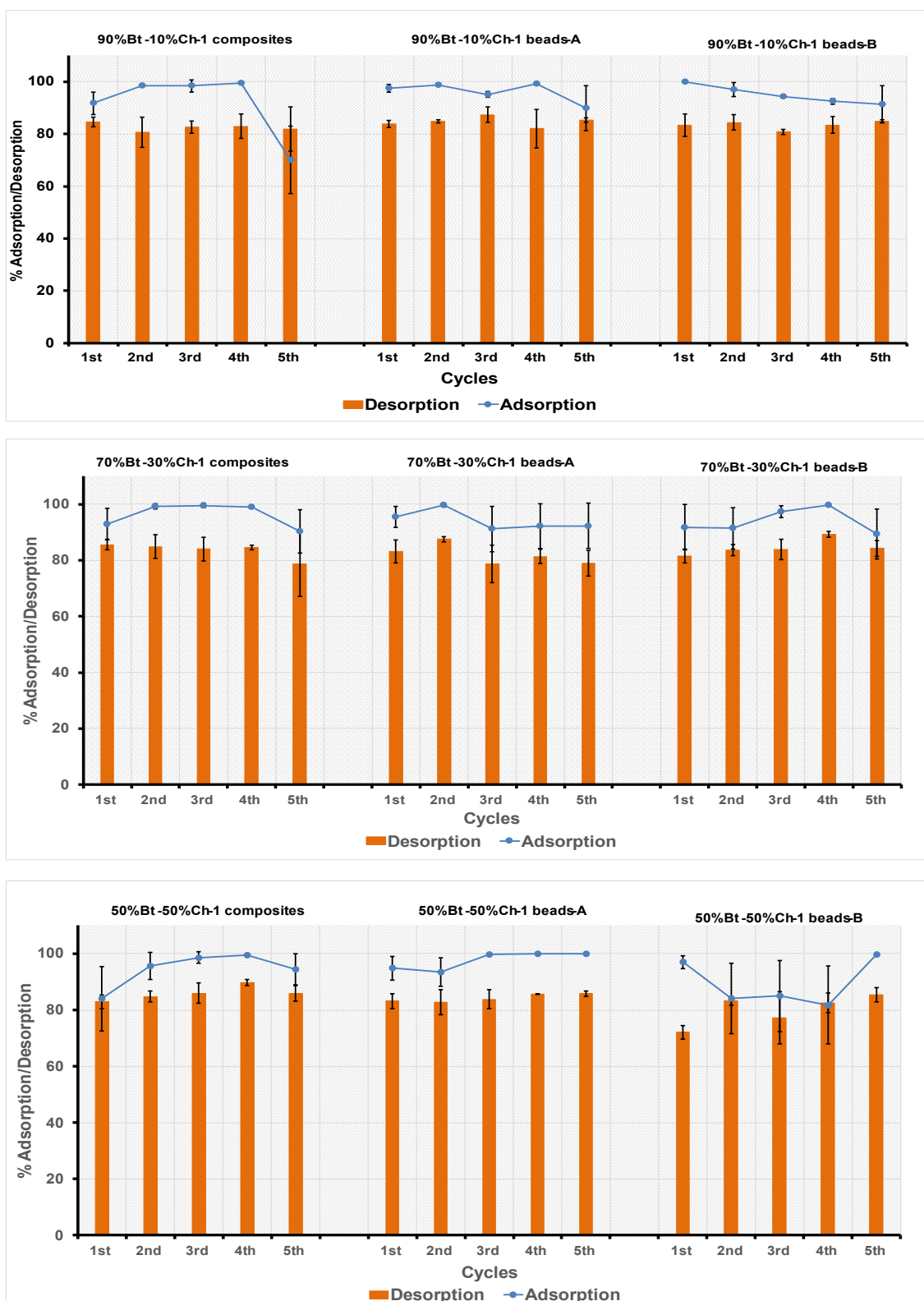
Appendix B19: Charts showing the Pb (II) adsorption efficiencies (%) of Bt-Ch-1 and Bt-Ch-2 composites/beads, chitosan-1, chitosan-2 and Na-bentonite.

Note: Initial Pb concentrations = 100 mg/L; pH = 4.5; adsorbent amount = 0.2 g; agitation time (at 230 rpm) = 60 minutes. Each bar represents mean ± standard deviation of three (3) different samples (n = 3).
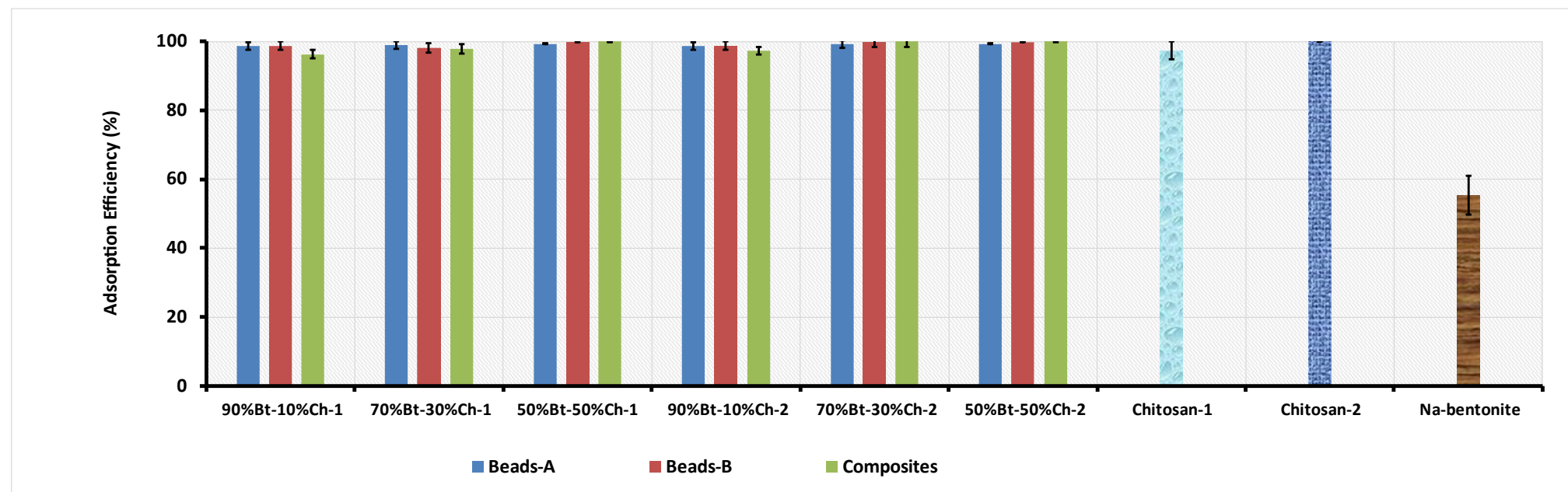
Appendix B20: Charts showing the serial % Adsorption/Desorption of Pb (II) ions adsorbed onto Bt-Ch-1 composites/beads. Desorbing agent = HCl (1.0 x 10^3 mmol/L)

Appendix B21: Charts showing the serial % Adsorption/Desorption of Pb (II) ions adsorbed onto Bt-Ch-2 composites/beads. Desorbing agent = HCl (1.0 x 10^3 mmol/L)
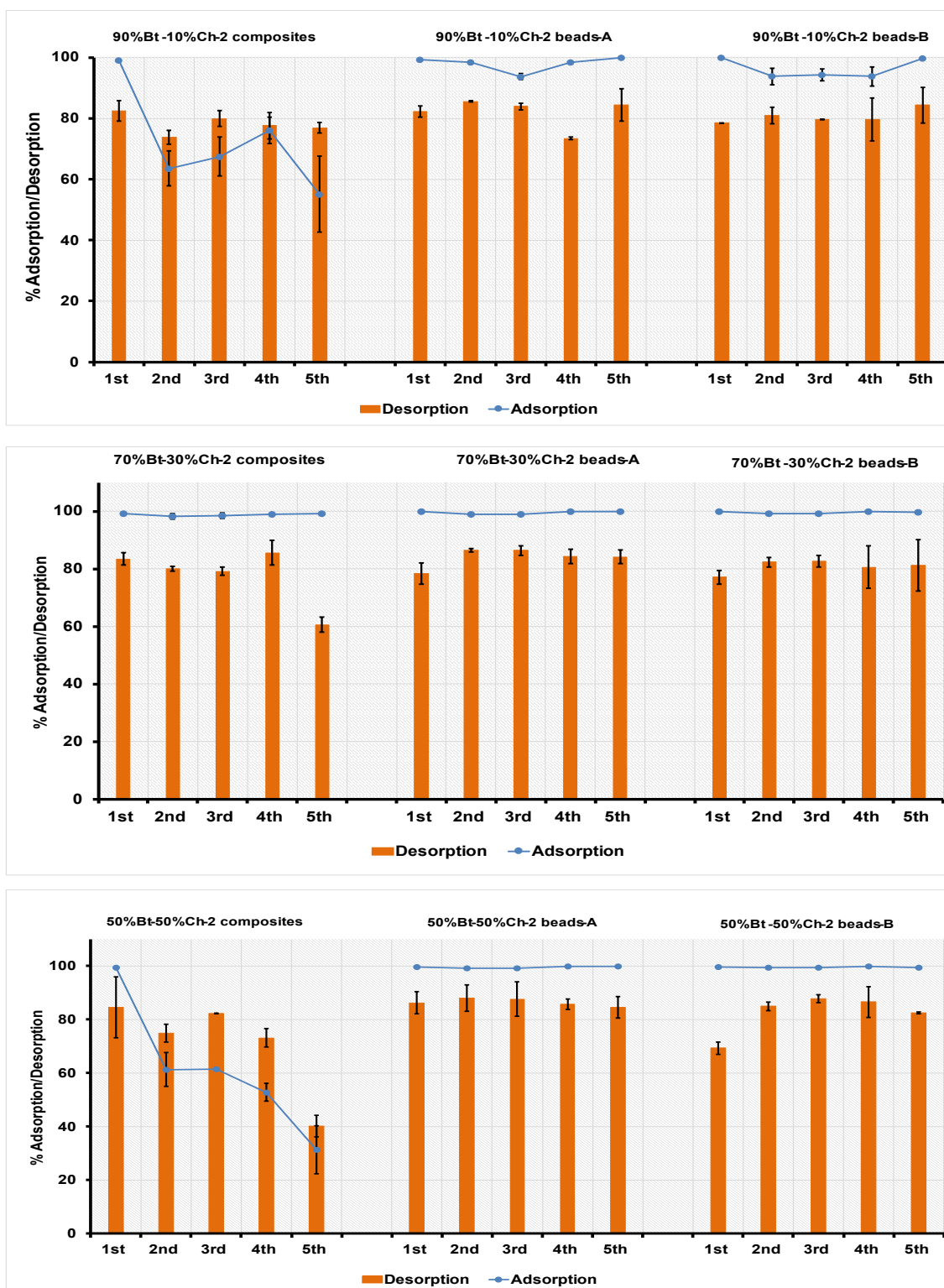
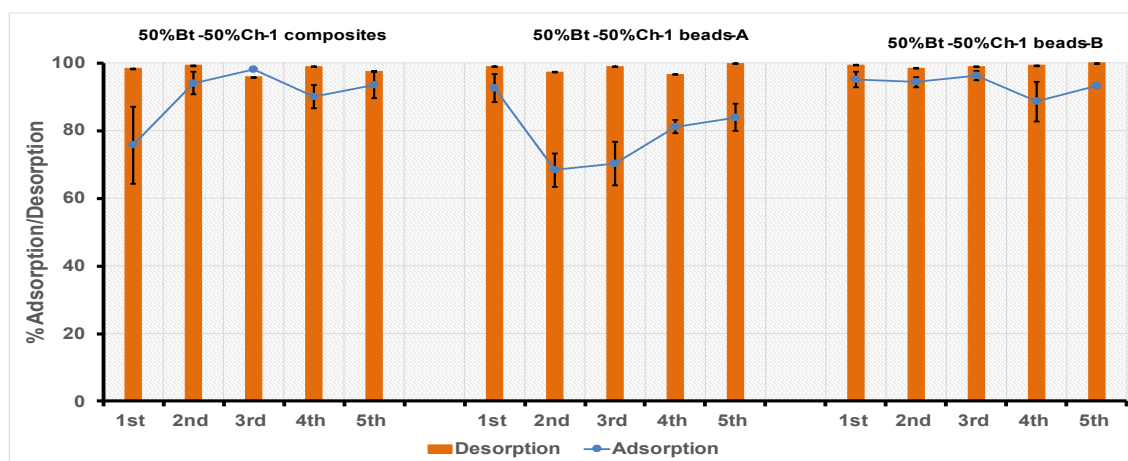**Appendix B22**: Charts showing the serial % Adsorption/Desorption of Pb (II) ions adsorbed onto Bt-Ch-1 composites/beads. Desorbing agent = EDTA (1.0 x 10^1 mmol/L)
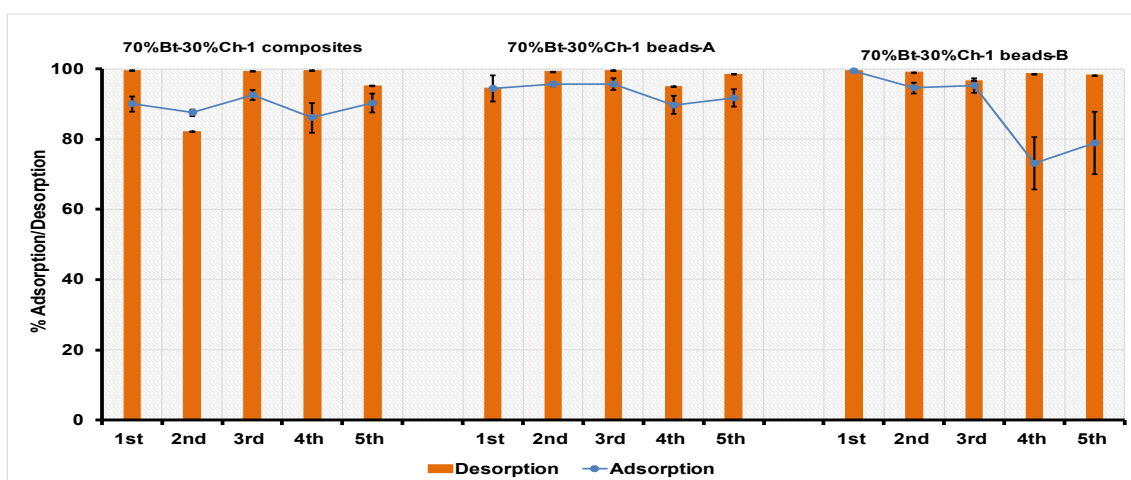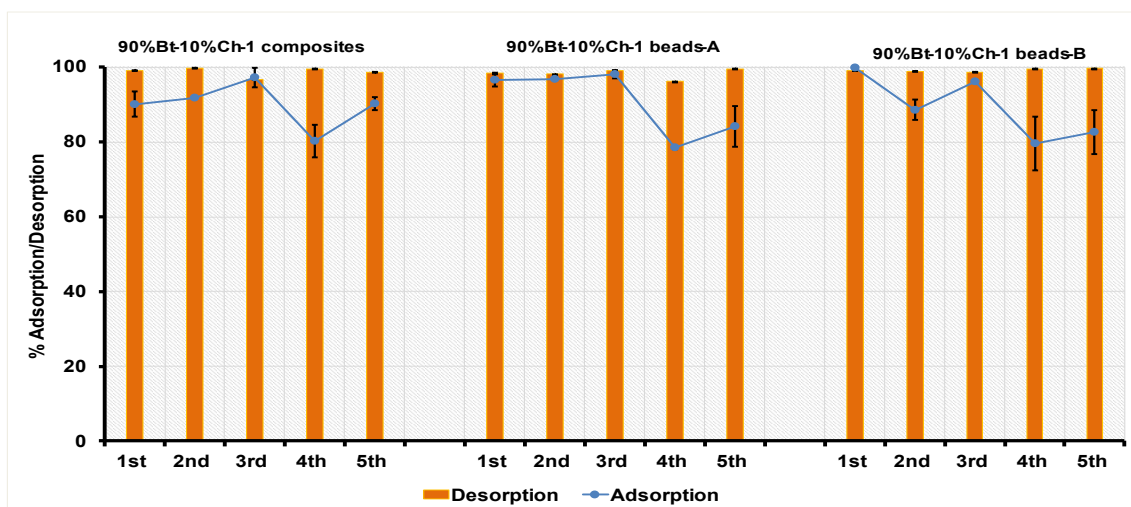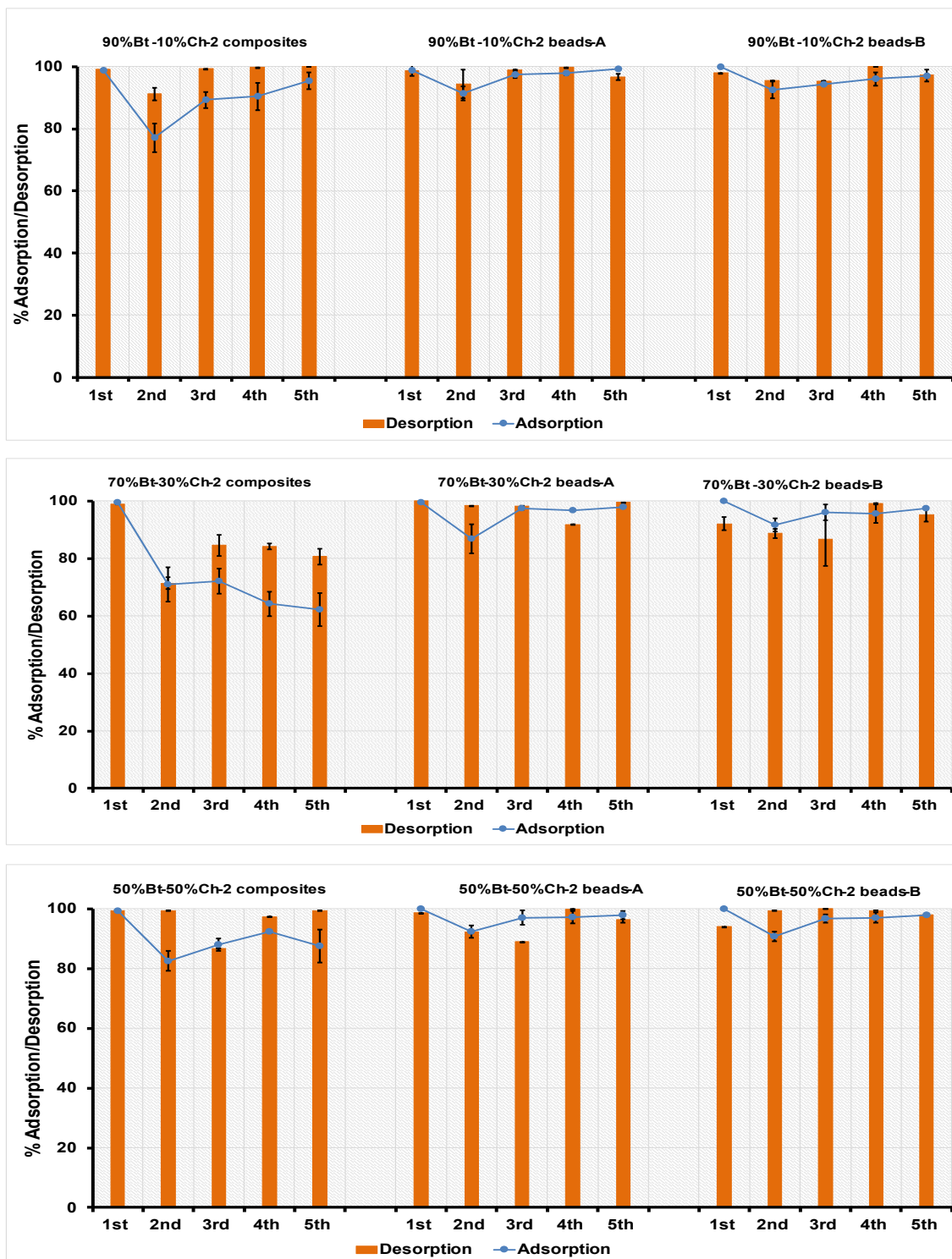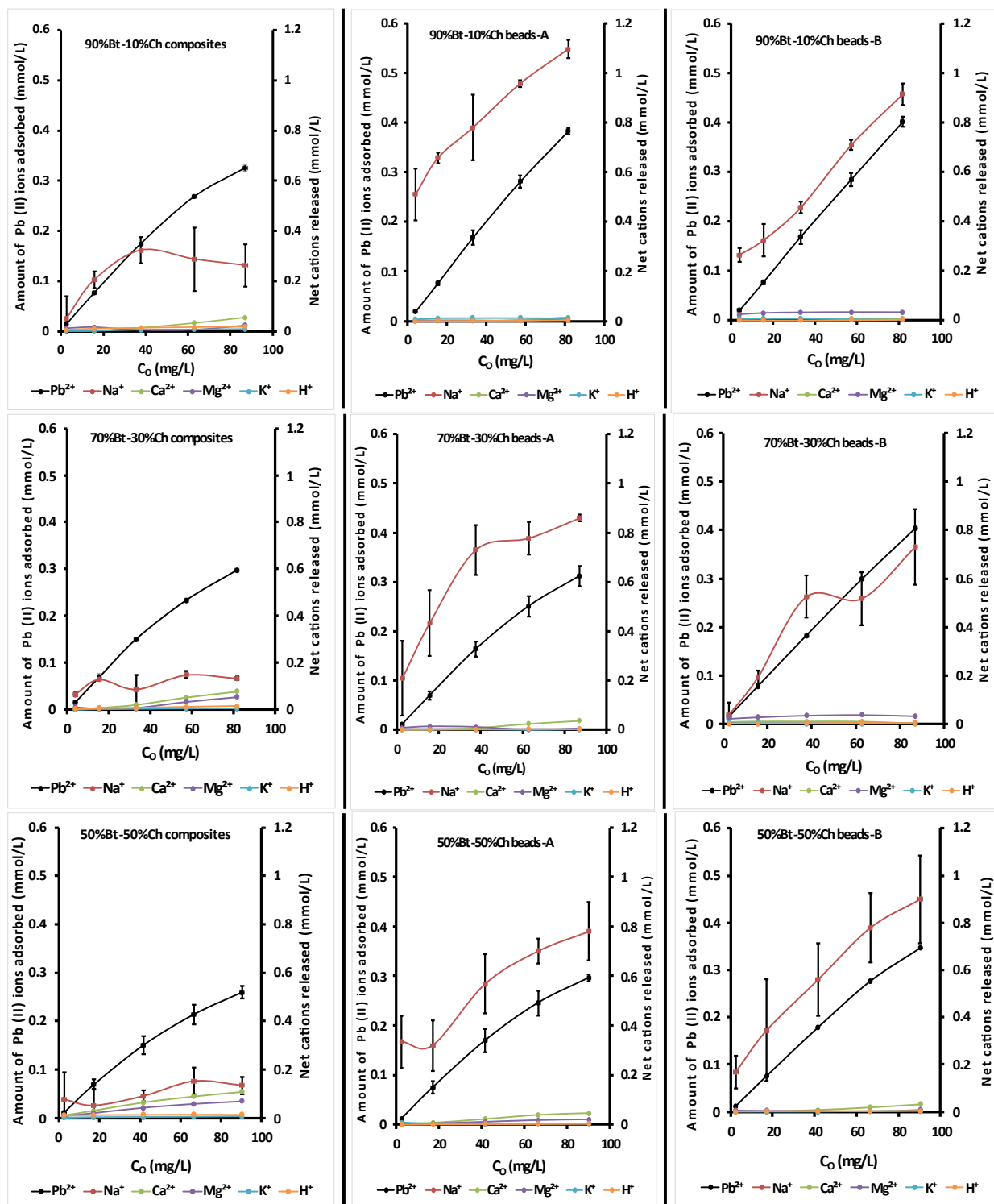
Appendix B23: Charts showing the serial % Adsorption/Desorption of Pb (II) ions adsorbed onto Bt-Ch-2 composites/beads. Desorbing agent = EDTA (1.0×10^1 mmol/L)

Appendix B24: Graphs showing the adsorption of Pb (II) ions and displacement of Na^+, Ca^{2+}, Mg^{2+}, K^+, and H^+ by 90%Bt-10%Ch (above), 70%Bt-30%Ch (middle), and 50%Bt-50%Ch (bottom) composites/beads.

Appendix C1: Adsorption factors (generated Design-Expert® 13 software) and response for optimal experimental design (I-optimal) concerning co-adsorption of Pb(II) and Cu(II) ion onto Bt-Ch composites/beads

Run	Factors					Response			
						Pb-Adsorption capacity (mg/g)		Cu-Adsorption capacity (mg/g)	
	A	B	C	D	E	Experimental	Predicted	Experimental	Predicted
1	5.66	0.10	50.00	10.00	X	7.67	6.70	7.79	5.54
2	2.08	0.20	105.78	78.15	Y	7.44	6.09	6.33	5.06
3	4.07	0.20	125.00	300.00	Y	15.30	16.49	15.91	15.05
4	6.00	0.20	50.00	209.29	X	4.55	4.47	4.94	3.50
5*	4.01	0.05	115.00	118.75	Y	20.99	19.68	22.61	20.58
6*	3.48	0.10	103.00	300.00	X	10.20	9.58	7.11	7.01
7	2.00	0.05	61.00	39.00	X	4.44	4.34	1.96	0.58
8	2.00	0.05	250.00	300.00	Y	9.38	10.06	4.77	4.98
9	2.00	0.13	50.00	198.50	Y	1.57	3.12	0.72	1.21
10	5.90	0.10	184.60	39.00	X	12.50	12.48	10.70	9.99
11	3.21	0.20	50.00	10.00	X	4.72	3.73	4.00	4.44
12	3.60	0.20	250.00	104.25	Y	17.43	16.58	20.17	19.64
13	2.00	0.20	190.00	220.25	X	6.51	5.94	3.17	3.52
14	6.00	0.05	50.00	300.00	Y	14.84	13.78	18.50	18.02
15	3.40	0.10	250.00	89.75	X	12.02	12.00	6.60	6.03
16	6.00	0.05	191.00	214.45	X	15.47	14.82	12.86	13.02
17	6.00	0.05	250.00	10.00	Y	12.61	13.33	25.05	25.64
18*	2.00	0.20	190.00	220.25	X	6.42	5.94	3.59	3.52
19	6.00	0.20	189.00	10.00	X	10.82	11.54	9.28	9.40
20	3.62	0.12	250.00	300.00	X	11.52	10.20	7.03	6.30
21*	3.40	0.10	250.00	89.75	X	11.99	12.00	6.16	6.03
22	2.00	0.18	170.00	10.00	Y	5.02	6.09	2.27	4.27
23	4.01	0.052	115.00	118.75	Y	18.97	19.68	19.99	20.58
24	6.00	0.20	50.00	10.00	Y	4.81	4.97	5.53	7.28
25	4.24	0.16	136.00	139.45	X	11.51	13.65	9.05	10.78
26*	5.82	0.13	192.00	201.40	Y	17.31	16.71	21.74	22.25
27	5.82	0.13	192.00	201.40	Y	17.63	16.71	23.24	22.25
28	4.98	0.05	50.00	186.30	X	11.06	12.74	8.35	11.69
29	3.48	0.10	103.00	300.00	X	9.65	9.58	6.52	7.01
30	5.8	0.20	250.00	300.00	X	9.44	10.73	10.32	11.06

A = pH; B = Adsorbent dosage; C = Initial concentration; D = Agitation time; E = Adsorbent type; X = Bt-Ch composites; Y = Bt-Ch beads-B; * = replicates (experimental run #5, #6, #18, #21 and #26 are the replicated experiments of run #23, #29, #13, #15, #27, respectively)

Appendix C2: Analysis of Variance (ANNOVA) of reduced quadratic model for the response (Pb adsorption capacity)

Source	Coefficient estimate	Sum of Squares	df	Mean Square	F-value	p-value	Remark
Model	15.93	679.69	11	61.79	40.13	< 0.0001	significant
A-pH	3.16	168.41	1	168.41	109.37	< 0.0001	
B-Adsorbent dosage	-1.66	46.25	1	46.25	30.04	< 0.0001	
C-Initial conc.	2.51	101.22	1	101.22	65.73	< 0.0001	
D-Agitation time	0.5384	4.29	1	4.29	2.79	0.1124	
E-Adsorbent type	1.74	81.03	1	81.03	52.62	< 0.0001	
BC	1.21	14.51	1	14.51	9.42	0.0066	
DE	0.9871	14.79	1	14.79	9.60	0.0062	
A²	-5.54	156.76	1	156.76	101.80	< 0.0001	
B²	1.88	18.44	1	18.44	11.98	0.0028	
C²	-3.40	56.98	1	56.98	37.00	< 0.0001	
D²	-1.87	17.23	1	17.23	11.19	0.0036	
Residual	--	27.72	18	1.54	--	--	
Lack of Fit	--	25.45	13	1.96	4.32	0.0582	not significant
Pure Error	--	2.27	5	0.4536	--	--	
Cor Total	--	707.40	29	--	--	--	

R^2 = 0.96; R^2_{adj}= 0.94; R^2_{pred} = 0.88; C.V (%) = 11.50; and Adequate precision = 21.10; df = Degree of freedom

Appendix C3: Analysis of Variance (ANNOVA) of reduced quadratic model for the response (Cu adsorption capacity)

Source	Coefficient estimate	Sum of Squares	df	Mean Square	F-value	p-value	Remark
Model	14.25	1459.85	15	97.32	32.46	< 0.0001	significant
A-pH	5.86	574.91	1	574.91	191.77	< 0.0001	
B-Adsorbent dosage	-1.03	16.80	1	16.80	5.60	0.0329	
C-Initial conc.	2.40	85.88	1	85.88	28.65	0.0001	
D-Agitation time	0.1559	0.3435	1	0.3435	0.1146	0.7400	
E-Adsorbent type	3.85	390.41	1	390.41	130.22	< 0.0001	
AB	-1.56	24.75	1	24.75	8.26	0.0123	
AC	1.70	25.61	1	25.61	8.54	0.0111	
AE	1.37	30.46	1	30.46	10.16	0.0066	
BC	1.69	27.02	1	27.02	9.01	0.0095	
BE	-0.9393	14.04	1	14.04	4.68	0.0483	
CE	1.55	36.38	1	36.38	12.14	0.0037	
A²	-5.13	129.20	1	129.20	43.10	< 0.0001	
B²	1.83	16.35	1	16.35	5.45	0.0349	
C²	-2.01	18.46	1	18.46	6.16	0.0264	
D²	-1.71	13.69	1	13.69	4.57	0.0507	
Residual	--	41.97	14	3.00	--	--	
Lack of Fit	--	37.05	9	4.12	4.18	0.0647	not significant
Pure Error	--	4.92	5	0.9840	--	--	
Cor Total	--	1501.82	29	--	--	--	

R^2 = 0.97; R^2_{adj}= 0.94; R^2_{pred} = 0.78; C.V (%) = 16.96; and Adequate precision = 19.81; df = Degree of freedom

Appendix C4: The non-linear single- and multi-component isotherms for co-adsorption of Pb(II)-Cu(II) by 70%Bt-30%Ch beads (adsorbent Y)

Note: at 25 ^{O}C. pH = 4.5; adsorbent amount = 0.05 g; agitation time (at 230 rpm) = 60 minutes; Initial concentrations of Pb(II) and Cu(II) ions in binary solution = 10 - 350 mg/L; Each data-point represents mean ± standard deviation of three (3) different experiments (n = 3)
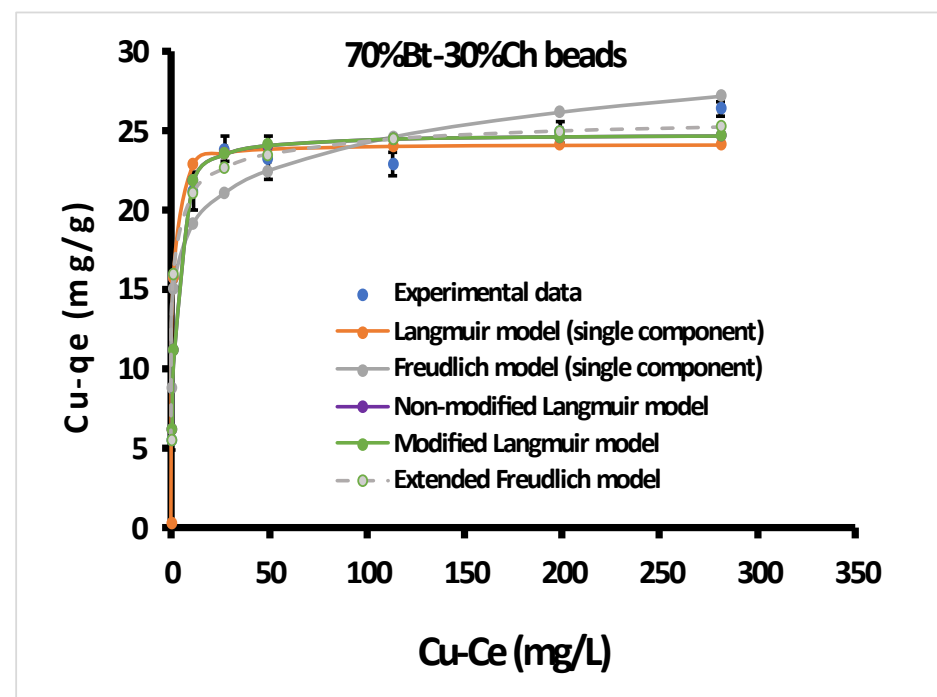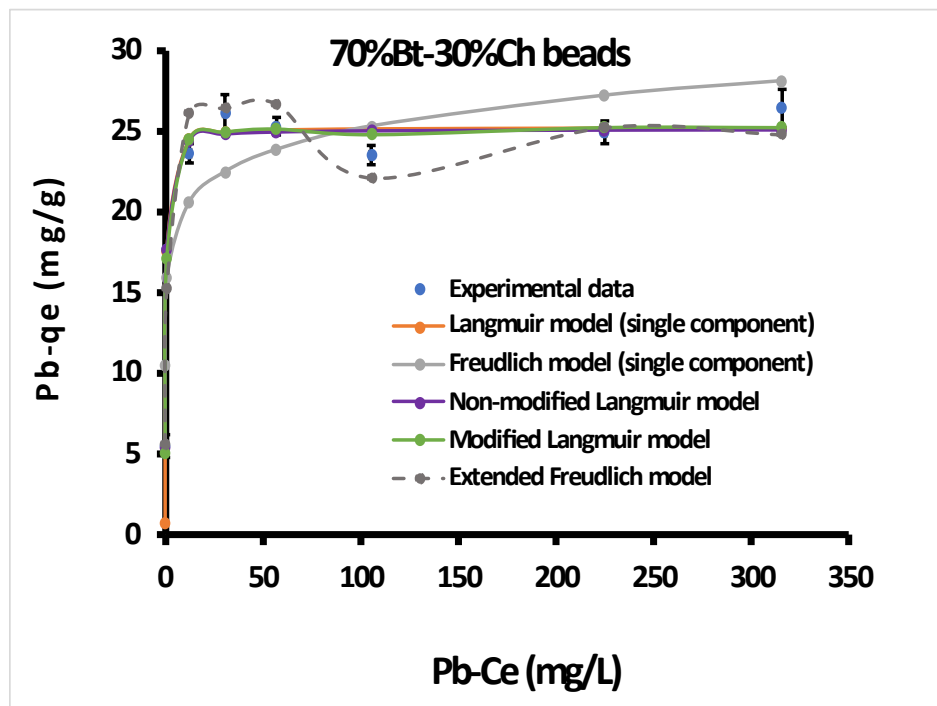
Appendix D1: Adsorption factors (generated Design-Expert® 13 software) and response for optimal experimental design (I-optimal) of As (III) ion adsorption onto Bt-Ch composites/beads

Run	Factors						Response	
							Adsorption efficiency (%)	
	A	B	C	D	E	F	Experimental	Predicted
1*	8.92	0.07	190.00	143.40	37.00	Y	1.953	1.964
2	9.00	0.43	50.00	10.00	28.15	Y	9.363	7.757
3	1.00	0.50	50.00	10.00	25.00	Z	19.498	18.621
4	1.00	0.50	50.00	300.00	55.00	X	9.847	10.233
5	1.00	0.21	50.00	105.70	55.00	Z	21.380	19.055
6	4.44	0.50	250.00	300.00	25.00	Y	9.311	12.589
7	5.08	0.05	250.00	300.00	32.50	Y	3.028	1.783
8	3.08	0.17	50.00	76.70	35.15	X	4.578	5.735
9	4.32	0.05	50.00	300.00	25.00	Y	1.949	1.813
10*	3.08	0.17	50.00	76.70	35.15	X	5.005	5.735
11	9.00	0.50	90.00	10.00	55.00	X	10.233	10.715
12	5.72	0.50	250.00	10.00	55.00	Y	5.564	5.812
13	1.08	0.48	109.00	166.57	43.00	Y	17.378	12.883
14	8.92	0.07	190.00	143.40	37.00	Y	1.644	1.964
15	5.44	0.24	221.00	184.00	55.00	X	3.755	3.418
16	1.00	0.05	200.00	300.00	25.00	X	0.684	0.585
17	5.36	0.32	154.00	10.00	40.90	Z	6.468	4.825
18	9.00	0.50	244.00	91.20	25.00	Z	9.122	8.078
19	8.80	0.05	250.00	10.00	25.00	X	0.025	0.030
20*	5.44	0.24	221.00	184.00	55.00	X	3.080	3.418
21	4.93	0.48	206.09	278.25	47.47	Y	9.513	9.727
22*	5.36	0.32	154.00	10.00	40.90	Z	4.338	4.825
23	5.24	0.05	147.00	300.00	52.00	Z	2.252	2.685
24	1.00	0.44	250.00	34.65	33.70	X	5.282	5.136
25	1.00	0.12	250.00	300.00	52.00	Y	5.386	5.212
26	7.48	0.50	50.00	218.80	45.70	Z	11.482	14.791
27	2.36	0.05	250.00	107.15	31.30	Z	10.965	9.938
28	9.00	0.05	250.00	10.00	55.00	Z	1.871	2.007
29	5.60	0.05	50.00	10.00	55.00	Y	0.924	0.964
30	9.00	0.50	250.00	300.00	41.35	X	13.804	14.125
31	9.00	0.38	110.00	300.00	55.00	Y	11.220	10.471
32	1.00	0.18	190.00	10.00	25.00	Y	2.734	2.921
33	9.00	0.28	50.00	300.00	32.99	Y	10.965	13.490
34	9.00	0.06	50.00	300.00	46.30	X	2.934	2.344
35	1.00	0.05	170.00	10.00	55.00	X	1.3008	1.217
36*	6.68	0.41	113.00	215.90	25.00	X	8.954	7.459
37	9.00	0.19	56.00	99.90	48.11	Z	5.338	4.149
38	1.00	0.05	132.00	157.53	43.00	Y	3.470	4.835
39	9.00	0.05	50.00	54.95	25.00	Z	0.299	0.298
40	1.00	0.50	250.00	268.10	55.00	Z	26.915	26.303
41	9.00	0.19	250.00	300.00	25.00	Z	2.411	2.761
42	6.68	0.41	113.00	215.90	25.00	X	7.779	7.459
43	1.00	0.31	98.00	300.00	30.40	Z	21.380	26.303

A = pH; B = Adsorbent dosage; C = Initial concentration; D = Agitation time; E = Temperature; F = Adsorbent type; X = Bt-Ch composites; Y = Bt-Ch beads-A; Z = Bt-Ch beads-B; * = replicates (experimental-runs #1, #10, #20, #22 and #36 are the replicated experiments of run #14, #8, #15, #17, #42, respectively)

Appendix D2: Analysis of Variance (ANNOVA) of reduced quadratic model for the response (As adsorption efficiency)

Source	Coefficient estimate	Sum of Squares	df	Mean Square	F-value	p-value	Remarks
Model	0.8624	12.60	26	0.4846	31.78	< 0.0001	significant
A-pH	-0.1718	0.9065	1	0.9065	59.46	< 0.0001	
B-Adsorbent dosage	0.4264	5.18	1	5.18	339.53	< 0.0001	
C-Initial conc.	-0.0553	0.1064	1	0.1064	6.98	0.0178	
D-Agitation time	0.1462	0.5205	1	0.5205	34.14	< 0.0001	
E-Temperature	0.0858	0.2607	1	0.2607	17.10	0.0008	
F-Adsorbent type	0.20/0.02	0.8698	2	0.4349	28.52	< 0.0001	
AB	0.1749	0.4668	1	0.4668	30.62	< 0.0001	
AD	0.0792	0.0875	1	0.0875	5.74	0.0291	
AE	0.1225	0.2116	1	0.2116	13.88	0.0018	
AF	0.06/0.13	0.4479	2	0.2239	14.69	0.0002	
BE	-0.13	0.2557	1	0.2557	16.77	0.0008	
BF	0.13/-0.03	0.2372	2	0.1186	7.78	0.0044	
CE	0.08	0.1163	1	0.1163	7.63	0.0139	
CF	-0.23/0.06	0.7581	2	0.3791	24.86	< 0.0001	
DE	-0.06	0.0634	1	0.0634	4.16	0.0583	
EF	0.08/-0.08	0.1139	2	0.0569	3.73	0.0467	
A^2	0.1653	0.1939	1	0.1939	12.72	0.0026	
B^2	-0.1795	0.1740	1	0.1740	11.41	0.0038	
C^2	0.1677	0.1682	1	0.1682	11.03	0.0043	
D^2	-0.2482	0.3639	1	0.3639	23.87	0.0002	
E^2	-0.1734	0.1790	1	0.1790	11.74	0.0035	
Residual	--	0.2440	16	0.0152	--	--	
Lack of Fit	--	0.2198	11	0.0200	4.14	0.0645	not significant
Pure Error	--	0.0242	5	0.0048	--	--	
Cor Total		12.84	42	--	--	--	

Base 10 log transformation (k = 0); R^2 = 0.98; R^2_{adj} = 0.95; R^2_{pred} = 0.85; C.V (%) = 18.98; and Adequate precision = 30.06; df = Degree of freedom

Appendix D3: The non-linear Langmuir/Freundlich (top) and Dubinin-Radushkevich (bottom) isotherms for adsorption of As(III) by 70%Bt-30%Ch beads-A (adsorbent Y)

Note: at 25, 40 and 55 ^{O}C. pH = 8.0; adsorbent amount = 0.2 g; agitation time (at 230 rpm) = 180 minutes; Initial Pb concentrations = 10 - 350 mg/L; Each data-point represents mean ± standard deviation of three (3) different experiments (n = 3).
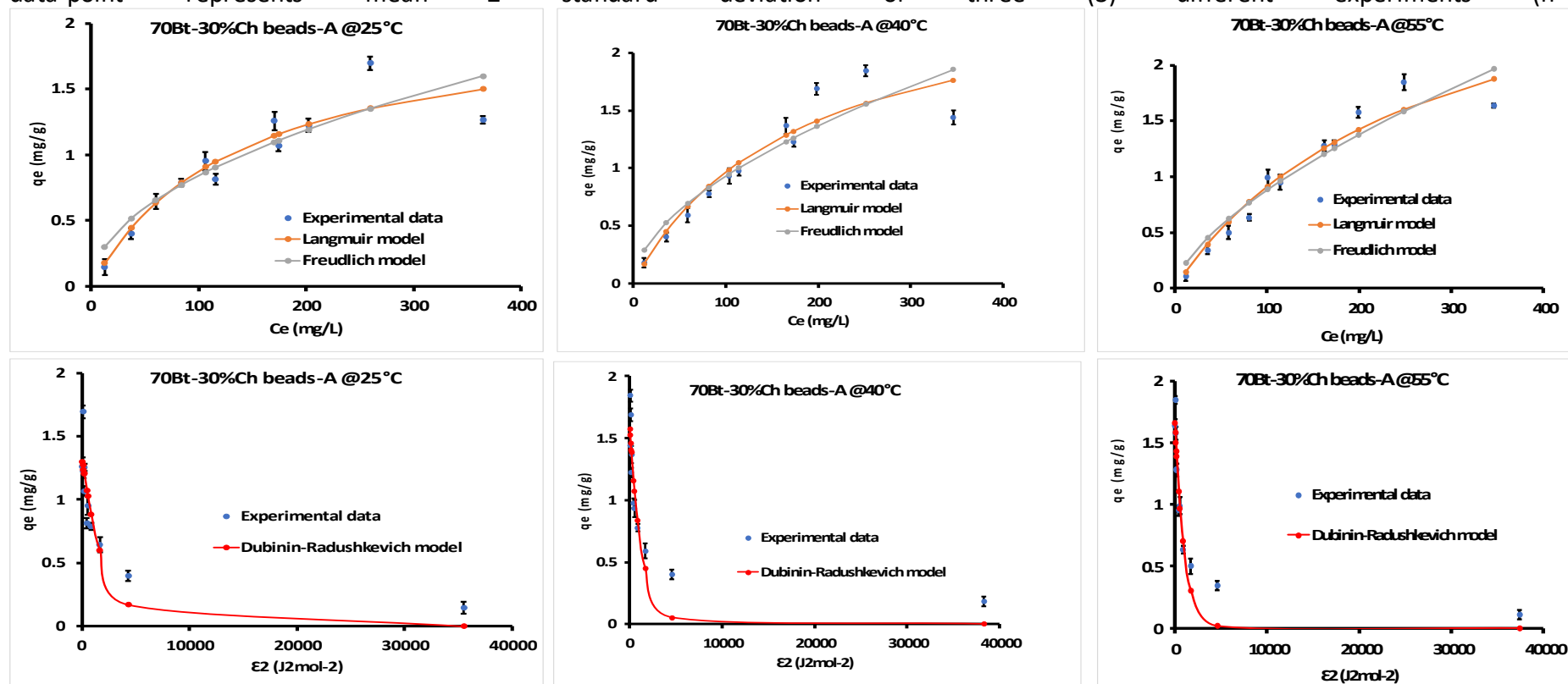
Appendix D4: The non-linear Langmuir/Freundlich (top) and Dubinin-Radushkevich (bottom) isotherms for adsorption of As(III) by 70%Bt-30%Ch beads-B (adsorbent Z)

Note at 25, 40 and 55 ^{O}C. pH = 8.0; adsorbent amount = 0.2 g; agitation time (at 230 rpm) = 180 minutes; Initial Pb concentrations = 10 - 350 mg/L; Each data-point represents mean ± standard deviation of three (3) different experiments (n = 3)
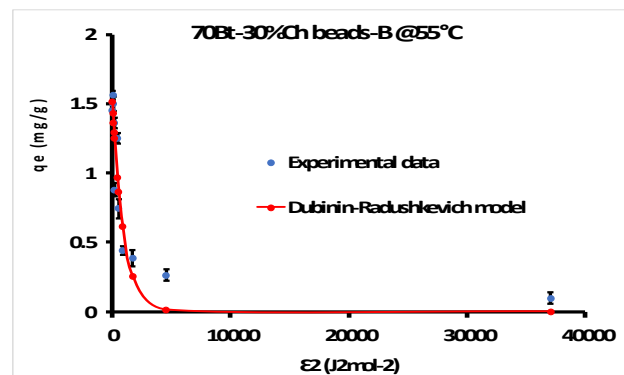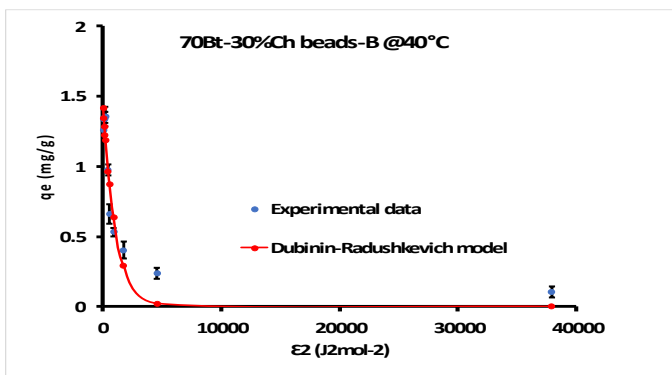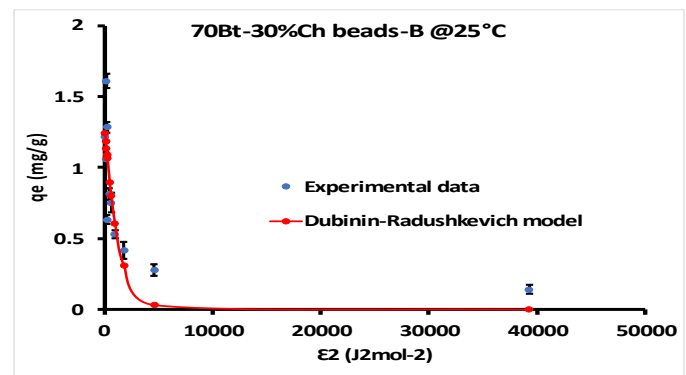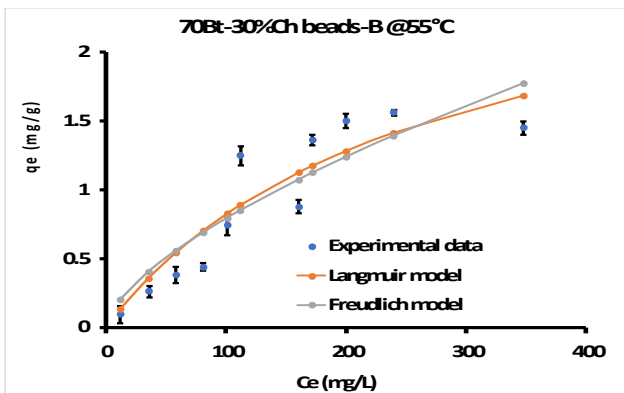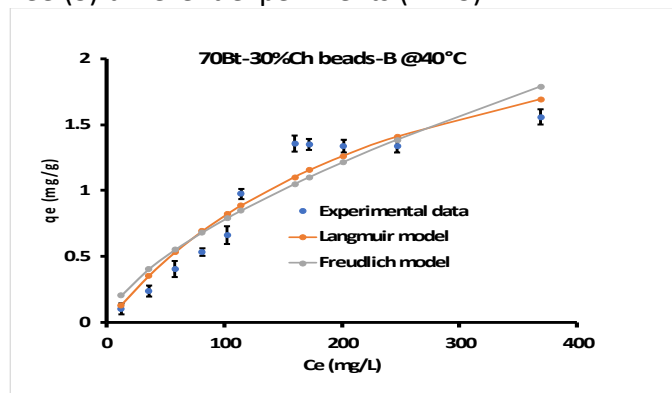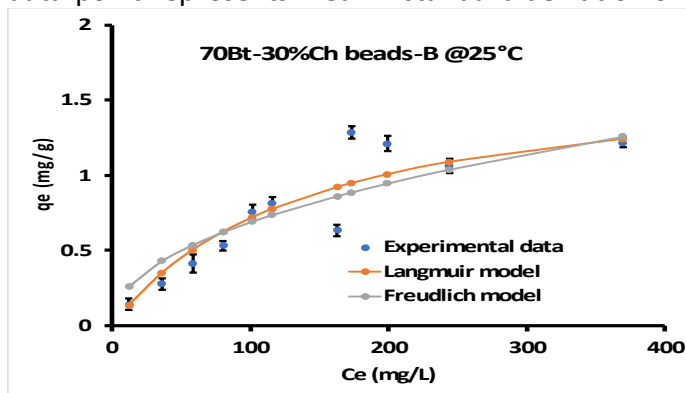
Appendix D5: The non-linear PFO, PSO and Elovich kinetic models for adsorption of As(III) by 70%Bt-30%Ch beads-A (adsorbent Y)

Note: at 25 ^{O}C. pH = 8.0; adsorbent amount = 0.2 g; Initial As(III) concentrations = 50 mg/L; agitation time (at 230 rpm) = 10 - 300 minutes; PFO = Pseudo-first order; PSO = Pseudo-second order. Each data-point represents mean ± standard deviation of three (3) different experiments (n = 3).
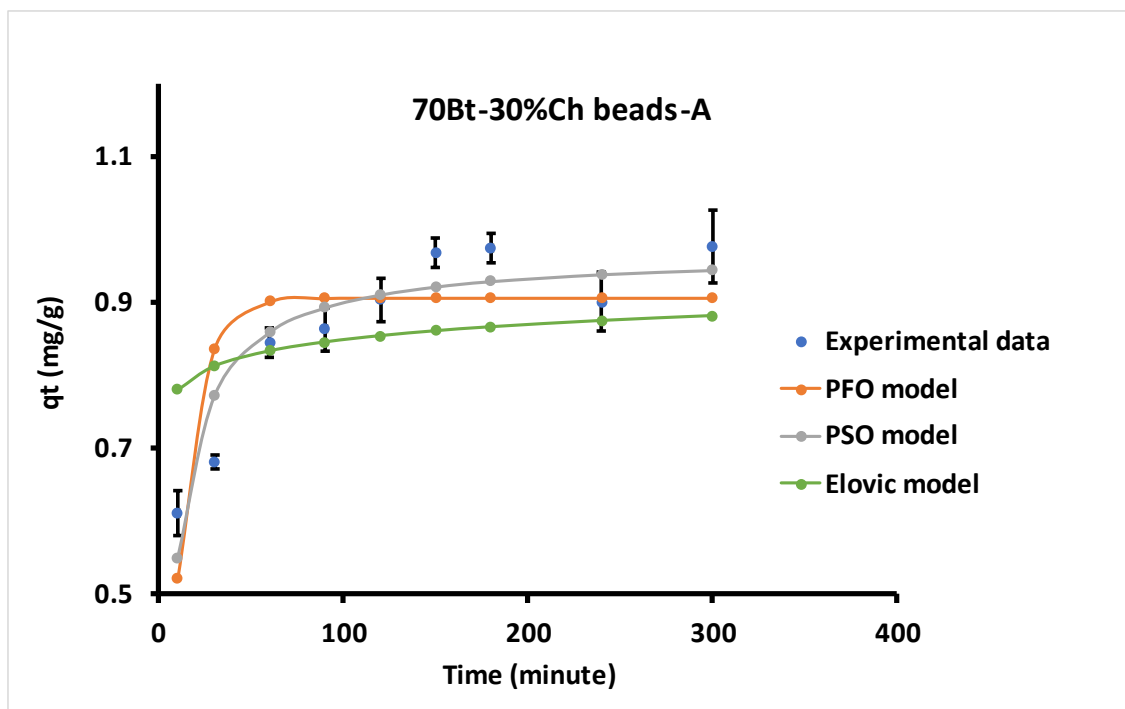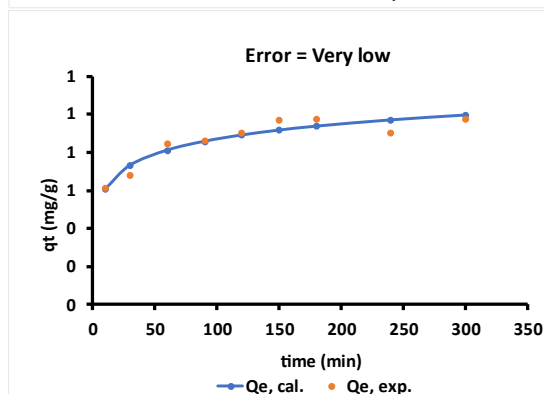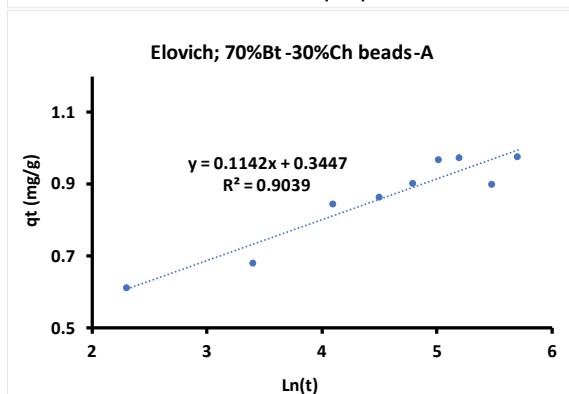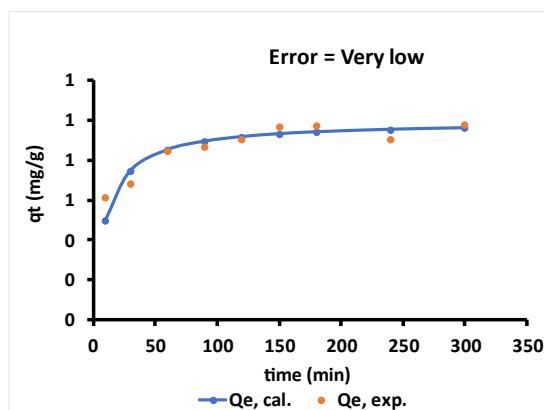
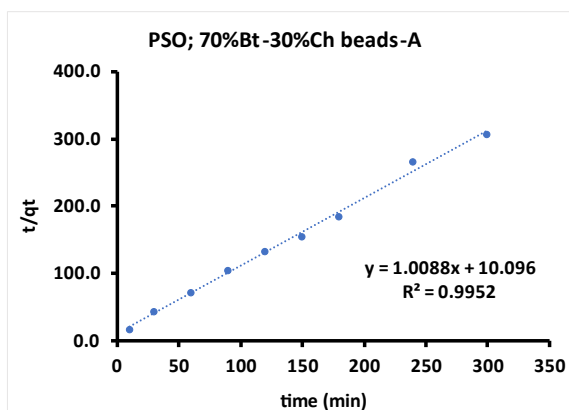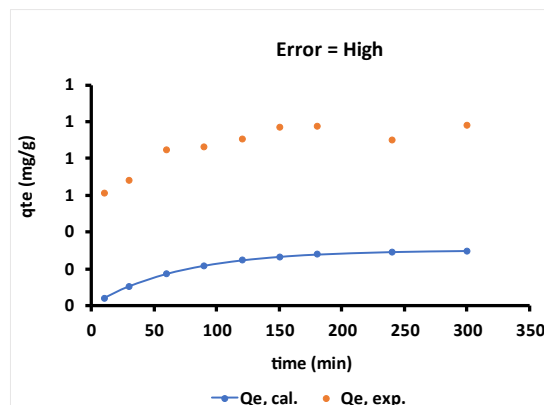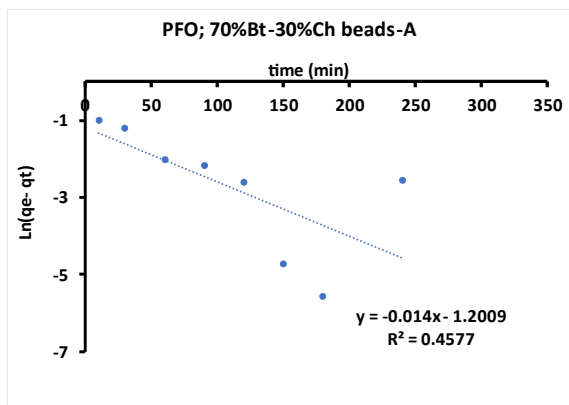**Appendix D6:** The non-linear PFO, PSO and Elovich kinetic models for adsorption of As(III) by 70%Bt-30%Ch beads-B (adsorbent Z)
Note: at 25 ^{O}C. pH = 8.0; adsorbent amount = 0.2 g; Initial As(III) concentrations = 50 mg/L; agitation time (at 230 rpm) = 10 - 300 minutes. Note: PFO = Pseudo-first order; PSO = Pseudo-second order. Each data-point represents mean ± standard deviation of three (3) different experiments (n = 3
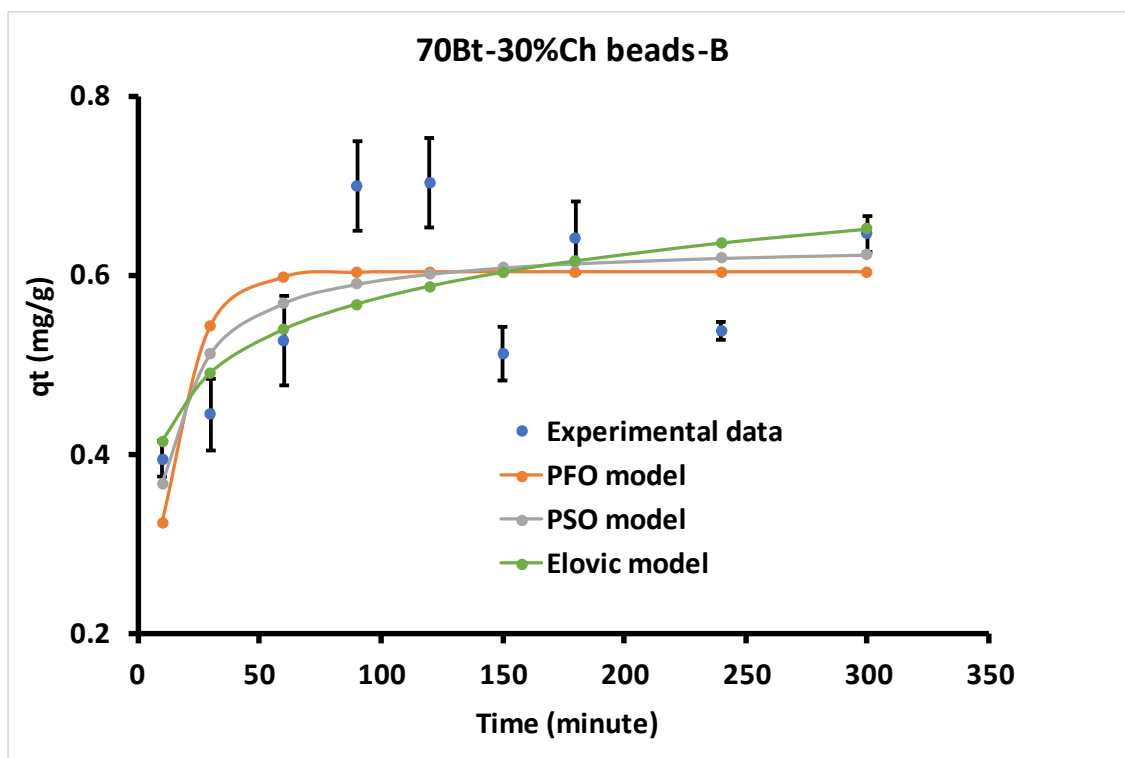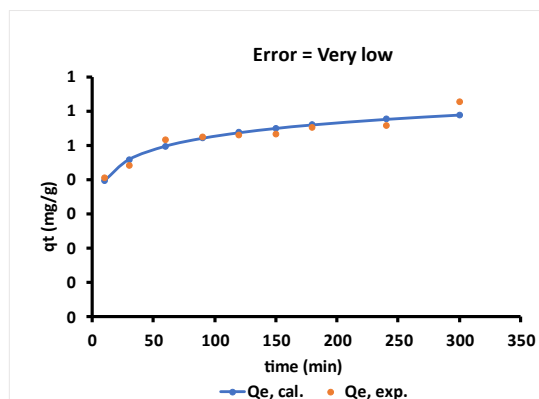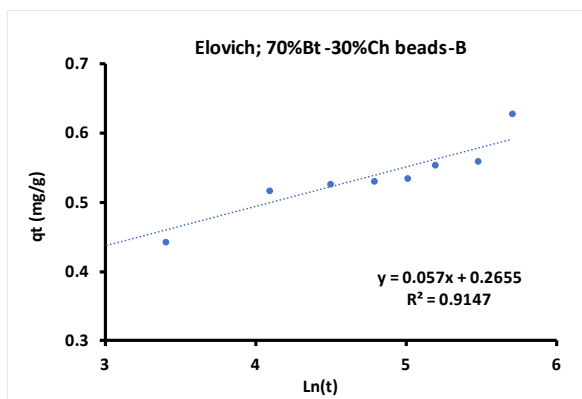
Appendix D7: The linear regression analysis of PFO, PSO and Elovich kinetic models for adsorption of As(III) by 70%Bt-30%Ch beads-A (adsorbent Y)

Note: at 25 ^{O}C. pH = 8.0; adsorbent amount = 0.2 g; Initial As(III) concentrations = 50 mg/L; agitation time (at 230 rpm) = 10 - 300 minutes; PFO = Pseudo-first order; PSO = Pseudo-second order. The average of the kinetic adsorption data was used to plot the linear regression graph.

PFO; 70%Bt-30%Ch beads-A

$y = -0.014x - 1.2009$
$R^2 = 0.4577$

Error = High

PSO; 70%Bt-30%Ch beads-A

$y = 1.0088x + 10.096$
$R^2 = 0.9952$

Error = Very low

Elovich; 70%Bt-30%Ch beads-A

$y = 0.1142x + 0.3447$
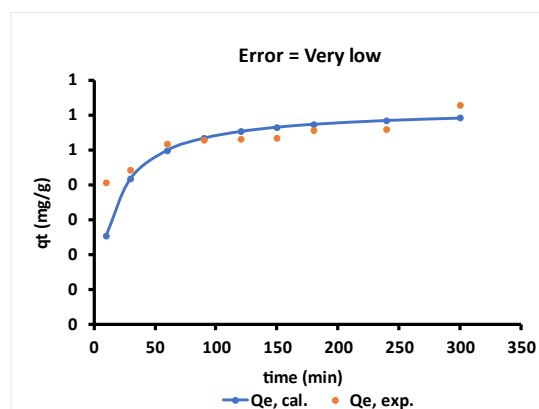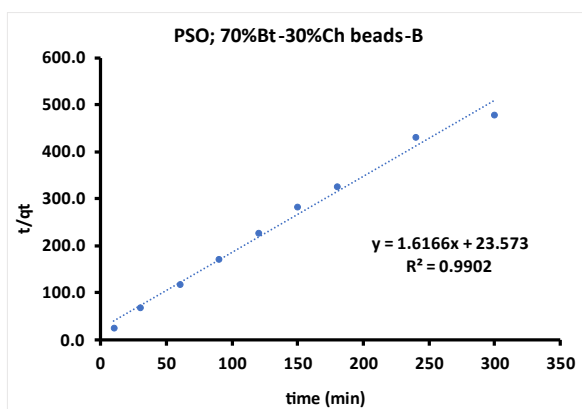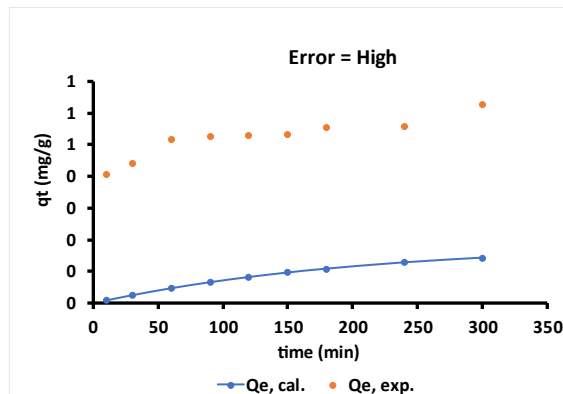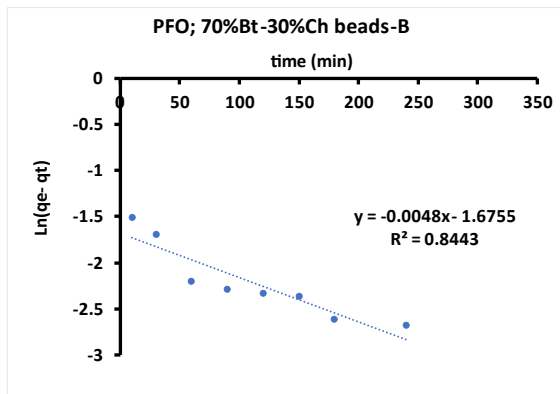$R^2 = 0.9039$

Error = Very low

Appendix D8: The linear regression analysis of PFO, PSO and Elovich kinetic models for adsorption of As(III) by 70%Bt-30%Ch beads-B (adsorbent Z)

Note: at 25 ^{O}C. pH = 8.0; adsorbent amount = 0.2 g; Initial As(III) concentrations = 50 mg/L; agitation time (at 230 rpm) = 10 - 300 minutes; PFO = Pseudo-first order; PSO = Pseudo-second order. The average of the kinetic adsorption data was used to plot the linear regression graph.

PFO; 70%Bt-30%Ch beads-B

$y = -0.0048x - 1.6755$
$R^2 = 0.8443$

Error = High

PSO; 70%Bt-30%Ch beads-B

$y = 1.6166x + 23.573$
$R^2 = 0.9902$

Error = Very low

Elovich; 70%Bt-30%Ch beads-B

$y = 0.057x + 0.2655$
$R^2 = 0.9147$

Error = Very low

Appendix E1: Adsorption factors (generated Design-Expert® 13 software) and response for optimal experimental design (I-optimal) concerning adsorption of As(III) ion onto Fe-Bt-Ch composites

| Run	Factors				Response Adsorption capacity (mg/g)	
	A	**B**	**C**	**D**	**Experimental**	**Predicted**
1*	4.50	0.20	121.00	197.05	9.101	9.243
2	9.00	0.05	100.00	221.89	12.120	12.023
3	4.10	0.19	250.00	10.00	7.809	7.786
4	9.00	0.20	50.00	300.00	6.199	6.192
5	2.00	0.20	50.00	10.00	3.826	3.849
6	9.00	0.05	250.00	256.50	11.550	11.482
7*	6.20	0.12	50.00	124.55	7.406	7.239
8*	2.00	0.12	170.00	124.55	8.777	9.122
9	9.00	0.05	70.00	10.00	8.650	8.670
10	6.09	0.13	168.00	34.65	10.530	9.768
11	6.24	0.12	170.00	300.00	11.664	12.303
12	2.00	0.05	50.00	300.00	5.055	5.078
13	3.85	0.05	250.00	223.15	10.300	10.233
14	3.86	0.05	104.00	10.00	7.085	7.176
15	2.00	0.20	250.00	300.00	10.773	10.715
16	9.00	0.19	250.00	214.45	10.555	10.233
17*	6.24	0.12	170.00	300.00	12.507	12.303
18	2.00	0.12	170.00	124.55	9.381	9.122
19	6.20	0.12	50.00	124.55	7.128	7.239
20	4.49	0.20	121.00	197.05	8.901	9.243
21	9.00	0.19	110.00	10.00	7.260	7.371
22*	4.49	0.20	121.00	197.05	9.635	9.243
23	4.94	0.15	250.00	178.28	10.555	10.965
24	9.00	0.08	250.00	10.00	7.864	8.039
25	2.07	0.15	50.00	299.76	4.989	4.910

*A = pH; B = Adsorbent dosage; C = Initial concentration; D = Agitation time; * = replicates (experimental-runs #1, #7, #8, #17 and #22 are the replicated experiments of run #20, #19, #18, #11, #20, respectively)*

Appendix E2: Analysis of Variance (ANOVA) of reduced quadratic model for the response (As-adsorption capacity)

| Source	Coefficient estimate	Sum of Squares	df	Mean Square	F-value	p-value	Remarks
Model	1.05	0.4012	14	0.0287	78.21	< 0.0001	significant
A-pH	0.061	0.0454	1	0.0454	123.79	< 0.0001	
B-Adsorbent dosage	-0.024	0.0074	1	0.0074	20.33	0.0011	
C-Initial conc.	0.094	0.1179	1	0.1179	321.81	< 0.0001	
D-Agitation time	0.056	0.0412	1	0.0412	112.39	< 0.0001	
AB	-0.030	0.0075	1	0.0075	20.36	0.0011	
AC	-0.036	0.0099	1	0.0099	27.09	0.0004	
AD	-0.002	0.0000	1	0.0000	0.0950	0.7643	
BC	0.030	0.0076	1	0.0076	20.70	0.0011	
BD	0.002	0.0000	1	0.0000	0.1148	0.7417	
CD	0.023	0.0039	1	0.0039	10.57	0.0087	
A²	-0.038	0.0057	1	0.0057	15.50	0.0028	
B²	-0.015	0.0009	1	0.0009	2.41	0.1517	
C²	-0.112	0.0530	1	0.0530	144.64	< 0.0001	
D²	-0.051	0.0102	1	0.0102	27.81	0.0004	
Residual	--	0.0037	10	0.0004	--	--	
Lack of Fit	--	0.0020	5	0.0004	1.23	0.4137	not significant
Pure Error	--	0.0016	5	0.0003	--	--	
Cor Total	--	0.4049	24	--	--	--	

Base 10 log transformation (k = 0); R^2 = 0.99; R^2_{adj}= 0.98; R^2_{pred} = 0.95; C.V (%) = 2.07; and Adequate precision = 33.96; df = Degree of freedom

Appendix E3: The non-linear Langmuir/Freundlich (top) and Dubinin-Radushkevich (bottom) isotherms for adsorption of As(III) by Fe-Bt-Ch-2 composites
Note: at 25, 40 and 55 ^{O}C. pH = 8.0; adsorbent amount = 0.1 g; agitation time (at 230 rpm) = 180 minutes; Initial Pb concentrations = 10 - 500 mg/L; Each data-point represents mean ± standard deviation of three (3) different experiments (n = 3).
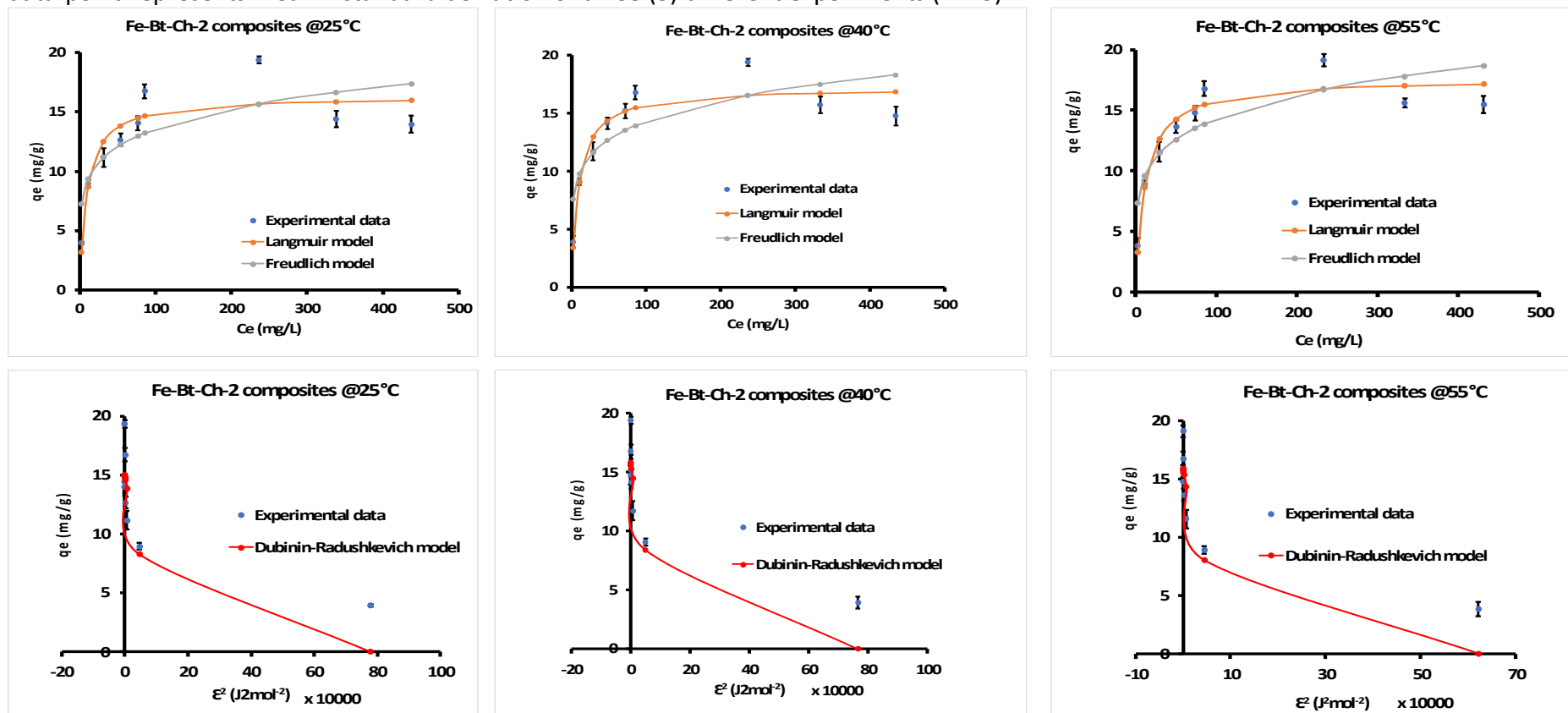
Appendix E4: The non-linear PFO, PSO and Elovich kinetic models for adsorption of As(III) by Fe-Bt-Ch-2.

Note: at 25 ^{O}C. pH = 8.0; adsorbent amount = 0.1 g; Initial As(III) concentrations = 50 mg/L; agitation time (at 230 rpm) = 10 - 300 minutes.; PFO = Pseudo-first order; PSO = Pseudo-second order. Each data-point represents mean ± standard deviation of three (3) different experiments (n = 3)

Fe-Bt-Ch-2 composites
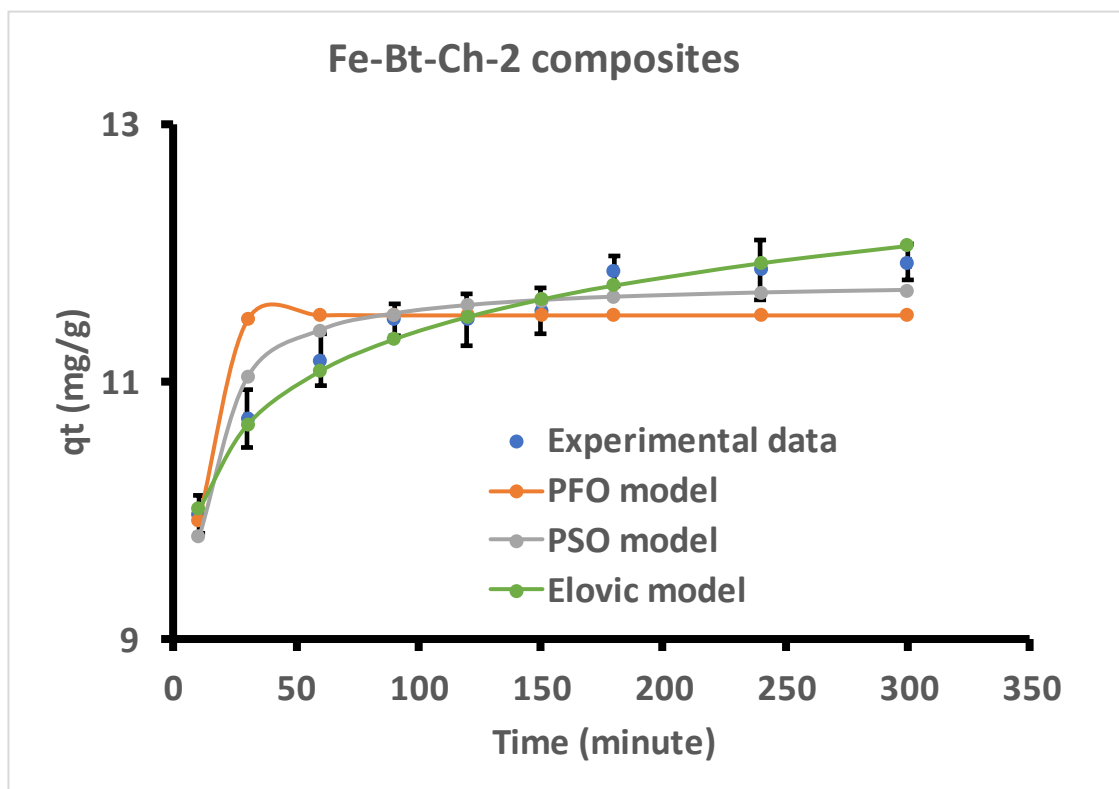
Appendix E5: The linear regression analysis of PFO, PSO and Elovich kinetic models for adsorption of As(III) by Fe-Bt-Ch-2 composites
Note: at 25 ^{O}C. pH = 8.0; adsorbent amount = 0.1 g; Initial As(III) concentrations = 50 mg/L; agitation time (at 230 rpm) = 10 - 300 minutes.; PFO = Pseudo-first order; PSO = Pseudo-second order. The average of the kinetic adsorption data was used to plot the linear regression graph.